UNIVERSITÉ DE MONTRÉAL

DISPLACEMENT-BASED PERFORMANCE ASSESSMENT OF RC SHEAR WALLS DESIGNED ACCORDING TO CANADIAN SEISMIC STANDARDS

KRASIMIRA ALEXIEVA
DÉPARTEMENT DES GÉNIES CIVIL, GÉOLOGIQUE ET DES MINES
ÉCOLE POLYTECHNIQUE DE MONTRÉAL

MÉMOIRE PRÉSENTÉ EN VUE DE L'OBTENTION
DU DIPLÔME DE MAÎTRISE ÈS SCIENCES APPLIQUÉES
(GÉNIE CIVIL)
DÉCEMBRE 2007

Your file Votre référence
ISBN: 978-0-494-36898-5
Our file Notre référence
ISBN: 978-0-494-36898-5

UNIVERSITÉ DE MONTRÉAL

ÉCOLE POLYTECHNIQUE DE MONTRÉAL

Ce mémoire intitulé:

DISPLACEMENT-BASED PERFORMANCE ASSESSMENT OF RC SHEAR WALLS DESIGNED ACCORDING TO CANADIAN SEISMIC STANDARDS

présenté par: ALEXIEVA Krasimira

en vue de l'obtention du diplôme de: Maîtrise ès sciences appliquées

a été dûment accepté par le jury d'examen constitué de:

Mme KOBOEVIC Sanda, Ph.D., président

M. BOUAANANI Najib, Ph.D., membre et directeur de recherche

M. BAGCHI Ashutosh, Ph.D., membre

ACKNOWLEDGEMENTS

I would like to express my deepest gratitude to my supervisor Professor Najib Bouaanani, Department of Civil, Geological and Mining Engineering at École Polytechnique de Montréal, for his invaluable guidance, constructive comments and suggestions during the whole research work. I would like to thank him sincerely for the encouragement provided and support through the preparation of this report, as well as for his appreciable advice about my professional career.

I would like to express my appreciation to all my professors from the Research Group in Structural Engineering at École Polytechnique de Montréal for their professional fulfillment and their manner to combine the theoretical part of teaching with the practice of Structural Engineering profession.

I owe special thanks to my husband and daughter for their unbelievable understanding, support and patience, especially at moments when they are not supposed to be part of the earthquake engineering research studies, but rather to enjoy time together.

I thank my parents and my husband's parents in Bulgaria for their continuing belief in me.

Last, but not the least, I would like to thank all my colleagues and friends for their continuous support and understanding.

RÉSUMÉ

Des approches de conception basées sur la performance parasismique des structures ont émergé récemment comme une alternative aux méthodes conventionnelles préconisées par les normes de conception modernes. La motivation sous-jacente à ces nouvelles techniques est de relier des niveaux anticipés d'aléas sismiques différents à des objectives spécifiques de performance structurale. La plupart de ces méthodes ont été validées cependant en utilisant des sollicitations sismiques typiques de l'ouest de l'Amérique du Nord, de l'Europe ou de l'Asie.

Ce projet de maîtrise a pour objective principal d'appliquer certaines approches basées sur le déplacement pour évaluer le comportement parasismique des murs de refend en béton armé dans le contexte normatif canadien. Trois bâtiments de bureaux avec des murs de refend et des cadres en béton armé sont dimensionnés et utilisés pour effectuer des analyses sismiques. Les trois bâtiments ont un plan de plancher identique, mais différentes hauteurs de 21 m, 42 m et 63 m, correspondant à 6, 12 et 18 étages, respectivement. Afin d'évaluer l'influence de la variabilité de l'aléa sismique entre l'est et l'ouest canadien, la conception parasismique et l'analyse de la performance structurale des trois bâtiments sont effectuées en considérant les deux sites de Montréal au Québec et de Vancouver en Colombie Britannique.

Les critères de dimensionnement parasismiques de la plupart des normes modernes, incluant le Code National du Bâtiment du Canada (CNBC 2005), recommandent l'application d'une conception basée sur l'évaluation de la force de cisaillement. Une telle démarche commence par le calcul de la force de cisaillement à la base d'une structure, requise pour maintenir un comportement linéaire élastique. Les accélérations spectrales fournies par la norme sont utilisées à cette fin. La structure est alors conçue pour une résistance en cisaillement de conception, obtenue en modifiant la force élastique à la base par des facteurs de force. Ces facteurs dépendent du type du système résistant aux forces latérales et tiennent compte de sa capacité en ductilité, ainsi que de sa réserve de résistance. Les

murs de refend étudiées dans ce projet sont considérés ductiles ($R_y = 3.5$). Les bâtiments sont alors soumis à une répartition des forces latérales équivalentes, obtenues par la distribution spatiale de la force de cisaillement à la base en fonction de la hauteur des bâtiments. Lorsque les déformations obtenues respectent les limites requises par la norme, le dimensionnement des composantes structurales telles que les murs de refend peut alors être effectué.

Trois méthodes basées sur la performance sont choisies pour ce projet : (i) la méthode du spectre de plastification (Aschheim, 2000), (ii) la méthode de conception basée sur l'évaluation directe du déplacement (Priestley et Kowalsky, 2000), et (iii) la méthode du spectre inélastique de déplacement (Chopra et Goel, 2001). Les trois méthodes ont été initialement établies pour un système à un seul degré de liberté. Elles sont basées sur le spectre inélastique de réponse sismique, obtenu à partir du spectre élastique en utilisant des facteurs dépendant de la ductilité. Pour faciliter la comprehension des fondements théoriques des trois méthodes, une formulation mathématique unifiée est développée dans le cadre de ce projet. La méthodologie des trois procédures choisies est basée essentiellement sur l'estimation des déplacements. En général, elles sont formulées de façon à satisfaire des critères de résistance des normes modernes de conception, et en même temps à assister les ingénieurs en structure pour limiter les déformations maximales et les déplacements inter-étages à des valeurs acceptables.

Ce projet présente aussi des méthodes d'estimation du déplacement cible et des indices inter-étages pour les structures multi-étagées, en développant des formules pour le profil déplacé des structures, à la base de la première forme de vibration. On pourrait utiliser aussi le spectre sumentionné pour déterminer des combinaisons différentes de résistance latérale et de ductilité, effectives pour limiter un déplacement cible et pour ductilités de déplacement requises, afin d'acheminer la performance désirée.

Des analyses non-linéaires temporelles des trois murs de refend sont effectuées en utilisant des excitations sismiques artificielles et historiques correspondant à l'aléa sismique

à Montréal et à Vancouver. Le programme d'analyse Ruaumoko est utilisé à cette fin. Un élément du mur avec des fibres multiple est choisi pour la modélisation de la section transversale du mur de refend en béton armé. Les résultats de tous les modèles d'analyse dans les deux villes montrent que les déplacements maximum obtenus par les méthodes basées sur la performance sont plus élevés que ceux obtenus par l'analyse dynamique préconisée par le CNBC 2005. Les critères de conception pour les déplacements inter-étage sont satisfaits pour les deux villes. En même temps, la résistance en cisaillement à la base obtenue par les méthodes basées sur la performance est moindre que celle résultant des analyses dynamiques. Un effet d'échelle a également été identifié dans les résultats de déplacement maximum et de plastification, ainsi que la force de cisaillement à la base maximum de conception et de plastification, obtenues par les méthodes de performance basée sur le déplacement.

Ce mémoire a présenté une étude de quelques procédures statiques non linéaires comme alternative au dimensionnement parasismique dans le contexte normatif Canadien. La simplicité d'utilisation de ces méthodes ainsi que les résultats obtenus montrent qu'elles peuvent effectivement être utilisées pour aboutir à une conception à la fois plus rationnelle et généralement plus économique que les techniques conventionnelles actuelles. Une validation expérimentale et un raffinement de ces nouvelles procédures sont cependant encore requis avant de pouvoir les adopter de façon définitive par la communauté des ingénieurs en structures.

ABSTRACT

Performance-Based Seismic Design (PBSD) methods were developed as an alternative to prescriptive current building codes. The underlying logic behind these techniques is to link specified structural performance objectives to one or more earthquake hazard levels. Most research on PBSD methods was validated using Western North America (WNA) ground motions however. This project aims mainly at investigating the use of some Displacement-Based approaches to assess the seismic performance of Reinforced Concrete (RC) shear walls in a Canadian code perspective.

The inelastic seismic response of reinforced concrete shear walls, as main members of the Seismic Force Resisting System (SFRS) was investigated using current engineering practice and compared to the seismic response after applying PBSD methods. Three reinforced concrete frame-shear wall office buildings with the same floor plan were investigated in the present study. The three buildings have different heights of 21 m, 42 m and 63 m corresponding to 6, 12 and 18 storeys, respectively. Seismic design and performance assessment of the three shear wall buildings were conducted assuming that they are located at the cities of Montréal, Québec, and Vancouver, British Columbia, to account for seismic hazard in Eastern and Western Canada, respectively.

Seismic provisions of current generation of building codes including the National Building Code of Canada (NBCC 2005), advocate the use of Force-Based Design (FBD) procedures. According to this approach, elastic base shear required to keep a ground shaken structure linear-elastic was first determined. Smoothened soil dependent elastic spectral accelerations were used for this purpose. The structure was then designed to have a yield strength obtained by dividing the elastic base shear by a force modification factor. This reduction factor depends on the lateral force-resisting system used, and is assumed to account for the structure's ductility capacity and inherent overstrength. The shear walls studied were assumed as ductile ($R_{\mathrm{d}} = 3.5$). The structures were then subjected to a set of equivalent lateral forces obtained from the vertical distribution of the design base shear over the

building height. Once the resulting deformations were checked to be within code prescribed limits, proportioning and detailing of the structural members followed.

Three Displacement-Based Design (DBD) approaches were explored in this work : (i) the Yield Point Spectra method (Aschheim, 2000), (ii) the Direct Displacement Based-Design method (Priestley and Kowalsky, 2000), and (iii) the Inelastic Displacement Spectra method (Chopra and Goel, 2001). To facilitate the understanding of the theoretical background of the three DBD techniques investigated, a unified mathematical formulation of the three methods was first developed in this project. The three techniques were developed initially for Single Degree of Freedom (SDOF) systems. They are based on inelastic response spectra, that can be derived from elastic spectra using ductility dependent factors.

The methodology of the three DBD procedures aims at a direct displacement-based structural design. They are indeed formulated to satisfy modern seismic design strength criteria and in the meantime to assist structural engineers to limit maximum deflections and inter-story drifts to acceptable values. In order to achieve these objectives, the conceptual methodology implements the use of an equivalent structural model of one degree of freedom. The present thesis also presents a new method of estimating the target displacement and the inter-story indexes of the multi-story buildings throughout establishing formulas for the deformed building shape, developed on the basis of the first deformation shape. Nonlinear time history analyses of the concrete shear walls were performed using site-specific ground motions for Montreal and Vancouver. Both synthetically generated and historical records were considered for the analyses carried out using the computer program Ruaumoko. A wall element with fiber discretization of the cross section was chosen for the modeling. Results for all models in both cities indicated that although the maximum displacements, obtained through PBSD have been found for some analyses much higher than those obtained by the NBCC 2005 dynamic analyses, they satisfied the target objectives for interstorey drift limits. In the same time, the design base shear strengths obtained through PBSD have been found lower than those obtained by the code

prescribed procedures. A size effect, function of the wall ratio for both cities, was also identified in the response of the maximum design and yield displacements, as well as for the design base shears obtained using the DBD methods.

This work presented original results following the application of some selected performance-based non-linear static procedures to buildings designed according to the Canadian seismic standards. It is found that the performance-based method investigated could represent an interesting alternative for seismic evaluation, and cost efficient design, while achieving target performance objectives. The results presented are however preliminary, and experimental validations and additional refinement are still required before these methods could be fully adopted by the structural engineering community.

CONDENSÉ EN FRANÇAIS

Au cours de l'histoire, les tremblements de terre ont causé de nombreuses pertes de vie et de propriétés. Aujourd'hui, même si de grands progrès ont été réalisés dans la domaine du génie parasismique, le risque sismique est généralement en augmentation à cause de l'urbanisation rapide à travers le monde. Pendant longtemps, les objectives principaux des critères de dimensionnement parasismique visaient à protéger les vies humaines et à éviter les effondrements suite à des tremblements de terre majeurs. Ces objectives étaient généralement établies à partir des critères minimums prescrits par les matériaux de construction, la résistance requise ou la déformation maximum acceptable sous chargement sismique.

Des tremblements de terre récents, notamment ceux de Loma Prieta (1989), Northridge (1994) et Hyogo-Ken Nambu (1995), ont marqué un grand tournant dans l'évolution des mesures parasismiques. Ils ont en effet montré que plusieurs structures conçues selon les normes conventionnelles se sont effondrée en perdant la totalité de leur capacité résistante. Suite à ces événements, les normes de conception parasismiques ont introduit des critères nouveaux afin d'obtenir une performance prévisible complémentaire aux objectives traditionnelles de protection de la vie humaine. De cette façon, les clauses basées sur la performance devraient garantir une fraction prévisible de la capacité fonctionnelle structurale et non-structurale des bâtiments.

L'objectif principal du présent projet de recherche est d'étudier l'application de méthodes simplifiées basées sur l'évaluation du déplacement pour analyser la performance sismique de murs de refend conçues selon la dernière édition des normes parasismiques canadiennes.

Les méthodes de conception basées sur la performance sismique ont émergés récemment comme des méthodes alternatives à celles plus conventionnelles préconisées par la plupart des normes de conception parasismiques internationales. La logique derrière de telles méthodes est de relier plusieurs niveaux d'aléas sismiques anticipés à des objectives spécifiques de performance structurale. La plupart de ces méthodes ont été validées en utilisant

des sollicitations sismiques typiques de l'ouest de l'Amérique du Nord, de l'Europe et de l'Asie. Ce projet de maîtrise a pour but principal d'étudier l'application de certaines approches basées sur le déplacement pour évaluer le comportement sismique des murs de refend en béton armé dans le contexte normatif canadien.

L'organization du projet de recherche commence par une revue des normes de conception modernes, telles le Code national du bâtiment du Canada (CNBC 2005) et la norme de dimensionnement des structures en béton CSA A23.3-04. Ces normes ont beaucoup évoluées au cours des dernières décennies et notamment, en 2004-2005, où des modifications majeures visant à les adapter aux avancées récentes dans le domaine de la réduction du risque sismique ont été introduites. Ces améliorations suivent les grandes lignes d'une nouvelle philosophie basées sur la performance des structures.

Plus concrètement, le CNBC 2005 utilise une nouvelle génération des cartes d'aléa sismique, générées pour plusieurs villes canadiennes. Les cartes sont basées sur l'estimation des valeurs médiannes des mouvements spécifiées pour un sol ferme avec une probabilité de dépassement de 2% en 50 ans correspondant à une période de retour de 2750 ans. Ces valeurs d'accélération sont représentées dans le CNBC 2005 sous le format d'un spectre de dimensionnement avec un amortissement de 5%, pour un sol ferme et avec une probabilité une probabilité de dépassement de 2% en 50 ans.

Deux types de calcul sismique sont préconisées dans le CNBC 2005 : (i) l'analyse dynamique spectrale et, (ii) la procédure de force statique équivalente. En général, le CNBC 2005 recommande l'application de l'analyse dynamique, mais l'utilisation de la force statique équivalente pourrait aussi être utilisée. D'abord son application est permise pour des structures avec des limitations en fonction du site, ou du type de la structure. En général, cette procédure commence par le calcul la force élastique à la base nécessaire à maintenir le comportement linéaire élastique de la structure soumise aux sollicitations sismiques. Les accélérations spectrales sont utilisées à cette fin. La structure est alors conçue pour une résistance en cisaillement de conception, obtenue en modifiant la force

élastique à la base par des facteurs de force. Ces facteurs dépendent du type du système résistant aux forces latérales et sont présumés tenir compte de la capacité en ductilité du système, ainsi que de sa réserve de résistance. Les bâtiments sont alors soumis à des forces latérales équivalentes distribuées selon la hauteur et obtenues à partir de la force de cisaillement à la base du bâtiment. Lorsque les déformations résultantes sont dans les limites de celles requises par le code, le dimensionnement des composantes structurales tels que les murs de refend peut alors être effectué.

Les nouvelles éditions des normes canadiennes s'orientent progressivement vers la conception basée sur la performance. Le CNBC 2005 a gardé la philosophie de 'conception par capacité'. Cette conception commence par l'hypothèse, que l'énergie induite lors d'un séisme, serait dissipée dans des locations spécifiques demandées (la zone plastique). La 'conception par capacité' exige que tous les autres éléments du système résistant aux forces latérales soient munis d'une résistance de réserve suffisante, pour éviter tout mécanisme non anticipé. Pour assurer que la plastification soit limitée à la base de la structure, la norme CSA A23.3-04 suggère que les moments de flexion et les forces de cisaillement à chaque étage en haut de la zone plastique soient multipliés par la relation de la résistance en flexion pondérées sur le moment en flexion (obtenu de l'effet des charges pondérées), où les deux dernières sont calculés au sommet de la zone plastique.

Un des changements les plus importants dans la norme CSA A23.3-04 est l'exigence que la capacité des murs de refend en rotation plastique soit plus grande que la demande de ces murs en rotation inélastique. Cette vérification de la ductilité, introduite pour la première fois dans les normes canadiennes, est un pas important vers les principes modernes de la conception basée sur la performance des structures. La demande plastique en rotation est calculée à la base du déplacement maximum au sommet de la structure et l'hypothèse que la rotule plastique soit localisée à une hauteur égale à la moitié de la dimension longitudinale du mur à la base. Le profil des déformations anticipé pour ces vérifications suit surtout le premier mode de vibration du système. Seules les exigences concernant les murs ductiles inclues dans la norme CSA A23.3-04 (Clause 21) sont envisagées dans ce

projet, telles les limitations sur les dimensions, les rotations, les moments fléchissant et les forces de cisaillement.

Le chapitre 3 aborde le sujet principal de ce projet de recherche, à savoir l'application des méthodes simplifiées basées sur l'évaluation des déplacements pour analyser la performance sismique des murs de refend conçues selon les normes parasismiques candiennes. Cette étude vise essentiellement à élucider la relation entre les niveaux de performance en déplacement des structures et les différents aléas sismiques au Canada. Une des premières explorations de cette relation a été présentée dans les documents Vision 2000 (1995) et le Blue Book (1999) produits par l'Association des ingénieurs en structure de Californie (SEAOC). DeVall (2003) a proposé une adaptation de ces relations dans le contexte du code canadien. Afin de relier les différents niveaux de performance des structures aux aléas sismiques anticipés, trois niveaux de risque sismique ont été considérés dans le présent projet, correspondant à des périodes de retour 75 ans (noté SHL-75), 475 ans (noté SHL-475) et 2475 ans (noté SHL-2500).

Des recherches récentes ont prouvé que les endommagements structuraux et non structuraux dans un bâtiment sont davantage reliés aux déplacements inter-étages d'une structure qu'au déplacement maximum se produisant au sommet. Par conséquent, un 'indice de déplacement inter-étage' est introduit dans le cadre de ce travail pour définir la relation entre les déplacements inter-étages et les niveaux d'aléas sismiques anticipés sur un site sonné. Le CNBC 2005 prescrit des limites seulement sur les déplacements inter-étages. L'effet des rotations à chaque étage est également important et devrait aussi être considéré. Des limites sur les rotations du mur de refnd sont donc introduites dans ce projet en s'inspirant de documents relatifs aux normes américaines de conception de nouvelles structures et de réhabilitations des structures existantes produits par l'Agence Fédérale de Gestion d'Urgence (FEMA). Deux profils de déplacements latéraux correspondant à des limites en déplacement inter-étages et en rotation sont donc proposés et utilisés dans ce projet. Ces profils sont établis en adoptant l'hypothèse simplificatrice d'une rotation inélastique constante à tous les étages de la structure et en utilisant une formule simplifiée

pour évaluer la courbure plastique d'un mur de refend.

Afin de faciliter la comprehension des fondements théorique des trois méthodes explorées, une formulation mathématique unifiée est d'abord proposée. La relation force-déplacement est représentée schématiquement par deux courbes, réelle et idéalisée bi-linéaire, afin d'introduire le rapport entre les forces et les déplacements élastiques et plastiques, tels le facteur modifiant la résistance à la plastification R_{y} et la ductilité du système. Deux types de spectres sont utilisés : élastique et inélastique. Parmi les spectres inélastiques, on a recours également à deux types de spectres inélastiques pour l'évaluation de la performance sismique : (i) le spectre de réponse inélastique d'accélération définissant les accélérations inélastiques maximum à différents niveaux de ductilité, en fonction de la période d'un système à un seul degré de liberté, et (ii) le spectre de réponse inélastique du déplacement définissant les déplacements inélastiques maximum à différents niveaux de ductilité, en fonction de la période d'un système à un seul degré de liberté.

Suite à une revue de littérature approfondie, deux méthodes de calcul des relations $R_{\mathrm{y}} - \mu - T$ sont considérées dans le cadre de ce travail : celle proposée par Nassar et Krawinkler (1991) et celle développée par Miranda (1993). La plupart des méthodes disponibles dans la litérature ont été validées en utilisant essentiellement des séismes typiques de l'ouest de l'Amérique du Nord. La méthode de Miranda (1993) tient compte de l'influence de différents types de sol, tandis que celle proposée par Nassar et Krawinkler détermine le facteur R_{y} seulement en fonction des propriétés du système structural. Une comparaison des deux méthodes est effectuée en déterminant les relations $R_{\mathrm{y}} - \mu - T$ pour les conditions de sol adaptées à la classification des types de sol du CNBC 2005. En comparant les résultats obtenus en utilisant les deux méthodes, on trouve que les facteurs R_{y} produits par les deux méthodes ont tendance à se rapprocher pour des niveaux de ductilités bas, *i.e.* 2 ou 3, et surtout pour des périodes fondamentales supérieures à 2 sec. Compte tenu de ces résultats et du fait que la méthode proposée par Miranda (1993) tient compte des variations des conditions de sol, cette dernière est adoptée pour la suite des analyses dans ce travail.

Tel que mentionné auparavant, la comprehension des différences entre plusieurs méthodes basées sur la performance peut être facilitée par leur formulation unifiée. Les trois techniques utilisées dans ce projet étaient initialement développées pour un système à un seul degré de liberté. Il devient alors très important de bien maîtriser les hypothèses adoptées pour généraliser ces méthodes à un bâtiment multi-étagé, pouvant être simulé généralement par un système à plusieurs degrés de liberté. Deux approches sont disponibles dans la littérature pour représenter la réponse dynamique des bâtiments multi-étagés par la réponse d'un système à un seul degré de liberté : (i) le système équivalent à un seul degré de liberté, et (ii) la structure de substitution. La première méthode est caractérisée par un déplacement plastique maximum au sommet et par un coefficient de résistance à la première plastification se produisant à la base du système équivalent. Ces deux paramètres sont multipliées par des facteurs de participation de masse et de forme, afin d'obtenir les valeurs correspondantes du système réel multi-étagé. Les deux facteurs de participation sont développés dans ce projet en fonction d'un profil de déplacement correspondant à un niveau d'aléa sismique donné. La méthode de la structure de substitution est basée sur l'hypothèse d'une force de cisaillement identique à la base des deux structures réelle et de substitution, ainsi que des déplacements maximum identiques aux sommets des deux structures. Ces deux conditions permettent de définir des propriétés effectives caractérisant la structure de substitution, à savoir sa masse, sa hauteur et sa rigidité effectives. Ces paramètres sont déterminées dans ce travail en fonction du profil cible des déplacements latéraux.

Le chapitre 3 présente ensuite trois méthodes d'évaluation basées sur la performance sismique, choisies suite à une revue de littérature approfondie : (i) la méthode du spectre de plastification (Aschheim, 2000), (ii) la méthode de conception basée sur l'évaluation directe du déplacement (Priestley et Kowalsky, 2000), et (iii) la méthode du spectre inélastique de déplacement (Chopra et Goel, 2001). Pour les fins de la clarification, un organigramme illustrant les étapes de chacune des trois méthodes est développé. Les trois procédures aboutissent à une force de cisaillement à la base du système réel multi-étagé,

correspondant à une force de plastification ou à une force ultime de conception selon la méthode utilisée.

La première méthode utilisée dans ce projet est la méthode du spectre de plastification (YPS) proposée par Aschheim et Black (2000). Comme son nom l'indique, cette procédure est basée sur la construction d'un spectre de réponse de plastification. Deux options sont possibles pour la construction d'un tel spectre : (i) le spectre de plastification 'exact' construit directement à partir des historiques temporels des mouvements sismiques, et (ii) le spectre de plastification 'lisse' construit à partir du spectre élastique en utilisant des facteurs de modification R_y. Dans ce projet de recherche, les spectres lisses sont adoptés pour examiner les performances sismiques des bâtiments choisis. La méthode du spectre de plastification utilise le système équivalent pour relier le système à un seul degré de liberté au à bâtiment multi-étagé.

La deuxième méthode explorée dans le cadre de ce projet est la méthode de conception basée sur l'évaluation directe du déplacement proposée par Priestley et Kowalsky (2000). Comparée à la précédente, cette méthode utilise la structure substituée pour modéliser la réponse du système inélastique. Elle est caractérisée par l'utilisation d'un profil cible de déplacement prédéterminé et par le spectre inélastique de réponse de déplacement pour des niveaux différents d'amortissement.

La troisième méthode basée sur la performance est celle utilisant le spectre inélastique de déplacement tel que proposée par Chopra et Goel (2001). La méthode a été généralement développée pour des systèmes à un seul degré de liberté. Pour les fins de ce projet, on a utilisé la structure substituée pour modéliser la réponse du système inélastique. La méthode du spectre inélastique utilise un profil cible de déplacement prédéterminé et des spectres inélastiques de réponse d'accélération pour des niveaux différents de ductilité. La procédure est itérative et inclue un rapport aux normes de conception, la faisant différer des autres méthodes ci-étudiées.

Le chapitre 4 applique les principes de la conception selon le CNBC 2005 et la norme CSA A23.3−04 pour trois murs de refend situés à deux endroits au Canada, soient Montréal et Vancouver. Trois bâtiments de bureaux, dont le système résistant aux forces latérales est présenté par des cadres dans la direction longitudinale et des murs de refend en béton armé dans la direction transversale, sont utilisés dans le projet. Tous les bâtiments ont le même plan et diffèrent seulement par leurs hauteurs de 21 m, 42 m et 63 m correspondent à 6, 12 et 18 étages. Puisque les murs de refend sont sujet de l'étude de ce projet pour l'application des méthodes de performance basée au déplacement plus tard, on fait la conception selon les normes canadiennes seulement pour ces murs de refend. Les fondations de tous les murs sont supposées comme assez rigides afin de transmettre les charges sismiques au sol et ne font pas l'objet de cette étude. La procédure des forces équivalentes statiques est d'abord appliquée pour définir les critères minimaux de la force de cisaillement à la base des murs et pour calibrer les résultats de l'analyse spectrale suivante tel que recommandé par le CNBC 2005. La période fondamentale utilisée pour cette procédure est calculée selon la formule empirique définie par le CNBC 2005 pour les murs de refend en béton multipliée deux fois. Tous les murs étaient considérés comme des murs ductiles et un facteur de modification de force $R_{\mathrm{d}} = 3.5$ est utilisé afin d'obtenir la force de conception à la base.

La méthode de l'analyse dynamique spectrale recommandée par le CNBC 2005 est ensuite appliquée pour obtenir les efforts de conception dans tous les murs pour les sites choisis. On a utilisé le programme ETABS (CSI) pour effectuer des analyses spectrales basées sur une modélisation tridimensionnelle des trois bâtiments en incluant des propriétés des sections effectives, telles que requis par la norme A23.3-04.

La comparaison des efforts tranchant à la base des murs de refend, calculés avec la méthode spectrale à ceux obtenus avec la procédure des forces équivalentes statiques a démontré deux points intéressants. Le premier point est que les forces de cisaillement obtenues par l'analyse pseudo-statique sont supérieures à celles obtenues par l'analyse spectrale pour les murs de hauteur modérée à élevée (bâtiments de 12 et de 18 étages). Cette différence

était attendue à cause des périodes fondamentales obtenues selon les analyses spectrales, et qui sont plus élevées que celles déterminées par la méthode statique équivalente. En plus, il a été observé que les dernières sont inférieures même à 80% des efforts calculées avec la méthode statique équivalente. Par contre, les efforts tranchants pour les bâtiments de 6 étages, obtenus par l'analyse spectrale gouvernent pour les deux sites étudiés. Le deuxième point important a mentionner est qu'on a pris comme limite minimale de calibration des efforts tranchants à la base des murs, 100% de la force de cisaillement, calculée par la méthode statique équivalente. La raison d'estimer ce pourcentage, au lieu de 80%, qui serait permis par le Code dans le cas de ce projet, est qu'on aurait augmenter de façon significative les efforts de flexion et de cisaillement anticipés de conception dans tous les étages. Puisque les exigences minimales du renforcement gouvernent pour tous les murs, sauf pour les bâtiments élevés à Vancouver, la différence parmi les moments de résistance probable et nominale et celle de l'effet des charges pondérées aurait augmenté, par conséquence - les efforts anticipés dans tous les étages et l'armature requise auraient augmenter de façon significative. Ensuite, on a effectué la conception des murs de refend selon les exigences spéciales sismiques de la norme A23.3-04 pour des murs ductiles. On devrait noter quelques points importants lors de la conception des murs pour les deux sites. Le premier était que les exigences de l'armature minimale gouvernaient pour les murs de refend ductiles des bâtiments situés à Montréal, tandis que pour Vancouver, cette observation était valide seulement pour le bâtiment de 6 étages. Comme un deuxième point, on a noté que les capacités en rotation plastiques sont satisfaites, c'est à dire plus grandes que les demandes en rotation plastique requises par la norme A23.3−04, pour tous les bâtiments à Montréal. En plus, pour les bâtiments de 6 à 12 étages, les demandes en rotation plastique étaient plus basses que les limites minimales, alors on a pris les dernières comme base de comparaison aux capacités obtenues. Puisque l'armature de flexion était conçue pour satisfaire les exigences minimales, établies par la norme A23.3−04, on pourrait dire que la conception avait résulté en une augmentation significative en armature. Par contre, pour la ville de Vancouver, ce sont les demandes en rotation plastique qui contrôlent la conception pour les bâtiments de 12 et de 18 étages, par conséquent, l'armature en flexion a été augmentée afin d'obtenir une plus grande ca-

pacité en rotation plastique pour ces murs de refend. Pour le bâtiment de 6 étages situé à Vancouver, on a noté que la limite minimum de demande en rotation plastique gouverne le dimensionnement.

Dans chapitre 5 les trois méthodes de performance choisies sont appliquées aux bâtiments conçus selon les normes canadiennes dans le chapitre précédent. Les bâtiments sont étudiés dans les deux sites de Montréal et de Vancouver, et pour trois niveaux de risque sismique SHL−75, SHL−475 et SHL−2500. Chacune des méthodes décrites auparavant a été présentée à l'aide d'un exemple. Pour toutes les méthodes, on a pris comme exemple le bâtiment de 6 étages à Montréal, soumis au séisme de niveau SHL-2500 et la procédure suivait les mêmes étapes décrites au chapitre 3. La première méthode du spectre de plastification commence par le calcul du déplacement de plastification au sommet, en utilisant les propriétés géométriques déjà définies de la structure. Ensuite, le déplacement maximum cible est calculé en prenant à chaque niveau la valeur gouvernant les profils en rotation vs. celui de déplacement inter-étage. Le rapport de ces deux valeurs nous a donné la ductilité utilisée pour construire le spectre de plastification. On a fait entrer le déplacement de plastification du système équivalent et le coefficient de réduction de la resistance à la base était rapporté. La procédure a fini par le calcul de la force de plastification à la base, en utilisant le facteur de participation de la masse.

La deuxième méthode basée sur l'évaluation directe du déplacement est utilisée par la suite. On commence par le développement des profils de déplacements. En utilisant le profil de contrôle, on calcule la masse et la hauteur effectives du la structure de substitution et le déplacement effectif au sommet de ce système. Le déplacement de plastification à cette hauteur, la ductilité et l'amortissement sont déterminés par la suite. On a construit le spectre inélastique de déplacement pour l'amortissement obtenu, dans lequel on a fait entrer le déplacement effectif, afin de raporter la période effective. La rigidité est ensuite obtenue pour en utilisant les transformation de la structure de substitution. La procédure a fini par le calcul de la force de cisaillement à la base.

La troisième méthode basée sur le spectre inélastique est présentée par la procédure itérative, telle que suggéré par Chopra et Goel (2001). De la même façon que la procédure précédente, on utilise le profil de déplacement de contrôle, le déplacement de plastification à la hauteur effective de la structure de substituion et la ductilité pour la première étape d'itération. On construit ensuite le spectre inélastique de déplacement correspondant à cette ductilité, dans lequel on reporte le déplacement effectif. La période correspondant à la première étape d'itération est donc obtenue et notée. La rigidité correspondante, la force de cisaillement et le moment de flexion requis sont ensuite déterminés. En utilisant la formule de la courbure de plastification, on re-calcule la rigidité du système effectif, et le déplacement de plastification. On compare le dernier au déplacement initialement anticipé et la procédure est répétée jusqu'à ce que la différence entre ces deux valeurs devienne négligeable. La procédure se termine par l'évaluation de la force de cisaillement à la base de la dernière étape d'itération. En comparant les forces de cisaillement à la base des murs de refend, une tendance attendue est validée pour toutes les méthodes basées sur la performance étudiées dans ce projet. La force de cisaillement à la base augmente pour les bâtiments élevés, et pour les niveaux de risque sismique plus élevés. Cette tendance est valide pour les deux villes de Montréal et de Vancouver. La comparaison des résultats obtenus pour les deux villes montre l'influence du site. Les forces de cisaillement obtenues pour Vancouver sont plus grandes que celles obtenues pour le cite de Montréal. Cette tendance est valide pour tous les bâtiments et pour tous les niveaux de risque sismique.

Le chapitre 6 présente les analyses temporelles non linéaires appliquées aux mêmes murs de refend pour les sites des deux villes de Montréal et de Vancouver. On a utilisé deux types d'excitations sismiques, artificielles et historiques. Pour les dernières, on a choisi deux événements historiques, ceux de Nahanni et de Saguenay. Les enregistrements artificiels, générés par Atkinson et Beresnev (1998) sont utilisés pour la période courte et longue pour chaque ville, dont la calibration pour le cite spécifique se faisait par des facteurs d'étalonnage. Afin de satisfaire les exigences du CNBC 2005 pour la conformité au spectre de 2% de probabilité en 50 années, on a généré les spectres correspondant aux historiques utilisées à l'aide du programme RSPMATCH. On a distingué deux types de

spectres de réponse générés : (i) des spectres 'proche', et (ii) des spectres 'vague'. La différence entre les deux était dans la convergence des derniers au spectre cible de conception, recommandé dans le CNBC 2005.

Le logiciel Ruaumoko est utilisé pour les analyses temporelles non linéaires. Pour la modélisation de la section transversale du mur de refend en béton armé, l'élément du type 'mur' est adopté. Les matériaux, le béton et l'armature, sont représentés par leurs diagrammes de contrainte-déformation pour le béton (Kent et Park) et par un courbe hystérèse bilinéaire pour l'armature. Les valeurs maximum des déplacements horizontaux, des forces de cisaillement et des moments de flexion par étage, sont présentées pour les trois murs de refend et pour les deux sites de Montréal et de Vancouver. Suite à la comparaison de ces résultats, on a constaté quelques points importants. Le premier est que les résultats obtenus à la base des événements sismiques 'proches' diffèrent de ceux, obtenus par les historiques étalonnées (à l'aide des facteurs de calibration seulement). Les historiques 'proches' donnent des efforts tranchants plus élevés, valident pour les événements de courte et de longue période, ainsi que pour les deux villes. Le deuxième point est que la résistance probable des murs en flexion est supérieure aux moments de conception pour tous les murs à Montréal. Par contre, pour les murs à Vancouver, cette résistance est dépassée pour la plupart des analyses, même pour les murs moins élevés. Le troisième point important est que les déplacements inter-étage maximum, rencontrent la limite de 2.5%, prescrite par le CNBC 2005 pour tous les murs dans les deux villes. Cette conclusion est valide pour toutes les analyses, incluant les événements étalonnés 'proches'.

Le chapitre 7 présente une comparaison des résultats des efforts tranchants et des déplacements maximum (au sommet) de tous les modèles d'analyse dans les deux villes. La comparaison montre que même les déplacements maximums, obtenus par les méthodes de performance sont plus élevés par rapport à ceux obtenus par l'analyse dynamique, procurée par le CNBC 2005, les critères de conception pour les déplacements inter-étage sont satisfaits. En même temps, la résistance en cisaillement à la base est inférieure à celle obtenue par les analyses du Code. Ce résultat est valide pour les forces de plastification

et les forces de cisaillement ultimes, et pour les deux villes. On a constaté aussi une tendance d'étalonnage pour toutes les méthodes de performance basée sur le déplacement, exprimée aussi bien pour le déplacement maximum et de plastification, que pour la force de cisaillement à la base maximum de conception et de plastification. Par conséquence, on pourrait rechercher des facteurs d'étalonnage afin d'obtenir des démarches préliminaires le plus proches possibles des résultats finaux.

Le dernier chapitre 8 propose des recommandations pour des recherches futures et des applications potentielles dans le domaine des méthodes de conception et d'analyse basées sur la performance sismique. Les méthodologies des trois procédures explorées dans le contexte normatif canadien ont pour but d'utiliser un déplacement cible relié à un niveau d'aléa sismique donné pour évaluer la performance sismique anticipé d'un bâtiment. Les méthodes sont formulées de façon à satisfaire les critères de résistance des codes modernes de conception parasismique et en même temps pour assister les ingénieurs en structure à limiter les déformations maximales et les déplacements inter-étages à des valeurs acceptables. Ce projet de mémoire présente des résultats originaux relatifs à l'application de procédures non linéaires statiques alternatives pour évaluer la performance des structures en tenant compte du contexte normatif canadien. Ces résultats sont cependant préliminaires, et doivent être complétés par une validation expérimentale et un raffinement des procédures avant leur généralisation dans la pratique de tous les jours.

TABLE OF CONTENTS

LIST OF TABLES

LIST OF FIGURES

LIST OF NOTATIONS AND ABBREVIATIONS

A_{e}	elastic pseudo-acceleration,
A_{y}	inelastic pseudo-acceleration,
b_{w}	wall web width,
B, B_x	parameter, quantifying for structural sensibility in torsion at level x,
c	distance from the extreme fibre in compression to the neutral axis of the wall, cohesion stress,
C_{y}	yield strength coefficient,
C_{y}^*	yield strength coefficient of the equivalent single degree of freedom system,
C^*	damping of the equivalent single degree of freedom system,
D_{nx}	in plane structure dimension at each floor level x,
e_x	eccentricity between the gravity center and the center of rigidity at floor x,
f'_{c}	maximum compressive stress of concrete,
f_{req}	required shear strength of the substitute single degree of freedom system,
F_a	acceleration-based site coefficient,
F_i	horizontal force acting on storey i, equivalent static horizontal force at each level i,
F_{t}	concentrated force at the top of the structure accounting for the higher, mode effects,
F_{x}	lateral force applied to Level x, total lateral force,
h_{eff}	height of the substitute single degree of freedom system,
h_i, h_{n}, h_x	height above the base (i=0) to level i, n, or x, where the base of the structure is that level at which horizontal earthquake motions are considered to be imparted to the structure,
h_{w}	height of shear wall,
I_{E}	importance factor of the structure,

J	reduction coefficient for base overturning moment,
J_x	reduction coefficient for overturning moment at level x,
K_{eff}	stiffness of the substitute single degree of freedom system,
K^*	stiffness of the equivalent single degree of freedom system,
ℓ_{p}	plastic hinge zone length,
l_{u}	nominal height of the wall section under consideration,
ℓ_{w}	length of shear wall,
$\mathbf{M}$	diagonal matrix containing lumped masses at the n floor levels,
$MDOF$	multiple degree of freedom system,
M_{eff}	mass of the substitute single degree of freedom system,
M_{f}	flexural resistance at the base of the wall, to account for the effect of the factored loads,
M_{n}	nominal flexural capacity,
$M_{\text{p}}, M_p w$	probable flexural capacity,
M_{r}	actural factored flexural resistance,
M_{req}	required flexural strength of the substitute single degree of freedom system,
M_{T}	total mass of the multiple degree of freedom system,
M_{v}	factor to account for higher mode effect on base shear,
M_x	overturning moment at level x,
M^*	mass of the equivalent single degree of freedom system,
P_{n}	earthquake provoked effort, transmitted between a coupled shear wall system elements,
P_{ns}	nominal net effort, due to a shrinkage at tension or compression of the concentrated or distributed reinforcement at the time of a plastic hinge formation,
P_{s}	axial effort of the section, due to surcharge and specified dead surcharges amount,

R_{d}	ductility related force modification factor,
R_{o}	overstrength related force modification factor,
R_{y}	yield strength factor,
$S_a(T)$	5% damped spectral response acceleration for a period T,
$SDOF$	single degree of freedom system,
T, T_{a}	period of vibration, fundamental lateral period of vibration of buildings,
T_{eff}	period of vibration of the substitute single degree of freedom system,
T_x	torsion moment, applied at each floor,
u_i, u_n	lateral displacements, relative to the building base, taken at i floor and n roof levels,
$u^*(t)$	lateral displacement of the equivalent single degree of freedom system,
$\ddot{u}_{\mathrm{g}}$	ground acceleration time history,
$\mathbf{U}$	vector containing lateral displacements u_i,
V	lateral earthquake design force at the base of the structure, shear force,
V_{c}	factored concrete shear resistance,
V_{d}	lateral earthquake design force at the base of the structure as determined by the dynamic analysis procedures,
V_{e}	elastic lateral earthquake design force at the base of the structure as determined by the dynamic analysis procedures,
V_{eff}	shear strength at the base of the substitute single degree of freedom system,
V_{f}	lateral earthquake design force at the base of the structure, to account for the effect of the factored loads,
V_{p}	probable shear capacity,
V_{r}	factored shear resistance,
V_{s}	factored transverse stell reinforcement shear resistance,
V_{y}	shear strength at yield,
V_{y}^*	yield strength of the equivalent single degree of freedom system,

W, W_i, W_x	seismic weight, dead load, portion of W which is located at or is assigned to level i or x respectively,
δ_{ave}	average storey displacement of structure extreme points at floor level x,
δ_{max}	maximum storey displacement of structure extreme points at floor level x,
Δ_{e}	peak earthquake-induced displacement,
Δ_{eff}	maximum lateral displacement of the substitute single degree of freedom system,
Δ_{f}	inelastic storey drift, due to factored loading,
Δ_i	lateral wall displacement at level i,
$\Delta_{i,\text{e}}, \Delta_{n,\text{e}}$	elastic portion of the wall displacement at level i and at roof level n,
$\Delta_{i,\text{p}}$	inelastic portion of the wall displacement at level i,
Δ_{u}	maximum inelastic storey drift,
Δ_{y}	displacement at yield,
Δ_{y}^*	yield displacement of the equivalent single degree of freedom system,
α	structural system post-yield stiffness coefficient'
α	mass participation factor,
ϵ_{cu}	peak strain of concrete at maximum compressive stress,
γ_{w}	nominal over strength factor,
Γ	shape participation factor,
ΓM^*	participating mass along given deformed shape,
λ	correction factor to account for the concrete density,
μ	structural ductility factor, structural displacement ductility factor,
ϕ_{c}	concrete resistance factor,
ϕ_{s}	reinforced steel resistance factor,
ϕ_{y}	yielding curvature,
$\boldsymbol{\phi}_j$	multistorey building shape at mode j,
θ_i	wall rotationt at level i,

$\theta_{i,\mathrm{e}}, \theta_{n,\mathrm{e}}$	wall elastic rotation at level i and at roof level n,
θ_{ic}	inelastic rotation capacity of the wall,
θ_{id}	inelastic rotation demand on the wall,
$\theta_{i,\mathrm{p}}$	wall plastic rotation at level i,
ω^*	frequency of vibration of the equivalent single degree of freedom system,
ψ	assumed shape vector representing the deformed configuration of the MDOF system,
ξ_{eff}	damping of the substitute single degree of freedom system,
ξ_{e}	initial elastic damping in the nonlinear system,
ξ_{h}	hysteretic damping in the nonlinear system,

LIST OF APPENDICES

CHAPTER 1

INTRODUCTION

1.1 Context

Throughout human history, earthquakes have resulted in immense loss of lives and property. Today, although significant progress has been achieved in the mitigation of earthquake hazard, the risk is even more increasing because of rapid urbanization in seismically prone regions. For many years, the main objectives of seismic design provisions in code standards worldwide have been primarily targeted towards safeguarding human life and avoiding major collapse in the aftermath of earthquake tremors. These objectives have been generally addressed by setting minimum *prescriptive* standards for construction materials, required strength and amount of deformation that may be tolerated under seismic loading. Complementary criteria that would ensure post-earthquake building functionality by confining damage to a certain level have not been considered explicitly in traditional building codes.

Recent damaging Loma Prieta (1989), Northridge (1994) and Hyogo-Ken Nambu (1995) earthquakes marked an important turn in seismic hazard mitigation. They showed that structures designed according to prescriptive codes generally failed short of meeting expected performance objectives, namely economical ones. As a result, recent seismic provisions are progressively implementing new criteria for an enhanced and predictable seismic performance in addition to satisfying traditional human safety objectives. It is hoped that these *performance-based* requirements would guarantee a predictable fraction of the structural as well as the nonstructural post-earthquake functional capacity of buildings.

On the other hand, Canadian standards for seismic design have continuously evolved to account for state-of-the-art advances in earthquake engineering. The last editions of the National Building Code of Canada (NBCC 2005) (CCBFC 2005), as well as the Design of Concrete Structures Standard CSA A23.3-04 (Canadian Standard Association 2004)

are major updates of the previous ones, namely in terms of seismic hazard assessment and seismic design provisions of reinforced concrete buildings. These new standards are currently being implemented in every day practice of the Canadian structural engineering community.

1.2 Problem Statement

Research on Performance-Based Seismic Design (PBSD) was rarely conducted within the Canadian context of seismic standards and codes of practice. Most of this research was also validated considering Western North America (WNA) seismic hazard or other similar environments. It is however widely accepted now that the effects of Eastern North America (ENA) ground motions should be addressed because of their particularly high frequency content. The objective-based format of the new edition of the National Building Code of Canada (CCBFC 2005) is a first step towards a balanced combination of performance- and prescriptive-based requirements. Rational and efficient methods to assess the seismic performance and vulnerability of new and existing structures designed according to Canadian seismic standards are however still required. Among the PBSD approaches, Displacement-Based Design (DBD) methods, with displacements as the primary design parameters, are gaining world-wide acceptance and are gradually being implemented in modern design standards. These methods still need validation and refinement before being fully adopted by the structural engineering community in Canada and elsewhere.

1.3 Objectives and Methodology

The main objective of this work is to investigate the use of simplified displacement-based approches to assess the seismic performance of shear walls designed according to the new Canadian seismic standards. Three promising simplified techniques are adapted to the Canadian context of seismic hazard assessment and seismic detailing requirements of concrete structures. The main steps summarizing the methodology adopted are to :

1. Design three cantilever shear walls with different heights and considering the effects

of ENA *vs.* WNA seismic hazards based on the seismic provisions of the NBCC 2005 and CSA A23.3-04;

2. Select three most promising displacement-based approaches based on an extensive literature revue;
3. Develop a unified mathematical formulation and terminology to describe the selected methods and identify basic assumptions;
4. Use the selected techniques to assess the seismic performance of the three shear walls designed previously;
5. Perform non linear time history analyses on the three shear walls to assess their seismic performance;
6. Compare the results obtained using different approaches and formulate recommandations.

1.4 Thesis Organization

The present thesis is divided in 8 chapters. Chapter 2 discusses the changes in the new concrete standard A23.3-04 and the National Building Code of Canada 2005 (NBCC 2005), regarding seismic requirements for the shear walls design, as elements of the seismic force resisting system.

The literature review, presented in Chapter 3, gives the main principles of three Displacement-Based Desing (DBD) approaches, namely : (i) the Yield Point Spectra method (Aschheim, 2000), (ii) the Direct Displacement Based-Design method (Priestley and Kowalsky, 2000), and (iii) the Inelastic Displacement Spectra method (Chopra and Goel, 2001).

In Chapter 4 design of the model is described and the analysis according the afore-noted standard documents last edition are presented. Three building models are analyzed using the Equivalent Static Force Procedure (ESFP) and the Linear Spectral Analysis (LSA) procedure, recommended by the NBCC 2005. Two sites (i.e. Montréal, QC and Vancouver, BC) are used for analysis, as representative for the seismic specificity of Eastern and Western Canada.

Chapter 5 performs analysis of the three models in both cities, following the three DBD approaches. A target displacement profile and the effective properties of the substitute structure are established as a general basis of those methods. Detailed calculations are demonstrated for the 6-storey building in Montréal under the three DBD methods and the results for all other buildings in both Montréal and Vancouver are tabulated and graphically represented.

Chapter 6 reflects the seismic demand of the three different height models for both sites through a nonlinear analysis performance. The chapter shows different seismic demands, characterizing Montréal and Vancouver seismic specificity and their compliance with the Code requirements.

Chapter 7 compares the shear walls behavior analyzed through standard force-based engineering practice with the corresponding models target-displacement profiling. Base shear forces and maximum displacements are used as a basis for comparison.

The last Chapter 8 has the objective to discuss the Displacement-Based Design methods application. It aims to qualify at that level of understanding the three researched methods, to mark out the conclusions from the performed analyses and to make recommendations for a further investigation work in that direction.

CHAPTER 2

REVIEW OF CANADIAN STANDARDS FOR SEISMIC DESIGN

2.1 Introduction

Concerns about both safe and economical seismic design of buildings are integrated more than ever in the new editions of the National Building Code of Canada (NBCC 2005) and the Canadian Standard CSA A23.3-04. New philosophy was reflected in the NBCC 2005 and CSA A23.3-04 through including new performance-based recommendations and restrictions for the structures seismic design. The Standard CSA A23.3-04 outlines those recommendations specifically to the ductile concrete shear walls structures.

The present chapter outlines the new provisions in the NBCC 2005 and CSA A23.3-04 for the seismic design of buildings having ductile shear walls as structural elements forming the seismic force resisting system (SFRS). Overview of the new national seismic hazard maps generation, used for the seismic design in NBCC 2005, is given. Two types of analyses recommended by the NBCC 2005 are presented : (i) the equivalent static force procedure, and (ii) the dynamic analysis procedure. That chapter presents, as well, the new dimensional restrictions and rotational limitations in the design of ductile reinforced concrete shear walls, recommended in the new standard CSA A23.3-04, are discussed.

2.2 National Building Code of Canada NBCC-2005

The National Building Code of Canada (NBCC) has undergone many changes since its first issue in 1941 (Tinawi 2004). A new edition of the Code (NBCC-2005) was recently proposed by the Canadian Commission on Building and Fire Codes and published by the National Research Council of Canada (NRCC) (CCBFC 2005). In this edition, the Canadian National Committee on Earthquake Engineering (CANCEE) implemented major modifications to the earthquake design requirements in Part 4 of the NBCC. The new seismic provisions aim at adapting the Canadian code to recent advances in earthquake

risk mitigation in order to afford better public protection against earthquakes. The main improvements that resulted from this recent revisions are outlined next.

2.2.1 Seismic Hazard Maps of Canada

The NBCC-2005 uses a new fourth generation of seismic hazard maps of Canada (Adams and Halchuk 2003). The maps are based on estimation of the median ground motion on firm soil sites for a probability of exceedence of 2 % in 50 years. Adams et Halchuk (2003) provided spectral acceleration values at four specific periods as well as peak ground accelerations for more than 650 Canadian localities. The values, which can be extracted from tables or read on seismic hazard maps, are used to construct approximate site-specific uniform hazard spectra.

The results summarizing of the median ground acceleration values are introduced into NBCC-2005 in a spectral acceleration format $S_a(T)$, 5 % damped, for a reference soil profile C and based on a 2 % probability of exceedence in 50 years. This probability level corresponds to a return period of 2475 years. The uniform hazard spectra represents an envelope of maximum response spectra for a range of periods when an elastic single degree a freedom system is submitted to specific earthquakes at a given site.

To estimate seismic hazard in Canada, as part of the incertitude, two source types are used as probabilistic models, such as the historical model (H) as first, and the regional (R) one, as second. The historical model, in general, uses relatively restricted zones, in the meaning - close to seismic sources, while the regional model is conceived for bigger zones, where important earthquakes could be produced. Both models H and R for the Eastern Canada were build up by Adams and Halchuk, while those for Western Canada - by Horner and Rogers.

In addition to the probabilistic models for the more active seismo-tectonic parts, Adams and Halchuk introduced a probabilistic model of type F for the most tectonically stable part of Canada and the deterministic model of type C for the subbduction zone of Cas-

cadia, where the last mentioned has generated big prehistoric earthquake events on the Vancouver island. To adopt a more realistic scenario for that part of Canada, one was chosen to use a deterministic model, instead of a probabilistic one and the seismic hazard of Cascadia was tabulated separately. But, in the meantime, a combination of these two models is suggested, so then the deterministic model with robust approach being combined to the probabilistic one. For design purposes aimed by the NBCC-2005, the values of the probabilistic model in combination with the last two models, such as the ones for Stable Canada and Cascadia subduction zone, result in one robust model (1995). The robust model is based simply on the maximum values of the four models for each grid point across Canada. The advantage of the robust model is that it ensures a good protection in both zones of high and low seismicity.

2.2.2 Methods of Analysis

Only the NBCC-2005 requirements related to shear walls earthquake resisting design are first reviewed. The NBCC-2005 propose two methods to establish the structural seismic analysis in Art.4.1.8.7 (CCBFC 2005) : the dynamic analysis method (Art. 4.1.8.12.) and the equivalent static force procedure (Art. 4.1.8.11.). The later method is permitted if at least one of the following conditions is satisfied :

- The product value $I_{\mathrm{E}}F_aS_a(0.2)$ is less than 0.35, where I_{E} denotes the seismic priority coefficient of the structure (Art. 4.1.8.5.), F_a is the acceleration coefficient for the site (Art. 4.1.8.4.) and $S_a(0.2)$ is the spectral response acceleration with 5 % damping, in terms of the gravity acceleration constant, for a period of $T = 0.2\,\mathrm{s}$ (Art. 4.1.8.4.) ;
- The structure is regular with a height less than 60 m and fundamental period T_{a} less than 2 s in each direction ;
- The structure is characterized with irregularity of type 1, 2, 3, 4, 5, 6 or 8, as described per Table 4.1.8.6. of the NBCC-2005, with a height less than 20 m and fundamental period less than 0.5 s.

2.2.2.1 Equivalent Static Force Procedure

The fundamental principle of that method is to determine the dynamic response of a structure to earthquake sollicitations in her first mode of vibration. For structures satisfying any of the afore listed conditions, the Equivalent Static Force Procedure (ESFP) determines the minimum shear force V at the structure base according to the following equation, (Art. 4.1.8.11) :

$$V = \frac{S(T_a) M_v I_E}{R_d R_o} W \tag{2.1}$$

where

- $S(T_a)$ is the response spectral acceleration with 5 % damping, expressed in terms of the gravity constant for a given fundamental period T_a (Art. 4.1.8.4.) ;
- M_v is the factor taking into account superior modes effect on the base shear force (Art. 4.1.8.11.) ;
- R_d is a force modification factor, reflecting the structural capacity of energy dissipation through out an inelastic behavior ($1 \leq R_d \leq 4$) (Art. 4.1.8.9.) ;
- R_o is a force modification factor, taking into account the structural over strength capacity ($1 \leq R_o \leq 2.5$) (Art. 4.1.8.9.) ;
- W is the dead load including 25 % of the snow load plus 60 % of any storrage load and 100 % of tank containing.

The minimum shear force V [Eq. (2.1)] should not be less than V_{min}, given by :

$$V_{min} = \frac{S(2.0) M_v I_E}{R_d R_o} W \tag{2.2}$$

In case of a lateral force resisting system (SRFS) with a value of R_d equal or bigger than 1.5, the minimum lateral force V should not exceed the force V_{max}, expressed by :

$$V_{max} = \frac{2}{3} \frac{S(0.2) M_v I_E}{R_d R_o} W \tag{2.3}$$

The fundamental period Ta for shear walls according to Art. 4.1.8.11.3.c) is calculated by the following Eq. (2.4) :

$$T_{\mathrm{a}} = 0.05\sqrt[4]{{h_n}^3} \tag{2.4}$$

where h_n is the total height of the structures in [m].

According to NBCC-2005 Art. 4.1.8.11.d) the fundamental period T_{a} used in the ESFP for shear walls, calculated by other methods of mechanics, shall be less than twice the one calculated per Eq. (2.4), (Art. 4.1.8.11). Thus Eq. (2.1) in Art. 4.1.8.11, gives the minimum shear force at the base of a structure, satisfying the requirements of Art. 4.1.8.6 of the NBCC 2005, previously denoted and imposes it as a basis of comparison and calibration, if necessary, with the shear force, resulting from a modal linear analysis.

The spacial distribution of the total seismic lateral force V is effectuated in such a manner, that one part F_{t} of it is a top force and corresponds to the following requirements (Art. 4.1.8.11) and the rest of the total force $V - F_{\mathrm{t}}$ is redistributed over the whole structure height according to Eq. (2.5) :

- the top force is $F_{\mathrm{t}} = 0.07 T_{\mathrm{a}} V$,
- the top force F_{t} is less than $0.25V$,
- F_{t} is considered as zero, if $T_{\mathrm{a}} \leq 0.7\,\mathrm{s}$

The lateral inertia force F_{x}, acting at floor level x is given by :

$$F_x = (V - F_{\mathrm{t}}) \left(\frac{W_x h_x}{\sum_{i=1}^{n} W_i h_i} \right) \tag{2.5}$$

where :

- W_x and W_i are the portions of the dead load corresponding to floor levels i and x ;
- h_x and h_i are the corresponding heights at floor levels i et x above the structure base ;
- n is the floor levels number.

The structure strength shall be verified for overturning effect caused by seismic forces [Eq. (2.5)] :

$$M_x = J_x \sum_{i=x}^{n} F_i(h_i - h_x) \tag{2.6}$$

where :

- J_x is the reduction coefficient of the overturning moment at floor level x, in function of the corresponding level height h_x, thus $J_x = 1.0$ for $h_x \geq 0.6h_n$ or $J + (1 - J)(\frac{h_x}{0.6h_n}$ for $h_x < 0.6h_n$ (Art.4.1.8.11).
- h_x and h_i are the corresponding heights at floor levels i et x above the structure base $(i = 0)$;
- n is the floor levels number ;
- F_i is the lateral force calculated at level i.

The coefficient J reflects the overturning base moment reduction (Table 4.1.8.11).

Taking into account torsional effects, the National Building Code of Canada 2005 requires that torsion moments T_x shall be applied at each floor level of the structure, considering moments caused by an eccentricity e_x between the gravity center and the center of rigidity in addition to the moments caused by an accidental eccentricity, equal to $\pm 0.1 D_{nx}$ [Eq. (2.7)] :

$$\begin{aligned} T_x &= F_x(e_x + 0.1D_{nx}) \\ T_x &= F_x(e_x - 0.1D_{nx}) \end{aligned} \tag{2.7}$$

where D_{nx} is the in plane structure dimension, perpendicular to the lateral force direction at each floor level x.

To quantify the structural sensibility in torsion, a parameter B was introduced in Art. 4.1.8.11, Sentence (9)(NBCC 2005), as the bigger value of B_x [Eq. (2.8)], calculated separately for both orthogonal directions of the structure at each floor level x. The torsional

sensitivity of a structure is schematically represented in Figure 2.1 (Tremblay 2005).

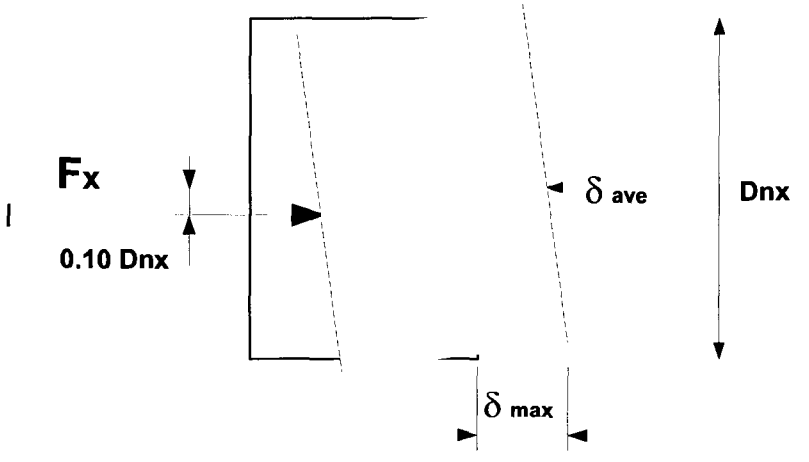

FIG. 2.1 Schematic representation of a torsional sensitivity of a structure.

$$B_x = \frac{\delta_{\max}}{\delta_{\text{ave}}} \tag{2.8}$$

where :

- $\delta_{\max}$ is the maximum storey displacement of structure extreme points at floor level x, in the earthquake direction, resulting from static equivalent lateral forces reacting at a distance $\pm 0.10 D_{\text{nx}}$ from the gravity center on each diaphragm ;
- δ_{ave} is the average storey displacement of structure extreme points at floor level x, in the earthquake direction, produced from the afore mentioned forces.
- D_{nx} is the plan dimension of the building at level x perpendicular to the direction of seismic loading being considered.

2.2.2.2 Dynamic Analysis Procedure

For its conformity to the requirements of NBCC 2005, the dynamic analysis shall be executed by one of the following methods :

- Performing a Linear Dynamic Analysis according to the Modal Response Spectrum

Method (MRSM), or according to the Numerical Integration Linear Time History Method (NILTHM). The exigence for using a time history analysis is that the time history record values shall be compatible to the 5 % damped response spectra with probability of exceedence 2 % in 50 years, required by the NBCC-2005 (Art.4.1.8.4.).

- Performing a Nonlinear Dynamic Analysis.

The code requires that the spectral acceleration values used in the Modal Response Spectrum Method shall be the design spectral acceleration values, $S(T)$, explained in this chapter. In the case of a Linear Dynamic Analysis, the base shear force V_{d} is calculated through multiplying the elastic shear force at the base, V_{e}, by a factor $\left(\frac{I_{\mathrm{E}}}{R_{\mathrm{d}} R_{\mathrm{o}}}\right)$. V_{e} results either from the MRSM or the NILTHM.

When the base shear force V_{d} is less than 80 % of the lateral force V, one is considered that $V_{\mathrm{d}} = 0.8V$, exception are irregular structures, where the maximum value is $V_{\mathrm{d}} = max\left(V_{\mathrm{e}}\left(\frac{I_{\mathrm{E}}}{R_{\mathrm{d}} R_{\mathrm{o}}}\right); 100\,\%V\right)$ (Art.4.1.8.12). V is calculated through the ESFP, described previously in that paragraph according to NBCC 2005 (Art.4.1.8.11.)

Taking into account the accidental torsion effects, which is produced in the same time as the lateral seismic forces, the NBCC-2005 requires one of the following methods being respected :

- Combining the static effects from torsion moments, caused by $F_{\mathrm{x}}(\pm 0.1 D_{\mathrm{nx}})$ at each floor level x where F_{x} was already established by equation 2.5 or calculated by a dynamic analysis ;
- The new code allows an accidental torsion $\pm 0.05 D_{\mathrm{nx}}$ being used at each floor level of the structure, when $B < 1.7$ was obtained through-out a three dimensional analysis performance (Art.4.1.8.12).

2.3 Concrete Standard CSA A23.3-04

Shear walls, as subject of the capacity design, required by the National Building Code of Canada 2005, shall conform to the special paraseismic design provisions of Clause

21 (Canadian Standard Association 2004). Structural design conforming to the Code required capacity design, begins with choosing a kinematically consistent mechanism, after which all other structural elements of the lateral force resisting system shall be conceived with sufficient reserve strength capacity, so then the previously chosen mechanism for energy dissipation would be maintained in the so defined locations without developing any additional mechanism throughout appearing deformations, as required by Clause 21.2.1 (Canadian Standard Association 2004). Shear walls, as part of the lateral force resisting system, shall be dimensioned in a manner, being of sufficient ductility and in the same time, of sufficient rigidity so to allow inelastic displacements without provoking any rupture in the structure itself. Locations, where one was assumed an inelastic behavior could be produced, are called plastic zones, chosen mainly at shear wall base. Plastic zones correspond to special requirements for shear walls design, minimum reinforcement in both directions, vertical and horizontal, as well as a minimum anchorage required and a depth of the zone in compression. The special requirements provided for the plastic hinge zone target a flexural hinging location in that specific locations in order to avoid plastification to occur out of the plastic hinge zone. Flexural moment restrictions, provided in the standard CSA A23.3-04 are conceived in order to achieve it.

2.3.1 Flexure Moment Restrictions

In general, each shear wall shall be conceived for plastic zones at each floor level, and thus conforming to the special seismic requirements, unless one is demonstrated that the plastification is limited at the structure base (Cl. 21.6.2.1). The concrete standard CSA A23.3-04 suggests as verification for that requirement, that flexure moments and shear forces, obtained throughout seismic analysis at each level above the plastic zone, shall be multiplied with the ratio of the factored moment resistance M_{r} to the factored moment M_{f}, where both moments are calculated for the superior part over the plastic zone. Graphical representation of the factored moment, obtained by design, the possible factored moment resistance and the capacity design moment of a shear wall is demonstrated in Figure 2.2.

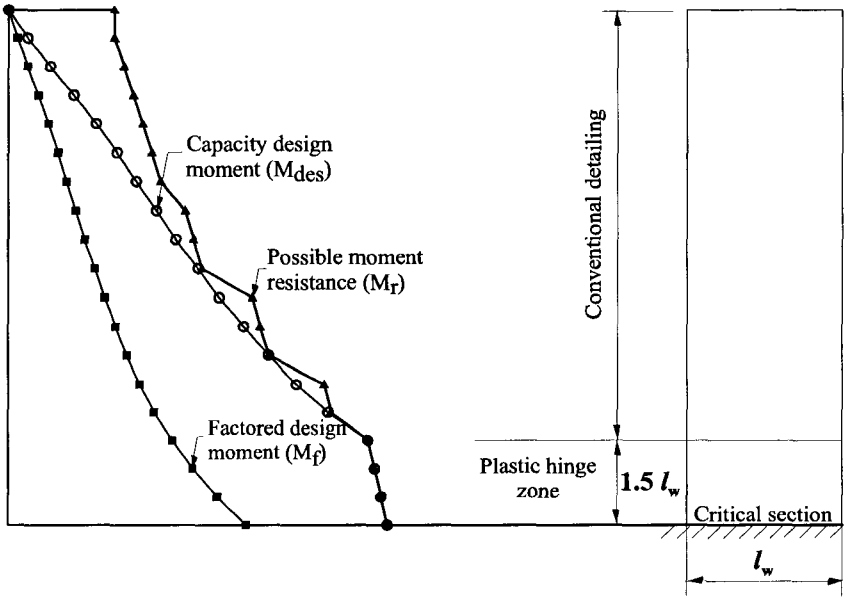

FIG. 2.2 Capacity design moment demands for ductile shear walls

2.3.2 Detailing of Shear Wall

Detailing of a ductile shear wall is performed through following steps :

- Loading on shear walls, according the National Building Code of Canada, (Art.4.1.3.1 and Table 4.1.3.2) shall be determined upon the combination of $1.0D + 0.5L + 0.25S + 1.0E$, where D is dead load, L - live load, S - snow load and E - seismic load ;
- Requirements for the minimum distributed and concentrated reinforcement, as well as for its anchorage and splicing are presented in details by Clauses 21.6.5 and 21.6.6 (Canadian Standard Association 2004). It shall be used at least two curtains of reinforcing bars, both verticals and horizontal, if in zones, developing plastic hinges, the factored shear force V_f is bigger than $0.18\lambda\phi_c\sqrt{f_c}A_{cv}$ (Cl. 21.6.5.3). Vertical reinforcing bars shall be placed outside horizontal ones.
- Verification of the resisting moment M_r is done after a preliminary design, so then it shall be bigger than the factored moment : $M_r \geq M_f$, where M_r is calculated upon using material coefficients for concrete and steel - $\phi_c = 0.65$ et $\phi_s = 0.85$, according to

CSA A23.3-04 (Clause 8.4.2 and 8.4.3).

2.3.3 Dimensional Restrictions of Shear Walls

Changes in dimensional restrictions limited the shear wall thickness in the plastic hinge zone $\frac{l_u}{14}$, as a minimum requirement, where l_u is the clear distance between floor levels (Cl. 21.6.3.2). In general, thickness restrictions for a shear wall in the plastic hinge zone, as $l_u 10$, are maintained from the ancient code seismic provisions (CCBFC 1995). Exception from the last requirement are parts of the shear wall, disposed at a distance bigger than half the distance between neutral axis and the end in compression of the shear wall section under factored forces acting on it.

2.3.4 Restrictions in Rotation

Important changes in shear walls design are related with displacements and rotational limitations. Shear walls, characterized by continuity in their transversal section over whole element length and which are envisaged with a plastic hinge at their base only, as it is the present case study, shall be verified for ductility demand according to Cl. 21.6.7, (Canadian Standard Association 2004). Special seismic provisions for ductile shear walls, $R_d = 3.5$ in present case, demand that the inelastic rotation θ_{id} (Cl. 21.6.7.2), calculated by Eq. (2.9), as demonstrated on Fig. 2.3.4, is smaller than the rotational inelastic capacity θ_{ic}, calculated by Eq. (2.10).

$$\theta_{id} = \frac{(\Delta_f R_o R_d - \gamma_w \Delta_f)}{\left(h_w - \frac{\ell_w}{2}\right)} \geq 0.004 \tag{2.9}$$

where :

- Δ_f - top shear wall displacement, due to factored loading,

  $\Delta_f R_o R_d$ - total displacement,

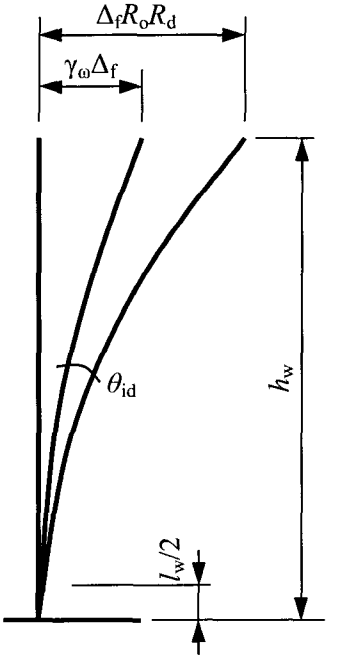

FIG. 2.3 Inelastic rotation

$\gamma_w \Delta_f$ - displacement elastic part,

γ_w - shear wall over strength factor, equal to the ratio of corresponding loading to nominal moment strength imposed on the wall versus factored loading imposed on the wall , $\frac{M_n}{M_f}$.

γ_w shall not be less than the value of 1.3,

ℓ_w - longest shear wall horizontal dimension in considered direction,

h_w - shear wall height.

The value of 0.004 is considered as a minimum rotational demand. Canadian standard (Cl. 21.6.7.3) express the rotational inelastic capacity according to Eq. (2.10) :

$$\theta_{ic} = \left(\frac{\epsilon_{cu} \ell_w}{2c} - 0.002 \right) \leq 0.025 \tag{2.10}$$

where : ϵ_{cu} - maximum elongation of extreme concrete fiber in compression at the moment of reinforcement ultimate relative deformation. $\epsilon_{cu} = 0.0035$, unless the shear wall section

in compression is confined as a column according standard requirements of Cl. 21.6.7.4 .
c - neutral axis depth, measured from the concrete section end in compression. The depth c could be determined through out calculating the factored flexural strength of the shear wall, submitted at axial loading P_s, P_n and P_{ns} or as well on the basis of Eq. (2.11) given by same standard (Cl. 21.6.7.3).

$$c = \frac{P_s + P_n + P_{ns} - \alpha_1 \phi_c f' c A_f}{\alpha_1 \beta_1 \phi_c f' c b_w} \tag{2.11}$$

where :

- A_f - flange area ;
- P_n - earthquake provoked effort, transmitted between elements of an coupled shear wall system. That effort shall be considered as the amount of shear efforts at both ends, corresponding to the coupling beam nominal flexural strength in the section upper part,
- P_{ns} - nominal net effort soliciting a section relative to the direction in study, due to a shrinkage at tension or compression of the concentrated or distributed reinforcement at the time of a plastic hinge formation,
- P_s - axial effort of the section, due to surcharge and specified dead surcharges amount,
- $\alpha_1 = 0.85 - 0.0015 f' c \geq 0.67$;
- $\beta_1 = 0.97 - 0.0025 f' c \geq 0.67$;

2.3.5 Shear Force Restrictions for Ductile Shear Walls

In order of not reducing the energy dissipation in an earthquake solicitation, special seismic provisions, provided by CSA A23.3-04 (Cl. 21.6.9.1) require that shear force at wall base do not control the shear wall capacity. Thus, shear walls shall possess much bigger shear strength that the one due to factored loading at the moment of developing a plastic hinge. The concrete standard demand that the factored shear resistance shall be bigger that the lesser of the following values :

1. Shear force, corresponding to a shear wall probable capacity in a plastic hinge zone. The design shear force is $V_{\mathrm{p}} = \gamma_{\mathrm{p}} V_{\mathrm{f}}$, where $\gamma_{\mathrm{p}} = \frac{M_{\mathrm{pw}}}{M_{\mathrm{f}}}$. The resisting probable moment M_{pw} is calculated on the basis of coefficients $\phi_{\mathrm{c}} = 1$, $\phi_{\mathrm{s}} = 1$ and $1.25 f_y$ and M_{f} is the moment due to factored loading.
2. Shear force, resulting from a seismic combination of factored loading, calculated on the basis of $R_{\mathrm{d}} R_{\mathrm{o}} = 1.0$. The concrete standard requires as well, that shear force due to factored effect loading takes into account superior modes inelastic effect.

In addition for the plastic hinge zone, Cl. 21.6.9.6 (Canadian Standard Association 2004) requires that the factored shear demand for a ductile shear wall is $V_{\mathrm{r}} = V_{\mathrm{c}} + V_{\mathrm{s}} \leq 0.1 \phi_{\mathrm{c}} f_c^{'} b_{\mathrm{w}} d_{\mathrm{v}}$ with exception that the inelastic rotational demand of a shear wall shall be less than 0.015, i.e. $\theta_{\mathrm{id}} < 0.015$. If $\theta_{\mathrm{id}} \leq 0.005$, the factored shear demand could not exceed $0.15 \phi_c f_c^{'} b_{\mathrm{w}} d_{\mathrm{v}}$. For factored shear demand between that limits, such as $0.005 < \theta_{\mathrm{id}} < 0.015$, the shear demand shall be calculated through out a linear interpolation.

CHAPTER 3

UNIFIED FORMULATION OF DISPLACEMENT-BASED DESIGN METHODS

3.1 Introduction

In the last decades, earthquakes have increased public awareness about the high cost associated with post-earthquake damage repair in addition to human life loss. Therefore modern seismic design concerns are expected to shift beyond life safety to economic considerations. However, the Building Code is still force-based and the interstorey drift ratio, verified in the end of the design procedure, gives no clear relation between the life safety goals and the expected performance level. Alternative performance-based design methods have been researched to accomplish those goals. Main principles of that methods are to target first the structure maximum displacement, in order to satisfy specific performance requirements, and then to define the system strength needed further for the system design.

3.2 Performance Based Design Methods

Throughout human history, earthquakes have resulted in immense loss of lives and property. Today, although significant progress has been achieved in the mitigation of earthquake hazard, the risk is even more increasing because of rapid urbanization in seismically prone regions. In this context, rational and efficient methods to assess both the seismic performance and vulnerability of new and existing structures are needed.

The seismic provisions of the current generation of building standards including the National Building Code of Canada (NBCC 2005), advocate the use of conventional Force-Based Design (FBD) procedures. According to this approach, elastic base shear required to keep a ground shaken structure linear-elastic is first determined, based on smoothened soil dependent elastic spectral accelerations. The structure is then designed to have a yield strength obtained by dividing the elastic base shear by a force modification factor. This

reduction factor depends on the lateral force-resisting system used, and is assumed to account for the structure's ductility capacity and inherent overstrength. The structure is then subjected to a set of equivalent lateral forces obtained from the vertical distribution of the design base shear over the building height. Once the resulting deformations are checked to be within code prescribed limits, proportioning and detailing of the structural members follow to insure a controlled ductile behaviour.

The FBD procedures, which are meant to be simple and economic, have generally served the profession to design safe structures. However, it was found based on recent severe earthquakes statistics, that structures designed according to prescriptive codes generally failed short after meeting the expected performance, namely economical ones and still modern codes do not provide connection between the seismic hazard level and the performance expected one, corresponding to the expected damage. During the last decade however, the international design community has shown a major interest in Performance-Based Seismic Design (PBSD) methods as alternatives to prescriptive current building codes (Vision-2000 1995; FEMA-273/274 1997). This evolution is aimed at giving the designer more flexibility to meet target performance and economic objectives, instead of restricting design validity to prescriptive strength and stiffness criteria. Among the new PBSD approaches, Displacement-Based Design (DBD) methods, with displacements as the primary design parameters, are gaining world-wide acceptance and are gradually being implemented in modern design standards. However, these methods still need validation and refinement before being fully adopted by the structural engineering community.

An extensive literature review has shown that three DBD methods are most effective for limiting roof drift and system ductility to target one or multiple performance objectives : (i) The Yield Point Spectra (YPS) method (Aschheim and Black 2000); (ii) the Direct Displacement-Based Design (DDBD) method (Priestley and Kowalsky 2000); and (iii) the Inelastic Design Spectra (IDS) method (Chopra and Goel 2001). The three DBD techniques are investigated in the current work while applied to shear walls submitted to new code prescribed Canadian seismic hazard (NBCC 2005).

3.2.1 Force-Displacement Response Modelling

The lateral force-displacement curve of a structure is shown in figure 3.1. An idealized bilinear force-displacement relationship and the linear relationship of the corresponding elastic system are also shown. We denote Δ_e and V_e the peak earthquake-induced displacement and corresponding resisting force of the elastic system. The yield displacement and corresponding yield strength of the bilinear system are denoted by Δ_y and V_y. The yield strength reduction factor R_y is defined by

$$R_y = \frac{V_e}{V_y} = \frac{\Delta_e}{\Delta_y} \tag{3.1}$$

Denoting Δ_u the peak earthquake-induced displacement, the system's displacement ductility factor is defined by

$$\mu = \frac{\Delta_u}{\Delta_y} = R_y \frac{\Delta_u}{\Delta_e} \tag{3.2}$$

Figure 3.1 also shows the design strength V_{des}, defined as the lateral elastic force divided by a force modification factor R_{des}

$$V_{des} = \frac{V_e}{R_{des}} \tag{3.3}$$

Art.4.1.8.9 of the NBCC-2005 defines two force modification factors : R_d to account for energy dissipation through inelastic deformations, and R_o to quantify potential overstrength in the structure.

3.2.2 Elastic and Inelastic Design Spectra

An inelastic Acceleration Design Response Spectrum (ADRS) is a constant ductility plot of inelastic pseudo-acceleration A_y against the natural period T of a SDOF oscillator (Chopra and Goel 2001). The elastic and yield strengths V_e and V_y are related to the elastic

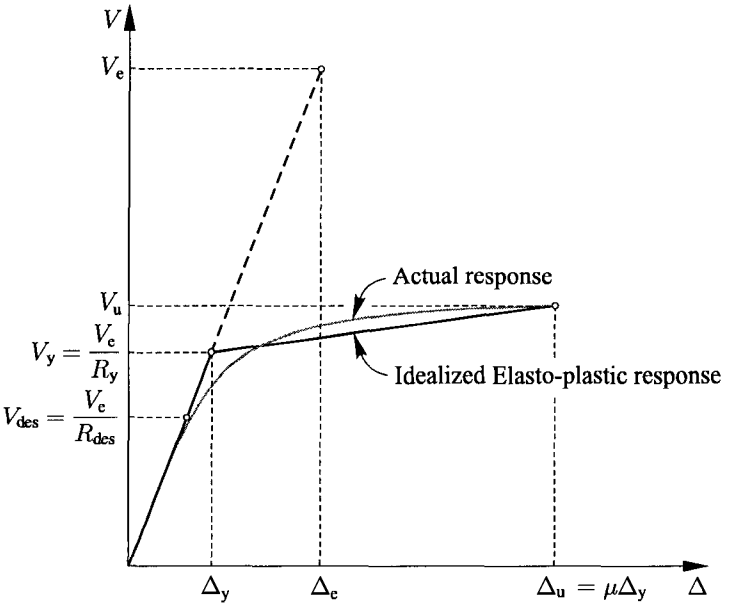

FIG. 3.1 Force-displacement relationships.

and yield pseudo-accelerations A_e and A_y by

$$V_e = \frac{A_e}{g} W \tag{3.4}$$

$$V_y = \frac{A_y}{g} W \tag{3.5}$$

where W is the weight of the SDOF system. The yield pseudo-acceleration A_y can then be written as

$$A_y = \frac{V_y}{V_e} A_e \tag{3.6}$$

or, using Eq. (3.1)

$$A_y = \frac{A_e}{R_y} \tag{3.7}$$

The constant-ductility inelastic ADRS can then be constructed by dividing the elastic ADRS by yield strength reduction factors R_y obtained for given ductility and natural period (Chopra and Goel 2001).

The inelastic Displacement Design Response Spectrum (DDRS) is a plot of the peak displacement Δ_u as a function of the system natural period T. It can be obtained using the following expression :

$$\Delta_u = \mu \frac{T^2}{4\pi^2} A_y = \mu \frac{T^2}{4\pi^2} \frac{A_e}{R_y} \tag{3.8}$$

Another type of inelastic spectra is the Yield Point Spectrum (YPS), defined as a plot of the yield points of SDOF oscillators having constant displacement ductility μ for a range of oscillator periods T (Aschheim and Black 2000). The yield points are plotted on the axes of yield displacement Δ_y and yield strength coefficient C_y, defined by

$$C_y = \frac{V_y}{W} \tag{3.9}$$

where W is the weight of the SDOF oscillator.

Yield point spectra can be generated using two approaches : (i) an 'exact' method where the largest strengths corresponding to a peak ductility demand are determined for a range of periods and ground motions (Figure 3.2a), and (ii) an approximate method based on code prescribed design spectra using smoothed relationships between yield strength reduction factor R_y, ductility μ and period T (Figure 3.2b). The second approach produces smoothed yield point spectra, and is clearly more attractive to maintain consistency with current design practice. The effectiveness of this approach has not been fully validated however, namely when applied to spectra from various seismic code provisions. Part of the present work investigates the effectiveness of using smoothed YPS obtained from Uniform Hazard Spectra (UHS) proposed in the new 2005 edition of the NBCC (NBCC 2005).

3.2.3 Strength Reduction Factors

Several researchers focused on developing ductility dependent yield strength factors (Nassar and Krawinkler 1991 ; Vidic *et al.* 1992 ; Miranda and Bertero 1994). A good account of these methods was presented by Miranda and Bertero (1994). The different approaches

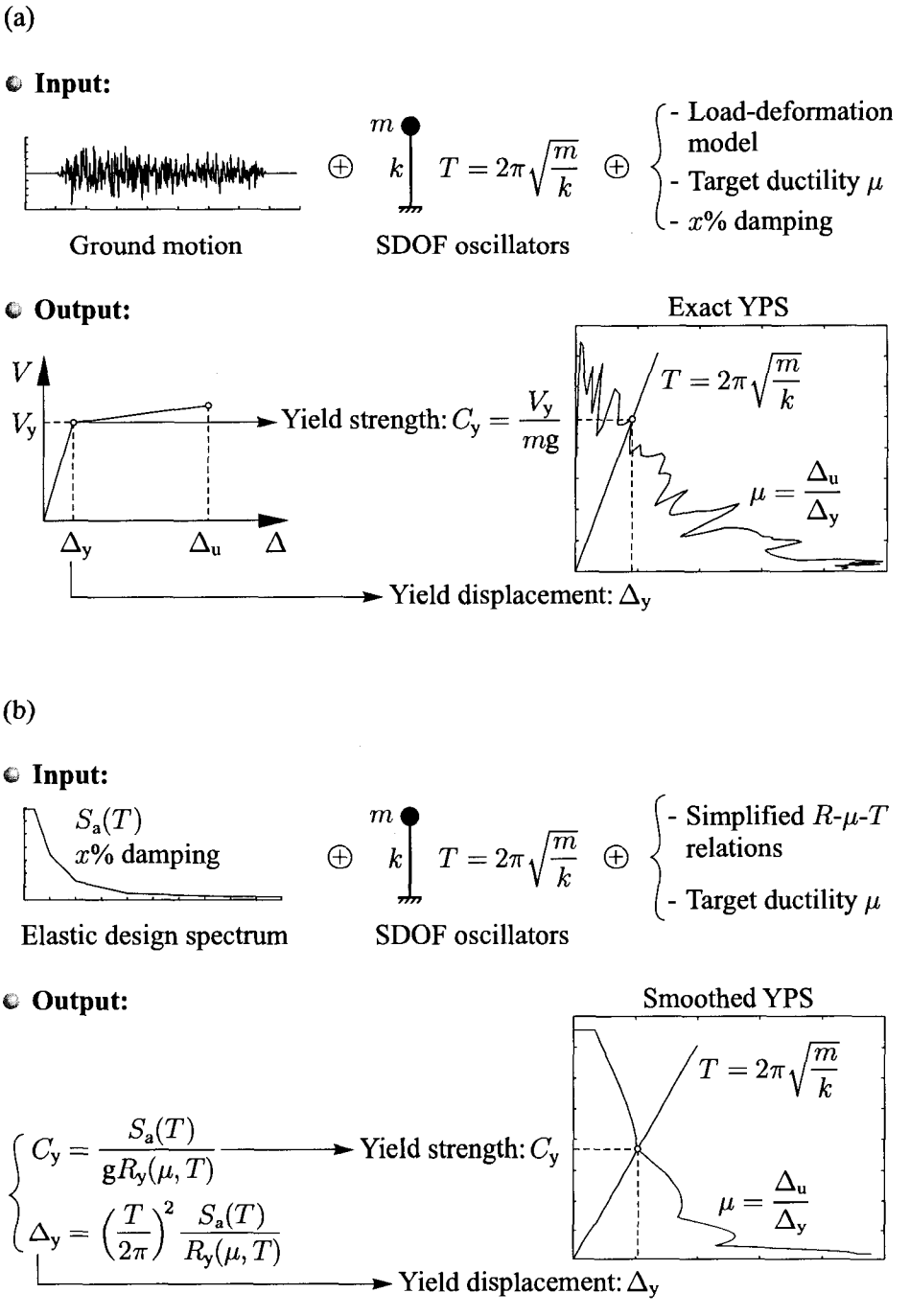

FIG. 3.2 Construction of Yield Point Spectra : (a) 'Exact' method; (b) Approximate method.

relie on assumed $R_y - \mu - T$ relationships to relate inelastic to elastic design spectra. For the purpose of the present study, methods proposed by Miranda (1993) and Nassar and Krawinkler (1991) are investigated.

3.2.3.1 Miranda Method

Miranda (1993) studied 124 different ground motions to evaluate the effects of earthquake magnitude, epicentral distance and local site conditions on yield strength reduction factors. The ground motions used were recorded on a large range of various soil conditions classified into three groups corresponding to rock, alluvium and very soft soil deposits with low shear wave velocities. Mean strength reduction factors for each soil group were computed based on the response of 5% damped bilinear SDOF systems with displacement ductilities ranging from 2 to 6. The study concluded that strength reduction factors are only slightly influenced by earthquake magnitude and epicentral distance, however, they are highly sensitive to soil conditions, especially for soft soil sites. Miranda (1993) proposed the following simplified expression to estimate strength reduction factors :

$$R_y(\mu) = \frac{\mu - 1}{\Phi} + 1 \geqslant 1 \tag{3.10}$$

in which Φ is a function depending on the SDOF system period T, the ductility μ and the site conditions as follows

$$\Phi = 1 + \frac{1}{(10-\mu)\,T} - \frac{1}{2T}\exp\left[-\frac{3}{2}\left(\ln T - \frac{3}{5}\right)^2\right] \quad \text{for rock sites} \tag{3.11}$$

$$\Phi = 1 + \frac{1}{(12-\mu)\,T} - \frac{2}{5T}\exp\left[-2\left(\ln T - \frac{1}{5}\right)^2\right] \quad \text{for alluvium sites} \tag{3.12}$$

$$\Phi = 1 + \frac{\overline{T}}{3T} - \frac{3\,\overline{T}}{4T}\exp\left[-3\left(\ln\frac{T}{\overline{T}} - \frac{1}{4}\right)^2\right] \quad \text{for soft soil sites} \tag{3.13}$$

where $\overline{T}$ is a predominant period defined as the period of the 5% damped SDOF system yielding the maximum relative velocity when submitted to the ground motion under

consideration (Miranda 1993). It is worth mentioning that for soft soils, the Φ parameter is very sensitive to small variations in the ratio $T/\overline{T}$ which is difficult to estimate (Miranda 1993). Consequently, the use of Eq. (3.13) should be associated with a higher level of uncertainty that Eqs. (3.11) and (3.12).

For the needs of the present work, Eqs. (3.11) to (3.13) are adapted to the site classification described in the NBCC 2005 by assuming the correspondence shown in Table 3.1. Figure 3.3 illustrates the variation of the strength reduction coefficient $R_{\mathrm{y}}(\mu)$ as a function of different soil types and displacement ductilities ranging from 2 to 6. For soil profile E, the ratio $T/\overline{T}$ is used instead of T along the periods axis. The curves clearly show that important variations of the yield strength reduction factor $R_{\mathrm{y}}(\mu)$ are mainly concentrated in the 0 s to 4 s range for rock soils, 0 s to 3 s for alluvium soils, and 0 s to $3\overline{T}$ for soft soils.

TAB. 3.1 Correspondence between soil groups proposed by Miranda (1993) and NBCC 2005 site classification

Soil groups in Miranda study (Miranda 1993)		NBCC 2005 site classification (CCBFC 2005)
Rock sites	$\Longleftrightarrow$	A, B
Alluvium sites	$\Longleftrightarrow$	C, D
Soft Soil sites	$\Longleftrightarrow$	E

Figures 3.4 and 3.5 portray inelastic response spectra obtained by dividing the NBCC-2005 UHS for Montréal and Vancouver, respectively, by corresponding yield strength reduction factors. Inelastic spectra are shown for displacement ductilities ranging from 2 to 6 considering the five soil profiles (A, B, C, D) listed in Table 3.1. Results for soft soil types are not presented since they require the estimation of the predominant period $\overline{T}$.

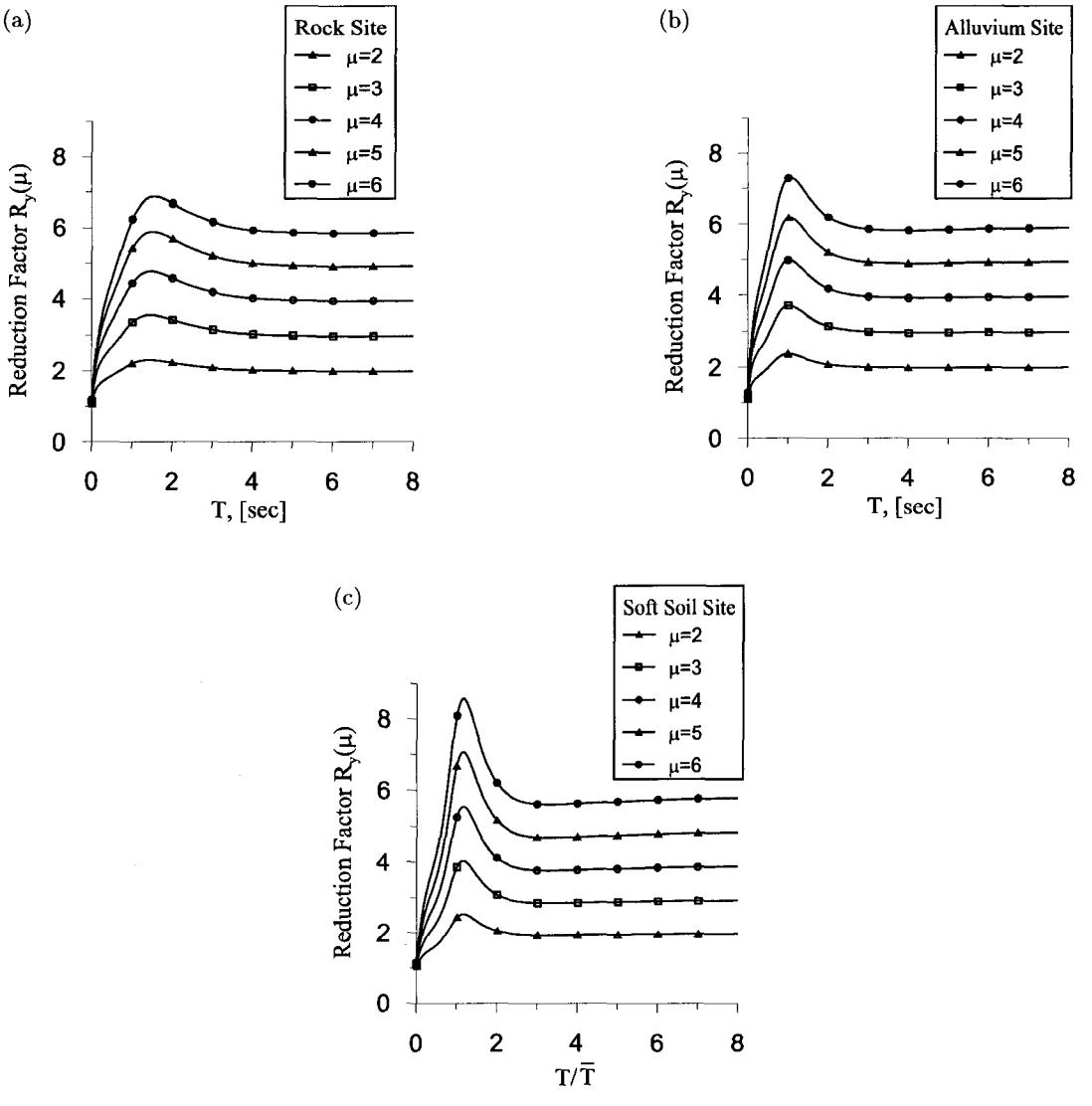

FIG. 3.3 Variation of strength reduction factor $R_y(\mu)$ obtained using Miranda (1993) method : (a) Rock site; (b) Alluvium site; and (c) Soft soil site.

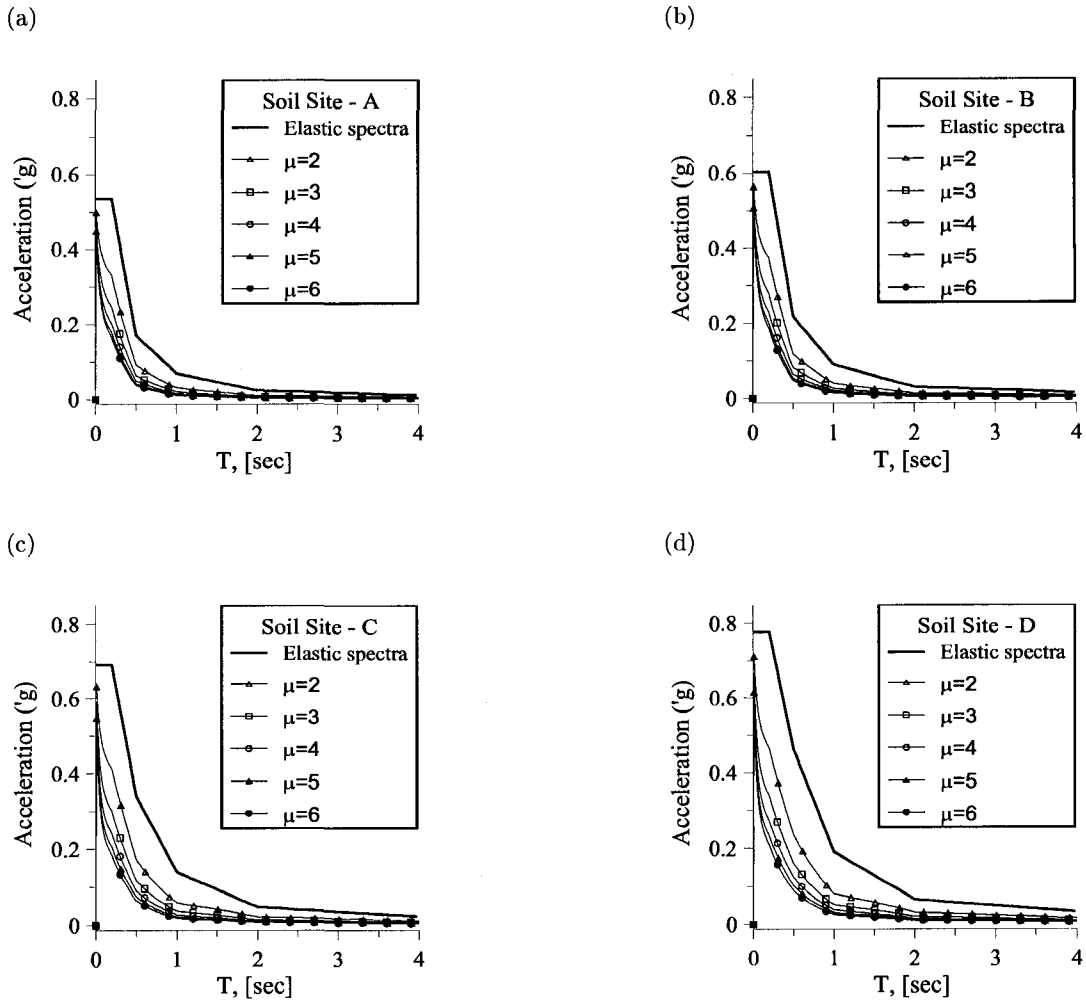

FIG. 3.4 Inelastic spectra for various soil profiles at Montréal with $R_y(\mu)$ obtained using Miranda (1993) method : (a) Soil type A ; (b) Soil type B ; (c) Soil type C ; (d) Soil type D.

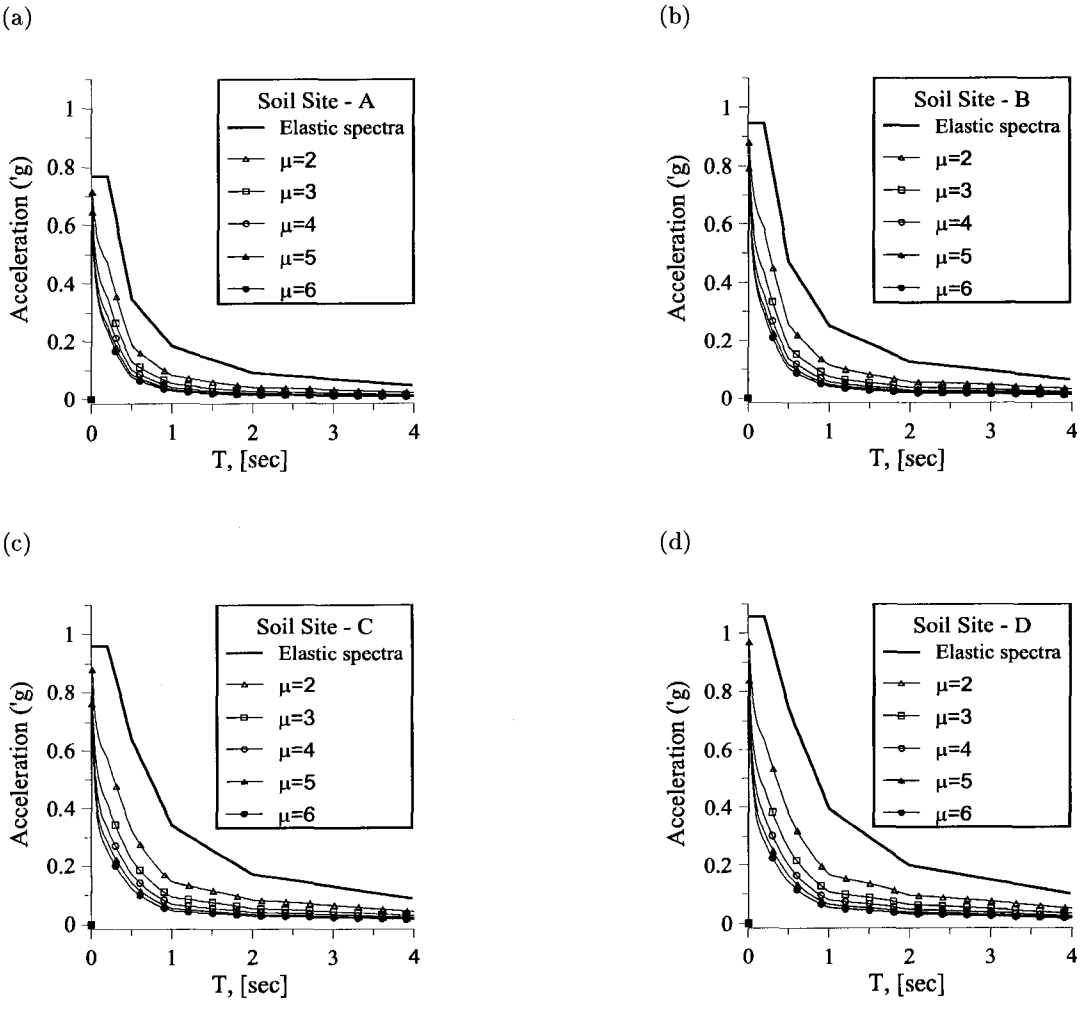

FIG. 3.5 Inelastic spectra for various soil profiles at Vancouver with $R_y(\mu)$ obtained using Miranda (1993) method : (a) Soil type A ; (b) Soil type B ; (c) Soil type C ; (d) Soil type D.

3.2.3.2 Nassar and Krawinkler Method

Nassar and Krawinkler (1991) studied the variation of $R_y(\mu)$ through the investigation of the dynamic response of Single Degree of Freedom (SDOF) nonlinear systems subjected to 15 ground motions recorded in the Western United States, mainly at alluvium and rock sites. Their study examined the sensitivity of the mean value of $R_y(\mu)$ to the epicentral distance and to structural system parameters, such as natural period T, strain-hardening ratio and inelastic material behavior. They concluded that the epicentral distance and stiffness degradation have a negligible influence on strength reduction factors. Based on the obtained results, Nassar and Krawinkler (1991) proposed a formula to estimate $R_y(\mu)$

$$R_y(\mu) = \left[c(\mu - 1) + 1\right]^{\frac{1}{c}} \tag{3.14}$$

where the coefficient c is given by

$$c(T, \alpha) = \frac{T^a}{1 + T^a} + \frac{b}{T} \tag{3.15}$$

in which α is the post-yield stiffness coefficient defined as a percentage of the initial system stiffness, and the parameters a and b are listed in Table 3.2.

TAB. 3.2 Parameters used in the Nassar and Krawinkler (1991) formulation.

α	a	b
0.00	1.00	0.42
0.02	1.00	0.37
0.10	0.80	0.29

The variation of the strength reduction coefficient $R_y(\mu)$ as a function of displacement ductilities ranging from 2 to 6 is illustrated in Figure 3.6. The three post-yield stiffness coefficients α listed in Table 3.2 are considered.

Figures 3.7 and 3.8 illustrate inelastic response spectra for the same range of displacement

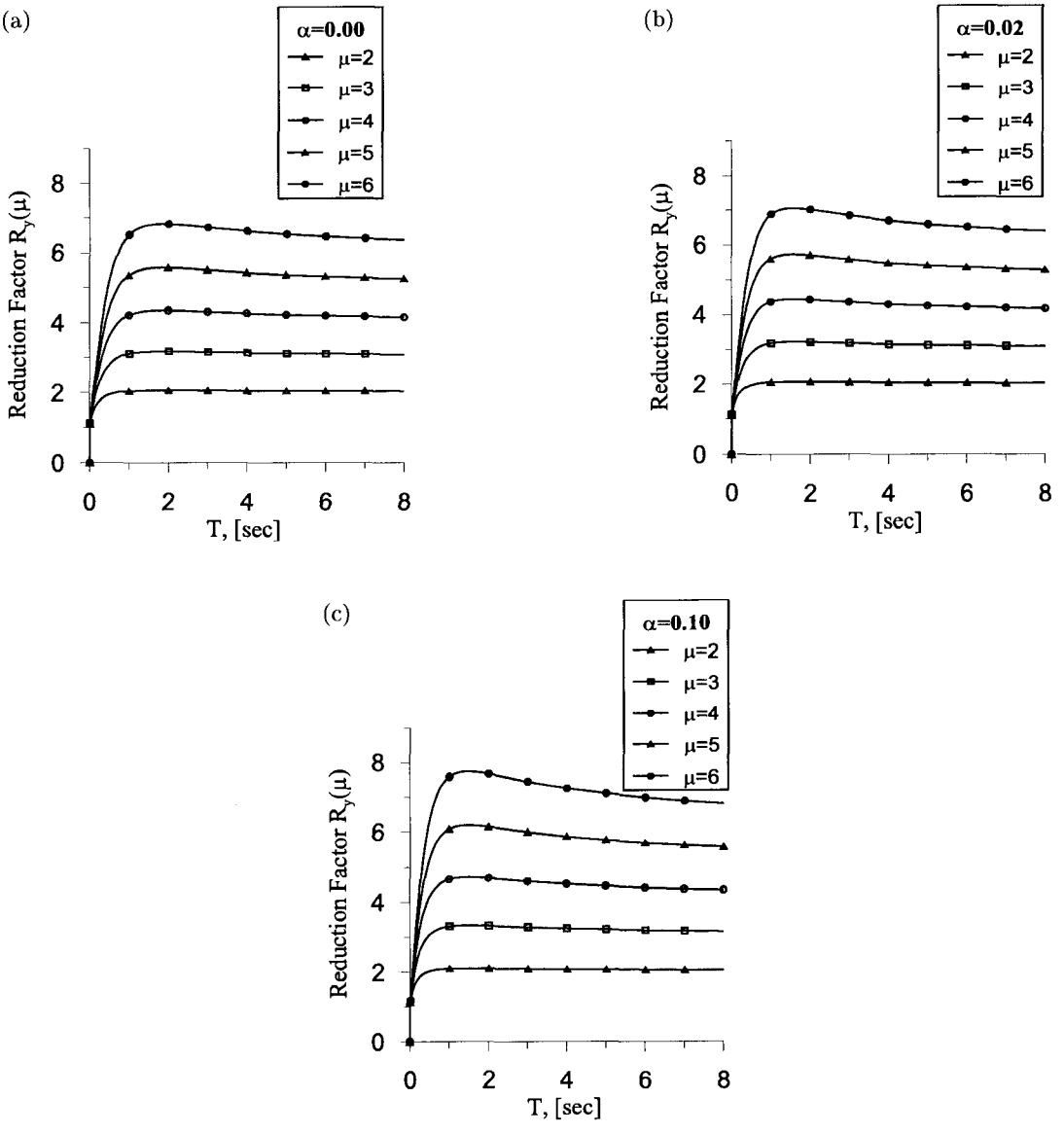

FIG. 3.6 Strength reduction coefficient $R_y(\mu)$ obtained using Nassar and Krawinkler (1991) method for different post-yield stiffness coefficients : (a) α=0.00; (b) α=0.02; and (c) α=0.10.

ductilities obtained by dividing the NBCC-2005 UHS for Montréal and Vancouver, respectivly, by yield strength reduction factors. For comparison purposes, inelastic spectra are shown for the same soil profiles (A, B, C, D and E) listed in Table 3.1. In fact, in this case, soil effects are accounted for only through the site dependence of the spectral accelerations according to the NBCC 2005. For illustration purposes, a value of $\alpha = 0$ is arbitrarily adopted to obtain the inelastic spectra in both cities.

The following two particularities of the Nassar and Krawinkler (1991) method can be pointed out :

- The method accounts for the elasto-plastic hysteretic behaviour through the coefficient c given by Eq. (3.15) ;
- The influence of soil conditions is not explicitly considered as in the method of Miranda (1993).

Strength reduction factors $R_y(\mu)$ determined using Miranda (1993) and Nassar and Krawinkler (1991) methods are shown in Fig. 3.9. An alluvium soil profile and a post-yield stiffness without hardening ($\alpha = 0$) are considered. It can be observed from Fig. 3.9 that the yield strength reduction factors obtained using Miranda (1993) method are generally higher than those obtained according to Nassar and Krawinkler (1991). The difference between both methods decreases however for lower displacement ductilities.

The inelastic response spectra obtained using both methods are also shown in Figs. 3.10 and 3.11. A soil profile C and a value of $\alpha = 0$ for the structural system are considered. It is clearly seen that the main differences between the two methods concentrate in the very short period range. For the purpose of the present work, the method proposed by Miranda (1993) is used mainly because it covers a wide range of ground motion types including East and West American earthquakes.

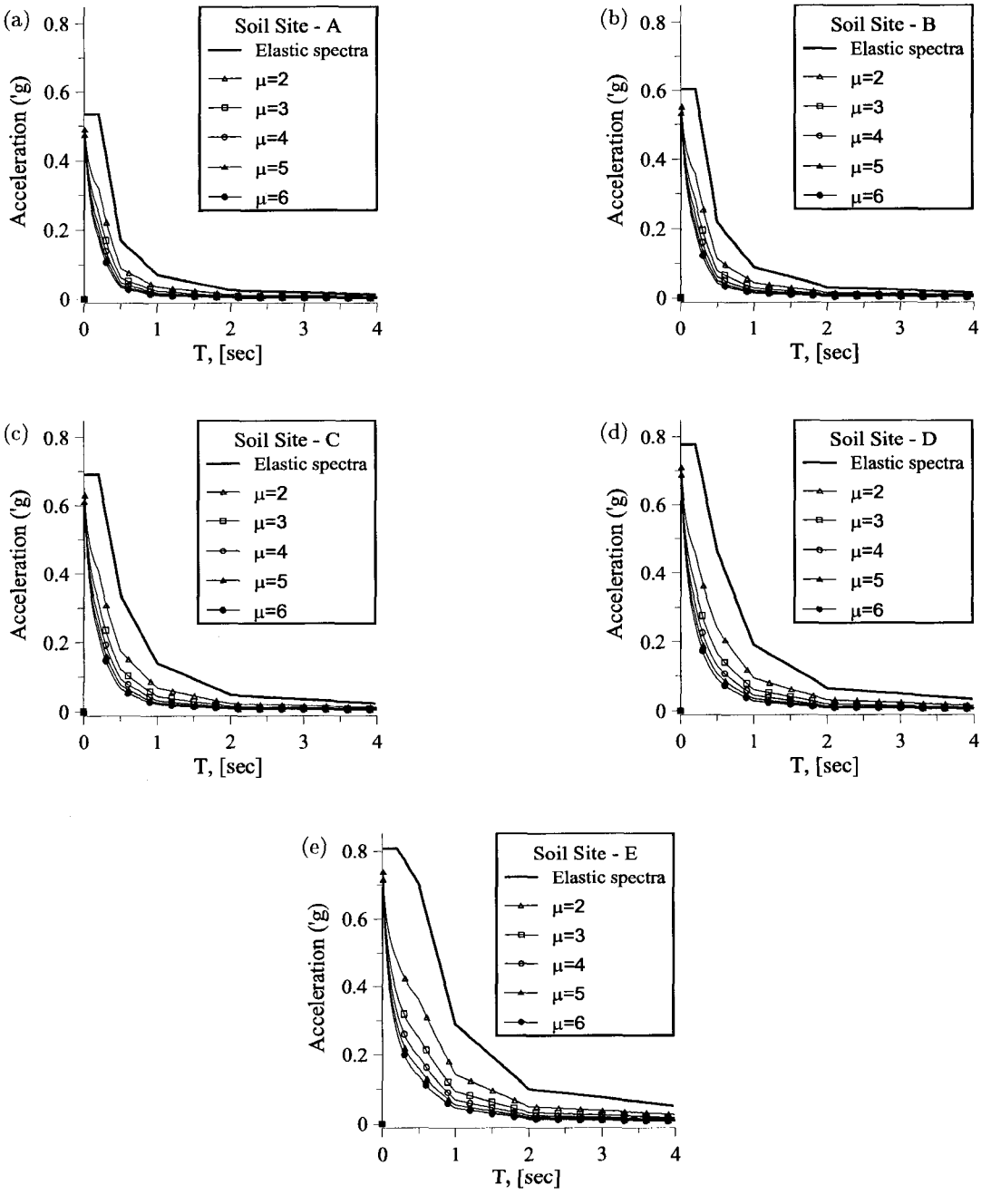

FIG. 3.7 Inelastic spectra for various soil profiles at Montréal with $R_y(\mu)$ obtained using Nassar and Krawinkler (1991) method : (a) Soil type A ; (b) Soil type B ; (c) Soil type C ; (d) Soil type D and (e) Soil type E.

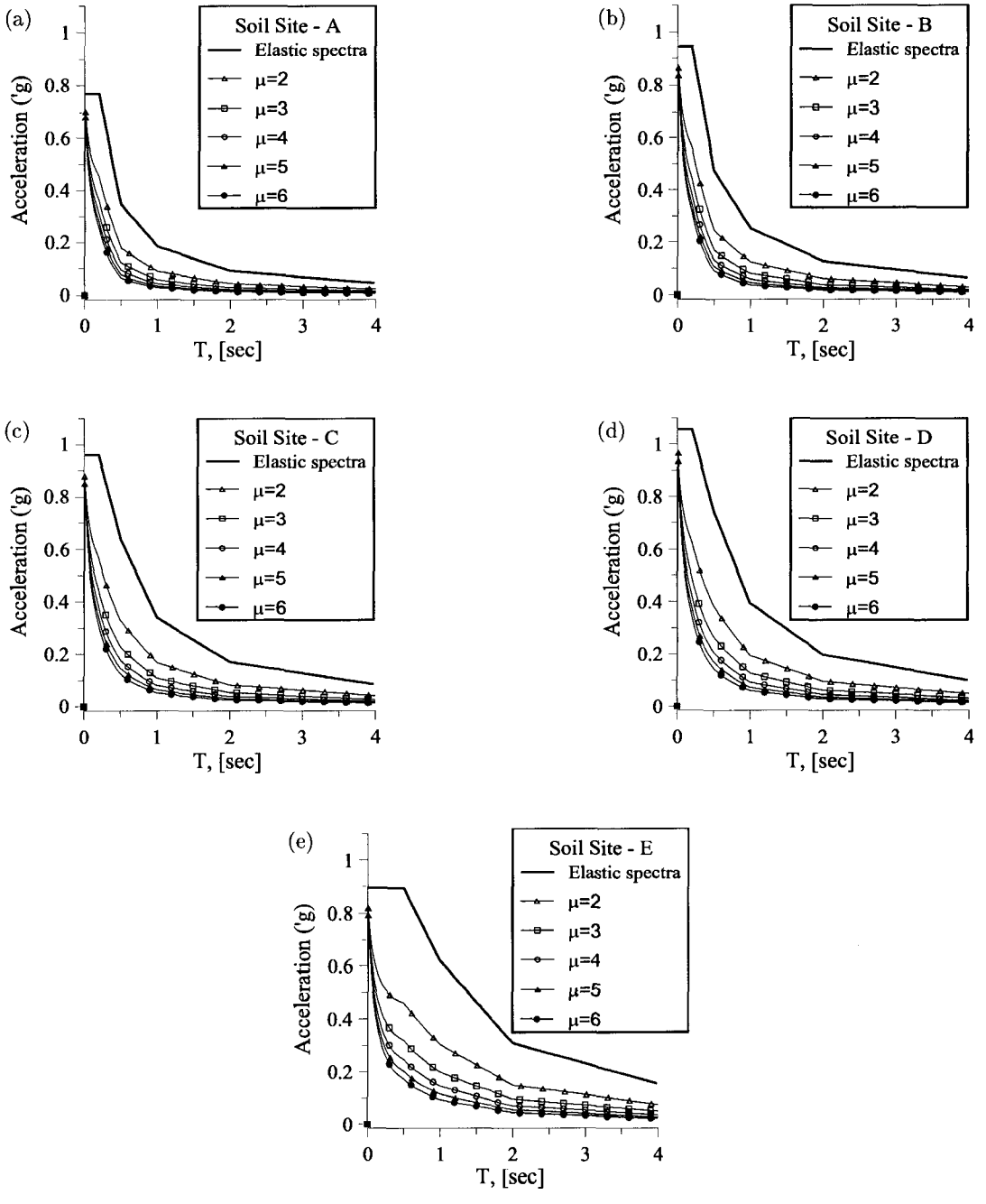

FIG. 3.8 Inelastic spectra for various soil profiles at Vancouver with $R_y(\mu)$ obtained using Nassar and Krawinkler (1991) method : (a) Soil type A ; (b) Soil type B ; (c) Soil type C ; (d) Soil type D and (e) Soil type E.

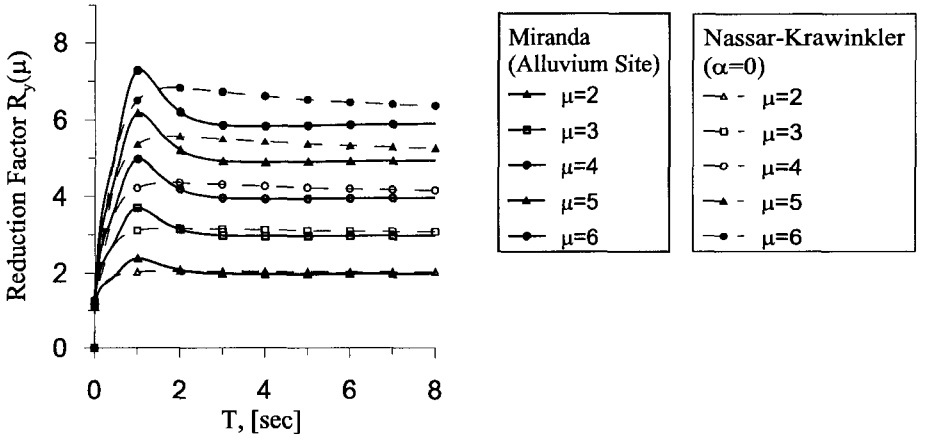

FIG. 3.9 Yield strength coefficient factor $R_y(\mu)$ obtained for various ductilities using Miranda (1993) and Nassar and Krawinkler (1991) methods.

3.2.4 Seismic Hazard Levels, Target Displacements and Performance Objectives

In the present work, three Seismic Hazard Levels (SHL) corresponding to return periods of approximately 2500 years (SHL-2500), 475 years (SHL-475) and 75 years (SHL-75) are considered to achieve specified performance objectives. The corresponding median (50^{th} percentile) spectral response accelerations expressed as a ratio to gravitational acceleration g are listed in Tables 3.3 and 3.4 for the cities of Montréal and Vancouver, respectively (Adams *et al.* 1999 ; CCBFC 2005). The values are given for the reference firm soil ground conditions of site Class C, and at periods of 0.2, 0.5, 1.0 and 2.0 seconds. The acceleration response spectra associated with the three seismic hazard levels for Montréal and Vancouver are shown in Figure 3.12.

As mentioned before, the main objective of Performance-Based Design is to closely relate expected performance levels to expected seismic hazard. Pioneering and comprehensive descriptions of such correlations are presented through the guidelines in SEAOC Vision 2000 (1995), FEMA-273/274 (1997), and SEAOC Blue Book (1999). To achieve adequate energy dissipation during earthquake excitation, critical regions of structural members

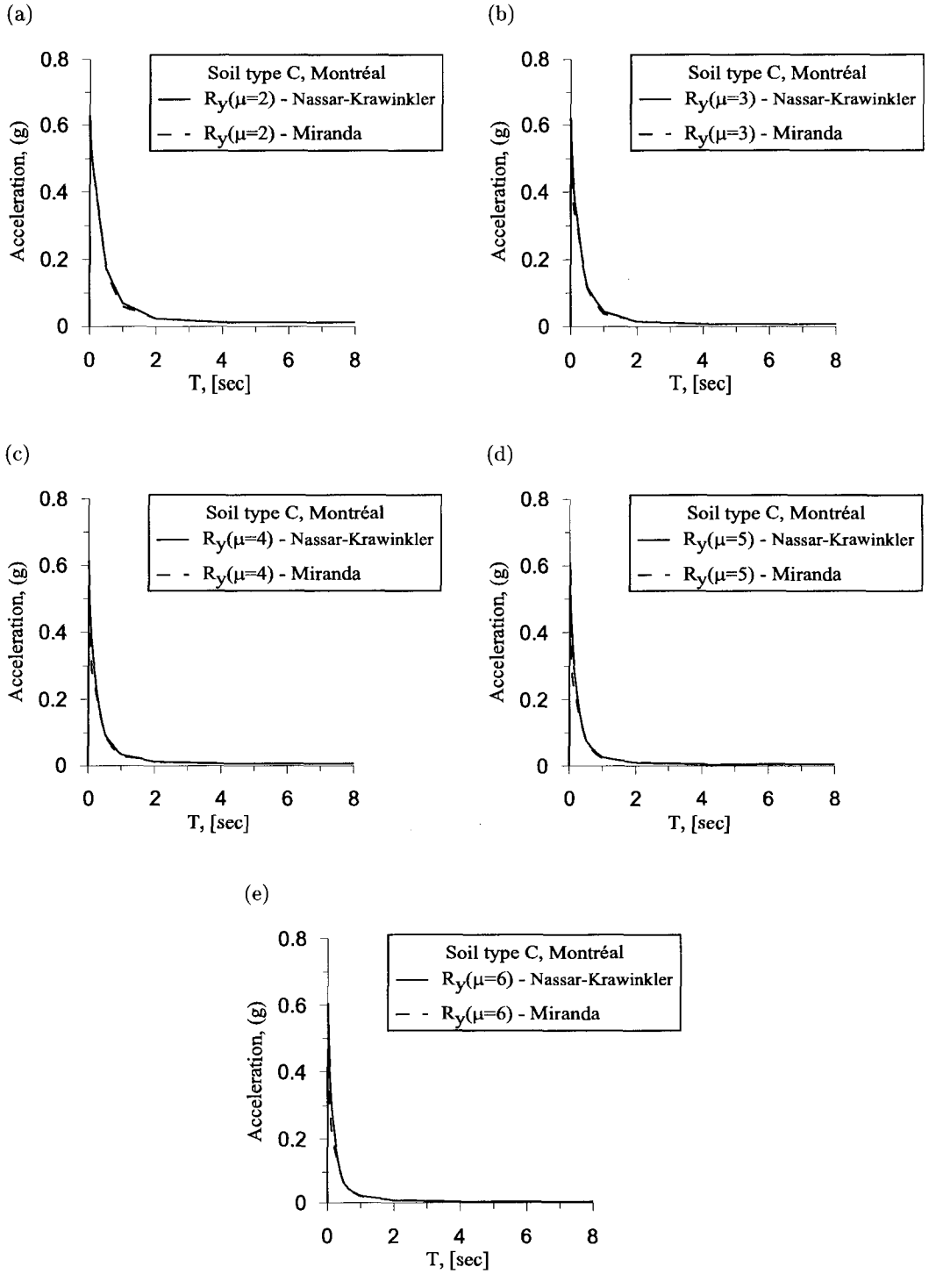

FIG. 3.10 Inelastic spectra generation for alluvium soil site at Montréal and various ductilities based on Miranda (1993) and Nassar-Krawinkler (1991) methods : (a) μ=2; (b) μ=3; (b) μ=3; (c) μ=4; (d) μ=5 and (e) μ=6.

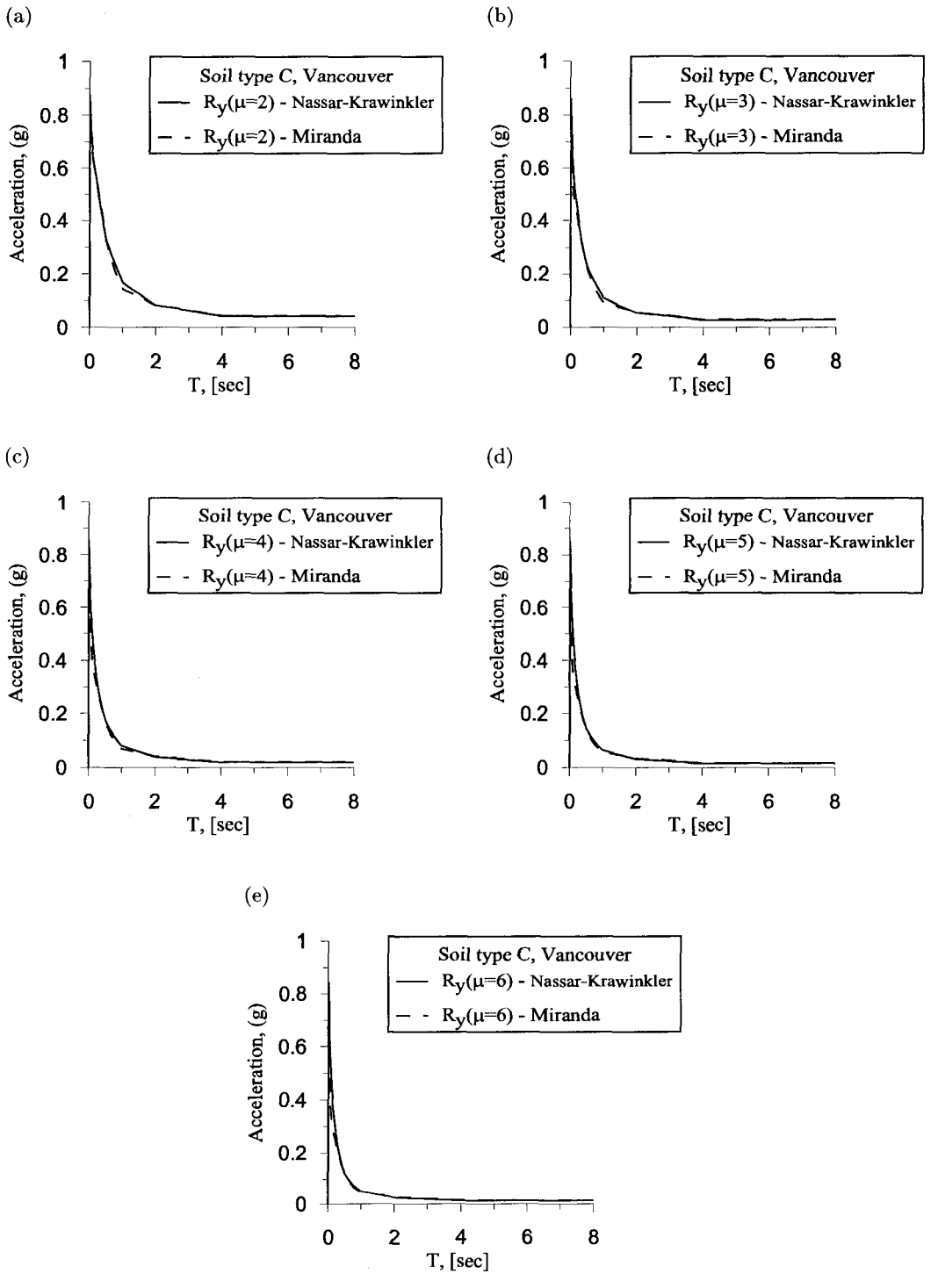

FIG. 3.11 Inelastic spectra generation for alluvium soil site in Vancouver and various ductilities based on Miranda (1993) and Nassar-Krawinkler (1991) methods : (a) μ=2; (b) μ=3; (b) μ=3; (c) μ=4; (d) μ=5 and (e) μ=6.

TAB. 3.3 Spectral response accelerations for three seismic hazard levels at the city of Montréal.

	SHL-75	SHL-475	SHL-2500
Probability of exceedance	50 % in 50 year	10 % in 50 years	2 % in 50 years
Return period	75 years	475 years	2500 years
Sa(0.2)	0.088	0.290	0.690
Sa(0.5)	0.036	0.130	0.340
Sa(1.0)	0.013	0.052	0.140
Sa(2.0)	0.004	0.016	0.048

TAB. 3.4 Spectral response accelerations for three seismic hazard levels at the city of Vancouver.

	SHL-75	SHL-475	SHL-2500
Probability of exceedance	50 % in 50 years	10 % in 50 years	2 % in 50 years
Return period	75 years	475 years	2500 years
$S_a(0.2)$	0.200	0.520	1.000
$S_a(0.5)$	0.140	0.350	0.670
$S_a(1.0)$	0.069	0.180	0.340
$S_a(2.0)$	0.034	0.089	0.180

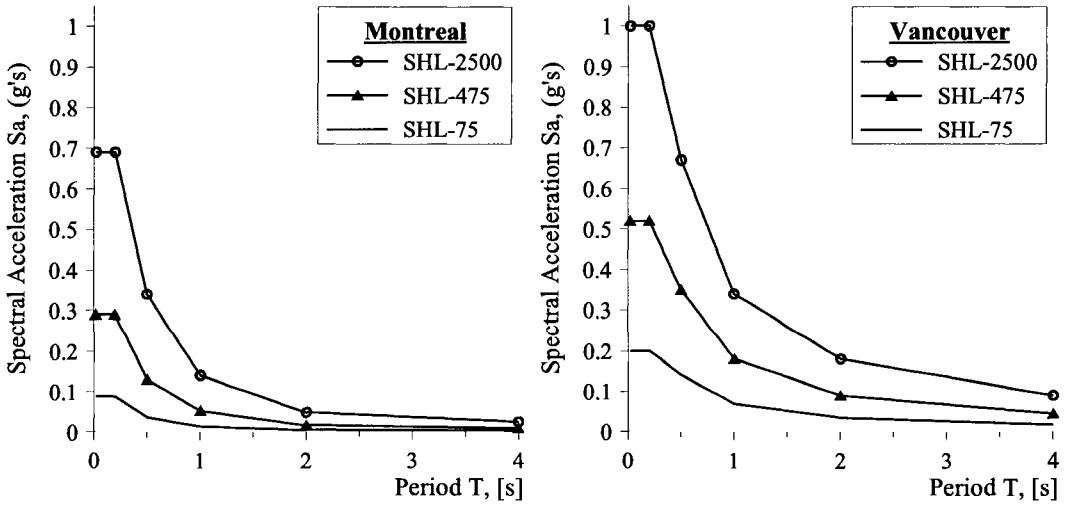

(a) Montréal (b) Vancouver

FIG. 3.12 Acceleration response spectra for different seismic hazard levels considered for the cities of Montréal and Vancouver.

should be sized and detailed to allow inelastic deformations within the limits of acceptable structural damage. On the other hand, it is now widely proven that nonstructural damage results in both significant hazard to occupants and major economic loss. It is also accepted that nonstructural damage is more related to interstorey drift, rather than overall lateral deflection of the building. In this report, the lateral displacement at level i is denoted by Δ_i, and the interstorey drift at level i by $\delta_i = \Delta_i - \Delta_{i-1}$. The seismic provisions of current building codes generally relate the structural and nonstructural damage at level i to Interstorey Drift Index IDI_i, defined as the percentage ratio of interstory lateral deflection to storey height

$$\mathrm{IDI}_i = \frac{\Delta_i - \Delta_{i-1}}{h_i - h_{i-1}} = \frac{\delta_i}{h_s^{(i)}} \tag{3.16}$$

where $h_s^{(i)}$ is the height of the i^{th} storey.

Art. 4.1.8.13 of the NBCC 2005 limits the maximum interstorey drift index to 1% for post-disaster buildings, 2% for schools, and 2.5% for all other buildings. These drift limits are inspired by the SEAOC Vision 2000 document (SEAOC 1995; Devall 2003), shown in Figs. 3.13 and 3.14. They can be related to the three seismic hazard levels SHL-

75, SHL-475 and SHL-2500 used in the present work. However, the displacement-based design methods investigated herein do not directly use interstorey drift index limits as an input, they rather require the definition of a target displacement profile of the structure considered. The construction of such a target displacement profile based on prescribed criteria is illustrated next for a shear wall building.

It can be assumed that the lateral wall displacement Δ_i at level i is comprised of an elastic portion $\Delta_{i,\mathrm{e}}$ and an inelastic or plastic portion $\Delta_{i,\mathrm{p}}$

$$\Delta_i = \Delta_{i,\mathrm{e}} + \Delta_{i,\mathrm{p}} \tag{3.17}$$

In the same fashion, the wall rotation θ_i at level i can be expressed as the sum of an elastic rotation $\theta_{i,\mathrm{e}}$ and a plastic rotation $\theta_{i,\mathrm{p}}$

$$\theta_i = \theta_{i,\mathrm{e}} + \theta_{i,\mathrm{p}} \tag{3.18}$$

Assuming that the elastic portion of the shear wall overall displacement coincides with its yield displacement (UBC 1997; Paulay 2001), and considering a lateral static load in the form of an inverted triangle, the elastic lateral displacement $\Delta_{i,\mathrm{e}}$ and elastic rotation $\theta_{i,\mathrm{e}}$ at level i located at wall height h_i are given by

$$\Delta_{i,\mathrm{e}} = \frac{\phi_\mathrm{y} h_i^2}{40 h_\mathrm{w}^3}\left(h_i^3 - 10 h_i h_\mathrm{w}^2 + 20 h_\mathrm{w}^3\right) \tag{3.19}$$

$$\theta_{i,\mathrm{e}} = \frac{\phi_\mathrm{y} h_i}{8 h_\mathrm{w}^3}\left(h_i^3 - 6 h_i h_\mathrm{w}^2 + 8 h_\mathrm{w}^3\right) \tag{3.20}$$

where ϕ_y is the wall yield curvature, and h_w the height of the shear wall. The yield curvature may be considered as the curvature at the first yielding of the wall extreme longitudinal reinforcement as reported in Paulay (2001). For load ratios less than about 0.15, Priestley and Kowalsky (1998) and Paulay (2002) have shown that for a wide range of

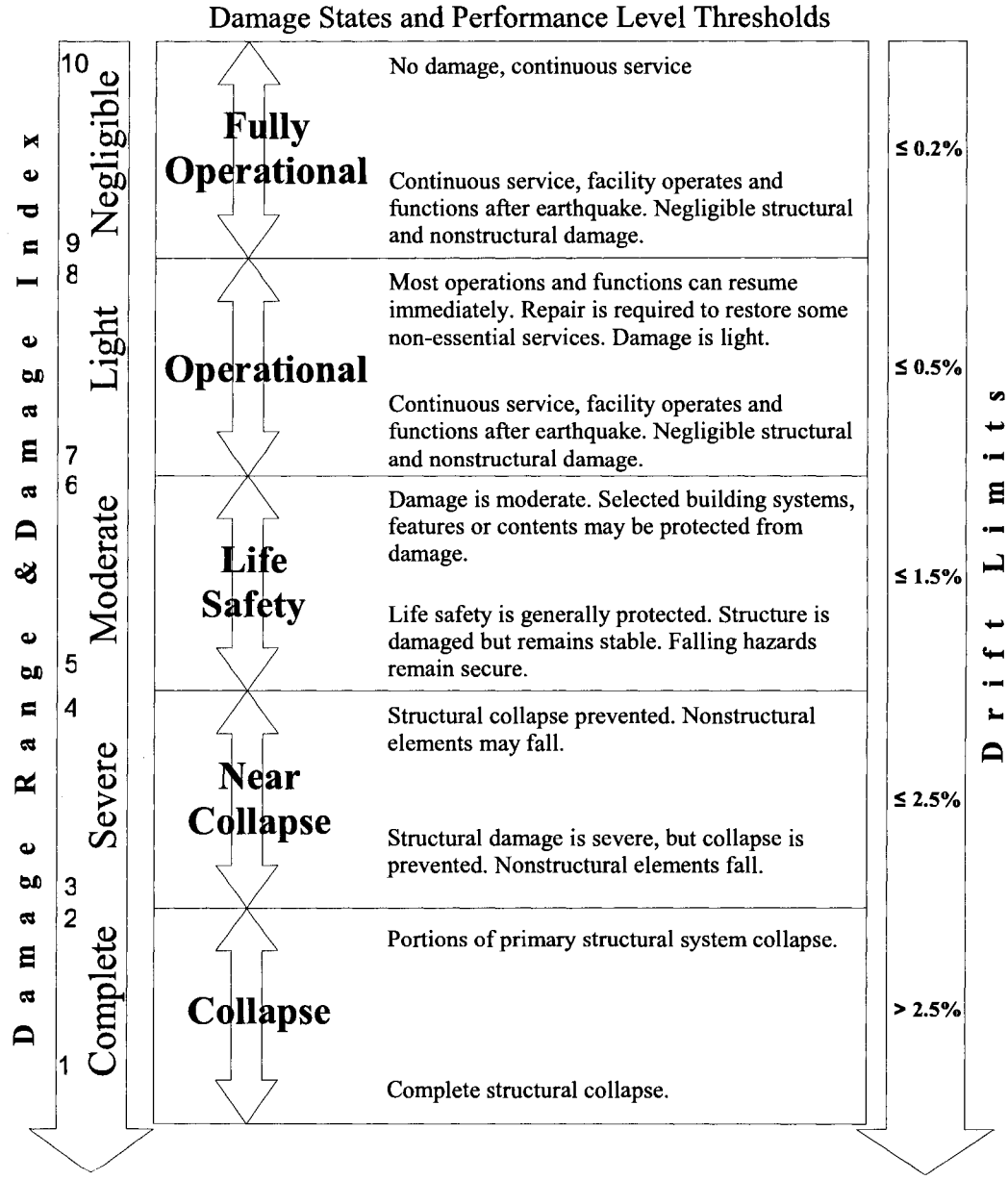

FIG. 3.13 Seismic damage spectrum from SEAOC Vision 2000, adjusted for NBCC 2005 drift requirements by DeVall (Devall 2003).

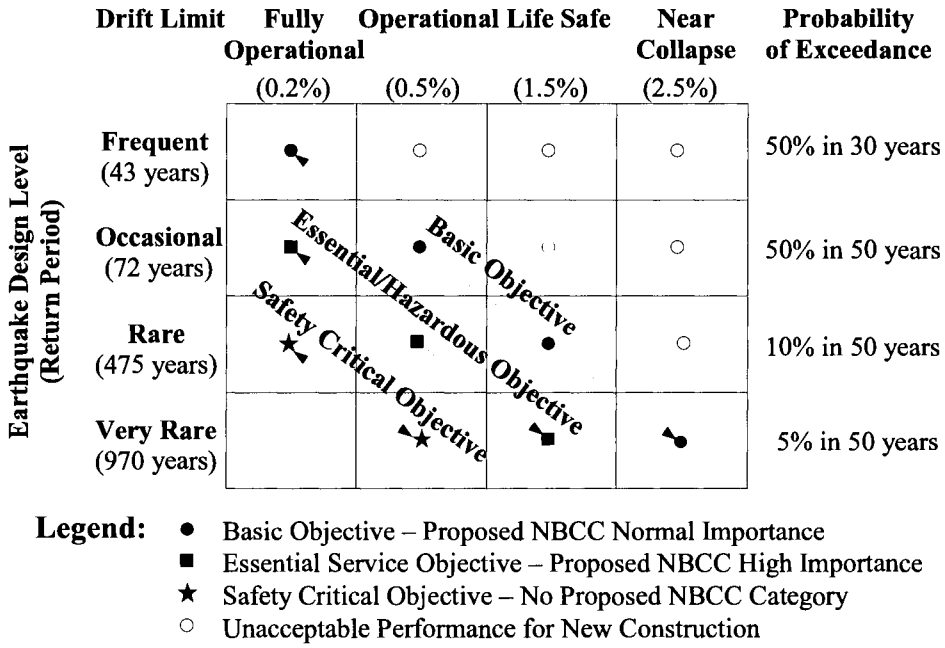

FIG. 3.14 Target performance objectives from SEAOC Vision 2000, adapted to NBCC 2005 drift requirements by DeVall (Devall 2003).

reinforcing steel ratios, the yield curvature can be approximated as

$$\phi_{\mathrm{y}} = \frac{2\varepsilon_{\mathrm{y}}}{\ell_{\mathrm{w}}} \tag{3.21}$$

According to Eqs. (3.19) and (3.20), the wall elastic displacement and rotation are maximum at roof level $h_n = h_{\mathrm{w}}$

$$\Delta_{n,\mathrm{e}} = \frac{11}{40}\phi_{\mathrm{y}} h_{\mathrm{w}}^2 \tag{3.22}$$

$$\theta_{n,\mathrm{e}} = \frac{3}{8}\phi_{\mathrm{y}} h_{\mathrm{w}} \tag{3.23}$$

The plastic lateral displacement $\Delta_{i,\mathrm{p}}$ at level i can be expressed as

$$\Delta_{i,\mathrm{p}} = \theta_{\mathrm{p}} \left(h_i - \frac{\ell_{\mathrm{p}}}{2} \right) \tag{3.24}$$

in which θ_{p} is the plastic hinge rotation at wall base, and ℓ_{p} the length of the plastic hinge. The inelastic rotation $\theta_{i,\mathrm{p}}$ at any level i is equal to the plastic hinge rotation θ_{p} at the base of the wall :

$$\theta_{i,\mathrm{p}} = \theta_n^{(\mathrm{p})} = \theta_{\mathrm{p}} \tag{3.25}$$

Note that the shear wall performance is assessed herein based on the assumption of plastic hinging at the wall base. The plastic rotation limit can be estimated either using interstorey drift limits prescribed by the NBCC 2005, or based on wall rotational capacity given in the CSA A23.3-2004 standard.

Equation (3.18) yields

$$\theta_{\mathrm{p}} = \theta_i - \theta_{i,\mathrm{e}} = \theta_n - \theta_{n,\mathrm{e}} = \theta_n - \frac{3}{8}\phi_{\mathrm{y}} h_{\mathrm{w}} \tag{3.26}$$

Using Eqs. (3.17), (3.19), (3.24) and (3.26), the lateral wall design displacement can be

written as

$$\Delta_i = \frac{\phi_y h_i^2}{40 h_w^3}\left(h_i^3 - 10 h_i h_w^2 + 20 h_w^3\right) + \left(\theta_n - \frac{3}{8}\phi_y h_w\right)\left(h_i - \frac{\ell_p}{2}\right) \tag{3.27}$$

which yields a target roof displacement

$$\Delta_n = \frac{11}{40}\phi_y h_w^2 + \left(\theta_n - \frac{3}{8}\phi_y h_w\right)\left(h_w - \frac{\ell_p}{2}\right) \tag{3.28}$$

The building Roof Drift Index RDI is defined as the percentage ratio of lateral displacement at roof level to total building height RDI $= \Delta_n / h_n$ (Figure 3.15). Hence, using Eq. (3.28)

$$\text{RDI} = \frac{\Delta_n}{h_n} = \frac{\Delta_n}{h_w} = \frac{11}{40}\phi_y h_w + \left(\theta_n - \frac{3}{8}\phi_y h_w\right)\left(1 - \frac{\ell_p}{2h_w}\right) \tag{3.29}$$

The rotation θ_n is approximately equal to the interstorey drift index at the top storey

$$\theta_n \approx \text{IDI}_n \tag{3.30}$$

Considering the code prescribed inter-story drift indices and using Eqs. (3.27) and (3.30), the target displacement profile corresponding to each of the performance levels described above can be determined. It is important to mention that this target profile is based solely on drift index limitations, and will be designated here as a *drift-controlled* displacement target profile. On the other hand, referring to Eq. (3.26), it can be seen that limitations on plastic hinging at the base of the wall may also control the target displacement profile. These target inelastic rotations can be obtained from setting target concrete compression or steel tension strain limit states. Canadian standards do not however specify such strain target values in terms of performance levels. For illustrative purposes, the target plastic hinge rotations proposed in the FEMA-273/274 are used to obtain what is designated herein as *rotation-controlled* target displacement profiles.

Table 3.5 summarizes the performance criteria used in the current work to obtain target

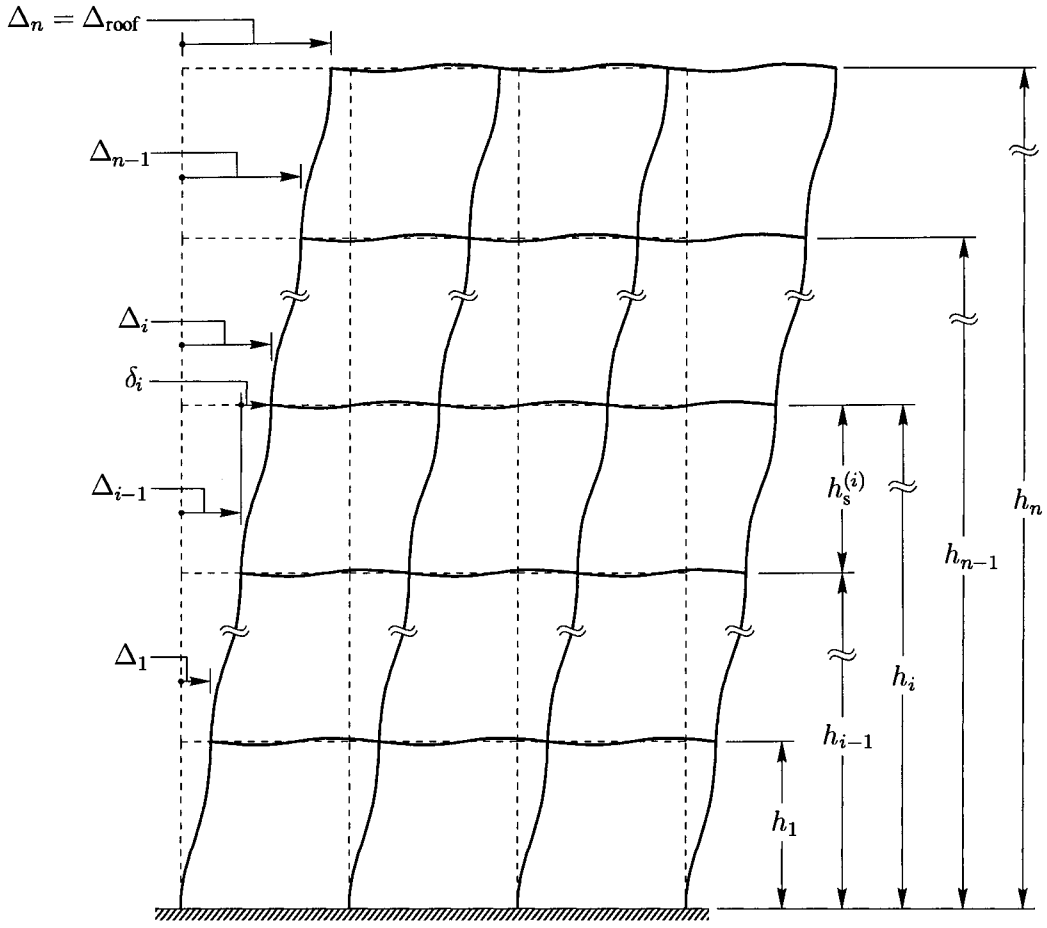

FIG. 3.15 Storey drifts Δ_i, interstorey drifts δ_i and heights h_i, $i = 1 \ldots n$, in a n-storey building.

drift- and rotation-controlled target displacement profiles as a function of seismic hazard levels.

TAB. 3.5 Seismic hazard levels and corresponding displacement performance objectives.

	Performance level		
	Post-disaster	Life safety	Near collapse
Seismic hazard level	SHL-75	SHL-475	SHL-2500
Interstorey drift limit (% of storey height)	0.5 %	1.5 %	2.5 %
Inelastic rotation limit (rad)	0.002	0.004	0.008

3.2.5 Equivalent Single Degree of Freedom and the Substitute Structure Method

It can be generally assumed that the dynamic response of a multistory building is governed by the equation of motion of a Multiple Degree Of Freedom System (MDOF)

$$\mathbf{M}\ddot{\mathbf{U}}(t) + \mathbf{C}\dot{\mathbf{U}}(t) + \mathbf{K}\mathbf{U}(t) = -\mathbf{M}\,\mathbf{1}\,\ddot{u}_g(t) \tag{3.31}$$

in which

- $\mathbf{U}$ is a vector containing lateral displacements u_i relative to the building base, taken at n floor levels, $i = 1 \ldots n$;
- $\mathbf{M}$ is a diagonal matrix containing lumped masses at the the n floor levels;
- $\mathbf{C}$ and $\mathbf{K}$ are the corresponding damping and stiffness matrices, respectively;
- $\mathbf{1}$ is a unit vector with n rows;
- $\ddot{u}_g$ is the ground acceleration time history.

Denoting u_n the relative displacement at the roof level, we can write

$$\mathbf{U}(t) = \boldsymbol{\psi}\, u_n(t) \tag{3.32}$$

where $\boldsymbol{\psi}$ is an assumed shape vector representing the deformed configuration of the MDOF system. Using Eq. (3.32) and Eq. (3.54) and pre-multiplying both sides of Eq. (3.31) by the transpose of the assumed deformed shape, yields

$$\boldsymbol{\psi}^{\mathrm{T}}\mathbf{M}\,\boldsymbol{\psi}\,\ddot{u}_n(t) + \boldsymbol{\psi}^{\mathrm{T}}\mathbf{C}\,\boldsymbol{\psi}\,\dot{u}_n(t) + \boldsymbol{\psi}^{\mathrm{T}}\mathbf{K}\,\boldsymbol{\psi}\,u_n(t) = -\boldsymbol{\psi}^{\mathrm{T}}\mathbf{M}\,\mathbf{1}\,\ddot{u}_{\mathrm{g}}(t) \tag{3.33}$$

which can be transformed into the equation of motion of an Equivalent Single Degree of Freedom (ESDOF)

$$\ddot{u}_n^*(t) + \frac{C^*}{M^*}\,\dot{u}_n^*(t) + \frac{K^*}{M^*}\,u_n^*(t) = -\ddot{u}_{\mathrm{g}}(t) \tag{3.34}$$

where the ESDOF displacement $u^*(t)$ is defined by

$$u^*(t) = \frac{u_n(t)}{\Gamma} \tag{3.35}$$

in which Γ is a participation factor defined by

$$\Gamma = \frac{\boldsymbol{\psi}^{\mathrm{T}}\mathbf{M}\,\mathbf{1}}{\boldsymbol{\psi}^{\mathrm{T}}\mathbf{M}\,\boldsymbol{\psi}} \tag{3.36}$$

and where the ESDOF mass M^*, damping C^* and stiffness K^* are given by

$$M^* = \boldsymbol{\psi}^{\mathrm{T}}\mathbf{M}\,\mathbf{1} \tag{3.37}$$

$$C^* = \Gamma\,\boldsymbol{\psi}^{\mathrm{T}}\mathbf{C}\,\boldsymbol{\psi} \tag{3.38}$$

$$K^* = \Gamma\,\boldsymbol{\psi}^{\mathrm{T}}\mathbf{K}\,\boldsymbol{\psi} \tag{3.39}$$

and the frequency of vibration of the ESDOF by

$$\omega^{*2} = \frac{K^*}{M^*} \tag{3.40}$$

Using Eqs. (3.37), (3.39) and (3.36), Eq. (3.40) expands to

$$\omega^{*2} = \frac{\Gamma\,\boldsymbol{\psi}^{\mathrm{T}}\mathbf{K}\,\boldsymbol{\psi}}{\boldsymbol{\psi}^{\mathrm{T}}\mathbf{M}\,\mathbf{1}} = \frac{\boldsymbol{\psi}^{\mathrm{T}}\mathbf{K}\,\boldsymbol{\psi}}{\boldsymbol{\psi}^{\mathrm{T}}\mathbf{M}\,\boldsymbol{\psi}} = \lambda_{\mathrm{R}} \tag{3.41}$$

where λ_{R} denotes the Rayleigh quotient (Chopra 2001).

It is to be mentioned that Eq. (3.35) can be written at yield as

$$\Delta_{\mathrm{y}}^{*} = \frac{\Delta_{n,\mathrm{y}}}{\Gamma} \tag{3.42}$$

where Δ_{y}^{*} denote the yield displacement of the ESDOF system and $\Delta_{n,\mathrm{y}}$ the yield displacement at the roof of the multistorey building. Both systems are illustrated in Fig. 3.16.

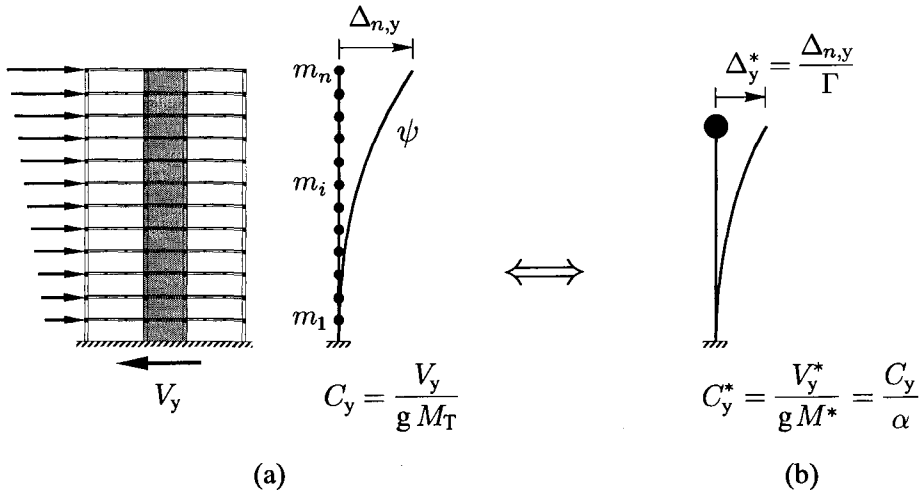

FIG. 3.16 Equivalent SDOF approximation : (a) MDOF system; (b) Equivalent SDOF system.

It can be seen that when the assumed deformed shape ψ coincides with a given mode shape ϕ_j of the multistorey building, Γ defines the corresponding modal participation factor and the product ΓM^{*} the participating mass along this deformed shape. The ESDOF frequency ω^{*} is then equal to the frequency of vibration ω_j at mode shape ϕ_j, since according to Eqs. (3.41), we have in this case

$$\omega^{*2} = \frac{\phi_j^{\mathrm{T}} \mathbf{K}\, \phi_j}{\phi_j^{\mathrm{T}} \mathbf{M}\, \phi_j} = \omega_j^2 \tag{3.43}$$

The yield strength V_{y}^{*} and the yield strength coefficient C_{y}^{*} of the ESDOF system are given by

$$V_{\mathrm{y}}^{*} = K^{*}\,\Delta_{\mathrm{y}}^{*} \tag{3.44}$$

and

$$\begin{aligned} C_{\mathrm{y}}^{*} &= \frac{V_{\mathrm{y}}^{*}}{\mathrm{g}\,M^{*}} \\ &= \frac{K^{*}}{\mathrm{g}\,M^{*}}\,\Delta_{\mathrm{y}}^{*} \end{aligned} \tag{3.45}$$

On the other hand, the base shear strength V_{y} of the MDOF system can be expressed as

$$\begin{aligned} V_{\mathrm{y}} &= \mathbf{1}^{\mathrm{T}}\mathbf{K}\mathbf{U}_{\mathrm{y}} \\ &= \mathbf{1}^{\mathrm{T}}\mathbf{K}\,\boldsymbol{\psi}\,\Delta_{n,\mathrm{y}} \end{aligned} \tag{3.46}$$

Denoting $M_{\mathrm{T}} = \mathbf{1}^{\mathrm{T}}\mathbf{M}\,\mathbf{1}$ the total mass of the MDOF system, the base shear strength coefficient at yield C_{y} of the multistorey building is given by

$$\begin{aligned} C_{\mathrm{y}} &= \frac{V_{\mathrm{y}}}{\mathrm{g}\,M_{\mathrm{T}}} \\ &= \frac{1}{\mathrm{g}}\,\frac{\mathbf{1}^{\mathrm{T}}\mathbf{K}\,\boldsymbol{\psi}}{\mathbf{1}^{\mathrm{T}}\mathbf{M}\,\mathbf{1}}\,\Delta_{n,\mathrm{y}} \end{aligned} \tag{3.47}$$

Using Eqs. (3.45) and (3.47), the ratio between the base shear strength coefficient at yield of the multistorey building and the yield strength coefficient of the ESDOF system can be expressed as

$$\frac{C_{\mathrm{y}}}{C_{\mathrm{y}}^{*}} = \frac{\left(\mathbf{1}^{\mathrm{T}}\mathbf{K}\,\boldsymbol{\psi}\right)}{\left(\boldsymbol{\psi}^{\mathrm{T}}\mathbf{K}\,\boldsymbol{\psi}\right)}\,\frac{\left(\boldsymbol{\psi}^{\mathrm{T}}\mathbf{M}\,\mathbf{1}\right)}{\left(\mathbf{1}^{\mathrm{T}}\mathbf{M}\,\mathbf{1}\right)} \tag{3.48}$$

which simplifies to

$$\frac{C_{\mathrm{y}}}{C_{\mathrm{y}}^{*}} = \frac{1}{M_{\mathrm{T}}}\,\frac{\left(\boldsymbol{\phi}_{j}^{\mathrm{T}}\mathbf{M}\,\mathbf{1}\right)^{2}}{\left(\boldsymbol{\phi}_{j}^{\mathrm{T}}\mathbf{M}\boldsymbol{\phi}_{j}\right)} \tag{3.49}$$

when the assumed deformed shape $\boldsymbol{\psi}$ coincides with mode shape $\boldsymbol{\phi}_j$ of the multistorey building.

For practical design purposes, the assumed deformed shape $\boldsymbol{\psi}$ is generally selected based on physical insight without necessarily coinciding with a given mode shape of the structure. In this case, Eq. (3.49) can be extended to

$$\frac{C_{\mathrm{y}}}{C_{\mathrm{y}}^{*}} = \frac{1}{M_{\mathrm{T}}} \frac{\left(\boldsymbol{\psi}^{\mathrm{T}}\mathbf{M}\,\mathbf{1}\right)^{2}}{\left(\boldsymbol{\psi}^{\mathrm{T}}\mathbf{M}\boldsymbol{\psi}\right)} \tag{3.50}$$

which can be further simplified to

$$\frac{C_{\mathrm{y}}}{C_{\mathrm{y}}^{*}} = \frac{\Gamma M^{*}}{M_{\mathrm{T}}} = \alpha \tag{3.51}$$

considering Eqs. (3.36) and (3.37). The ratio α of the participating mass ΓM^{*} to the total mass M_{T} is called the participating or the effective mass factor.

Using Eqs. (3.47) and (3.51), the base shear strength at yield of the multistorey building is obtained as

$$V_{\mathrm{y}} = \alpha\, \mathrm{g}\, M_{\mathrm{T}}\, C_{\mathrm{y}}^{*} \tag{3.52}$$

Different types of assumed deformed shape vectors $\boldsymbol{\psi}$ were proposed in the literature, including triangular or quadratic shapes (SEAOC 1995 ; ATC 1996 ; SEAOC 1999 ; Aschheim and Black 2000). In the present work, two assumed deflected shapes are considered :

- An assumed inverted triangular shape vector

$$\psi_i = \frac{h_i}{h_{\mathrm{w}}} \qquad i = 1 \ldots n \tag{3.53}$$

- An assumed quintic shape vector based on the displacement profile given by Eq. (3.27)

$$\psi_i = \frac{\Delta_i}{\Delta_n} \qquad i = 1 \ldots n \tag{3.54}$$

As can be seen, the shape vector ψ is normalized to have a unit value at the building roof level. Replacing Eq. (3.53) or Eq. (3.54) into Eqs. (3.36) and (3.51), the participation factor Γ and the mass participation factor α can be obtained as

$$\Gamma = h_{\mathrm{w}} \frac{\sum_{i=1}^{n} m_i h_i}{\sum_{i=1}^{n} m_i h_i^2} \; ; \qquad \alpha = \frac{1}{M_{\mathrm{T}}} \frac{\left(\sum_{i=1}^{n} m_i h_i \right)^2}{\sum_{i=1}^{n} m_i h_i^2} \tag{3.55}$$

for the assumed triangular shape vector [Eq. (3.53)] and

$$\Gamma = \Delta_n \frac{\sum_{i=1}^{n} m_i \Delta_i}{\sum_{i=1}^{n} m_i \Delta_i^2} \; ; \qquad \alpha = \frac{1}{M_{\mathrm{T}}} \frac{\left(\sum_{i=1}^{n} m_i \Delta_i \right)^2}{\sum_{i=1}^{n} m_i \Delta_i^2} \tag{3.56}$$

for the assumed quintic shape vector [Eq. (3.54)].

The procedure described previously assumes that the base shear strength of the MDOF system and the yield strength of the ESDOF are different. Another technique known as the *substitute structure* procedure was proposed by some researchers (Gulkan and Sozen 1974; Shibata and Sozen 1976). It is based on the following assumptions :

- the base shears of the MDOF and the ESDOF systems are the same as illustrated in Fig. 3.17;
- the ESDOF is characterized by an effective stiffness K_{eff} defined as a secant stiffness at peak response $\Delta_{\mathrm{u}} = \Delta_{\mathrm{eff}}$ (Fig. 3.17c);
- the work done by the lateral earthquake forces on both systems is the same.

Assuming a nondimensional shape vector ψ representing a target deformed configuration of the multistorey building [Eq. (3.54); Fig. 3.17a], the first and last assumptions translate

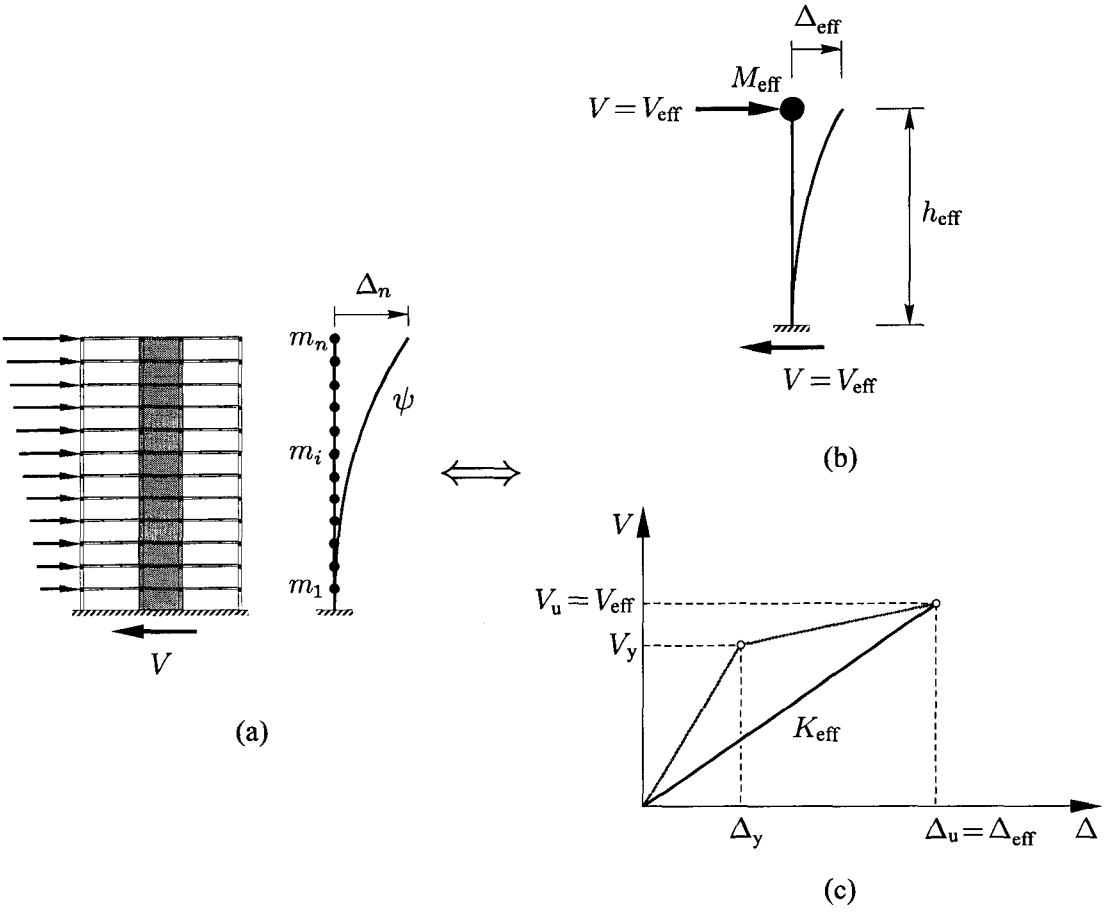

FIG. 3.17 Substitute structure method.

into

$$V_{\text{eff}} = \Delta_n \, \mathbf{1}^{\mathrm{T}} \mathbf{K} \boldsymbol{\psi} \tag{3.57}$$

$$V_{\text{eff}} \, \Delta_{\text{eff}} = \Delta_n^2 \, \boldsymbol{\psi}^{\mathrm{T}} \mathbf{K} \boldsymbol{\psi} \tag{3.58}$$

which yields

$$\Delta_{\text{eff}} = \Delta_n \frac{\boldsymbol{\psi}^{\mathrm{T}} \mathbf{K} \boldsymbol{\psi}}{\mathbf{1}^{\mathrm{T}} \mathbf{K} \boldsymbol{\psi}} \tag{3.59}$$

or, using a modal shape approximation

$$\begin{aligned} \Delta_{\text{eff}} &= \Delta_n \frac{\boldsymbol{\psi}^{\mathrm{T}} \mathbf{M} \boldsymbol{\psi}}{\mathbf{1}^{\mathrm{T}} \mathbf{M} \boldsymbol{\psi}} \\ &= \frac{\sum_{i=1}^{n} m_i \Delta_i^2}{\sum_{i=1}^{n} m_i \Delta_i} \end{aligned} \tag{3.60}$$

The effective mass of the ESDOF system is given by

$$\begin{aligned} M_{\text{eff}} &= \frac{\Delta_n}{\Delta_{\text{eff}}} \left(\mathbf{1}^{\mathrm{T}} \mathbf{M} \boldsymbol{\psi}^{\mathrm{T}} \right) \\ &= \frac{\sum_{i=1}^{n} m_i \Delta_i}{\Delta_{\text{eff}}} \end{aligned} \tag{3.61}$$

Equating the overturning moments at the bases of the ESDOF system and the multistory building results in

$$h_{\text{eff}} = \frac{\sum_{i=1}^{n} m_i \Delta_i h_i}{\sum_{i=1}^{n} m_i \Delta_i} \tag{3.62}$$

where h_{eff} is the height of the ESDOF system which coincides with the height of the resultant lateral seismic force.

The substitute structure is also characterized by an effective damping ratio ξ_{eff} defined as the sum of an initial elastic damping ξ_{e} in the nonlinear system, and a hysteretic damping ξ_{h} due to energy dissipation during hysteretic loop response

$$\xi_{\text{eff}} = \xi_{\text{e}} + \xi_{\text{h}} \tag{3.63}$$

Assuming a 5 % initial elastic damping and a Takeda degrading stiffness hysteretic model (Takeda *et al.* 1970), Kowalsky *et al.* (1995) developed an expression to estimate effective damping ξ_{eff} as a function of displacement ductility μ

$$\xi_{\text{eff}} = 0.05 + \frac{1}{\pi}\left(1 - \frac{0.95}{\sqrt{\mu}} - 0.05\sqrt{\mu}\right) \tag{3.64}$$

3.3 Yield Point Spectra Method

The Yield Point Spectra (YPS) method is based on stable yield displacement instead of the more sensitive period of vibration (Aschheim and Black 2000). It is also most likely to be adopted by the structural engineering community because of it produces a base shear that can be distributed according to current detailing practice. The method can be used for preliminary or detailed seismic design of new buildings, as well as for the evaluation or rehabilitation of existing structures.

One important step in the YPS method is the construction of yield point spectra described in section 3.2.2. As mentioned previously, the Yield Point Spectra used in this work are smoothed ones derived from the Uniform Hazard Spectra (UHS) proposed in the new 2005 edition of the NBCC (CCBFC 2005). The YPS method procedure is illustrated in the flowchart of Figure 3.18. On the one hand, when applied to a SDOF structure, the main steps of the method can be summarized as follows :

Step 1 : Estimate the roof yield displacement $\Delta_{n,\text{y}}$ of the structure based on preliminary geometrical and material properties. It can be assumed that the roof yield displacement $\Delta_{n,\text{y}}$ is equal to the elastic roof displacement $\Delta_{n,\text{e}}$ given

by Eq. (3.22). The yield curvature ϕ_y can be estimated using Eq. (3.21);

Step 2 : Fix a target roof displacement Δ_n satisfying a desired performance objective. This target displacement can be obtained from a displacement-controlled or a rotation-controlled performance objective as described in section 3.2.4. In the present work, the target roof displacement given by Eq. (3.28) is considered;

Step 3 : Calculate the corresponding system displacement ductility demand μ of the structure, defined as the ratio of the peak displacement Δ_u to the yield displacement Δ_y

$$\mu = \frac{\Delta_n}{\Delta_{n,y}} \tag{3.65}$$

Step 4 : Construct a Yield Point Spectrum corresponding to the displacement ductility demand μ, as described in section 3.2.2;

Step 5 : Determine the required yield strength coefficient C_y using the constructed Yield Point Spectrum.

Step 6 : Determine the required base shear strength V_y using the reported, from the previous step, yield strength coefficient and Eq. 3.9.

The steps described above can be extended to MDOF systems, based on approximating their displacement response by the deformed shape of a SDOF system as described in section 3.2.5. This approximation yields appropriate results for buildings with a predominant fundamental mode response. The participation factor Γ [Eq. (3.36)] and the mass participation factor α [Eq. (3.51)] are then used to relate an MDOF system to its equivalent SDOF system. A multistorey building can then be analyzed by applying the YPS procedure described above to its equivalent SDOF system. This procedure is illustrated later when applied to cantilever shear wall buildings (Chapter 5).

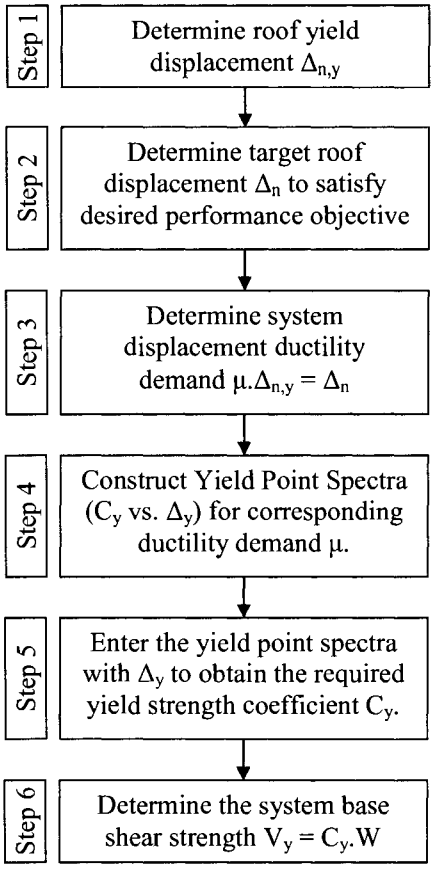

FIG. 3.18 Flowchart of YPS method (Aschheim, 2000).

3.4 Direct Displacement-Based Design Method

The Direct Displacement-Based Design (DDBD) approach (Kowalsky *et al.* 1995; Priestley and Kowalsky 2000) is based on the substitute structure technique presented in section 3.2.5. The method consists of modelling the nonlinear response of an inelastic system by using a substitute structure characterized by an effective stiffness K_{eff}, an effective damping ξ_{eff} and an effective period T_{eff} as described below. The DDBD procedure is illustrated in the flowchart of Figure 3.19. The main steps of the method can be summarized as follows :

Step 1 : Assume a target displacement profile over structure height to satisfy code prescribed drift limits, or other damage control criteria to satisfy given performance objectives. In this work, the target displacement profile Δ_i given by Eq. (3.27) is adopted. The yield curvature ϕ_{y} can be estimated according to Eq. (3.21).

Step 2 : Determine the effective displacement Δ_{eff}, the effective mass M_{eff} and the effective height h_{eff} of the substitute structure using Eqs. (3.60) to (3.62)

Step 3 : Determine the yield displacement $\Delta_{\text{eff,y}}$ at the height of the resultant lateral seismic force h_{eff} using Eq. (3.19)

$$\Delta_{\text{eff,y}} = \frac{\phi_{\text{y}} h_{\text{eff}}^2}{40 h_{\text{w}}^3}\left(h_{\text{eff}}^3 - 10 h_{\text{eff}} h_{\text{w}}^2 + 20 h_{\text{w}}^3\right) \tag{3.66}$$

Step 4 : Calculate the displacement ductility

$$\mu = \frac{\Delta_{\text{eff}}}{\Delta_{\text{eff,y}}} \tag{3.67}$$

Step 5 : Determine the effective damping ratio ξ_{eff} of the substitute structure according to Eq. (3.64);

Step 6 : Construct a 5 % damped inelastic displacement spectrum based on a 5 % dam-

ped pseudo-acceleration spectrum using the relation

$$\Delta_{\mathrm{e}}^{(5\,\%)} = \frac{T^2}{4\pi^2} A_{\mathrm{e}} \tag{3.68}$$

Step 7 : Determine the displacement spectrum for effective damping ξ_{eff} using the relation proposed in the Eurocode EC8 (Eurocode 1998)

$$\Delta_{\mathrm{e}}^{(\xi_{\mathrm{eff}})} = \Delta_{\mathrm{e}}^{(5\,\%)} \sqrt{\frac{7}{2+\xi_{\mathrm{eff}}}} \tag{3.69}$$

where $\Delta_{\mathrm{e}}^{(5\,\%)}$ and $\Delta_{\mathrm{e}}^{(\xi_{\mathrm{eff}})}$ are the spectral displacements at 5 % and ξ_{eff} damping values, respectively.

Step 8 : Calculate the effective period T_{eff}, the effective stiffness K_{eff} and the base shear $V_{\mathrm{u}} = V_{\mathrm{eff}}$ using (Priestley and Kowalsky 2000)

$$T_{\mathrm{eff}} = T_{\mathrm{c}} \frac{\Delta_{\mathrm{eff}}}{\Delta_{\mathrm{c}}} \sqrt{\frac{2+\xi_{\mathrm{eff}}}{7}} \tag{3.70}$$

$$K_{\mathrm{eff}} = \frac{4\pi^2 M_{\mathrm{eff}}}{T_{\mathrm{eff}}^2} = \frac{4\pi^2 M_{\mathrm{eff}}}{T_{\mathrm{c}}^2} \frac{\Delta_{\mathrm{c}}^2}{\Delta_{\mathrm{eff}}^2} \left(\frac{7}{2+\xi_{\mathrm{eff}}} \right) \tag{3.71}$$

$$V_{\mathrm{eff}} = K_{\mathrm{eff}} \Delta_{\mathrm{eff}} = \frac{4\pi^2 M_{\mathrm{eff}}}{T_{\mathrm{c}}^2} \frac{\Delta_{\mathrm{c}}^2}{\Delta_{\mathrm{eff}}} \left(\frac{7}{2+\xi_{\mathrm{eff}}} \right) \tag{3.72}$$

where T_{c} and Δ_{c} are, respectively, a corner period and the corresponding displacement on the inelastic displacement spectrum. A corner period $T_{\mathrm{c}} = 4\,\mathrm{s}$ corresponding to the maximum period of NBCC 2005 uniform hazard spectra is considered in this work.

3.4.1 Comments

- Direct Displacement-Based Design Method (DDBD), proposed by Priestley and Kowalsky (2000) is relatively fast procedure.
- Design procedure starts with predetermined target interstorey drift.
- DDBD suggests the use of a set of design displacement spectra, generated for different

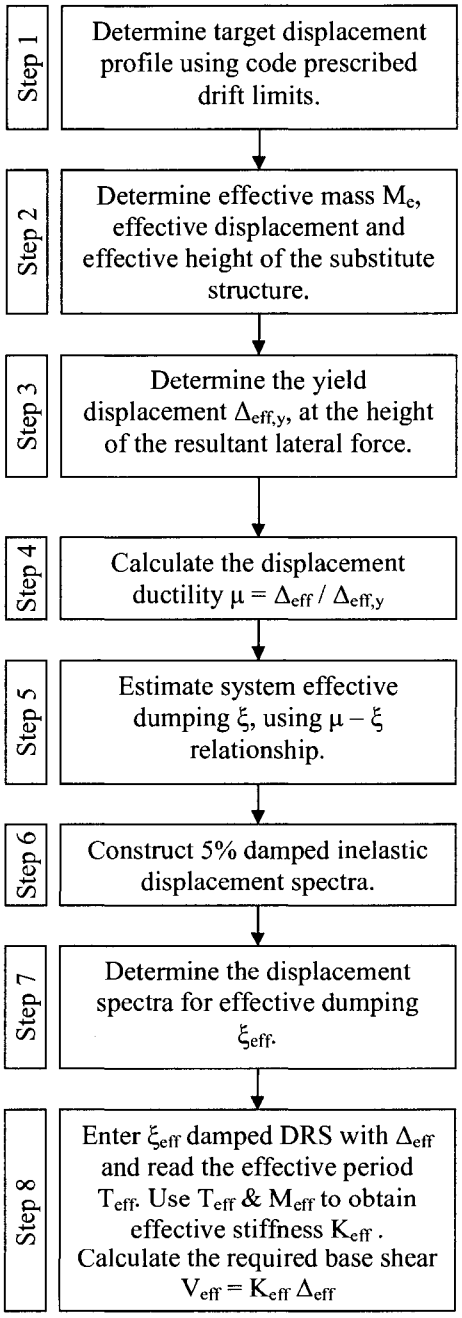

FIG. 3.19 Flowchart of DDBD method (Priestley and Kowalsky, 2000).

damping levels. For comparison purpose Figures 3.20 and 3.21 show development of displacement design response spectra (DDRS) with different damping values, for three specific soil profiles in Montréal and Vancouver. DDRS generation is based on the 5 % damped acceleration design response spectra (ADRS), required by NBCC-2005 (CCBFC 2005) and is performed by a 'home-made' procedure using the program MATLAB. Three specific soil profiles are chosen for the DDRS development, such as : soil profile A, representative for rock and firm soils, C - for intermediate profiles (dense soil) and E - for poor soils or with potential liquifaction.

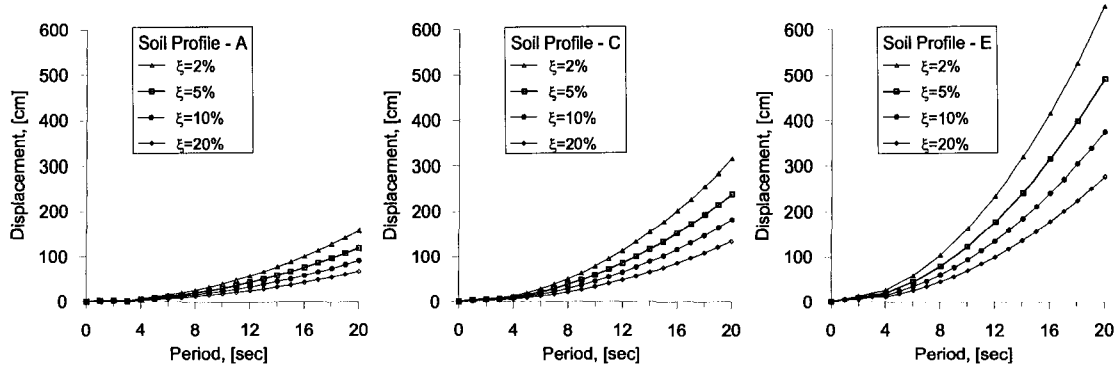

(a) Soil Profile A (b) Soil Profile C (c) Soil Profile E

FIG. 3.20 Displacement response spectrums generated for different damping values for soil profiles A, C and E in Montréal.

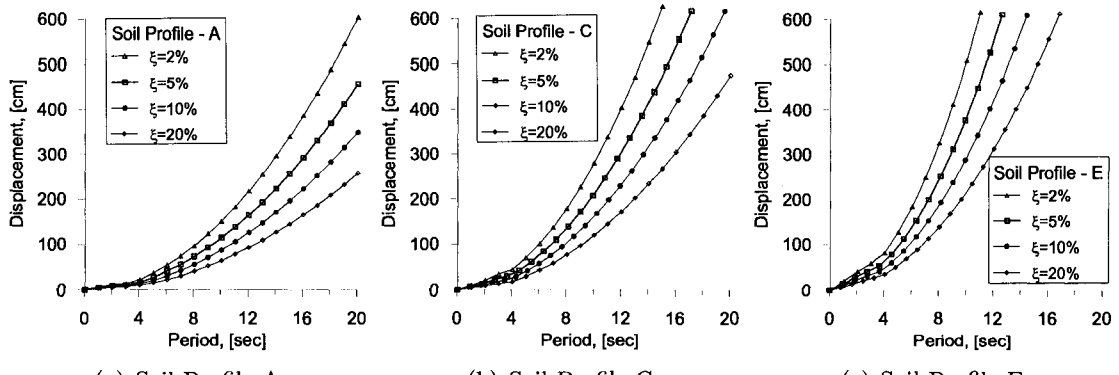

(a) Soil Profile A (b) Soil Profile C (c) Soil Profile E

FIG. 3.21 Displacement response spectrums generated for different damping values for soil profiles A, C and E in Vancouver.

The substitute structure period is expected, in general, to be longer than the one of the

initially elastic structure ($T_{\text{eff}} \approx \sqrt{\mu} T_i$), where T_i is the initial and elastic period. Thus, DDRS are supposed to be developped for longer periods than the expected ADRS. From other side, the DDBD method (Priestley and Kowalsky 2000) impose a limite for the period, because structural displacements, corresponding to longer periods, tend to decrease to the value of peak ground displacement (PGD). The european code of seismicity EC8 (Eurocode 1998) suggests a limit of 3 sec for the period, with the idea that longer values cause displacements absolutely independent of it.

3.5 Inelastic Design Spectra Method

In this text, the Inelastic Design Spectra (IDS) method refers to the direct displacement-based design procedure proposed by Chopra and Goel (1999; 2001) and it is illustrated in the flowchart of Figure 3.22. The method is initially formulated for a SDOF system and its application is illustrated using an example representing a bridge pier (Chopra and Goel 2001). In the present work, the IDS method is generalized to MDOF systems using the substitute structure assumption. The main steps of the method can then be summarized as follows :

Step 1 : The system yield displacement Δ_y is initially estimated as the value, defined in the Direct Displacement-Based Design Method (*Step* 3);

Step 2 : The acceptable hinge inelastic rotation at the base θ_p is assumed, as listed in Table 3.5;

Step 3 : Similarly to Δ_y, the effective target displacement Δ_{eff}, the effective mass M_{eff} and the effective height h_{eff} of the substitute structure are initially estimated, defined in the Direct Displacement-Based Design Method (*Step* 2), using Eqs. (3.60). For the following steps in the iteration procedure Δ_{eff} is defined as per Chopra example (Chopra and Goel 2001) : $\Delta_{\text{eff}} = \Delta_y + h_{\text{eff}}\theta_p$, where Δ_y results from the last iteration step;

Step 4 : Calculate the displacement ductility

$$\mu = \frac{\Delta_{\text{eff}}}{\Delta_y} \tag{3.73}$$

Step 5 : Construct inelastic displacement design spectra for the calculated design ductility μ;

Step 6 : Enter the inelastic displacement spectra with Δ_{eff} to read the corresponding period T_1 for the first iteration ductility;

Step 7 : Compute the initial elastic stiffness k using

$$k = \frac{4\pi^2}{{T_1}^2} M_{\text{eff}}; \tag{3.74}$$

Step 8 : Determine the required yield strength using

$$f_{\text{y}} = f_{\text{req}} = k\Delta_{\text{y}}; \tag{3.75}$$

Step 9 : The required flexural strenght M_{req}, based on the required yield strength is calculated : $M_{\text{req}} = f_{\text{req}} h_{\text{eff}}$. Structural system members are then designed to provide design flexural strength M_{u}, bigger or at least equal to the required flexural strength M_{req};

Step 10 : The initial elastic stiffness is then redefined - $k_{\text{des}} = 3\dfrac{EI_{\text{eff}}}{h_{\text{eff}}^3}$, where the effective system property is defined as - $EI_{\text{eff}} = M_{\text{u}}/\phi_{\text{y}}$.

Step 11 : The corresponding yield displacement is then recalculated : $\Delta_{\text{y,des}} = \dfrac{f_{\text{y}}}{k_{\text{des}}}$ for the so-designed structural system ;

Step 12 : The estimated yield displacement Δ_{y} from Step 1 is compared to the obtained yield displacement $\Delta_{\text{y,des}}$ [*Step* 11];

Step 13 : Steps 1 to 11 are repeated until a desired yield displacement difference is obtained.

Step 14 : The final design shear strength V_{u} corresponds to f_{y}, resulting from the last iteration number.

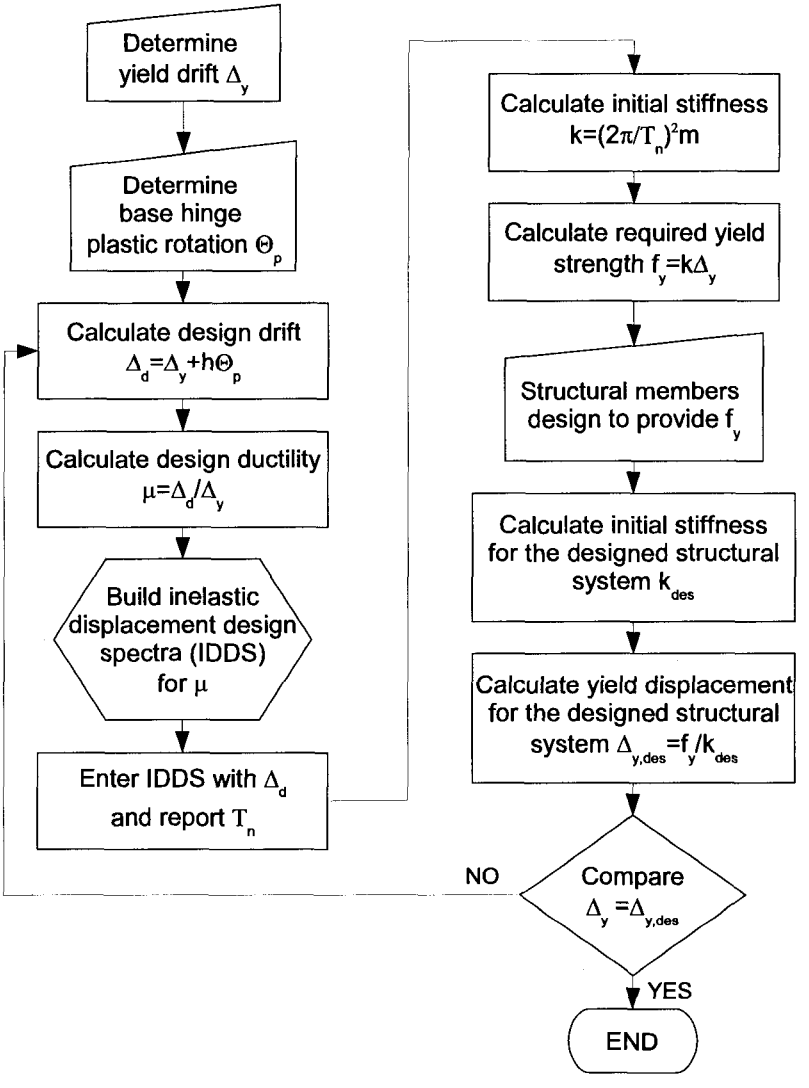

FIG. 3.22 Flowchart of IDS method (Chopra and Goel, 2001).

3.5.1 Comments

For Chopra DBD method performance, some assumptions were implemented in the procedure input data.

- The DBD method using inelastic design spectra, proposed by Chopra and Goel (2001) starts with determination of the system target displacement and corresponding design ductility. For the purpose of the present study, the yield displacement Δ_y, which is used was based on a Priestley and Kowalsky research [Priestley *et al.* 1996] and is described in more details in the presented herein DDBD procedure .
- The target displacement Δ_u is assumed to be the more conservative value from the one, calculated upon the interstorey drift limit, restricted by the NBCC 2005 [CCBFC 2005] and as second, restricted by the plastic rotation at hinge base. A more detailed explanation of Δ_u is included in the afore-mentioned DDBD procedure.
- No recommendations were made in the Displacement-based design method proposed by Chopra for the base shear distribution throughout structure members. Therefore, for the present research study, the vertical distribution of the shear force with respect to weight and height, implemented in the Equivalent Static Force Procedure, required by NBCC 2005, was assumed.
- For calculating the effective elastic stiffness k_{des}, Chopra and Goel refer in a procedure example [Chopra and Goel 2001] to an idealized single degree of freedom (SDF) system with a stiffness, shown in Eq. (3.76) :

$$k_{\text{des}} = \frac{3EI_{\text{eff}}}{h^3}; \tag{3.76}$$

where, E is the elastic modulus of concrete and for I_{eff}, MacGregor's formula for member subjected to lateral load and included in the American Concrete Institute design provisions ACI 318-95, was chosen. As per Canadian concrete norm CSA A23.3-04, Clause 21.2.5.2.1, I_{eff} for shear walls is shown in Eq. (3.77), where I_{g} is the gross wall section property :

$$I_{\text{eff}} = I_{\text{g}} \left(0.6 + \frac{P}{A_{\text{g}}\, f_c'}\right) \tag{3.77}$$

CHAPTER 4

DESIGN ACCORDING TO CANADIAN CODE STANDARDS

4.1 Introduction

This chapter describes the structures studied in this work as well as their design and detailing according to the Canadian code standards : NBCC 2005 (CCBFC 2005) and CSA 23.3-04 (Canadian Standard Association 2004). The main objective of that chapter is to research the seismic performance of a ductile concrete shear wall system, used as a Seismic Force Resisting System in a loading direction for three multistory buildings (6-, 12 and 18-storeys), designed according to the NBCC 2005 and CSA A23.3-04 requirements.

4.2 Buildings Description

Three reinforced concrete frame-shear wall office buildings with the same floor plan shown in Figure 4.1 are considered in the present study. The three buildings have different heights of 21 m, 42 m and 63 m corresponding to 6, 12 and 18 storeys, respectively, as illustrated in Figure 4.1b. The overall dimensions of the buildings are inspired from examples in previous publications [Mitchell and Paultre 1994 ; CPCA 1995]. For easier reference, the 6-, 12- and 18-storey buildings are denoted B6, B12, and B18.

The building foundations are not subject to design in the present study. It is assumed that all lateral load supporting systems have an adequate foundation, capable of transmitting the earthquake induced forces into the ground.

The typical floor plan of the three buildings consists of two 9 m office bays and a central 6 m corridor bay in the longitudinal N-S direction. Resistance to lateral forces in this direction is provided by four concrete frames located following the three bays. In the transversal E-W direction, the lateral force resisting system is made of eight concrete frames and two shear walls. The typical floor area is $A_{\text{floor}} = 24.5 \times 42.5 = 1041.25\,\text{m}^2$.

The structures are symmetrical in both directions, and it is assumed for simplicity that all storeys have the same floor-to-floor height of 3.5 m. A concrete compressive strength $f'_c = 30\,\text{MPa}$, and a steel yield strength $f_y = 400\,\text{MPa}$ are considered. Calculations are conducted assuming that the three buildings are located at the cities of Montréal, Québec, and Vancouver, British Columbia, to account for seismic hazard in Eastern and Western Canada, respectively.

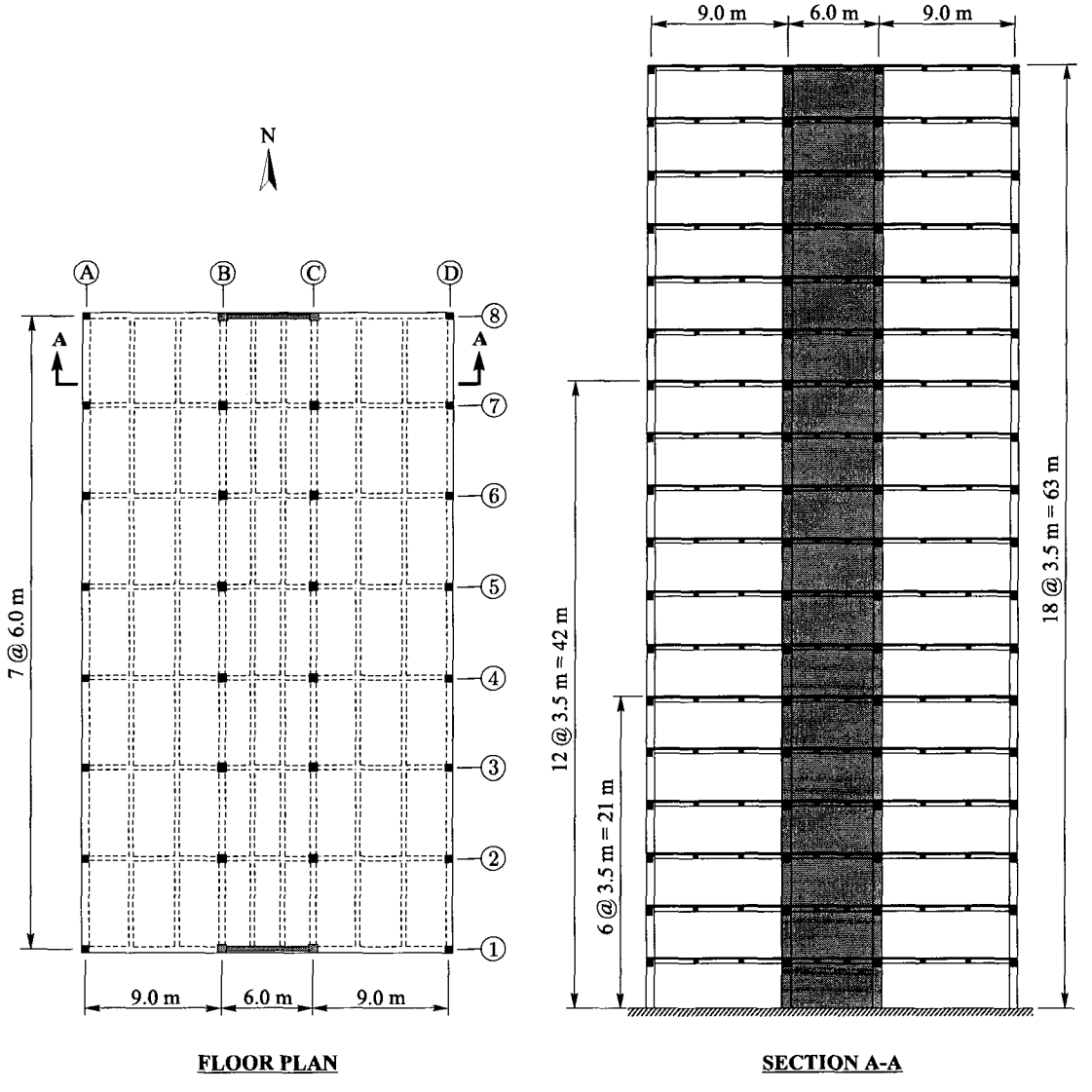

FIG. 4.1 Buildings studied : (a) Typical floor plan ; (b) Elevations.

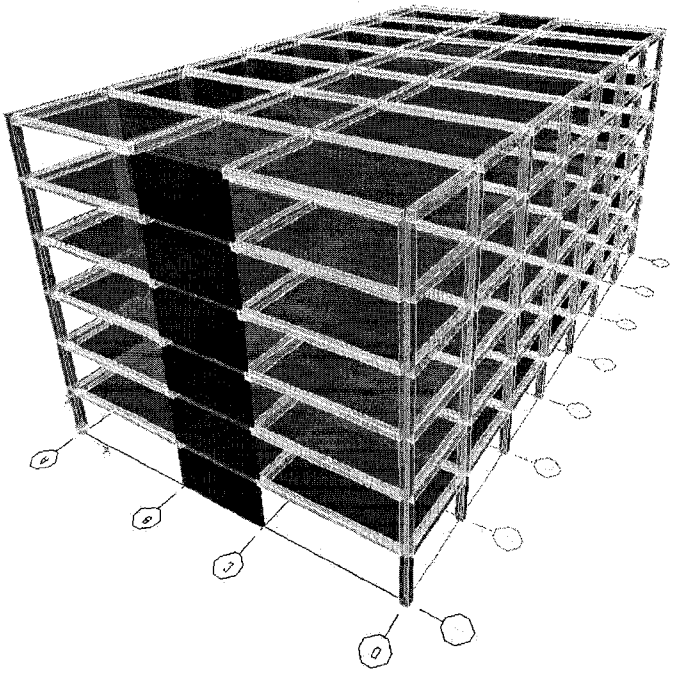

FIG. 4.2 3D view of the 6-storey building.

The one-way slab floor system consists of a 110 mm thick slab spanning in the transverse direction, supported by beams in the longitudinal direction. Primary beams are part of the four moment resisting frames spanning along grid lines A, B, C and D in the longitudinal direction. All other beams in both directions are designated as secondary. The dimensions of primary and secondary beams, as well as of exterior and interior columns for each of the three buildings are listed in Table 4.1.

Wind effects are not included in the present study. As required by NBCC 2005 and specified in previous chapter of that project, the buildings are designed for load combinations including principal loads "$1.0\,D + 1.0\,E$", and principal and companion loads[1] "$1.0\,D + 1.0\,E + 0.5\,L + 0.25\,S$". The next two sections describe the gravity and seismic loads considered to design the three buildings.

[1]The building is not intended for a storage occupancy, equipment area or service room

TAB. 4.1 Dimensions of the beams and columns of the three buildings studied.

		Columns		Beams	
Building	Level	Exterior (mm)	Interior (mm)	Primary (mm)	Secondary (mm)
B6	1–6	500×500	550×550	400×550	300×350
B12	7–12	500×500	550×550	400×550	300×350
	1–6	500×500	600×600	400×600	300×350
B18	13–18	500×500	550×550	400×550	300×350
	11–12	500×500	600×600	400×550	300×350
	1–10	500×500	600×600	400×600	300×350

4.3 Gravity Loads

The dead and live loads acting on the three buildings are determined according to NBCC 2005 requirements for a building with office occupancy. A typical office floor loading of $2.4\,\mathrm{kN/m^2}$ is applied all over the floor areas except at the 6 m–wide corridor bay where an assembly floor loading of $4.8\,\mathrm{kN/m^2}$ is considered. Additional dead loads of $0.5\,\mathrm{kN/m^2}$ and $0.5\,\mathrm{kN/m^2}$ are applied at all floor levels to represent partition and mechanical equipment loadings, respectively. A dead load of $1.0\,\mathrm{kN/m^2}$ is added to the self-weight of the roof slab to account for architectural roof specifications, such as insulation, hydro-membrane, gravel and possible mechanical outlets. The roof snow loading S is determined using the formula given in Article 4.1.6.2 of NBCC 2005

$$S = I_s\left[S_s(C_b C_w C_s C_a) + S_r\right] \tag{4.1}$$

where

- I_s is the importance factor for snow load [Table 4.1.6.2][2] ;
- S_s is the 1-in-50 year ground snow load in kPa [Appendix C, Table C-2][2] ;

[2]Reference to NBCC 2005 [CCBFC 2005]

- C_b is the basic roof load factor [Art. 4.1.6.2 (2)][2];
- C_w is the wind exposure factor [Art. 4.1.6.2 (2)–(3)][2];
- C_s is the slope factor [Art. 4.1.6.2 (5)–(7)][2];
- C_a is the shape factor [Art. 4.1.6.2 (8)][2];
- S_r is the 1-in-50 year associated rain load in kPa [Appendix C, Table C-2][2]. S_r must be less than $S_s(C_b C_w C_s C_a)$

The following coefficients are considered for the buildings studied

$$I_s = 1\,; \qquad C_b = 0.8\,; \qquad C_w = 1\,; \qquad C_s = 1\,; \qquad C_a = 1$$

According to Table C-2 of Appendix C, the following 1-in-50 year ground snow load and associated rain load are adopted

$$\begin{aligned} \text{Montréal} &: \quad S_s = 2.6\,\text{kPa}\,; \quad S_r = 0.4\,\text{kPa} \\ \text{Vancouver} &: \quad S_s = 1.8\,\text{kPa}\,; \quad S_r = 0.2\,\text{kPa} \end{aligned}$$

which yields the snow loads

$$\begin{aligned} \text{Montréal} &: \quad S = 1 \times [2.6 \times (0.8 \times 1 \times 1 \times 1) + 0.4] = 2.48\,\text{kN/m}^2 \\ \text{Vancouver} &: \quad S = 1 \times [1.8 \times (0.8 \times 1 \times 1 \times 1) + 0.2] = 1.64\,\text{kN/m}^2 \end{aligned}$$

Table 4.2 summarizes the dead and live loads acting on the buildings.

The axial load transmitted through each shear wall is calculated as suggested in Table 4.1.3.2 of the NBCC 2005, considering a combination of " 100% dead load + 50% live load" for all floor levels and a combination of " 100% dead load + 25% snow load" at the roof level. According to Art. 1.1.5.9 of the NBCC 2005, live loads excluding snow loading are reduced as a function of the structural element tributary area A. In this case, a reduction factor of $0.3 + \sqrt{9.8/A}$ is applied to tributary areas A greater that $20\,\text{m}^2$. Tables 4.3 to 4.8 present the variation with height of axial load carried by each shear wall,

TAB. 4.2 Dead and live loads considered.

Loading location	and type	Load (kN/m^2)	Description
Roof :	Live	2.48	Full snow load for Montréal
		1.64	Full snow load for Vancouver
	Dead	1.0	Roofing and mechanical service loading
Floor :	Live	2.4	Typical office floor loading on two 9 m–wide bays
	Live	4.8	Typical assembly floor loading on 6 m–wide corridor bay
	Dead	–	Reinforced concrete structural members, calculated at 23.5 kN/m^2
	Dead	0.5	Typical partition loading on all floors
	Dead	0.5	Typical mechanical service loading on all floors

as well as the corresponding total axial load at the center of mass of each of the three buildings studied. Details of load calculations are given in Appendix I.

TAB. 4.3 Axial loading transmitted by a shear wall in B6 building.

		Montréal		Vancouver	
	Dead load	Live load	Cumulated load	Live load	Cumulated load
	P_{DL}	P_{LL}	$P_{DL} + 0.5P_{LL}$	P_{LL}	$P_{DL} + 0.5P_{LL}$
Level	(kN)	(kN)	(kN)	(kN)	(kN)
6	423	123	453	81	443
5	405	148	933	148	922
4	405	124	1400	124	1390
3	405	120	1866	120	1855
2	405	118	2330	118	2320
1	405	105	2788	105	2777

4.4 Seismic Loads

4.4.1 Basic Assumptions and Parameters

The present study focuses on the seismic response of the considered buildings in the N-S direction (Figure 4.1). Although the lateral resistance in this direction is provided by the combined action of moment frames and cantilever shear walls, it is assumed for simplicity that the N-S horizontal seismic loads are resisted only by the two shear walls, where half of the total seismic load in the considered direction is transmitted to each wall. Columns and beams are assumed to resist only gravity loads. A site class C (Firm soil) is considered. According to Table 4.1.8.9 of the NBCC 2005, ductility and over-strength factors for a ductile shear wall are taken as $R_d = 3.5$ and $R_o = 1.6$. An importance factor $I_E = 1$ is considered for a building with a normal importance as per Table 4.1.8.5 of the NBCC 2005. Denoting h_w the total height (in meters) above the base of each building, the fundamental lateral period T_a of the structure is determined as per Article 4.1.8.11

TAB. 4.4 Total axial load acting at the center of mass of the B6 building.

		Montréal		Vancouver	
	Dead load	Snow load	Cumulated load	Snow load	Cumulated load
	P_{DL}	P_{SL}	$P_{DL} + 0.25P_{SL}$	P_{SL}	$P_{DL} + 0.25P_{SL}$
Level	(kN)	(kN)	(kN)	(kN)	(kN)
6	6647	2582	7293	1708	7074
5	6509	–	13802	–	13583
4	6509	–	20311	–	20092
3	6509	–	26819	–	26601
2	6509	–	33328	–	33110
1	6509	–	39837	–	39619

of the NBCC 2005 and equation (2.4), yielding periods of 0.49 s, 0.82 s and 1.12 s for the B6, B12 and B18 buildings, respectively.

According to Article 4.1.8.11.d of the NBCC 2005, other established methods of structural mechanics can be used to determine the fundamental period, provided that the result is less than twice the vibration period calculated using Eq. (2.4).

In the present work, the three buildings are modeled using the commercial software for structural analysis ETABS (Computers and Structures Inc, 2004). A three-dimensional model of the buildings was used. A 3-D view of the 6-storey building is shown in Figure 4.2. The seismic mass of each floor level as assigned as a lumped mass at the center of mass of each storey. All the floor slabs were modelled as rigid diaphragms.

To account for cracking of structural members under seismic excitation, effective member properties obtained by reducing the initial gross section properties are used as described in Clause 21.2.5.2 of the CSA-A23.3-04. According to Table 21.1 of CSA-A23.3-04, the effective moments of inertia of the structural slabs and beams are the gross properties multiplied by reduction coefficients of 0.2 and 0.4, respectively. The effective member

TAB. 4.5 Axial loading transmitted by a shear wall in the B12 building.

		Montréal		Vancouver	
	Dead load	Live load	Cumulated load	Live load	Cumulated load
	P_{DL}	P_{LL}	$P_{DL} + 0.5P_{LL}$	P_{LL}	$P_{DL} + 0.5P_{LL}$
Level	(kN)	(kN)	(kN)	(kN)	(kN)
12	423	123	453	81	443
11	405	148	933	148	922
10	405	124	1400	124	1390
9	405	120	1866	120	1855
8	405	118	2330	118	2320
7	405	105	2788	105	2777
6	408	92	3242	92	3231
5	408	90	3695	90	3684
4	408	88	4147	88	4136
3	408	87	4598	87	4587
2	408	86	5048	86	5038
1	408	85	5499	85	5488

TAB. 4.6 Total axial load acting at the center of mass of the B12 building.

		Montréal		Vancouver	
	Dead load	Snow load	Cumulated load	Snow load	Cumulated load
	P_{DL}	P_{SL}	$P_{DL} + 0.25P_{SL}$	P_{SL}	$P_{DL} + 0.25P_{SL}$
Level	(kN)	(kN)	(kN)	(kN)	(kN)
12	6647	2582	7293	1708	7074
11	6509	–	13802	–	13583
10	6509	–	20311	–	20092
9	6509	–	26819	–	26601
8	6509	–	33328	–	33110
7	6509	–	39837	–	39619
6	6632	–	46469	–	46179
5	6632	–	53100	–	52738
4	6632	–	59732	–	59370
3	6632	–	66363	–	66001
2	6632	–	72995	–	72633
1	6632	–	79626	–	79264

TAB. 4.7 Axial loading transmitted by a shear wall in the B18 building.

		Montréal		Vancouver	
	Dead load	Live load	Cumulated load	Live load	Cumulated load
	P_{DL}	P_{LL}	$P_{DL} + 0.5P_{LL}$	P_{LL}	$P_{DL} + 0.5P_{LL}$
Level	(kN)	(kN)	(kN)	(kN)	(kN)
18	423	123	453	81	443
17	405	148	933	148	922
16	405	124	1400	124	1390
15	405	120	1866	120	1855
14	405	118	2330	118	2320
13	405	105	2788	105	2777
12	405	92	3239	92	3229
11	405	90	3690	90	3679
10	408	88	4141	88	4131
9	408	87	4593	87	4582
8	408	86	5043	86	5033
7	408	85	5494	85	5483
6	408	84	5943	84	5933
5	408	83	6392	83	6382
4	408	82	6841	82	6831
3	408	81	7290	81	7280
2	408	81	7738	81	7728
1	408	80	8186	80	8176

TAB. 4.8 Total axial load acting at the center of mass of the B18 building.

		Montréal		Vancouver	
	Dead load	Snow load	Cumulated load	Snow load	Cumulated load
	P_{DL}	P_{SL}	$P_{DL} + 0.25P_{SL}$	P_{SL}	$P_{DL} + 0.25P_{SL}$
Level	(kN)	(kN)	(kN)	(kN)	(kN)
18	6647	2582	7293	1708	7074
17	6509	–	13802	–	13583
16	6509	–	20311	–	20092
15	6509	–	26819	–	26601
14	6509	–	33328	–	33110
13	6509	–	39837	–	39619
12	6560	–	46397	–	46179
11	6560	–	52957	–	52738
10	6632	–	59589	–	59370
9	6632	–	66220	–	66001
8	6632	–	72852	–	72633
7	6632	–	79483	–	79264
6	6632	–	86115	–	85896
5	6632	–	92746	–	92527
4	6632	–	99378	–	99159
3	6632	–	106009	–	105790
2	6632	–	112641	–	112422
1	6632	–	119272	–	119053

properties for column and wall members depend on the level of axial compression acting at each floor level. Tables 4.9 to 4.11 present the variation of the reduction coefficients for columns and walls along building height. The notations P_W, P_{IC} and P_{EC} designate the axial loading transferred through a shear wall (SW), an internal column(IC) and an external column (EC), respectively. Detailed calculations are shown for a single shear wall in Appendix I. The reduction coefficients are obtained according to Clause 21.2.5.2.2 of the CSA-A23.3-04

$$\alpha_C = 0.5 + 0.6\frac{P_s}{f'_c A_g} \tag{4.2}$$

$$\alpha_W = 0.6 + \frac{P_s}{f'_c A_g} \tag{4.3}$$

where P_s is the axial load P_W, P_{IC} or P_{EC} at the base of the wall, f'_c the concrete compressive strength and A_g the corresponding member gross area.

TAB. 4.9 Effective Member Reduction Coefficients for the B6 building.

	Montréal			Vancouver			Reduction		
	Axial Loading			Axial Loading			Coefficients		
	P_W	P_{IC}	P_{EC}	P_W	P_{IC}	P_{EC}	α_W	α_{IC}	α_{EC}
Level	(kN)	(kN)	(kN)	(kN)	(kN)	(kN)	–	–	–
6	453	272	177	443	262	171	0.61	0.52	0.51
5	933	579	366	922	570	360	0.61	0.54	0.53
4	1400	875	544	1390	866	538	0.62	0.56	0.54
3	1866	1170	719	1855	1160	714	0.63	0.58	0.56
2	2330	1463	894	2320	1453	889	0.63	0.60	0.57
1	2788	1749	1069	2777	1740	1063	0.64	0.62	0.59

Tables 4.9, 4.10 and 4.11 clearly show that the snow loading difference in Montréal and Vancouver sites reflects negligibly the total tributary loading to both shear walls and columns (interior and exterior) in a way, that the corresponding reduction coefficients

TAB. 4.10 Effective Member Reduction Coefficients for the B12 building.

	Montréal			Vancouver			Reduction		
	Axial Loading			Axial Loading			Coefficients		
	P_W	P_{IC}	P_{EC}	P_W	P_{IC}	P_{EC}	α_W	α_{IC}	α_{EC}
Level	(kN)	(kN)	(kN)	(kN)	(kN)	(kN)	–	–	–
12	453	272	177	443	262	171	0.61	0.52	0.51
11	933	579	366	922	570	360	0.61	0.54	0.53
10	1400	875	544	1390	866	538	0.62	0.56	0.54
9	1866	1170	719	1855	1160	714	0.63	0.58	0.56
8	2330	1463	894	2320	1453	889	0.63	0.60	0.57
7	2788	1749	1069	2777	1740	1063	0.64	0.62	0.59
6	3242	2037	1243	3231	2027	1237	0.65	0.61	0.60
5	3695	2323	1417	3684	2314	1411	0.65	0.63	0.61
4	4147	2609	1591	4136	2600	1585	0.66	0.64	0.63
3	4598	2894	1764	4587	2885	1759	0.67	0.66	0.64
2	5048	3179	1938	5038	3169	1932	0.67	0.68	0.66
1	5499	3463	2111	5488	3453	2105	0.68	0.69	0.67

TAB. 4.11 Effective Member Reduction Coefficients for the B18 building.

	Montréal			Vancouver			Reduction		
	Axial Loading			Axial Loading			Coefficients		
	P_W	P_{IC}	P_{EC}	P_W	P_{IC}	P_{EC}	α_W	α_{IC}	α_{EC}
Level	(kN)	(kN)	(kN)	(kN)	(kN)	(kN)	–	–	–
18	453	272	177	443	262	171	0.61	0.52	0.51
17	933	579	366	922	570	360	0.61	0.54	0.53
16	1400	875	544	1390	866	538	0.62	0.56	0.54
15	1866	1170	719	1855	1160	714	0.63	0.58	0.56
14	2330	1463	894	2320	1453	889	0.63	0.60	0.57
13	2788	1749	1069	2777	1740	1063	0.64	0.62	0.59
12	3239	2034	1242	3229	2025	1237	0.65	0.61	0.60
11	3690	2318	1416	3679	2308	1410	0.65	0.63	0.61
10	4141	2604	1592	4131	2594	1586	0.66	0.64	0.63
9	4593	2889	1768	4582	2879	1762	0.67	0.66	0.64
8	5043	3173	1943	5033	3164	1938	0.67	0.68	0.66
7	5494	3457	2119	5483	3448	2113	0.68	0.69	0.67
6	5943	3741	2294	5933	3731	2289	0.68	0.71	0.68
5	6392	4024	2470	6382	4014	2464	0.69	0.72	0.70
4	6841	4306	2645	6831	4297	2639	0.70	0.74	0.71
3	7290	4589	2820	7280	4579	2814	0.70	0.75	0.73
2	7738	4871	2995	7728	4861	2989	0.71	0.77	0.74
1	8186	5153	3170	8176	5143	3164	0.72	0.79	0.75

for calculating members effective properties are equal for both cities. An estimation of reduction coefficients average values for corresponding members and structure models is generalized in Table 4.12.

TAB. 4.12 Average Effective Member Reduction Coefficients.

		Column	
Building	Shear wall	Interior	Exterior
B6	0.62	0.57	0.55
B12	0.64	0.61	0.59
B18	0.66	0.66	0.63

However, structural members modeling for all buildings and for both cites, performed throughout the ETABS software, was based on the specific reduction coefficients corresponding to each structural member (shear wall, interior and exterior column). The shear walls modelling was based on the differentiated coefficients by floors, as listed in Tables 4.9 to 4.11. The columns modelling as based on the average coefficients, listed in Table 4.12.

The modal analysis of each of the three buildings resulted in the following fundamental mode periods 1.71 s, 3.12 s and 5.19 s for the B6, B12 and B18 buildings, respectively. For the three buildings, modal analyses lead to periods greater than twice that determined using Eq. (2.4). Consequently, seismic lateral load calculations, according the ESFP are conducted using fundamental periods twice the period prescribed by the code (Eq. 2.4 of that project), yielding 0.98 s, 1.64 s and 2.24 s for the B6, B12 and B18 buildings, respectively, shown in Figure 4.3.

4.4.2 Design Spectral Accelerations

As mentioned above, the three buildings are designed for Montréal and Vancouver sites. The NBCC 2005 prescribed Seismic Hazard Level is defined by a 2% probability of exceedance in 50 years, which corresponds to a return period of approximately 2500 years.

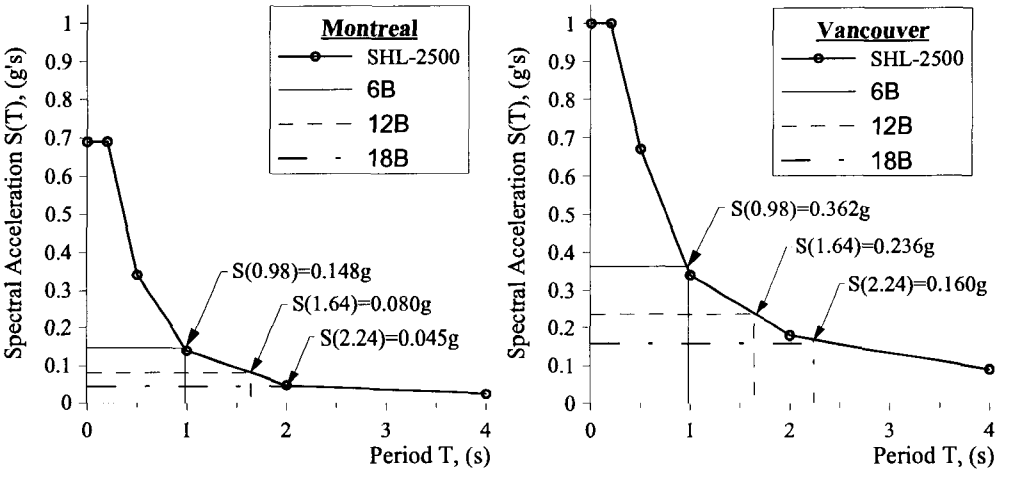

(a) Montréal design spectrum (b) Vancouver design spectrum

FIG. 4.3 Design spectral response acceleration values for B6, B12 and B18 buildings in Montréal and Vancouver.

The corresponding median (50^{th} percentile) 5% damped spectral response accelerations expressed as a ratio to gravitational acceleration g are listed in Table 4.13 for the cities of Montréal and Vancouver, respectively [CCBFC 2005]. The values are given for the reference firm soil ground conditions of site Class C, and at periods of 0.2, 0.5, 1.0 and 2.0 seconds.

According to Article 4.1.8.4.4 of the NBCC 2005, the acceleration and velocity based site coefficients F_{a} and F_{v} are obtained from Tables 4.1.8.4.B and 4.1.8.4.C using linear interpolation for intermediate values of $S_{\text{a}}(0.2)$ and $S_{\text{a}}(1.0)$, yielding $F_{\text{a}} = 1.0$ and $F_{\text{v}} = 1.0$. The design spectral accelerations $S(T)$ are determined using linear interpolation for intermediate values of period T as specified in Article 4.1.8.4.6 of the NBCC 2005. These

calculations are presented next for Montréal :

$$\text{For } T \leqslant 0.2\,\text{s}: \quad S(T) = F_\text{a}\, S_\text{a}(0.2) = 1.0 \times 0.69\,\text{g} = 0.69\,\text{g}$$

$$T = 0.5\,\text{s}: \quad S(T) = \min[F_\text{v}\, S_\text{a}(0.5); F_\text{a}\, S_\text{a}(0.2)] = 1.0 \times 0.34\,\text{g} = 0.34\,\text{g}$$

$$T = 1.0\,\text{s}: \quad S(T) = F_\text{v}\, S_\text{a}(1.0) = 1.0 \times 0.14\,\text{g} = 0.14\,\text{g}$$

$$T = 2.0\,\text{s}: \quad S(T) = F_\text{v}\, S_\text{a}(2.0) = 1.0 \times 0.048\,\text{g} = 0.048\,\text{g}$$

$$T \geqslant 4.0\,\text{s}: \quad S(T) = \frac{1}{2} F_\text{v}\, S_\text{a}(2.0) = \frac{1}{2} \times 1.0 \times 0.048\,\text{g} = 0.024\,\text{g}$$

TAB. 4.13 Median spectral response accelerations for the cities of Montréal and Vancouver.

	Spectral response accelerations			
Location	$S_\text{a}(0.2)$ (g)	$S_\text{a}(0.5)$ (g)	$S_\text{a}(1.0)$ (g)	$S_\text{a}(2.0)$ (g)
Montréal	0.690	0.340	0.140	0.048
Vancouver	1.000	0.670	0.340	0.180

4.4.3 Seismic Lateral Load Calculations

For convenient reference, seismic lateral load calculations are illustrated here for the B6 building located at Montréal and subjected to a seismic hazard corresponding to 2% probability of exceedance in 50 years. To obtain the seismic design forces, a Dynamic Analysis Procedure is recommended in the NBCC 2005 [Art. 4.1.8.12] and used for design in that project. The Equivalent Static Force Procedure [Art. 4.1.8.11], known from former code edition may be used only for structures that meet some specific conditions, described in the previous chapter of the present work. For the buildings studied herein, the orthogonal directions coincide with the N-S and E-W directions.

The structures B6 and B12 studied herein satisfy the second condition and the equivalent static force procedure (ESFP) could be applied. For the B18, as adopted in that project,

the ESFP is not permitted by the NBCC 2005 for both height and fundamental period do not correspond to the conditions, previously specified. For illustrational purpose, the step by step procedure is described here for the B6 building in Montréal :

Step 1 : The fundamental period used for seismic load calculations for the B6 building is $T_{\mathrm{a}} = 0.98\,\mathrm{s}$ [Section 4.4.1].

Step 2 : The spectral acceleration $S(T_{\mathrm{a}})$ is determined using line interpolation between $S(0.5) = 0.34\,\mathrm{g}$ and $S(1.0) = 0.14\,\mathrm{g}$ for $T_{\mathrm{a}} = 0.98\,\mathrm{s}$

$$S(T_{\mathrm{a}}) = \frac{0.98 - 1.0}{0.5 - 1.0}\Big[S(0.5) - S(1.0)\Big] + S(1.0) = 0.148\,\mathrm{g}$$

Step 3 : The importance, ductility and over strength factors for a ductile shear wall are taken as $I_{\mathrm{E}} = 1$, $R_{\mathrm{d}} = 3.5$ and $R_{\mathrm{o}} = 1.6$ [Section 4.4.1].

Step 4 : The higher mode factor $M_{\mathrm{v}} = 1.0$ is determined from Table 4.1.8.11 for fundamental period $T_{\mathrm{a}} = 0.98\,\mathrm{s} \leqslant 1.0\,\mathrm{s}$ and ratio

$$\frac{S_{\mathrm{a}}(0.2)}{S_{\mathrm{a}}(2.0)} = \frac{0.69}{0.048} = 14.38 \geqslant 8.0$$

Step 5 : The base shear is given by [Art. 4.1.8.11]

$$V = \frac{S(T_{\mathrm{a}})M_{\mathrm{v}}I_{\mathrm{E}}}{R_{\mathrm{d}}R_{\mathrm{o}}}\,W = \frac{0.148 \times 1.0 \times 1.0}{3.5 \times 1.6}\,W = 0.0264\,W$$

The base shear shall not be less than V_{min}

$$V_{\mathrm{min}} = \frac{S(2.0)M_{\mathrm{v}}I_{\mathrm{E}}}{R_{\mathrm{d}}R_{\mathrm{o}}}\,W = \frac{0.048 \times 1.0 \times 1.0}{3.5 \times 1.6} = 0.0086\,W$$

and since $R_{\mathrm{d}} = 1.6 \geqslant 1.5$, V shall not be greater that V_{max}

$$V_{\mathrm{max}} = \frac{2}{3}\,\frac{S(0.2)M_{\mathrm{v}}I_{\mathrm{E}}}{R_{\mathrm{d}}R_{\mathrm{o}}}\,W = \frac{2 \times 0.69 \times 1.0 \times 1.0}{3 \times 3.5 \times 1.6}\,W = 0.0821\,W$$

Considering the seismic load of the B6 building $W = 39626\,\mathrm{kN}$, the design

base shear is

$$V = 0.0264\,W = 0.0264 \times 39837 = 1050\,\text{kN}$$

Step 6 : The base shear force is vertically distributed over the height of the building. The force concentrated at the roof level is

$$F_\text{t} = 0.07\,T_\text{a}\,V = 0.07 \times 0.98 \times 1050 = 72\,\text{kN}$$

which is less than

$$F_{t,\text{max}} = 0.25\,V = 0.25 \times 1050 = 263\,\text{kN}$$

The remainder of the lateral force, $V - F_\text{t}$ is distributed along the building height, including the top level, as given by the formula in Art. 4.1.8.11 6

$$F_x = (V - F_\text{t}) \left(\frac{W_x h_x}{\sum_{i=1}^{6} W_i h_i} \right)$$

Tables 4.14 to 4.16 summarize the lateral load and shear force calculations for the B6, B12 and B18 buildings located in Montréal, calculated through Equivalent Static Force Procedure without taking into account the accidental torsion effect.

Following tables 4.17 to 4.19 summarize the lateral load and shear force calculations for the B6, B12 and B18 buildings located in Vancouver, calculated through Equivalent Static Force Procedure without taking into account the accidental torsion effect.

4.5 Spectral Analysis Results

Table 4.21 summarize the design values for the lateral earthquake force at the base of each model shear wall, denoted as V_f. As shown in section 2.2, the dynamic lateral earthquake

TAB. 4.14 Lateral load calculations for the B6 building, located in Montréal.

Floor level	Height h_x (m)	Weight W_x (kN)	Lateral Force F_x (kN)	Shear Force V_x (kN)
6	21.00	7293	375	375
5	17.50	6509	225	600
4	14.00	6509	180	780
3	10.50	6509	135	915
2	7.00	6509	90	1005
1	3.50	6509	45	1050

TAB. 4.15 Lateral load calculations for the B12 building, located in Montréal.

Floor level	Height h_x (m)	Weight W_x (kN)	Lateral Force F_x (kN)	Shear Force V_x (kN)
12	42.00	7293	478	478
11	38.50	6509	220	698
10	35.00	6509	200	898
9	31.50	6509	180	1078
8	28.00	6509	160	1238
7	24.50	6509	140	1378
6	21.00	6632	122	1500
5	17.50	6632	102	1602
4	14.00	6632	82	1684
3	10.50	6632	61	1745
2	7.00	6632	41	1785
1	3.50	6632	20	1806

TAB. 4.16 Lateral load calculations for the B18 building, located in Montréal.

Floor level	Height h_x (m)	Weight W_x (kN)	Lateral Force F_x (kN)	Shear Force V_x (kN)
18	63.00	7293	632	632
17	59.50	6509	195	827
16	56.00	6509	184	1011
15	52.50	6509	172	1184
14	49.00	6509	161	1345
13	45.50	6509	149	1494
12	42.00	6560	139	1633
11	38.50	6560	127	1761
10	35.00	6632	117	1878
9	31.50	6632	105	1983
8	28.00	6632	94	2077
7	24.50	6632	82	2159
6	21.00	6632	70	2229
5	17.50	6632	59	2288
4	14.00	6632	47	2335
3	10.50	6632	35	2370
2	7.00	6632	23	2393
1	3.50	6632	12	2405

TAB. 4.17 Lateral load calculations for the B6 building, located in Vancouver.

Floor level	Height h_x (m)	Weight W_x (kN)	Lateral Force F_x (kN)	Shear Force V_x (kN)
6	21.00	7074	874	874
5	17.50	6509	539	1413
4	14.00	6509	431	1845
3	10.50	6509	323	2168
2	7.00	6509	216	2384
1	3.50	6509	108	2491

TAB. 4.18 Lateral load calculations for the B12 building, located in Vancouver.

Floor level	Height h_x (m)	Weight W_x (kN)	Lateral Force F_x (kN)	Shear Force V_x (kN)
12	42.00	7074	958	958
11	38.50	6509	450	1409
10	35.00	6509	409	1818
9	31.50	6509	369	2187
8	28.00	6509	328	2514
7	24.50	6509	287	2801
6	21.00	6632	248	3048
5	17.50	6632	206	3255
4	14.00	6632	167	3422
3	10.50	6632	125	3547
2	7.00	6632	83	3630
1	3.50	6632	42	3672

TAB. 4.19 Lateral load calculations for the B18 building, located in Vancouver.

Floor level	Height h_x (m)	Weight W_x (kN)	Lateral Force F_x (kN)	Shear Force V_x (kN)
18	63.00	7074	1155	1155
17	59.50	6509	379	1534
16	56.00	6509	357	1890
15	52.50	6509	334	2225
14	49.00	6509	312	2537
13	45.50	6509	290	2826
12	42.00	6560	270	3096
11	38.50	6560	247	3343
10	35.00	6632	227	3570
9	31.50	6632	204	3775
8	28.00	6632	182	3956
7	24.50	6632	159	4115
6	21.00	6632	136	4251
5	17.50	6632	114	4365
4	14.00	6632	91	4456
3	10.50	6632	68	4524
2	7.00	6632	45	4569
1	3.50	6632	23	4592

force, V_d is calculated through multiplying the elastic shear force at the base V_e by the ratio $\left(\frac{I_E}{R_d R_o}\right)$. Although all models structure is determined as regular, as demonstrated in Annex II for B calculated by Eq. 2.8, the design base shear V_f is the greater value of $100\%V$ and V_d. Both values of V and V_d were obtained using the 3-D modelized buildings in ETABS, as previously noted in the present chapter. Both models were performed including the accidental torsional effects, according to Eq. 2.7. The lateral forces used for the static loading pattern is calculated according Eq. 2.5 for the minimum lateral force V, Eq. 2.1. Forces F_x are tabulated by floors for each model in Tables 4.14 to 4.19.

TAB. 4.20 Shear strengths at the base of buildings in B6, B12 and B18models, located in Montréal and Vancouver.

	Montréal			Vancouver		
	B6	B12	B18	B6	B12	B18
Site coefficients F_a or F_v	1	1	1	1	1	1
Fundamental period T_a (s)	0.98	1.65	2.24	0.98	1.65	2.24
Spectral accel. $S(T_a)$ (g)	0.148	0.080	0.045	0.352	0.236	0.160
Product $S(T_a)M_v$	0.148	0.127	0.113	0.352	0.259	0.192
Importance factor I_E	1.0	1.0	1.0	1.0	1.0	1.0
Force modification factor R_d	3.5	3.5	3.5	3.5	3.5	3.5
Force modification factor R_o	1.6	1.6	1.6	1.6	1.6	1.6
Seismic building weight W (kN)	39837	79626	119272	39619	79264	119053
Static base shear V (kN)						
Acc. torsion not included	1050	1806	2405	2491	3672	4592

Tables 4.22 to 4.24 summarize walls design shear (V_f), moment (M_f) and displacement (Δ_{des}) values for the B6, B12 and B18 buildings located in Montréal and Vancouver, resulting from Spectral Analysis (included accidental torsion effect). The displacement values, noted in that tables as Δ_{des}, represent the total lateral deflection of the walls at the building roof : $\Delta_{des} = \Delta_f R_d R_o$.

TAB. 4.21 Flexural and shear strengths at the base of one shear wall under design loads in B6, B12 and B18models, located in Montréal and Vancouver.

	Montréal			Vancouver		
	B6	B12	B18	B6	B12	B18
Static base shear V (kN)						
Acc. torsion included	622	1069	1427	1469	2336	2718
Dynamic base shear V_d (kN)	791	828	863	1581	1804	1823
Design base shear V_f (kN)	791	1069	1427	1581	2336	2718
Design base overturning moment M_f (kNm)	7556	9193	14369	13460	22981	34185

TAB. 4.22 Spectral analysis results for one shear wall in B6 building, located in Montréal and Vancouver.

	Montréal			Vancouver		
Level	V_f (kN)	M_f (kNm)	Δ_{des} (m)	V_f (kN)	M_f (kNm)	Δ_{des} (m)
6	313	804	0.050	530	1353	0.116
5	369	2319	0.031	909	3210	0.087
4	369	3271	0.022	1190	5505	0.063
3	479	4147	0.014	1379	8017	0.040
2	640	5438	0.007	1468	10669	0.021
1	791	7555	0.003	1581	13460	0.007

TAB. 4.23 Spectral analysis results for one shear wall in B12 building, located in Montréal and Vancouver.

	Montréal			Vancouver		
Level	V_f (kN)	M_f (kNm)	Δ_{des} (m)	V_f (kN)	M_f (kNm)	Δ_{des} (m)
12	297	746	0.187	599	1495	0.625
11	432	1560	0.165	886	3142	0.553
10	448	2296	0.144	998	4784	0.482
9	411	2830	0.123	1043	6273	0.413
8	406	3212	0.104	1090	7693	0.345
7	453	3453	0.085	1174	9002	0.279
6	517	3565	0.067	1317	10438	0.218
5	593	3866	0.051	1500	12097	0.161
4	712	4233	0.036	1707	14001	0.112
3	859	5102	0.023	1933	16513	0.068
2	968	6385	0.012	2093	19327	0.033
1	1069	9193	0.004	2336	22981	0.011

TAB. 4.24 Spectral analysis results for one shear wall in a B18 building, located in Montréal and Vancouver.

	Montréal			Vancouver		
Level	V_f (kN)	M_f (kNm)	Δ_{des} (m)	V_f (kN)	M_f (kNm)	Δ_{des} (m)
18	305	752	0.346	494	1230	1.252
17	484	1630	0.319	834	2720	1.172
16	522	2454	0.292	966	4287	1.101
15	499	3103	0.265	1012	5732	1.013
14	497	3623	0.239	1052	7108	0.942
13	551	4036	0.214	1118	8370	0.862
12	617	4463	0.190	1199	9674	0.783
11	661	4880	0.167	1276	10947	0.698
10	690	5373	0.144	1353	12414	0.616
9	724	5811	0.122	1446	13788	0.534
8	769	6344	0.102	1564	15409	0.452
7	793	6859	0.083	1659	17039	0.366
6	802	7403	0.065	1735	18853	0.279
5	887	8075	0.049	1912	20956	0.217
4	1018	9048	0.034	2102	23548	0.150
3	1171	10373	0.021	2305	26456	0.089
2	1277	12191	0.011	2419	30040	0.052
1	1427	14369	0.004	2718	34185	0.015

Graphical representation for the shear, moment and displacement values, listed in Tables 4.22 to 4.24 is given in Figures 4.4 to 4.7 for the B6, B12 and B18 buildings located in Montréal and Vancouver.

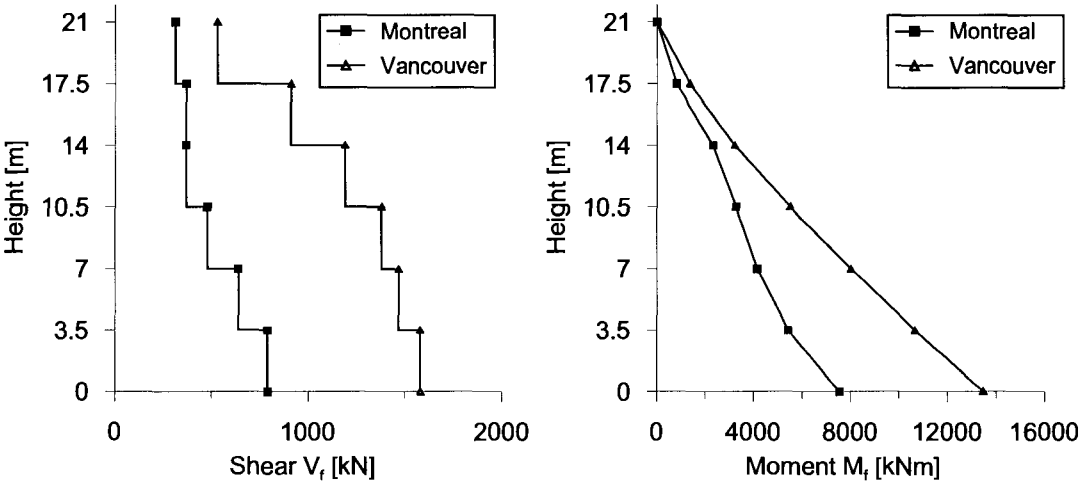

(a) Shear Diagram (b) Moment Diagram

FIG. 4.4 Spectral analysis results for the B6 building in Montréal and Vancouver

4.6 Shear Wall Dimensioning

4.6.1 Dimensioning for CSA 23.3-04 Requirements

The shear walls for all models B6, B12 and B18 in both cities are detailed according to the special seismic provisions of CSA A23.3-04 for ductile shear walls. Following are the basic dimensioning characteristics for all models shear walls :

1. The plastic hinge zone lenght is assumed as denoted in Clause 21.6.2.2, Item a) : $1.5 \times \ell_w = 1.5 \times 6.6 = 9.9\,\text{m}$, where ℓ_w is the lenght of the shear wall. Therefore the first three storeys are dimensioned as a plastic hinge zone.
2. The flexural reinforcement is composed of concentrated vertical bars (CVB) in the shear wall ends (columns) and of two curtains of uniformly distributed vertical bars in the wall web (DVB).

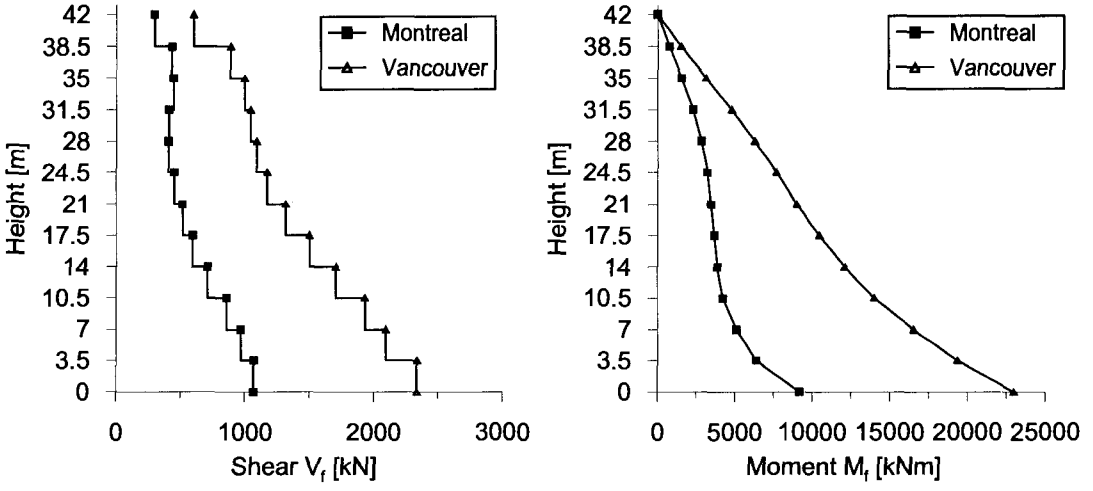

(a) Shear Diagram (b) Moment Diagram

FIG. 4.5 Spectral analysis results for the B12 building in Montréal and Vancouver

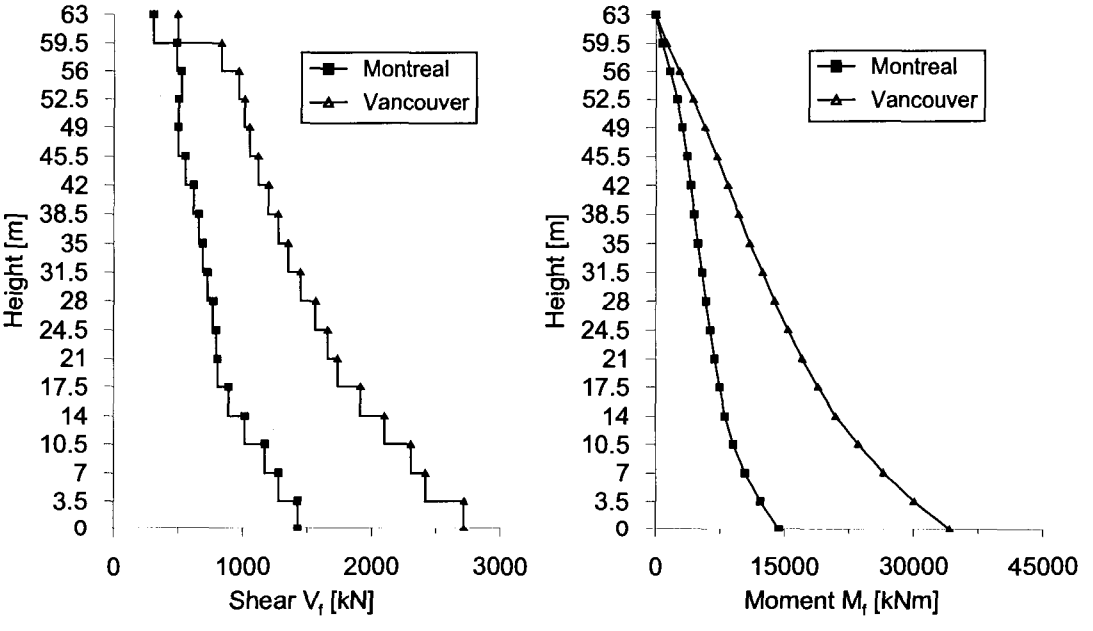

(a) Shear Diagram (b) Moment Diagram

FIG. 4.6 Spectral analysis results for the B18 building in Montréal and Vancouver

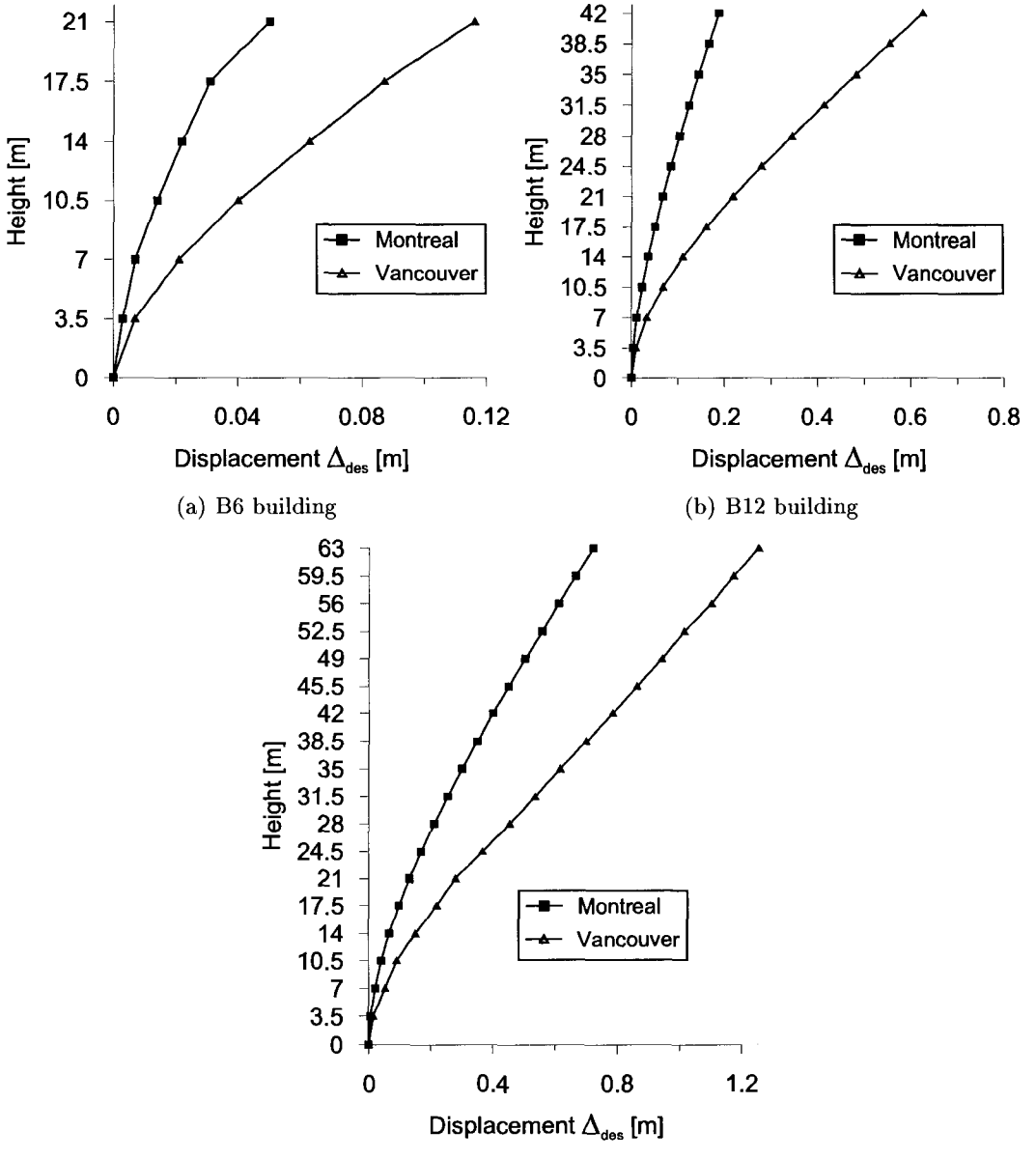

(a) B6 building

(b) B12 building

(c) B18 building

FIG. 4.7 Displacement results from spectral analysis for shear wall in B6, B12 and B18 in Montréal and Vancouver

3. The minimum CVB area is assumed as the greater of :
   - $0.01A_g = 0.01 \times 600 \times 600 = 3600\,mm^2$ Because a detailed analysis for the lateral force resisting system will not be performed in the other direction (N-S) of the building, columns are accounted as members of four ductile moment-resisting frames ($R_d = 4$). According to Clause 21.4.3.1, CSA A23.3-04, the mimimum reinforcement ratio for the longitudinal bars in that members is $0.01A_g$, where A_g is the gross area of the section.
   - $0.0015\ell_w b_w = 0.0015 \times 6600 \times 300 = 2970\,mm^2$ - the minimum area of concentrated reinforcement in ductile shear walls, according to Clause 21.6.6.4 in areas of plastic hinge zone.
   - $0.001\ell_w b_w = 0.001 \times 6600 \times 300 = 1980\,mm^2$ - the minimum area of concentrated reinforcement in ductile shear walls, according to Clause 21.6.6.3 for areas outside the plastic hinge zone.

   Therefore a minimum area of $3600\,mm^2$ has to be provided at all concentrated reinforcement locations in all models, which is satisfied with 8M25 ($A_s = 8 \times 500 = 4000\,mm^2$).
4. The vertical (flexural) reinforcement is based on the factored moment resistance of the cantilever shear wall matching or exceeding the factored moment demand after the formation of the plastic hinge.
5. The shear reinforcement is composed of two curtains of uniformly distributed horizontal bars (DHB). That reinforcement in the plastic hinge zone is governed by the shear strength to develop the probable flexural capacity.
6. The horizontal (shear) reinforcement in the plastic hinge region is based on the shear strength required to develop the probable flexural capacity, $V_p = \gamma_p V_f = \frac{M_{pw}}{M_f} V_f$. Outside the plastic zone, it is based on the shear strength required to develop the factored one.

Moment and shear design values are determined at each level of the shear walls according the requirements of the norm CSA A23.3-04, Clauses 21.6.2.2 and 21.6.9.1 for a ductile shear wall. Dimensioning in details is given in Table 4.25 for the 6-storey building in

Montréal. The shear and moment values, used for dimensioning the wall, result from the Spectral Dynamic Analysis, listed in Table 4.22 and the axial loading transmitted by that shear wall is listed in Table 4.3. Following the Code requirements, a reinforcement layout is specified, as shown in Table 4.25. After that a sectional analysis for the concrete section with the predetermined reinforcement layout is performed throughout the program RESPONSE 2000 [Bentz and Collins 2000]. The resulting nominal - M_n, factored - M_r and probable - M_{pw} flexural resistances are listed in the same table.

Based on the shear and moment values, resulting from the Spectral Dynamic Analysis and listed in Tables 4.22 to 4.24, as well as the axial loading transmitted by each shear wall, listed in Tables 4.3, 4.5 and 4.7, shear walls for the three models have been dimensioned using aforementioned new NBCC-2005 and CSA A23.3-04 requirements. Resulting flexural and shear strenghts at the shear walls base are shown in 4.27. Reinforcement detailing for all models in both cities is presented by the reinforcement layouts in Figures 4.8 to 4.13.

TAB. 4.25 Dimensioning of one shear wall in B6 building, located in Montréal.

Lev.	V_f	M_f	Shear wall reinforcement			M_n	M_r	M_{pw}
			CVB in	Distributed		$f'_c = 1$	$f'_c = 0.65$	$f'_c = 1$
			column	Vertical	Horizontal	$f_s = 1$	$f_s = 0.85$	$f_s = 1.25$
	(kN)	(kNm)	(-)	(-)	(-)	(kNm)	(kNm)	(kNm)
6	313	804	8M25	M10@260	M15@400	22143	14526	26805
5	369	2320	8M25	M10@260	M15@400	23542	15947	28168
4	369	3271	8M25	M10@260	M15@400	24874	17322	29440
3	479	4147	8M25	M10@260	M15@200	26183	18639	30732
2	640	5438	8M25	M10@260	M15@200	27449	19991	32194
1	791	7555	8M25	M10@260	M15@200	28849	21266	33393

TAB. 4.26 Dimensioning of one shear wall in B6 building, located in Montréal (Continue).

Level	γ	γ_w	γ_p	M_{des}	V_{des}
	M_r/M_f	M_n/M_f	M_p/M_f	$M_f \times \gamma_m$	$V_f \times \gamma_m$
				(kNm)	(kN)
6	18.07	27.55	33.35	4256	1655
5	6.88	10.2	12.15	12280	1952
4	5.29	7.60	9.00	17322	1952
3	4.49	6.31	7.41	18639	2119
2	3.68	5.05	5.92	19991	2828
1	2.81	3.82	**4.42**	21266	3494

4.6.2 Shear Walls Ductilities

As denoted in Chapter 2, CSA A23.3-04 demands as part of the special seismic provisions for ductile shear walls ($R_d = 3.5$) that the inelastic rotational capacity of the wall, θ_{ic}, shall be greater than inelastic rotational demand, θ_{id}, in order to ensure the wall ductility in the hinge region.

The inelastic rotational demand θ_{id} and the inelastic rotational capacity θ_{ic} are calculated by Eq. (2.9) and Eq. (2.10) respectively. The calculated inelastic rotational demands and capacities for the three models B6, B12 and B18 for both cities are listed in Table 4.28.

It could be noted from the same table, that the inelastic rotational demands (values in brackets) for models B6 and B12 in Montréal are far below the minimum required by CSA A23.3-0, Clause 21.6.7.2 : $\theta_{id} \geq 0.004$. Therefore a rotational demand $\theta_{id} = 0.004$ was assigned for the those shear walls. The reason for that is mainly the great flexural overstrength of the shear walls, based on the minimum reinforcement requirements in CSA A23.3-04 for the lateral resisting force systems in both directions.

TAB. 4.27 Flexural and shear strengths at the base of one shear wall under design loads in B6, B12 and B18models, located in Montréal and Vancouver.

Parameter	Montréal			Vancouver		
	B6	B12	B18	B6	B12	B18
Design base overturning moment, M_f (kNm)	7556	9193	14369	13460	22981	34185
Factored moment resistance, M_r (kNm)	21266	28696	35151	21233	32567	54485
Nominal moment resistance, M_n (kNm)	28849	35355	41521	28856	40142	66335
Probable moment resistance, M_{pw} (kNm)	33393	39310	45249	33371	45029	75710
Wall overstrength factor at nominal flexural capacity, γ_w [3]	3.82	3.85	2.89	2.14	1.75	1.94
Wall overstrength factor, at probable flexural capacity, γ_p [4]	4.42	4.28	3.15	2.48	1.96	2.21
Design base shear, V_f (kN)	791	1069	1427	1581	2336	2718
Design base probable shear, V_r (kN)	3494	4571	4495	3920	4577	6021

TAB. 4.28 Inelastic rotational demands and capacities of one shear wall in B6, B12 and B18models, located in Montréal and Vancouver.

Parameter	Montréal			Vancouver		
	B6	B12	B18	B6	B12	B18
Elastic deflection at roof level, Δ_f (mm)	9	33	62	20	112	224
Yield deflection at roof level, Δ_y (mm) $\Delta_y = \gamma_w \Delta_f$	34	129	179	43	195	434
Total deflection at roof level, $\Delta_f R_d R_o$ (mm)	50	187	346	116	625	1252
Inelastic rotational demand, θ_{id} (rad) $\theta_{id} \geq 0.004$ (rad)	0.004 (0.0009)	0.004 (0.0015)	0.0072	0.004 (0.0039)	0.0103	0.0137
Inelastic rotational capacity, θ_{ic} (rad)	0.0186	0.0105	0.0081	0.0186	0.0112	0.0138

Figures 4.8 to 4.13 visualize resulting shear walls detailing for both cities.

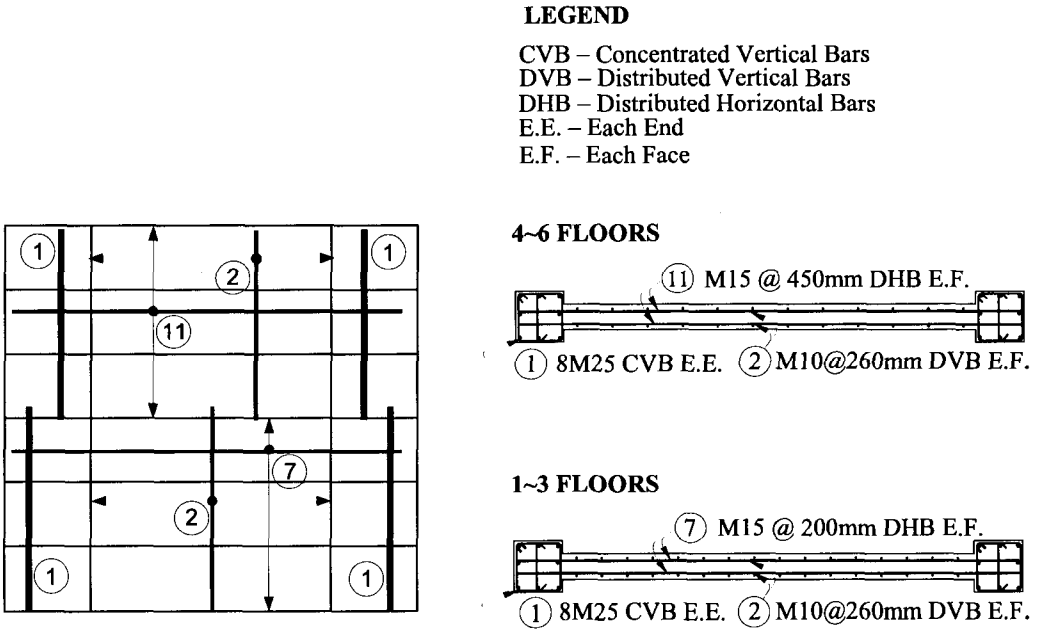

FIG. 4.8 Shear wall reinforcement in B6 building located in Montréal.

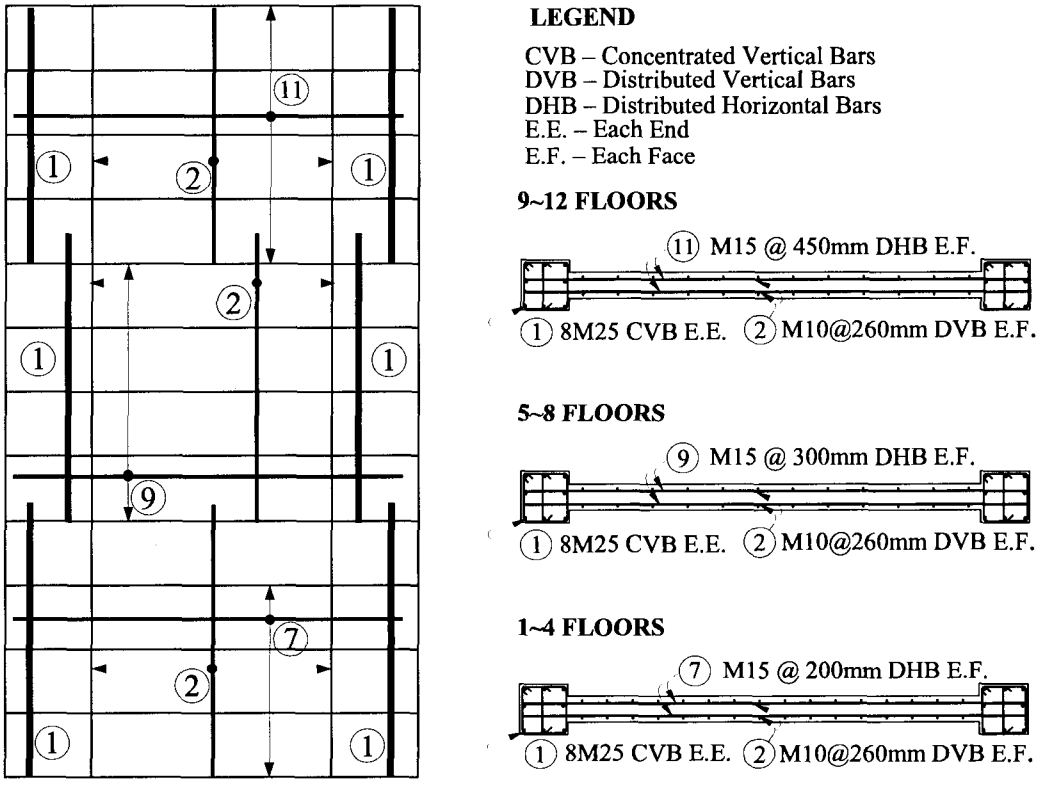

FIG. 4.9 Shear wall reinforcement in B12 building located in Montréal.

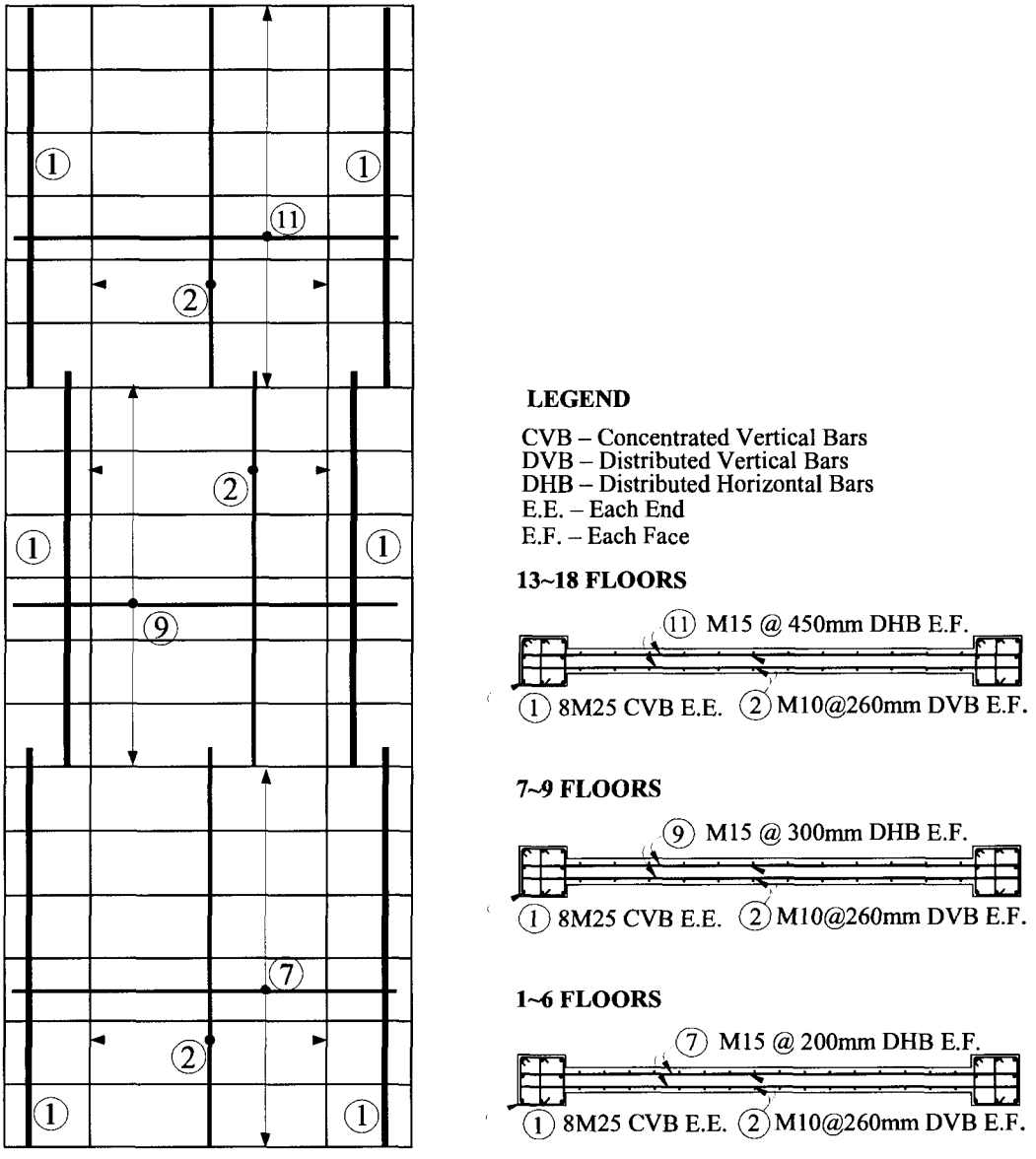

FIG. 4.10 Shear wall reinforcement in B18 building located in Montréal.

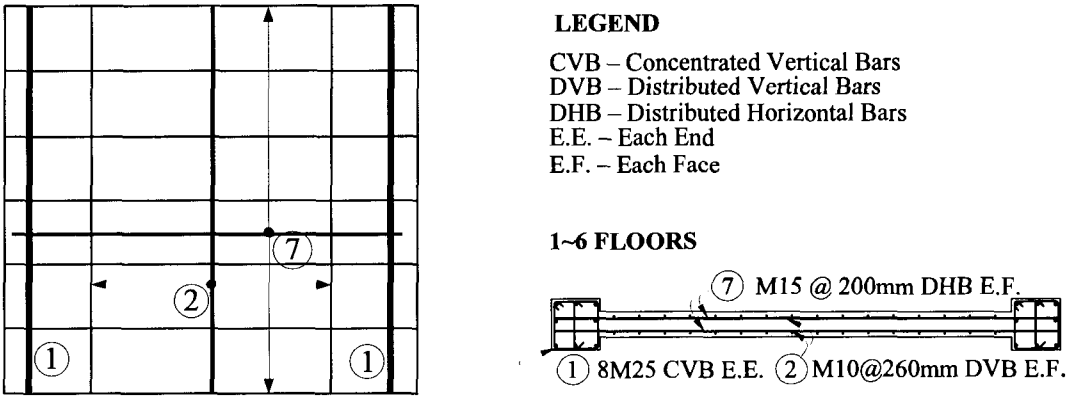

FIG. 4.11 Shear wall reinforcement in B6 building located in Vancouver.

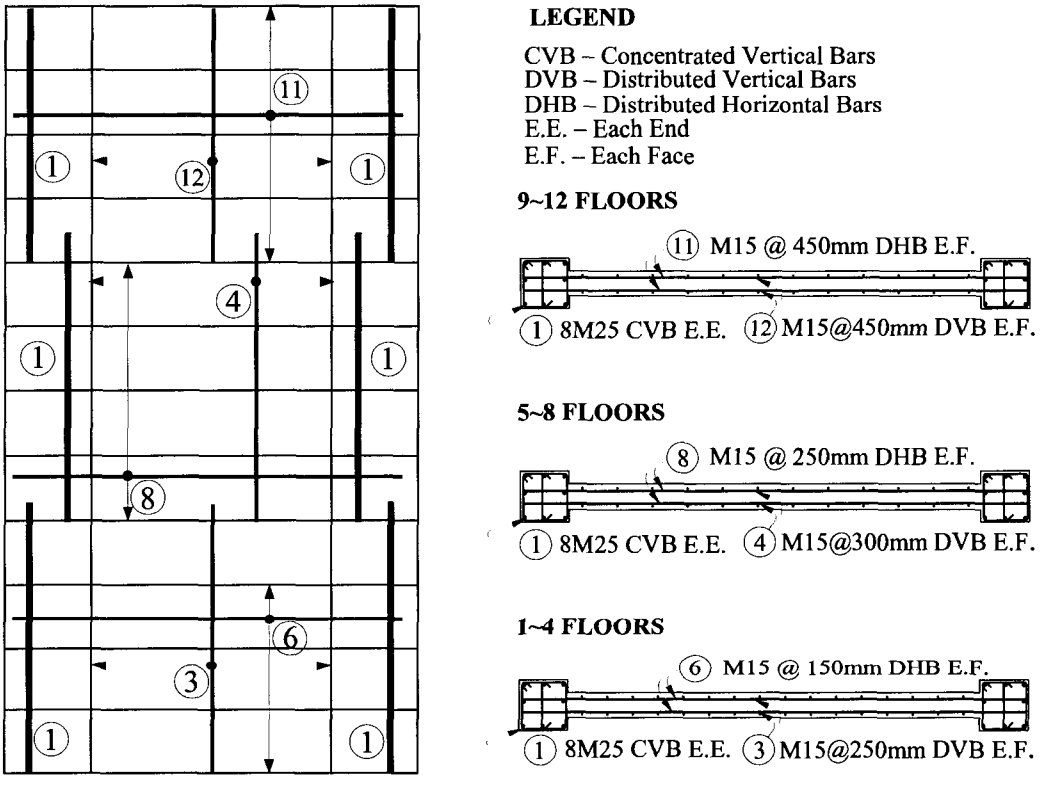

FIG. 4.12 Shear wall reinforcement in B12 building located in Vancouver.

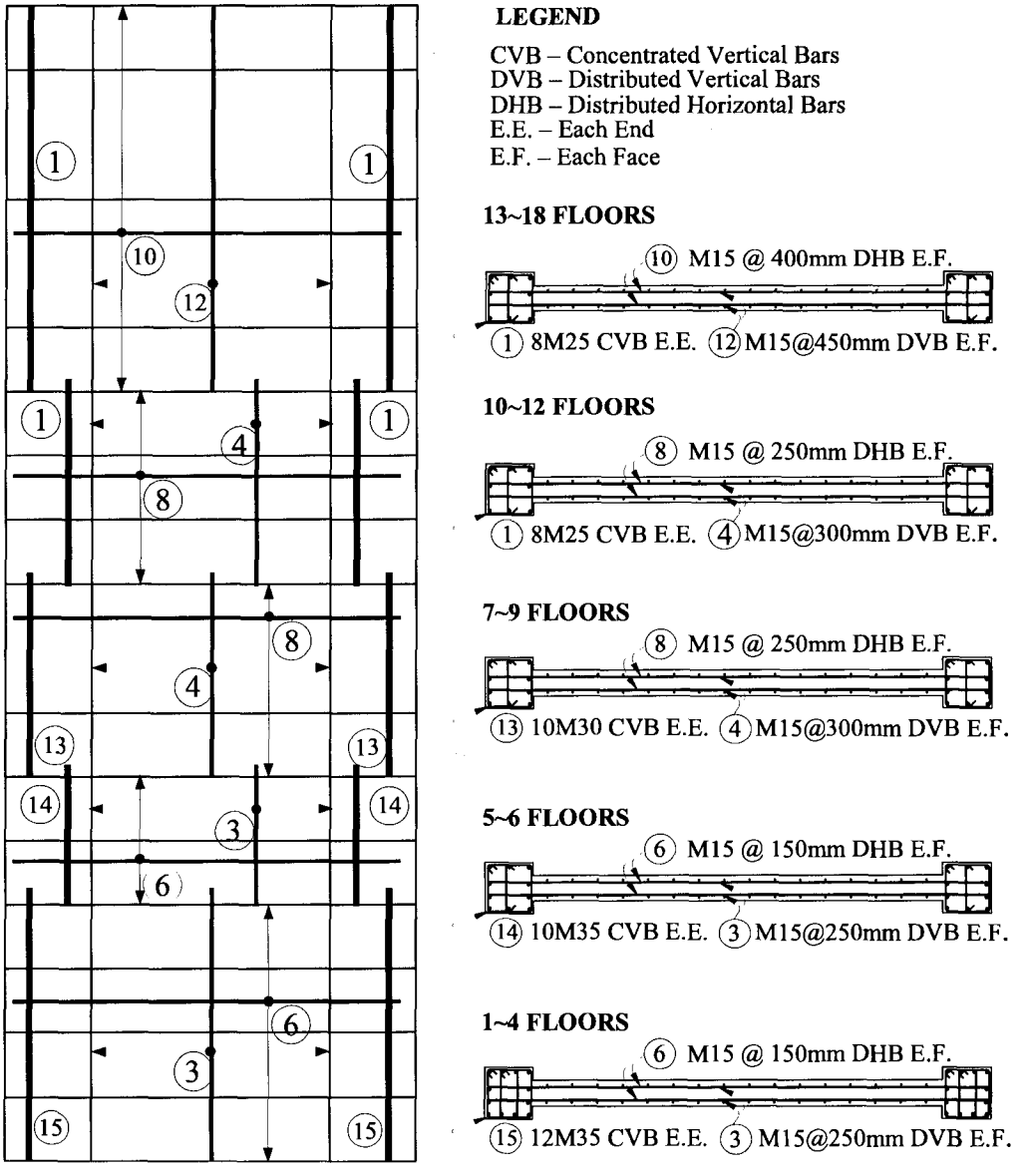

FIG. 4.13 Shear wall reinforcement in B18 building located in Vancouver.

CHAPTER 5

DISPLACEMENT-BASED ASSESSMENT OF THE SEISMIC PERFORMANCE

5.1 Introduction

In this chapter, the assessment of the seismic performance of the three cantilever shear wall building designed in Chapter 4 is presented using the three displacement-based approaches described in Chapter 2, *i.e.* : (i) The Yield Point Spectra (YPS) method (Aschheim and Black 2000) ; (ii) the Direct Displacement-Based Design (DDBD) method (Priestley and Kowalsky 2000) ; and (iii) the Inelastic Design Spectra (IDS) method (Chopra and Goel 2001).

5.2 Yield Point Spectra Method

The procedure described in section 3.3 is applied here to the three cantilever shear wall buildings. The different calculation steps are illustrated in detail for the B6 building.

Step 1 : The yield curvature of the three cantilever shear walls can be estimated according to Eq. (3.21)

$$\phi_{\mathrm{y}} = \frac{2\varepsilon_{\mathrm{y}}}{\ell_{\mathrm{w}}} = \frac{2 \times 0.002}{6.6} = 6.061 \times 10^{-4}\,\mathrm{m}^{-1}$$

It is assumed that the yield displacement $\Delta_{n,\mathrm{y}}$ is equal to the elastic displacement $\Delta_{n,\mathrm{e}}$. The latter is given by Eq. (3.22) under the assumption of a triangular distributed seismic load. Thus, the yield displacement at the roof of the B6 building is given by

$$\Delta_{n,\mathrm{y}} = \frac{11}{40}\phi_{\mathrm{y}} h_{\mathrm{w}}^2 = \frac{11 \times 6.061 \times 10^{-4} \times 21^2}{40} = 0.074\,\mathrm{m} \qquad (5.1)$$

Step 2 : The target roof displacement Δ_n is determined using Eq. (3.28) for perfor-

mance objectives corresponding to drift-controlled or rotation-controlled limits described in Table 3.5. The resulting roof target displacements for the B6 building are presented in Table 5.1. Values in bold are the minimum target performance objectives to be satisfied.

Step 3 : The target displacement ductility μ for each seismic hazard level is obtained by dividing the minimum target drift by the yield displacement determined in the previous step. The target displacement ductilities for the B6 building are also shown in Table 5.1.

TAB. 5.1 Performance objectives in terms of drift limits for the B6 building.

	Performance level		
	Post disaster	Life safety	Near collapse
Seismic hazard level	SHL-75	SHL-475	SHL-2500
Drift-controlled Δ_n (m)	**0.078**	0.271	0.465
Rotation-controlled Δ_n (m)	0.112	**0.151**	**0.228**
Target ductility μ	1.054	2.041	3.081

Step 4 : Construct a Yield Point Spectra corresponding to the target displacement ductility μ[*Step* 3].

To find the yield displacement of the ESDOF system representing the B6 building, the participation factor Γ is first determined according to Eq. (3.55)

$$\Gamma = h_{\mathrm{w}} \frac{\sum_{i=1}^{6} m_i h_i}{\sum_{i=1}^{6} m_i h_i^2} = 1.367 \tag{5.2}$$

The ESDOF yield displacement is then given by Eq. (3.42)

$$\Delta_{\mathrm{y}}^{*} = \frac{\Delta_{n,\mathrm{y}}}{\Gamma} = \frac{0.074}{1.367} = 0.054\,\mathrm{m}$$

Step 5 : The ESDOF yield displacement is entered into the Yield Point Spectrum constructed for the target displacement ductility μ [*Step* 3] and the corresponding seismic hazard level. This is illustrated in Figure 5 for the B6 building when located in Montréal and considering seismic hazard level SHL-2500.

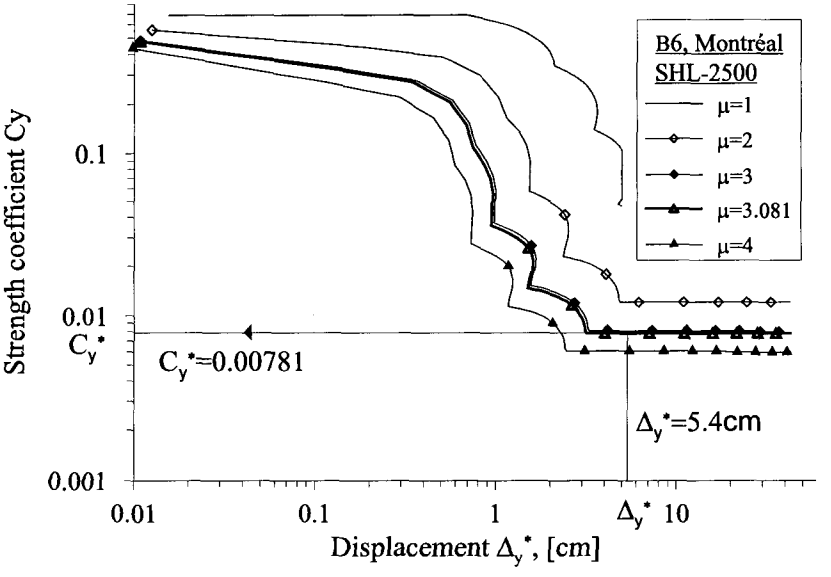

FIG. 5.1 Use of Yield Point Spectrum to obtain the ESDOF yield strength coefficient corresponding to a target displacement ductility for the B6 building located in Montréal under SHL-2500 seismic hazard.

It is to be mentioned that the Yield Point Spectra used here are smoothed ones derived from the NBCC 2005 response spectrum (see section 3.2.2). The required yield strength coefficient $C_y^* = 0.00781$ is obtained by graphical construction as shown in Figure 5. To obtain the base shear strength coefficient C_y at yield of the B6 building, the mass participation factor α is first determined using Eq. (3.55) based on an assumed triangular profile

$$\alpha = \frac{1}{M_T} \frac{\left(\sum_{i=1}^{6} m_i h_i\right)^2}{\sum_{i=1}^{6} m_i h_i^2} = 0.809 \tag{5.3}$$

The base shear strength coefficient at yield of the B6 building is then given by Eq. (3.51)

$$C_y = \alpha C_y^* = 0.809 \times 0.00781 = 0.00632 \tag{5.4}$$

Step 6 : The required base shear strength V_y is then calculated using the reported, from the previous step, yield strength coefficient C_y and Eq. (3.47)

$$V_y = g\, M_T\, C_y = 9.81 \times 4060.9 \times 0.00632 = 252\,\text{kN} \tag{5.5}$$

Steps 1 to 5 are repeated to find the required base shears for the buildings studied considering the different seismic hazard levels described previously. Figures 5.2 to 5.7 illustrate the Yield Point Spectra used and the reading of the shear strength coefficients C_y^*. The results are summarized in Table 5.2 for the two locations of Vancouver and Montréal.

TAB. 5.2 Base shear calculations using the Yield Point Spectra method for the three buildings submitted to three seismic hazard levels.

		Montréal			Vancouver		
		C_y^*	C_y	V_y (kN)	C_y^*	C_y	V_y (kN)
SHL-75							
	B6	0.00193	0.00156	62	0.02070	0.01674	663
	B12	0.00220	0.00171	136	0.01700	0.01324	1049
	B18	0.00220	0.00169	202	0.01700	0.01307	1557
SHL-475							
	B6	0.00393	0.00318	127	0.03900	0.03154	1249
	B12	0.00520	0.00405	322	0.02904	0.02261	1792
	B18	0.00765	0.00588	702	0.04266	0.03281	3907
SHL-2500							
	B6	0.00781	0.00632	252	0.05200	0.04200	1666
	B12	0.01150	0.00895	713	0.04089	0.03183	2523
	B18	0.01408	0.01083	1292	0.05003	0.03848	4581

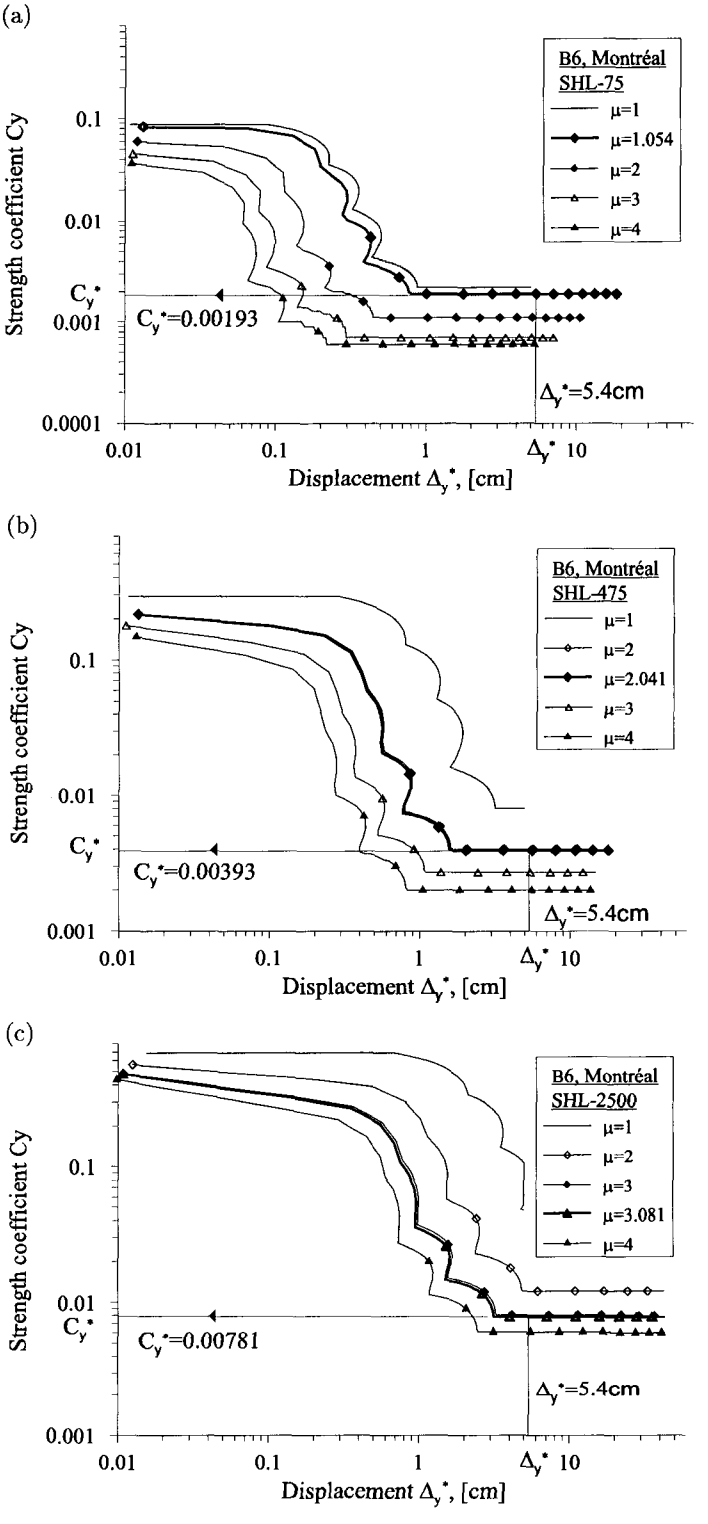

FIG. 5.2 Yield Point Spectra for the B6 building in Montréal for different seismic hazard levels : (a) SHL-75 ; (b) SHL-475 ; and (c) SHL-2500.

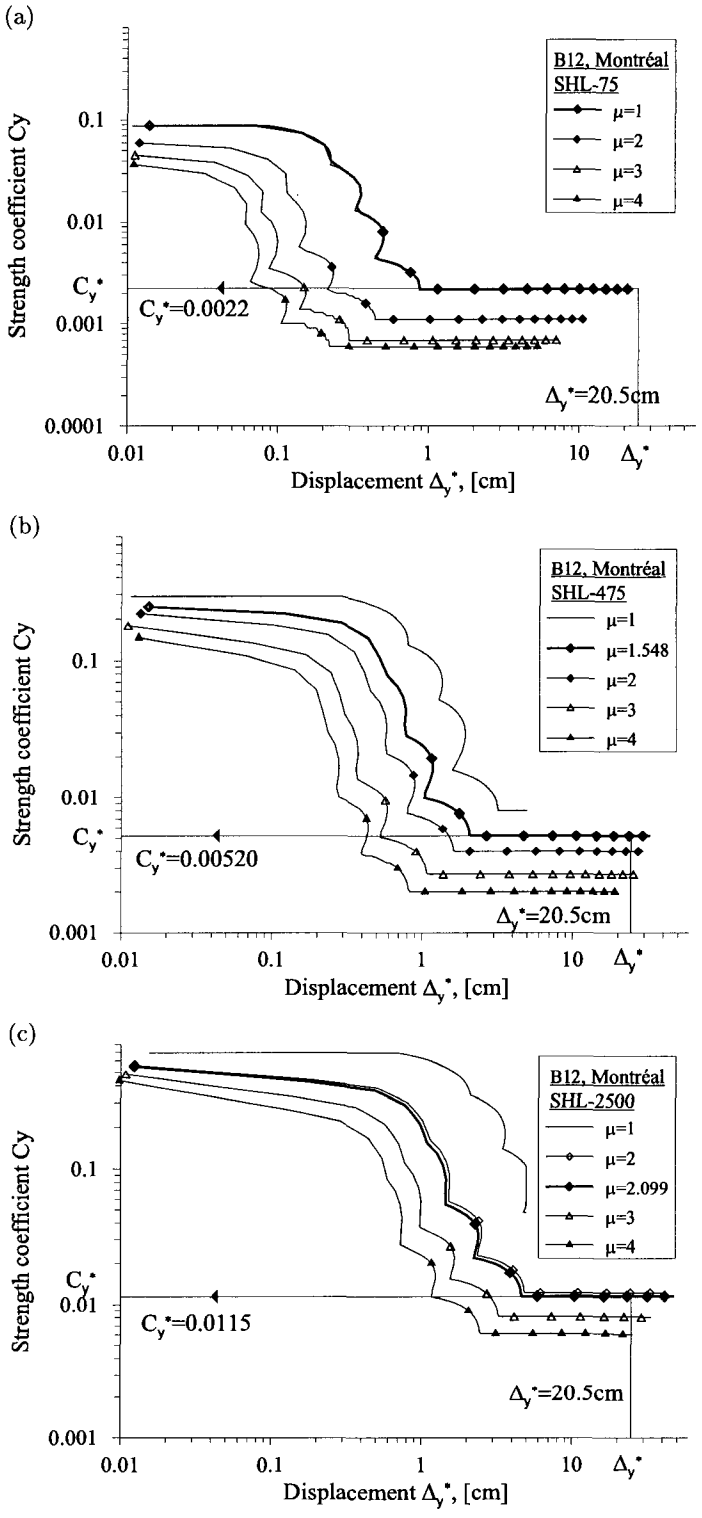

FIG. 5.3 Yield Point Spectra for the B12 building in Montréal for different seismic hazard levels : (a) SHL-75 ; (b) SHL-475 ; and (c) SHL-2500.

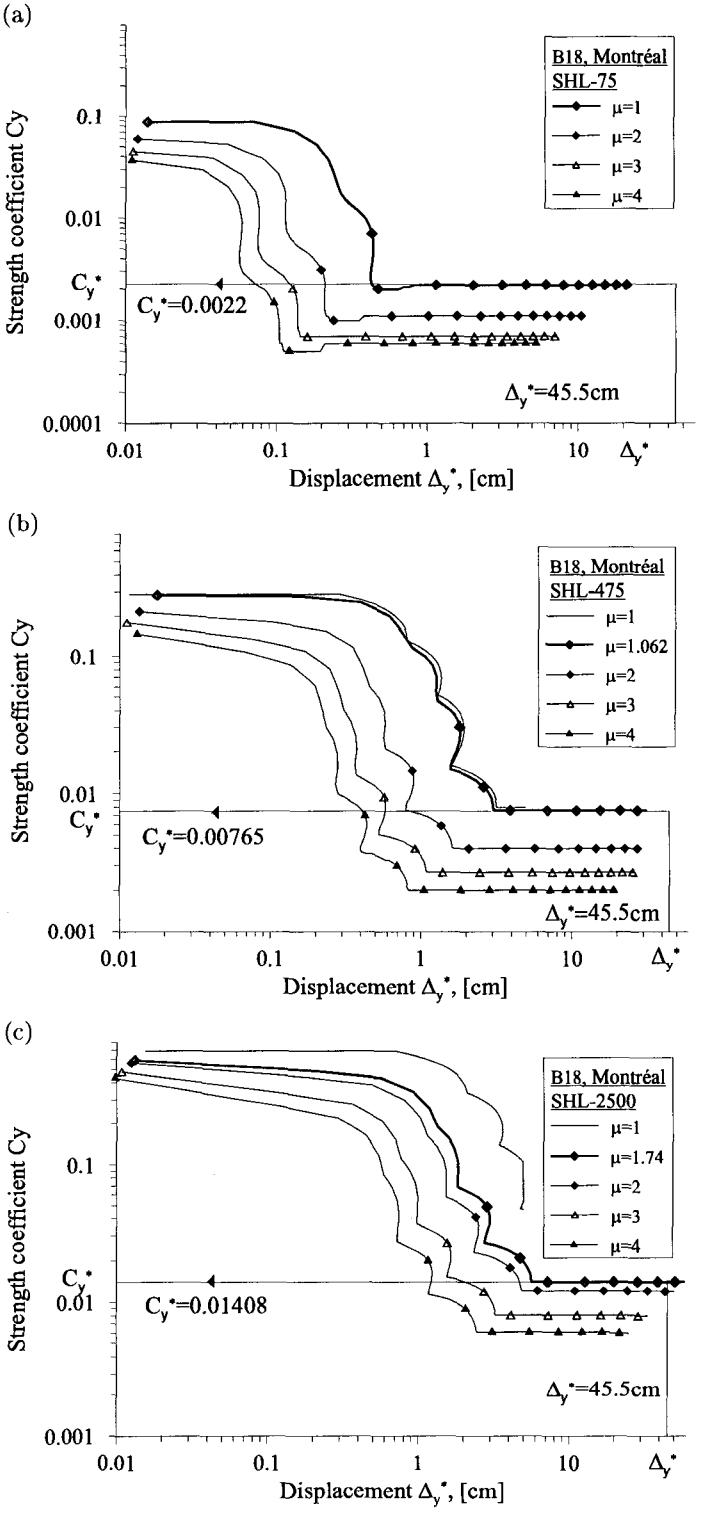

FIG. 5.4 Yield Point Spectra for the B18 building in Montréal for different seismic hazard levels : (a) SHL-75 ; (b) SHL-475 ; and (c) SHL-2500.

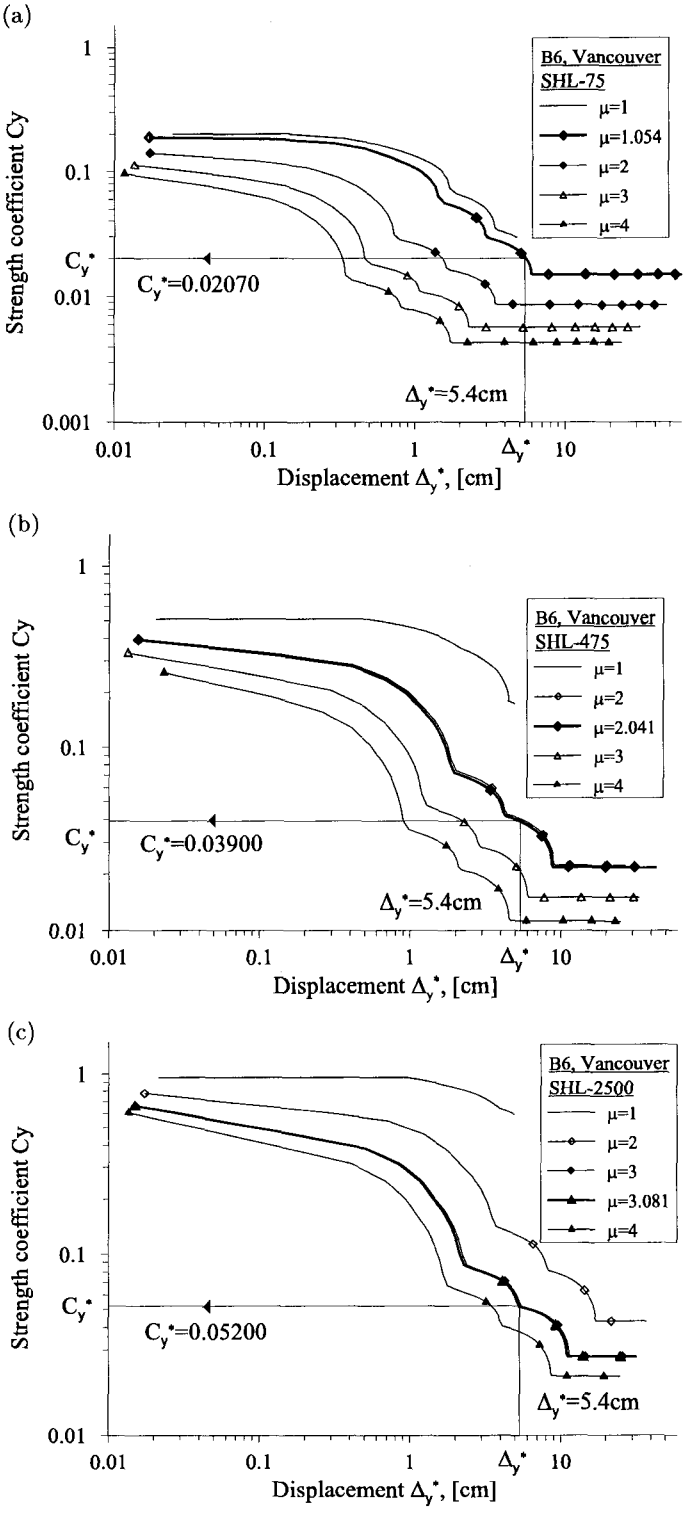

FIG. 5.5 Yield Point Spectra for the B6 building in Vancouver for different seismic hazard levels : (a) SHL-75 ; (b) SHL-475 ; and (c) SHL-2500.

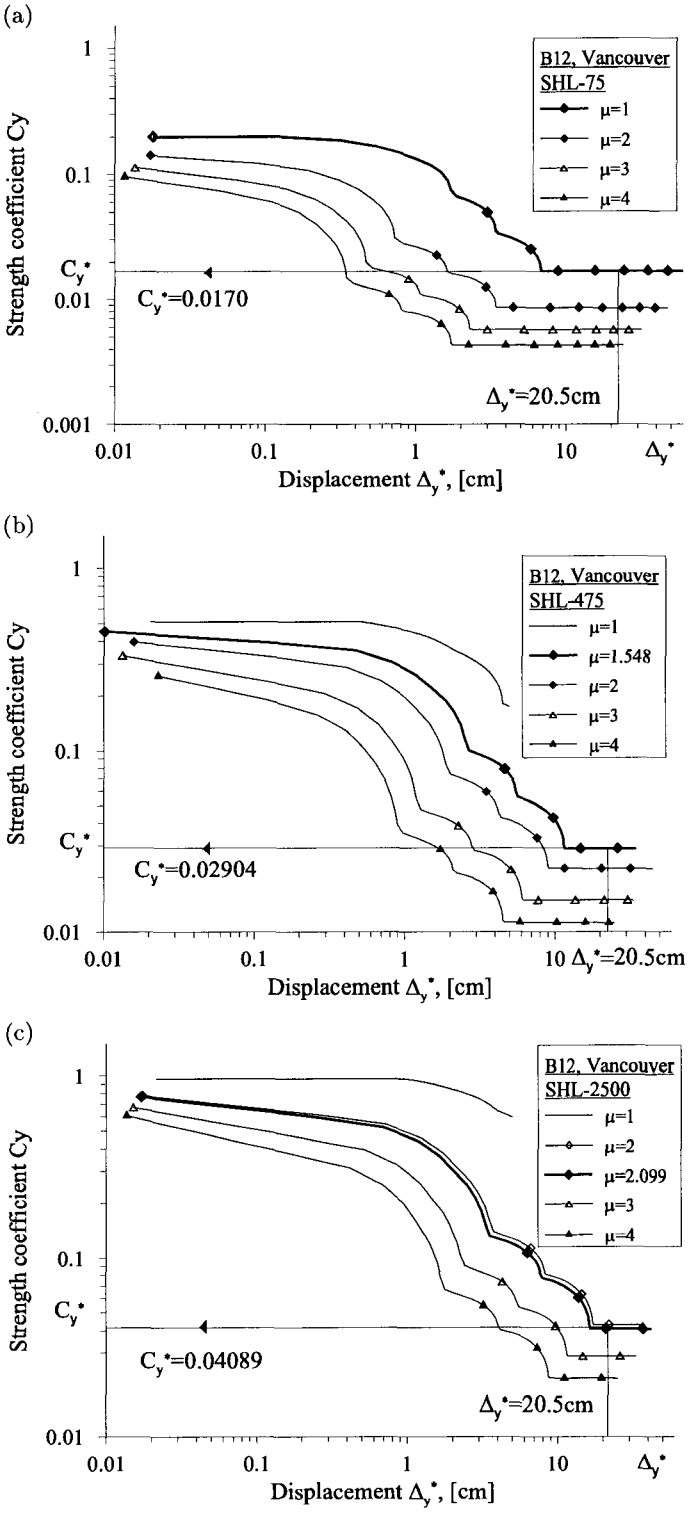

FIG. 5.6 Yield Point Spectra for the B12 building in Vancouver for different seismic hazard levels : (a) SHL-75 ; (b) SHL-475 ; and (c) SHL-2500.

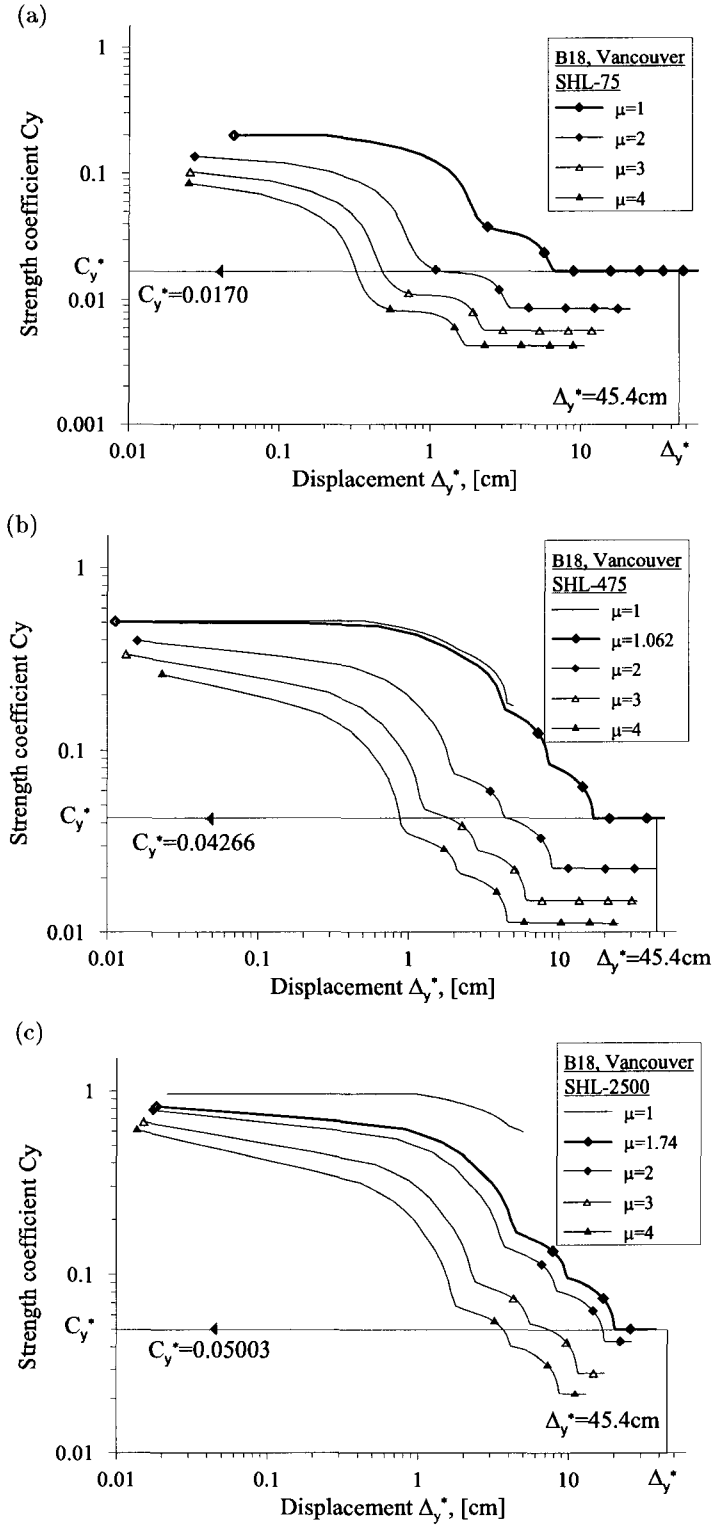

FIG. 5.7 Yield Point Spectra for the B18 building in Vancouver for different seismic hazard levels : (a) SHL-75 ; (b) SHL-475 ; and (c) SHL-2500.

5.3 Direct Displacement-Based Method

The direct displacement-based design method described in chapter 3 is applied first to the B6 building located in Montréal. Three seismic hazard levels SHL-75, SHL-475 and SHL-2500 are considered.

Step 1 : The target displacement profile is calculated using Eq. (3.27) as shown in Table 5.3. Fig. 5.8 represents drift-controlled and rotation controlled target displacement profiles for the B6 building submitted to three seismic hazard levels SHL-75, SHL-475 and SHL-2500. Minimum target performance displacement profiles are shown in bold in Table 5.3 and are represented by thicker lines in Fig. 5.8.

TAB. 5.3 Target displacement profile emph *vs.* expected performance levels for the B6 building.

	Performance level					
	SHL-75		SHL-475		SHL-2500	
Height h_i (m)	Drift-based Δ_i (m)	Rotation-based Δ_i (m)	Drift-based Δ_i (m)	Rotation-based Δ_i (m)	Drift-based Δ_i (m)	Rotation-based Δ_i (m)
21.0	**0.078**	0.112	0.271	**0.151**	0.465	**0.228**
17.5	**0.061**	0.089	0.219	**0.120**	0.378	**0.184**
14.0	**0.046**	0.065	0.169	**0.090**	0.293	**0.139**
10.5	**0.033**	0.043	0.122	**0.061**	0.210	**0.096**
7.0	**0.022**	0.023	0.076	**0.034**	0.129	**0.055**
3.5	**0.009**	0.007	0.028	**0.011**	0.046	**0.018**

Step 2 : Using Eq. (3.60), Eq. (3.61) and Eq. (3.62) the design peak displacement Δ_{eff}, the effective mass M_{eff} and the effective height h_{eff} of the equivalent SDOF system of the B6 building in Montréal are calculated in details for SHL-2500 and shown in Table 5.4.

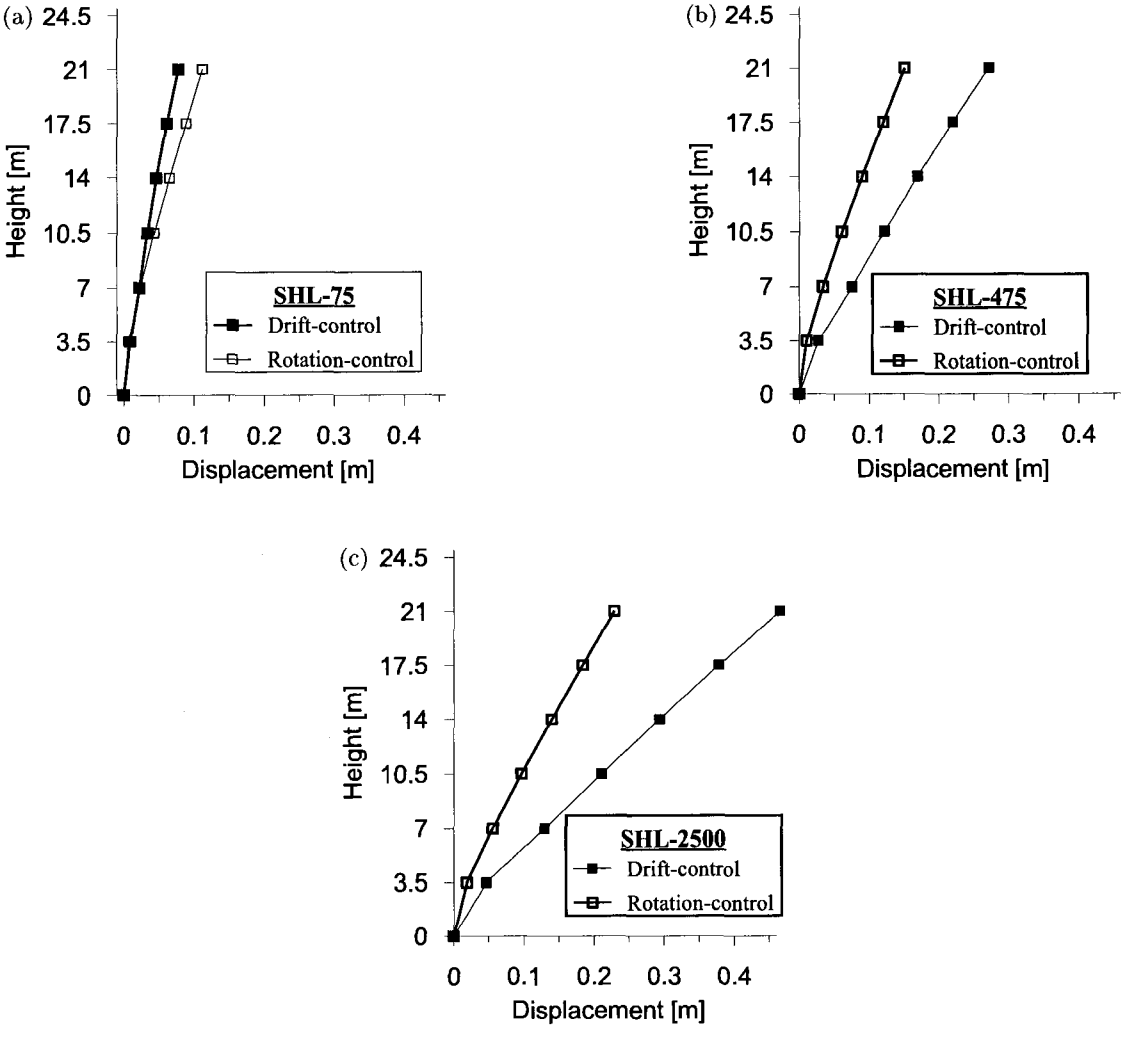

FIG. 5.8 Target displacement profile for B6 building under SHL-75, SHL-475 and SHL-2500 seismic hazards : (a) Seismic Hazard Level SHL-75; (b) Seismic Hazard Level SHL-475 and (c) Seismic Hazard Level SHL-2500.

TAB. 5.4 Preparative calculations for B6 building equivalent SDOF system properties.

Level (m)	m_i ($\times 10^3$ kg)	Δ_i (m)	$m_i\Delta_i$ ($\times 10^3$ kg m)	$m_i\Delta_i^2$ ($\times 10^3$ kg m^2)	$m_i\Delta_i h_i$ ($\times 10^3$ kg m^2)
21.0	743.4	0.228	169.7	38.7	3564.1
17.5	663.5	0.184	121.8	22.4	2132.1
14.0	663.5	0.139	92.4	12.9	1293.7
10.5	663.5	0.096	63.7	6.1	669.3
7.0	663.5	0.055	36.6	2.0	256.4
3.5	663.5	0.018	12.1	0.2	42.3
$\sum$	4060.9		4961.4	82.4	7957.8

$$\Delta_{\text{eff}} = \frac{\sum_{i=1}^{n} m_i\Delta_i^2}{\sum_{i=1}^{n} m_i\Delta_i} = \frac{82.4 \times 10^3}{496.4 \times 10^3} = 0.166\,\text{m} \tag{5.6}$$

$$M_{\text{eff}} = \frac{\sum_{i=1}^{n} m_i\Delta_i}{\Delta_{\text{eff}}} = \frac{496.4 \times 10^3}{0.166} = 2992.2 \times 10^3\,\text{kg} \tag{5.7}$$

$$h_{\text{eff}} = \frac{\sum_{i=1}^{n} m_i\Delta_i h_i}{\sum_{i=1}^{n} m_i\Delta_i} = \frac{7957.8 \times 10^3}{496.4 \times 10^3} = 16.03\,\text{m} \tag{5.8}$$

Step 3 : The yield curvature of the B6 building is first estimated according to Eq. (3.21)

$$\phi_{\text{y}} = \frac{2\varepsilon_{\text{y}}}{\ell_{\text{w}}} = \frac{2 \times 0.002}{6.6} = 6.061 \times 10^{-4}\,\text{m}^{-1}$$

Assuming a triangular distributed seismic force, the yield displacement Δ_{y} at the height of the resultant lateral seismic force is calculated using Eq. (3.66).

TAB. 5.5 Properties of the equivalent SDOF system of the B6 building in Montréal .

	Seismic hazard level		
Equivalent SDOF properties	SHL-75	SHL-475	SHL-2500
Peak displacement Δ_{eff} (m)	0.055	0.109	0.166
Effective mass M_{eff} (10^3 kg)	3106.35	2938.86	2992.2
Effective height h_{eff} (m)	15.76	16.15	16.03

For example, under seismic hazard level SHL-2500

$$\begin{aligned}\Delta_{\text{eff,y}} &= \frac{\phi_{\text{y}} h_{\text{eff}}^2}{40 h_{\text{w}}^3}\left(h_{\text{eff}}^3 - 10 h_{\text{eff}} h_{\text{w}}^2 + 20 h_{\text{w}}^3\right) \\ &= \frac{6.061 \times 10^{-4} \times 16.03^2}{40 \times 21^3}\left(16.03^3 - 10 \times 16.03 \times 21^2 + 20 \times 21^3\right) \\ &= 0.050\,\text{m}\end{aligned}$$

The yield displacements corresponding to the considered three seismic hazard levels are summarized in Table 5.6.

Step 4 : The displacement ductilities corresponding to the three seismic hazard levels are calculated as the ratios of Δ_{eff} to $\Delta_{\text{eff,y}}$ as shown in Table 5.6.

Step 5 : The effective damping ratios ξ_{eff} for the three seismic hazard levels are determined using Eq. (3.64) and summarized in Table 5.6.

TAB. 5.6 Yield displacements, displacement ductilities and effective damping ratios for the B6-storey building.

	Seismic hazard level		
	SHL-75	SHL-475	SHL-2500
Yield displacement Δ_{y} (m)	0.05	0.05	0.05
Displacement ductility μ	1.14	2.17	3.33
Effective damping ratio ξ_{eff} (%)	6.8	13.9	17.30

Step 6 : Construct a 5% damped inelastic displacement spectra based on a 5% damped pseudo-acceleration spectrum using Eq. (3.68).

Step 7 : Determine the displacement spectra for effective damping ξ_{eff} using the relation proposed by Eurocode EC8 ([Eurocode 1998])

$$\Delta_{\text{e}}^{(\xi_{\text{eff}})} = \Delta_{\text{e}}^{(5\%)} \sqrt{\frac{7}{2+\xi_{\text{eff}}}} \tag{5.9}$$

where $\Delta_{\text{e}}^{(5\%)}$ and $\Delta_{\text{e}}^{(\xi_{\text{eff}})}$ are the spectral displacements at 5% and ξ_{eff} damping values, respectively. Development of displacement spectrums for different damping values ξ is demonstrated in Figure 5.9 for the the three seismic hazard levels.

Step 8 : Based on the reported from Figure 5.9 effective period T_{eff}, the effective stiffness K_{eff} and design base shear V_{eff} are calculated using (Priestley and Kowalsky 2000). For example, under seismic hazard level SHL-2500 K_{eff} and V_{eff} are as follows :

$$K_{\text{eff}} = \frac{4\pi^2 M_{\text{eff}}}{T_{\text{eff}}^2} = \frac{4\pi^2 2992.20 \times 10^3}{6.8} = 2554.7 \times 10^3\,\text{N/m} \tag{5.10}$$

$$V_{\text{u}} = V_{\text{eff}} = K_{\text{eff}}\,\Delta_{\text{eff}} = 2554.7 \times 10^3 \times 0.166 = 424\,\text{kN} \tag{5.11}$$

The Direct Displacement-Based Design Method is then applied to the studied buildings in Montréal and Vancouver for the trhee seismic levels. Identically to the B6 building in Montréal, the drift-controlled and rotation controlled target displacement profiles are first illustrated in Figures 5.10 and 5.11 and then the displacement spectrums are developped in Figures 5.12 to 5.16. The corresponding results for the cases studied herein are summarized in Tables 5.7, 5.8 and 5.9.

5.4 Inelastic Design Spectra Method

The Inelastic Design Spectra method for Displacement-based design (IDS) is illustrated here as a step by step procedure for the B6 building, located in Montréal and subjected

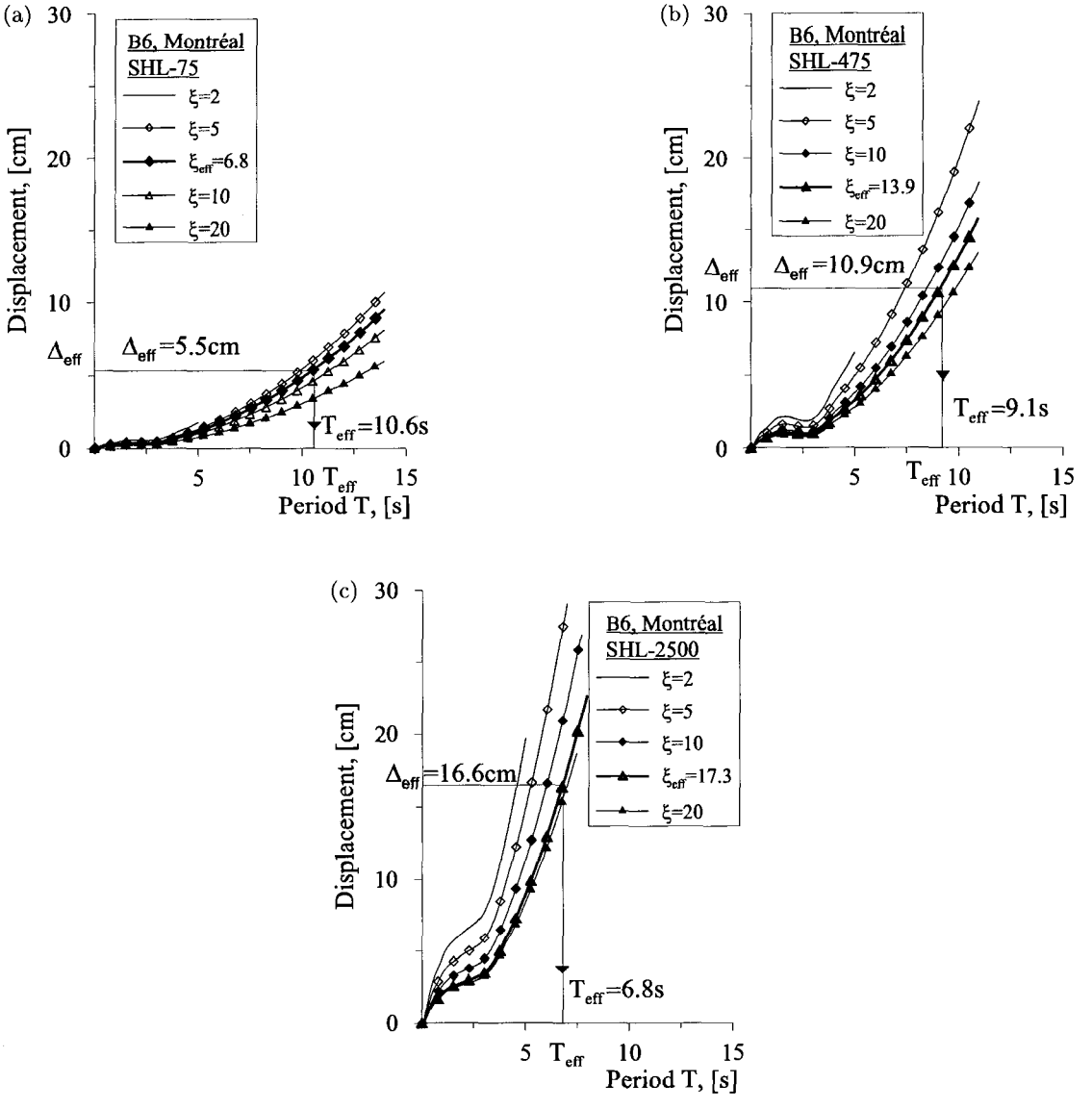

FIG. 5.9 Displacement Spectra for different damping values ξ for the B6 building in Montréal : (a) Seismic Hazard Level SHL-75; (b) Seismic Hazard Level SHL-475 and (c) Seismic Hazard Level SHL-2500.

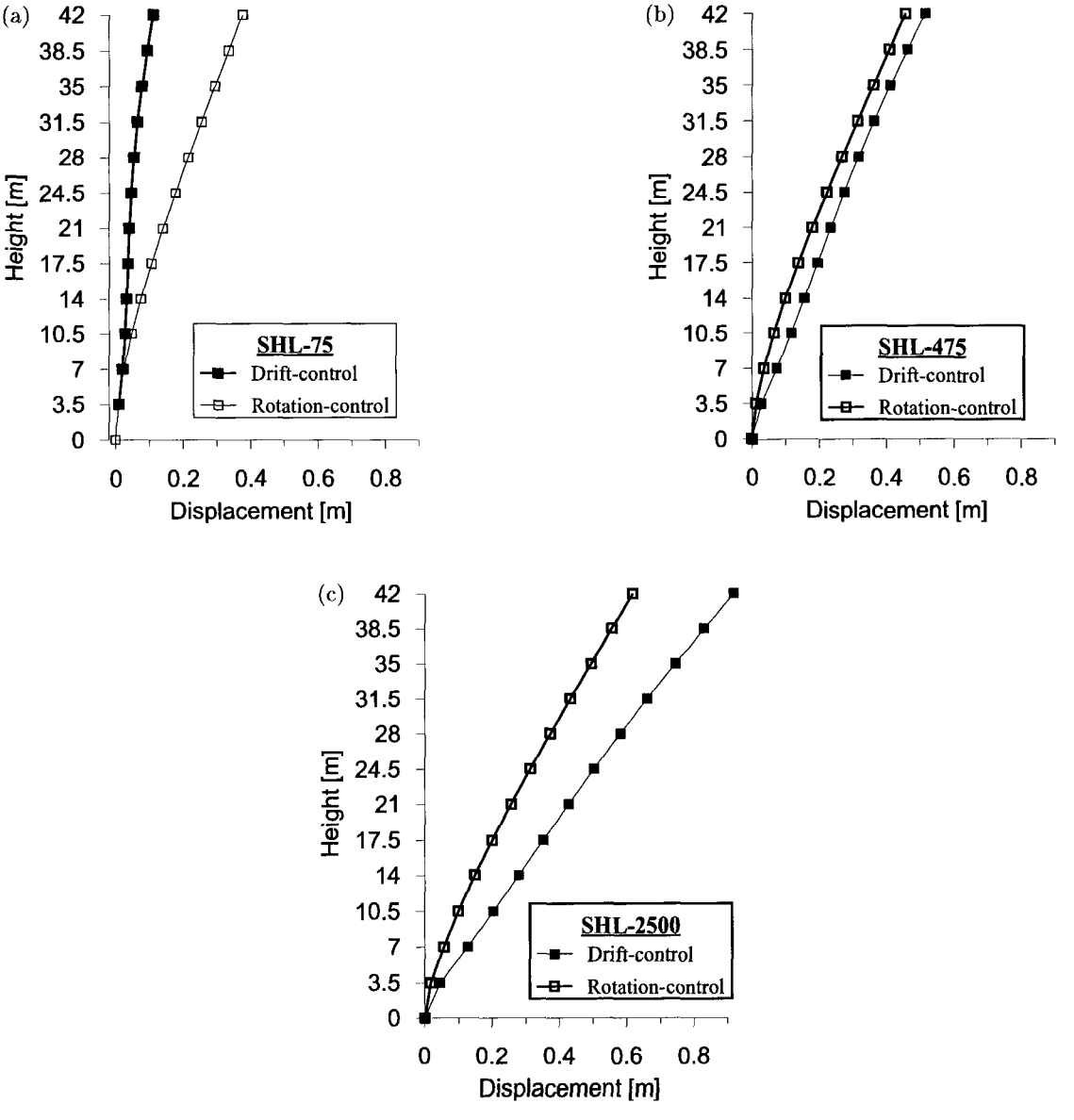

FIG. 5.10 Target displacement profile for B12 building under SHL-75, SHL-475 and SHL-2500 seismic hazards : (a) Seismic Hazard Level SHL-75 ; (b) Seismic Hazard Level SHL-475 and (c) Seismic Hazard Level SHL-2500.

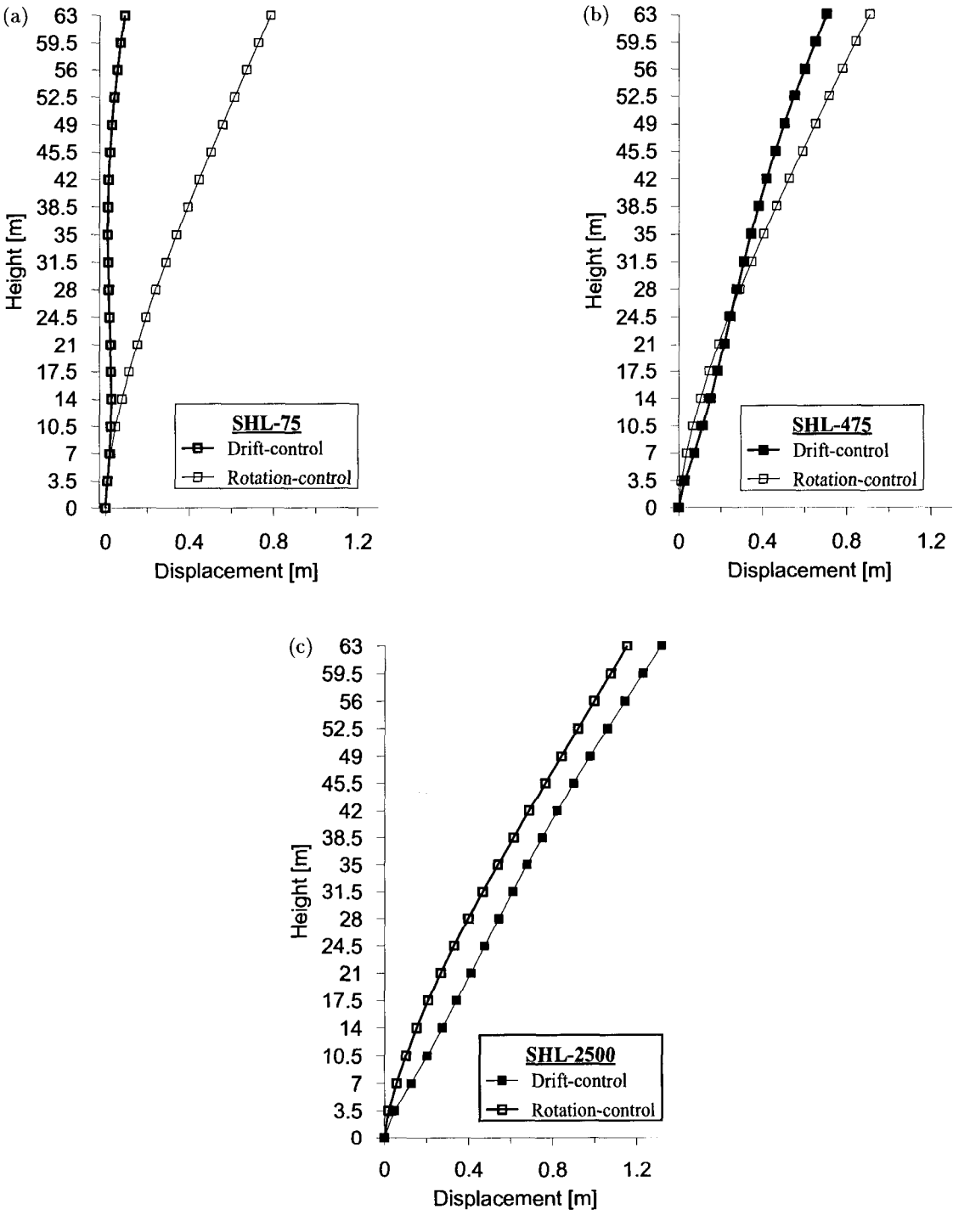

FIG. 5.11 Target displacement profile for B18 building under SHL-75, SHL-475 and SHL-2500 seismic hazards : (a) Seismic Hazard Level SHL-75 ; (b) Seismic Hazard Level SHL-475 and (c) Seismic Hazard Level SHL-2500.

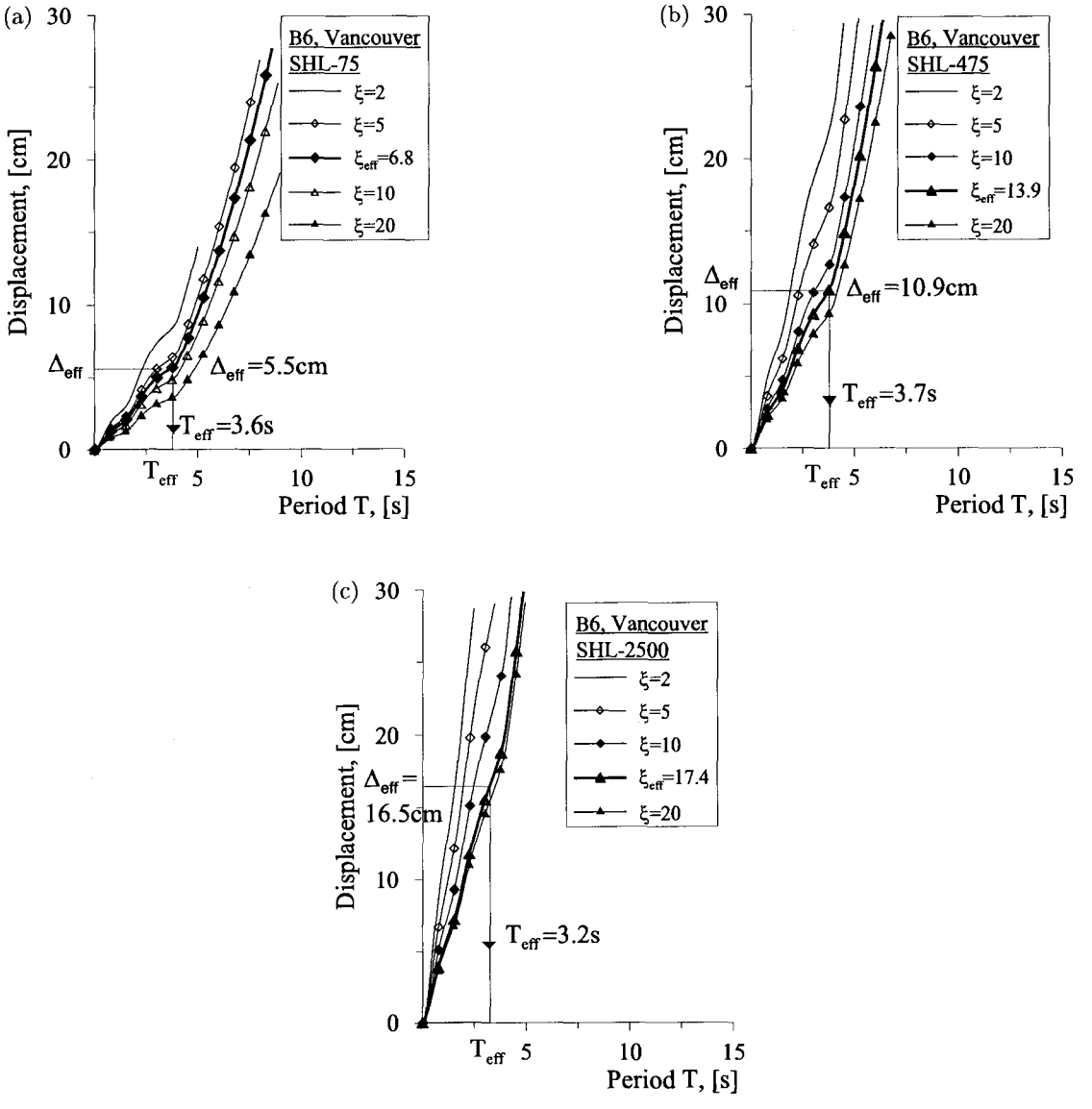

FIG. 5.12 Displacement Spectra for different damping values ξ for the B6 building in Vancouver : (a) Seismic Hazard Level SHL-75; (b) Seismic Hazard Level SHL-475 and (c) Seismic Hazard Level SHL-2500.

TAB. 5.7 Properties of the equivalent SDOF system of the B6 building in Montréal and Vancouver.

Equivalent SDOF	Montréal			Vancouver		
properties	SHL-75	SHL-475	SHL-2500	SHL-75	SHL-475	SHL-2500
Δ_{eff} (m)	0.055	0.109	0.166	0.055	0.109	0.165
M_{eff} (10^3 kg)	3106.35	2938.86	2992.2	3087.85	2919.84	2973.11
h_{eff} (m)	15.76	16.15	16.03	15.71	16.10	15.98
Δ_{y} (m)	0.05	0.05	0.05	0.18	0.18	0.18
μ	1.14	2.17	3.33	1.14	2.17	3.33
ξ_{eff} (%)	6.8	13.9	17.3	6.8	14.0	17.4
T_{eff} (s)	10.62	9.10	6.80	3.55	3.74	3.24
K_{eff} (10^3 N/m)	1091.4	1401.1	2554.7	9673.0	8240.9	11181.0
V_{eff} (kN)	60	153	424	532	898	1848

TAB. 5.8 Properties of the equivalent SDOF system of the B12 building in Montréal and Vancouver.

Equivalent SDOF	Montréal			Vancouver		
properties	SHL-75	SHL-475	SHL-2500	SHL-75	SHL-475	SHL-2500
Δ_{eff} (m)	0.068	0.349	0.631	0.068	0.349	0.630
M_{eff} (10^3 kg)	6090.20	6115.39	6110.82	6064.80	6085.72	6080.73
h_{eff} (m)	29.65	29.80	29.81	29.59	29.75	29.76
Δ_{y} (m)	0.177	0.178	0.179	0.176	0.178	0.178
μ	1.00	1.96	3.53	1.00	1.96	3.54
ξ_{eff} (%)	5.0	13.0	17.8	5.0	13.0	17.8
T_{eff} (s)	11.15	16.03	13.33	4.01	6.80	7.08
K_{eff} (10^3 N/m)	1933.9	939.5	1357.7	14889.8	5195.8	4789.0
V_{eff} (kN)	132	328	857	1014	1811	3016

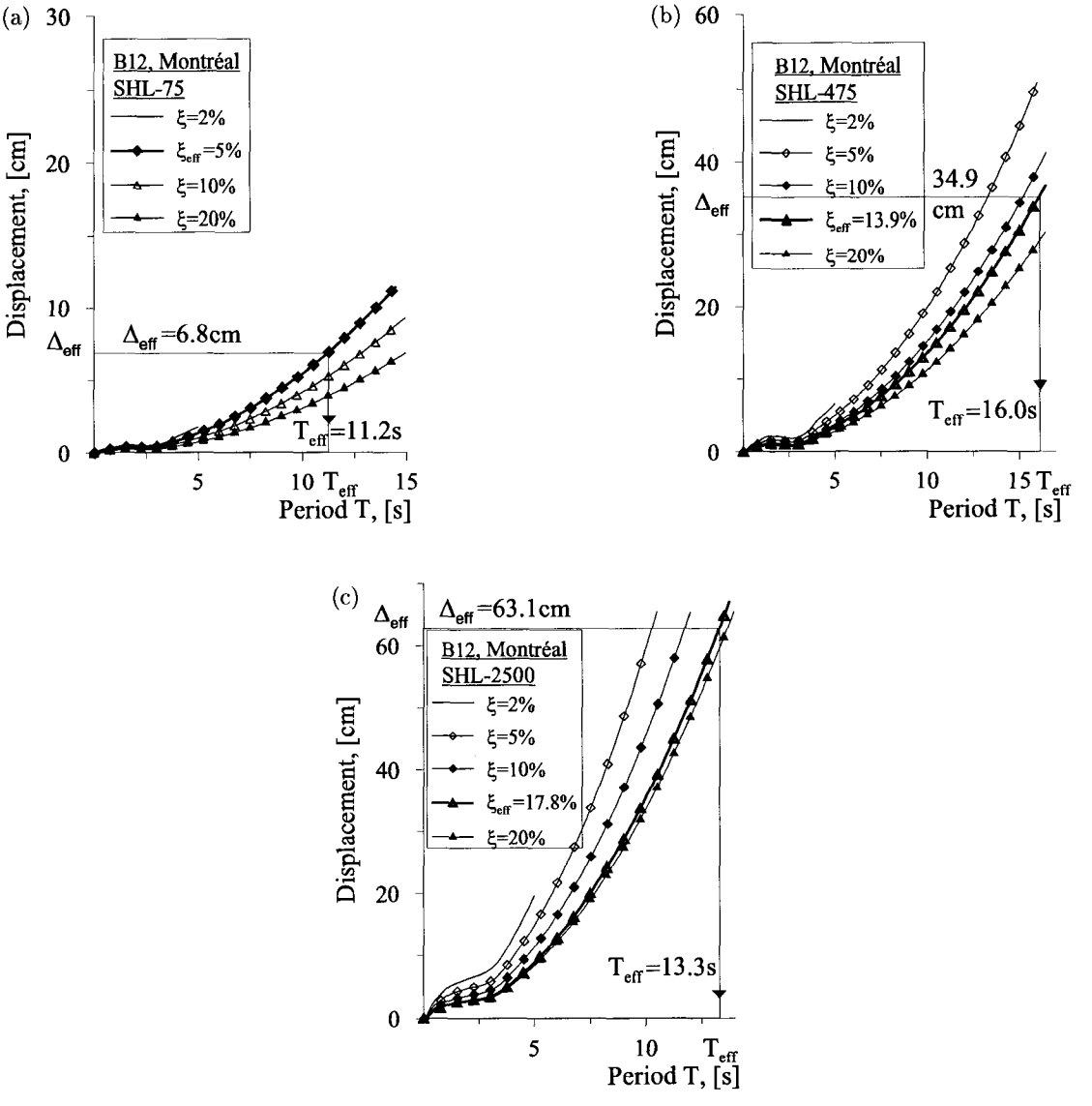

FIG. 5.13 Displacement Spectra for different damping values ξ for the B12 building in Montréal : (a) Seismic Hazard Level SHL-75; (b) Seismic Hazard Level SHL-475 and (c) Seismic Hazard Level SHL-2500.

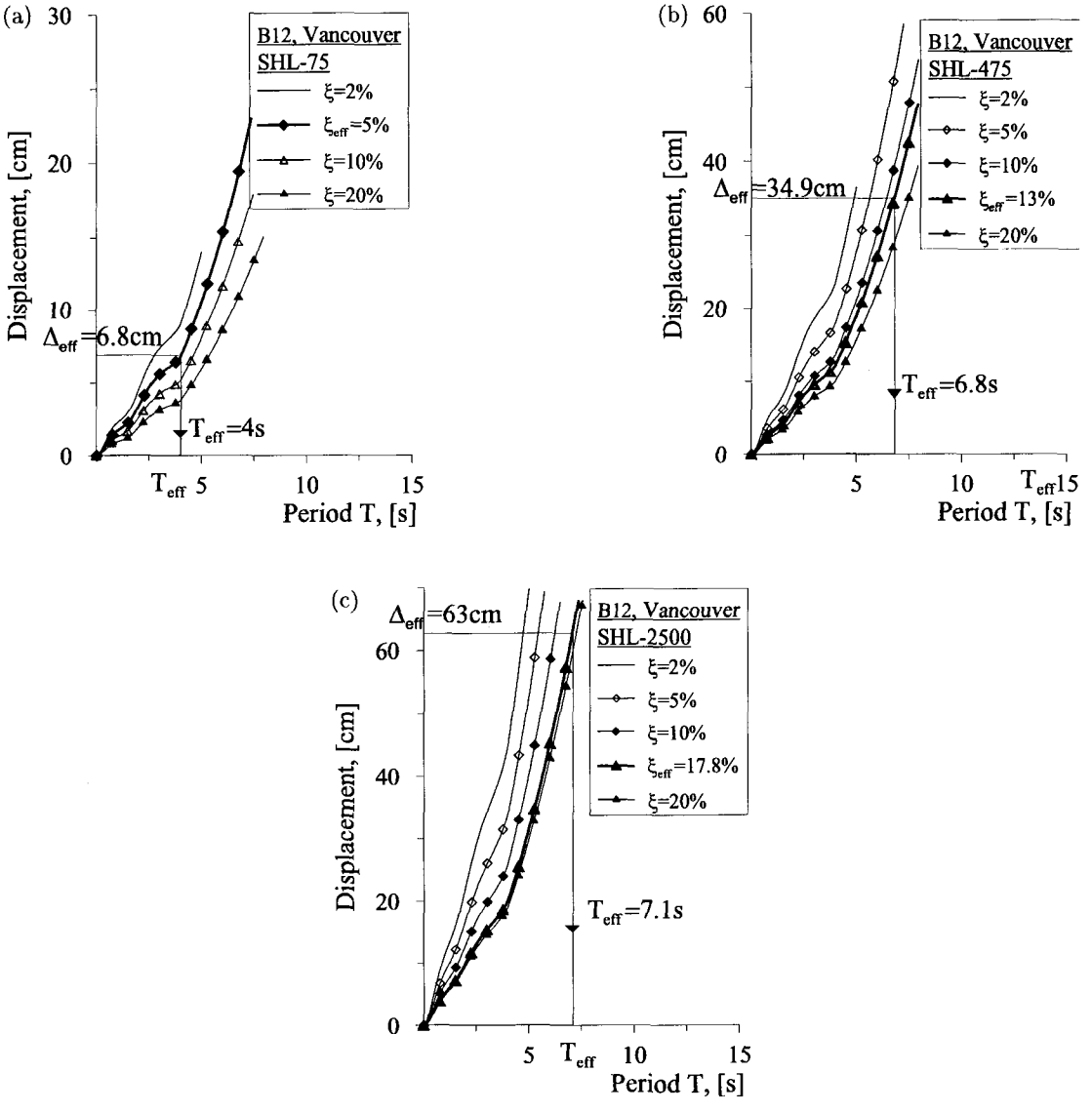

FIG. 5.14 Displacement Spectra for different damping values ξ for the B12 building in Vancouver : (a) Seismic Hazard Level SHL-75; (b) Seismic Hazard Level SHL-475 and (c) Seismic Hazard Level SHL-2500.

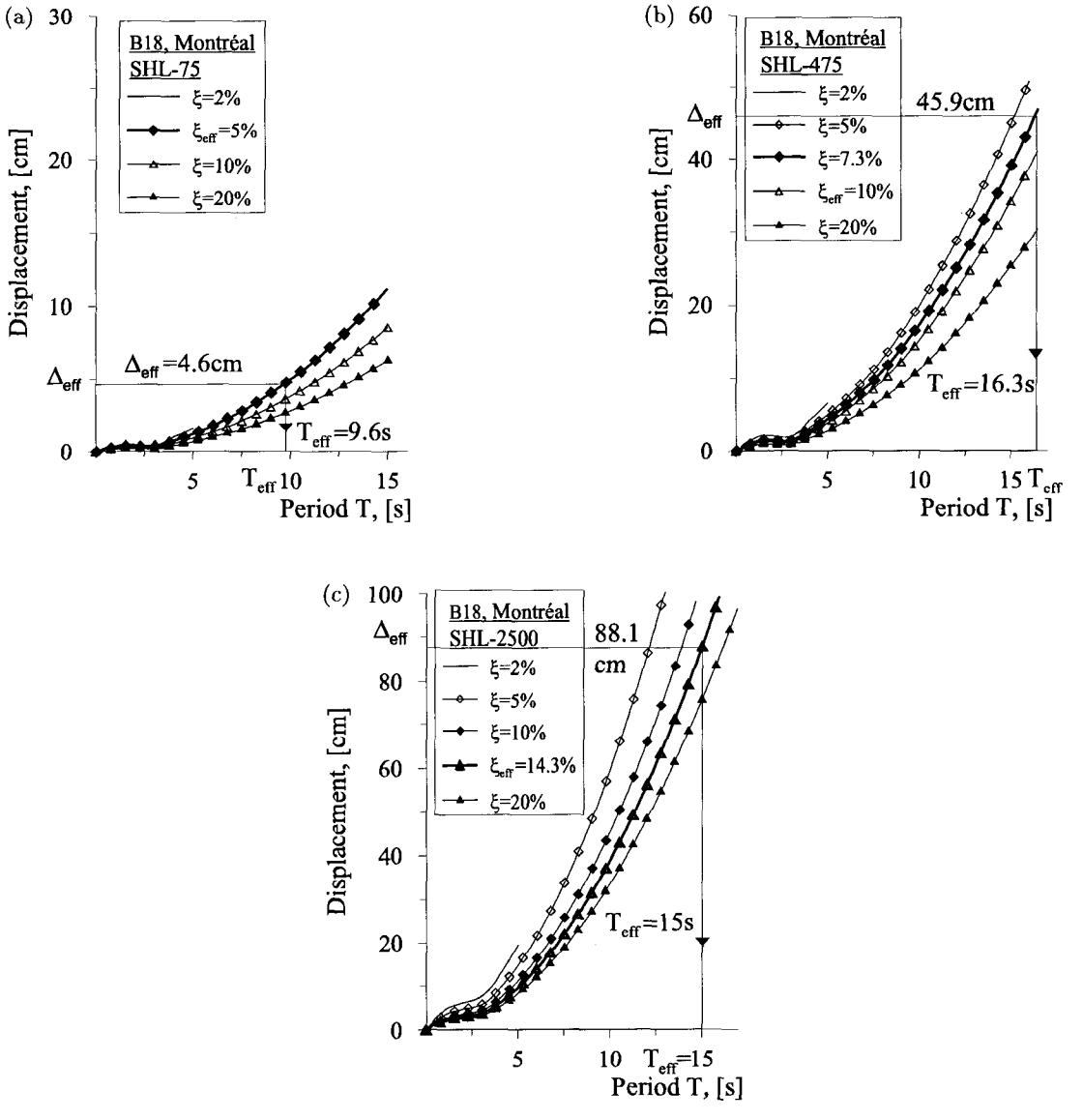

FIG. 5.15 Displacement Spectra for different damping values ξ for the B18 building in Montréal : (a) Seismic Hazard Level SHL-75; (b) Seismic Hazard Level SHL-475 and (c) Seismic Hazard Level SHL-2500.

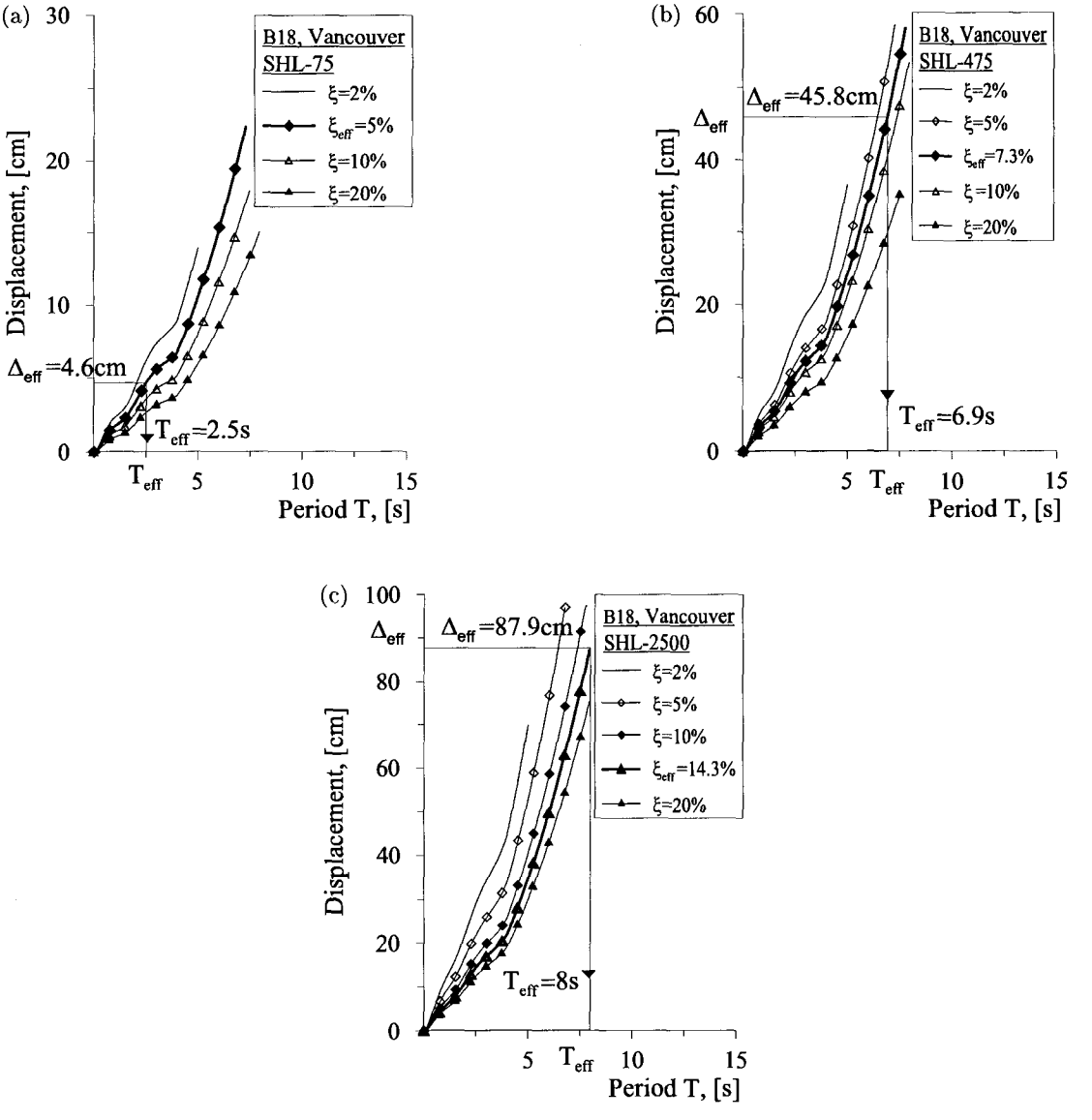

FIG. 5.16 Displacement Spectra for different damping values ξ for the B18 building in Vancouver : (a) Seismic Hazard Level SHL-75; (b) Seismic Hazard Level SHL-475 and (c) Seismic Hazard Level SHL-2500.

TAB. 5.9 Properties of the equivalent SDOF system of the B18 building in Montréal and Vancouver.

Equivalent SDOF	Montréal			Vancouver		
properties	SHL-75	SHL-475	SHL-2500	SHL-75	SHL-475	SHL-2500
Δ_{eff} (m)	0.046	0.459	0.881	0.046	0.458	0.879
M_{eff} (10^3 kg)	7689.84	9155.42	9145.95	7687.58	9139.46	9129.15
h_{eff} (m)	42.62	43.72	43.77	42.50	43.65	43.70
Δ_{y} (m)	0.373	0.388	0.389	0.371	0.387	0.388
μ	1.00	1.18	2.27	1.00	1.18	2.27
ξ_{eff} (%)	5.0	7.3	14.3	5.0	7.3	14.4
T_{eff} (s)	9.62	16.30	15.03	2.47	6.90	7.98
K_{eff} (10^3 N/m)	3280.4	1360.4	1598.3	49745.7	7578.5	5659.6
V_{eff} (kN)	152	625	1407	2288	3473	4975

to seismic hazard level SHL-2500.

Step 1 : The system yield displacement Δ_{y} is initially estimated as the value, defined in the Direct Displacement-Based Design Method (Section 3.4) - $\Delta_{\text{y}} = 0.05\,\text{m}$, listed in Table 5.7 for the B6 building in Montréal ;

Step 2 : The acceptable hinge inelastic rotation at the base is assumed as $\theta_{\text{p}} = 0.008\,\text{rad}$, as listed in Table 3.5 ;

Step 3 : Similarly to Δ_{y}, the system target displacement is initially estimated as the value, defined in the Direct Displacement-Based Design Method (Section 3.4) - $\Delta_{\text{eff}} = 0.166\,\text{m}$, listed in Table 5.7 for the B6 building in Montréal. For the following steps in the iteration procedure Δ_{eff} is defined as per Chopra example (Chopra and Goel 2001) : $\Delta_{\text{eff}} = \Delta_{\text{y}} + h_{\text{eff}}\theta_{\text{p}} = \Delta_{\text{y}} + 16.03 \times 0.008$, where $h_{\text{eff}} = 16.03\,\text{m}$ was perviously defined in Table 5.7, Section 3.4 and Δ_{y} resulted from the last iteration step ;

Step 4 : The design displacement ductility is $\mu = \Delta_{\text{eff}}/\Delta_{\text{y}} = 0.166/0.05 = 3.3$;

Step 5 : Build inelastic displacement design spectra for the calculated design ductility μ, as shown in Figure 5.17 ;

Step 6 : Enter the inelastic displacement spectra with $\Delta_{\text{eff}} = 0.166$ to read the corresponding period $T = 5.22$s for the first iteration ductility $\mu = 3.3$;

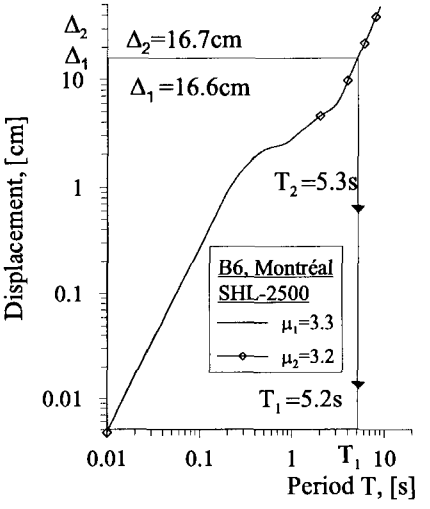

FIG. 5.17 Inelastic displacement spectra development in order to obtain the system period T_{n} at corresponding ductility for the B6 building located in Montréal for SHL-2500.

Step 7 : The initial elastic stiffness k is computed by $k = \dfrac{4\pi^2}{T^2} M_{\text{eff}} = \dfrac{4\pi^2}{5.22^2} \dfrac{2992200}{2 \times 10^5} = 21.68\,\text{kN/cm}$; The effective mass $M_{\text{eff}} = 2992.2 \times 10^3\,\text{kg}$, corresponding to the SDOF system (effective system), was previously calculated by the Direct Displacement-Based Design Method (Section 3.4) and the value was listed in Table 5.7 for the B6 building in Montréal. The calculations in Chopra's DBD method are performed for a single shear wall.

Step 8 : The required yield strength $f_{\text{req}} = k\Delta_{\text{y}} = 21.68 \times 5 = 108\,\text{kN}$;

Step 9 : The required flexural strenght M_{req}, based on the required yield strength is calculated : $M_{\text{req}} = f_{\text{req}} h_{\text{eff}} = 108 \times 16.03 = 1731\,\text{kNm}$.

Unless research is performed for the shearwall behaviour under different seismic hazard levels SHL-475 and SHL-75 and thus the minimum required reinforcement ratio for such a behaviour, the design moment flexural strength M_{u} in the present study is chosen as the required flexural strength, which in our case

is : $M_u = M_{req} = 1731\,\text{kNm}$. Therefore, the design lateral yield strength V_u would be : $V_u = f_{req} = 108\,\text{kN}$

Step 10 : The initial elastic stiffness is then redefined - $k_{des} = 3\frac{EI_{eff}}{h_{eff}^3} = 3\frac{2.866 \times 10^6}{16.03^3 \times 100} = 20.9\,\text{kN/cm}$, where the effective system property is defined as - $EI_{eff} = M_u/\phi_y = 1731/0.00606 = 2.866 \times 10^6\,\text{kN}m^2$.

Step 11 : The corresponding yield displacement is determined : $\Delta_{y,des} = \frac{V_u}{k_{des}} = \frac{108}{20.9} = 5.19\,\text{cm}$ for the so-designed structural system ;

Step 12 : The estimated yield displacement $\Delta_y = 5\,\text{cm}$ [Step 1] is compared to the obtained yield displacement $\Delta_{y,des} = 5.19\,\text{cm}$ [Step 11] ;

Step 13 : Steps 1 to 11 are repeated until a desired yield displacement difference is obtained. In the present case a satisfactory yield displacement difference was obtained after two iterations giving a shearwall lateral yield strength of $V_u = 111\,\text{kN}$ per wall and so then $V_u = 2 \times f_{req} = 2 \times 111 = 222\,\text{kN}$ as a building base shear.

TAB. 5.10 Results of iterative DBD procedure for 6-storey shearwall in Montréal using inelastic design spectrum for SHL-2500.

No	Δ_y (cm)	Δ_{eff} (cm)	μ	T (s)	k (kN/cm)	f_{req} (kN)	M_{req} (kNm)	EI_{eff} (kNm^2)	k_{des} (kN/cm)	$\Delta_{y,des}$ (cm)
1	5.00	16.6	3.3	5.2	21.68	108	1731	2866050	20.9	5.19
2	5.19	16.7	3.2	5.3	21.43	111	1783	2941950	21.4	5.19

The Chopra method procedure for Displacement-based design (DBD) using inelastic design spectra is applied for the three models of 6-, 12- and 18-storeys buildings, located in Montréal and Vancouver, subjected to the three seismic hazard levels SHL-75, SHL-475 and SHL-2500. Steps [1] to [11] of the afore-described Chopra method, are tabulated in details for each building and for each seismic hazard level and are represented in Annex IV. Following is a comparative Table 5.11 with the final results for the yielding lateral and flexural strengths and the yield displacements obtained for the models under the three

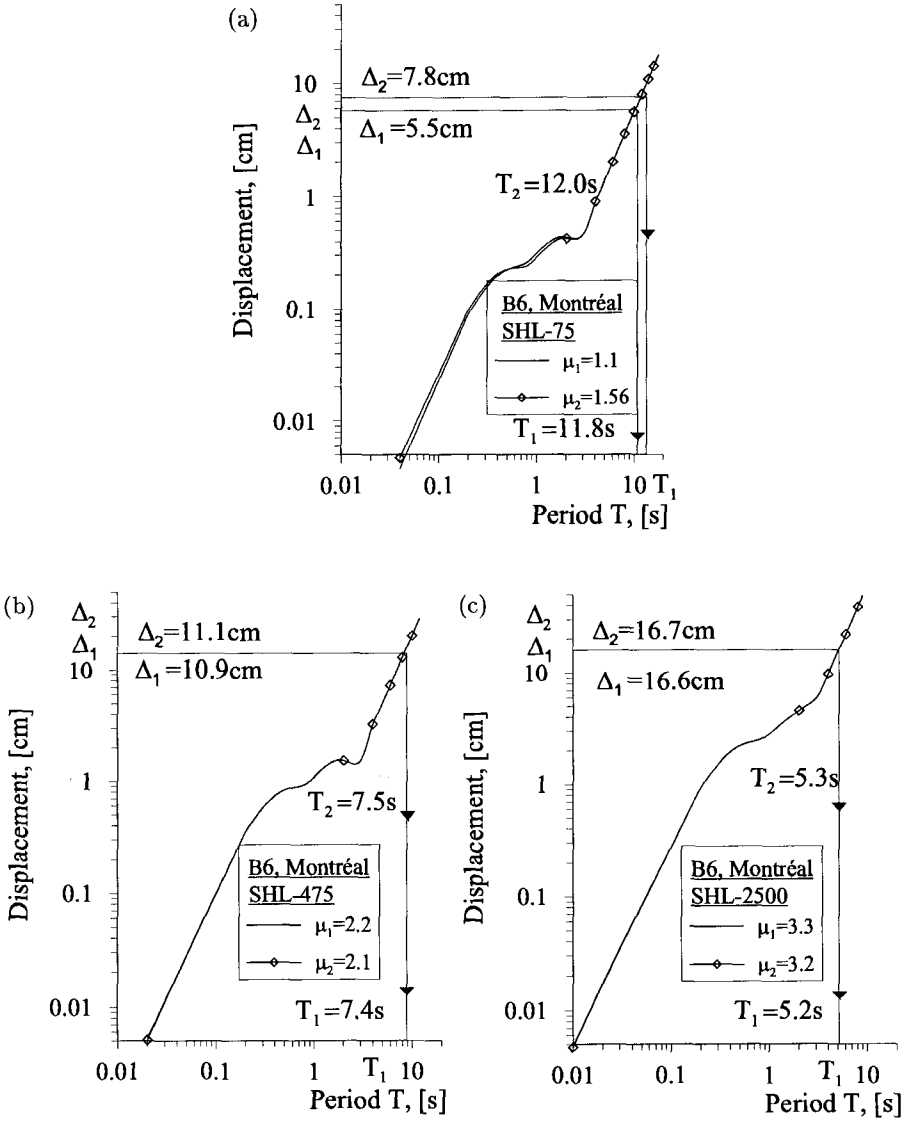

FIG. 5.18 Displacement Spectra for different ductility values μ for the B6 building in Montréal : (a) Seismic Hazard Level SHL-75; (b) Seismic Hazard Level SHL-475 and (c) Seismic Hazard Level SHL-2500.

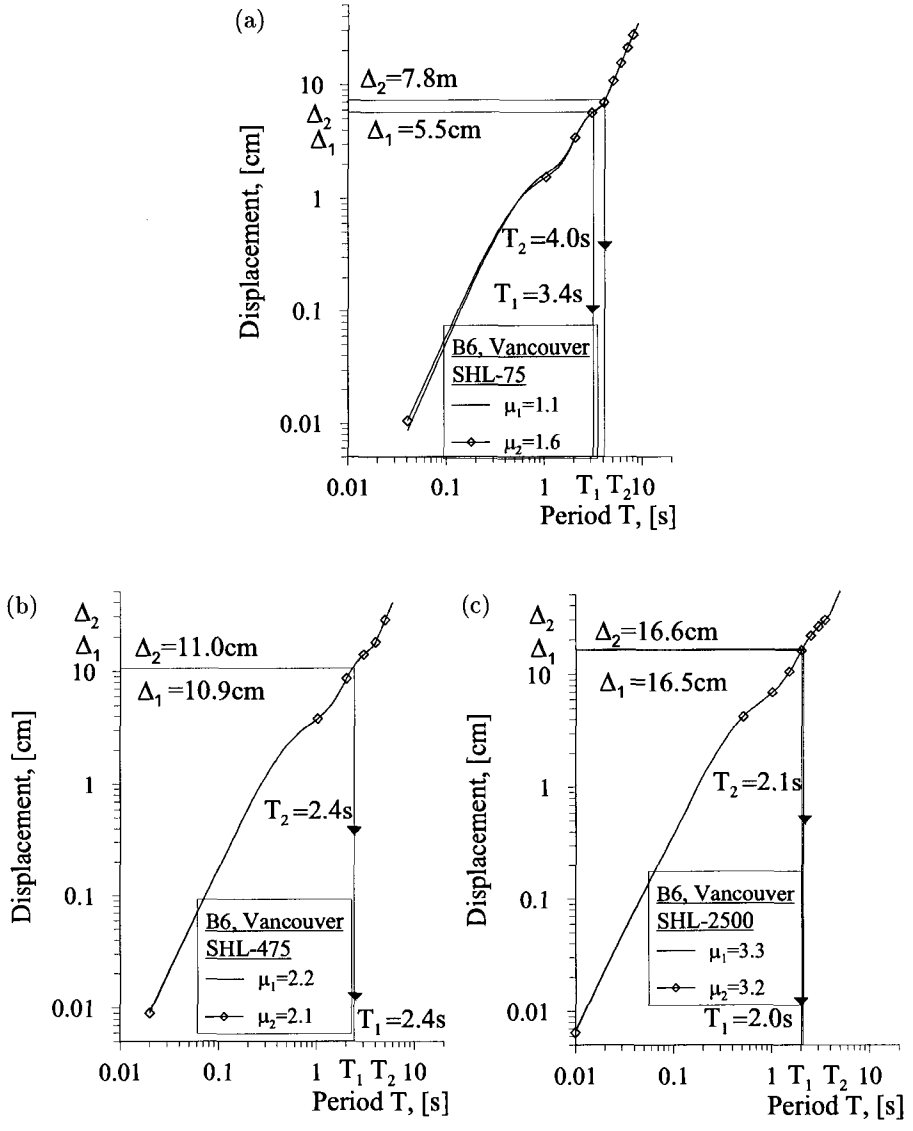

FIG. 5.19 Displacement Spectra for different ductility values μ for the B6 building in Vancouver : (a) Seismic Hazard Level SHL-75; (b) Seismic Hazard Level SHL-475 and (c) Seismic Hazard Level SHL-2500.

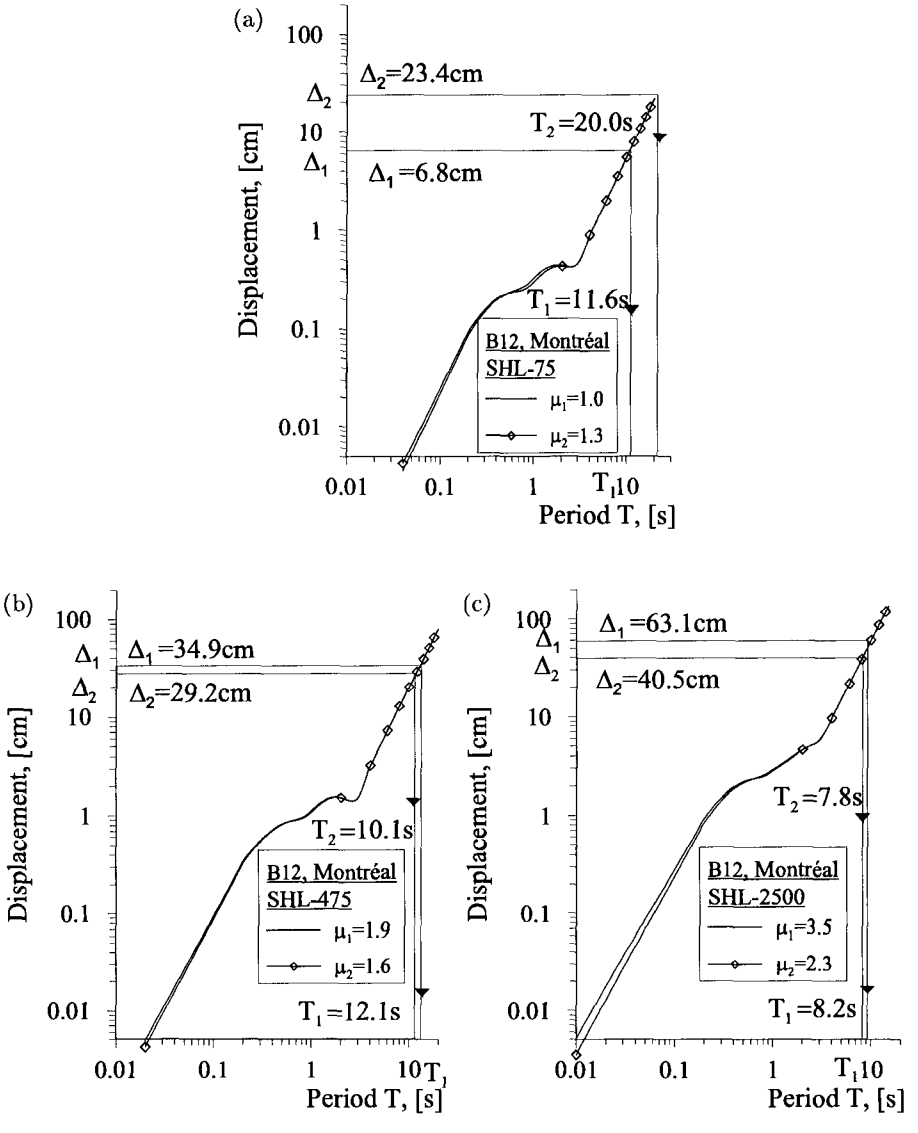

FIG. 5.20 Displacement Spectra for different ductility values μ for the B12 building in Montréal : (a) Seismic Hazard Level SHL-75; (b) Seismic Hazard Level SHL-475 and (c) Seismic Hazard Level SHL-2500.

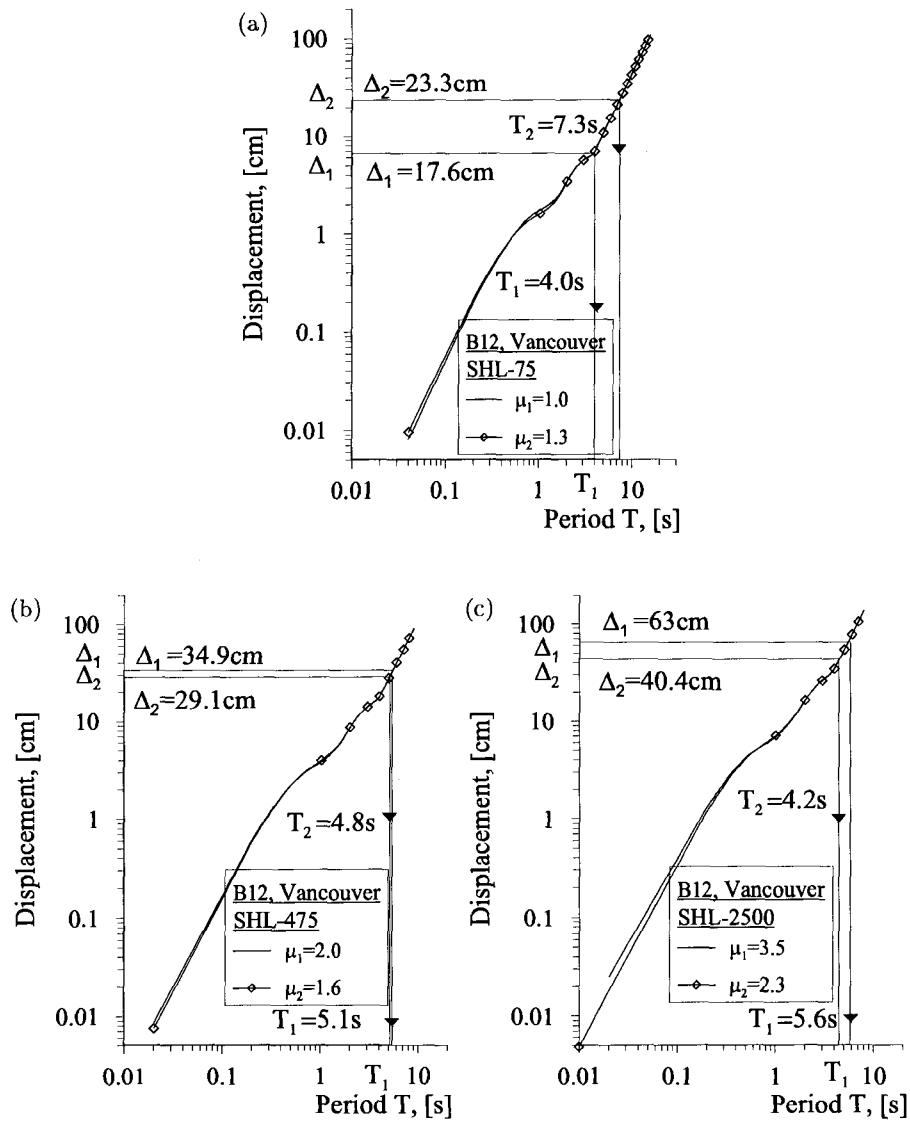

FIG. 5.21 Displacement Spectra for different ductility values μ for the B12 building in Vancouver : (a) Seismic Hazard Level SHL-75; (b) Seismic Hazard Level SHL-475 and (c) Seismic Hazard Level SHL-2500.

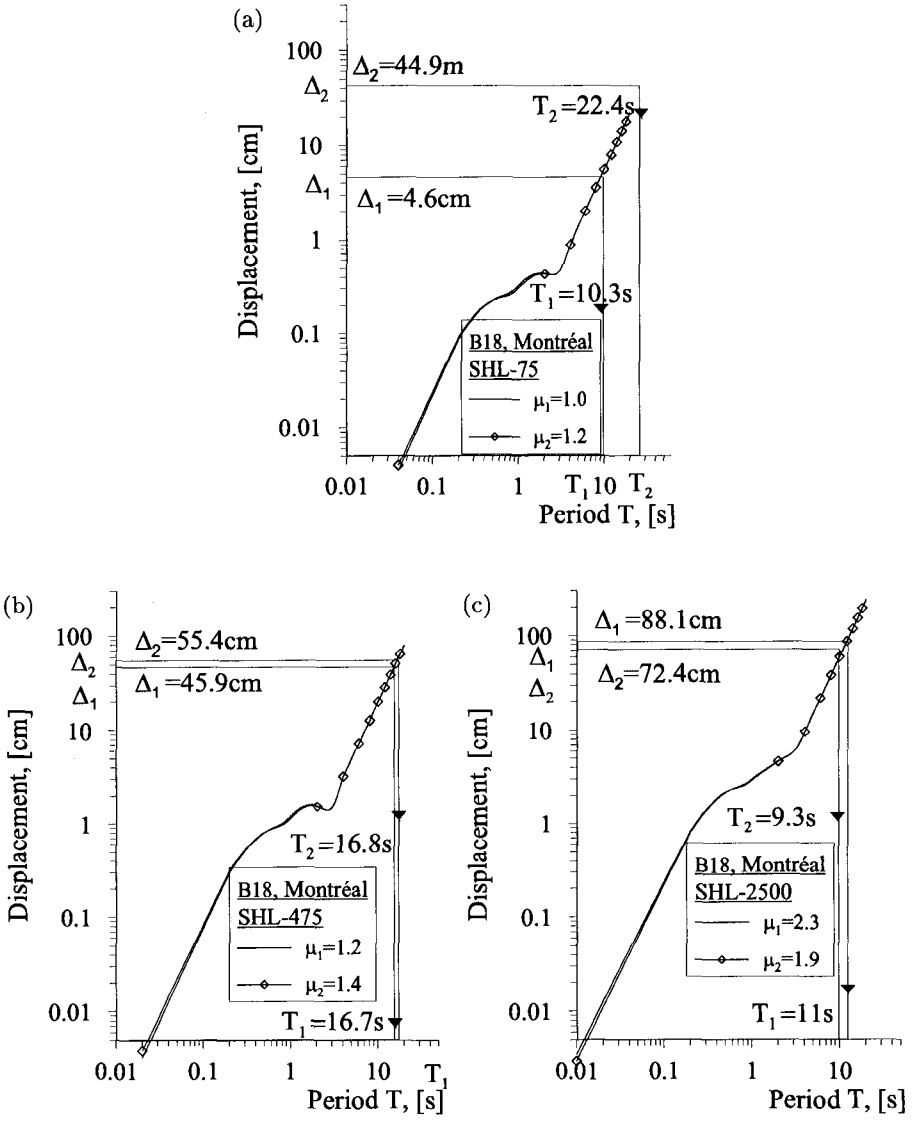

FIG. 5.22 Displacement Spectra for different ductility values μ for the B18 building in Montréal : (a) Seismic Hazard Level SHL-75; (b) Seismic Hazard Level SHL-475 and (c) Seismic Hazard Level SHL-2500.

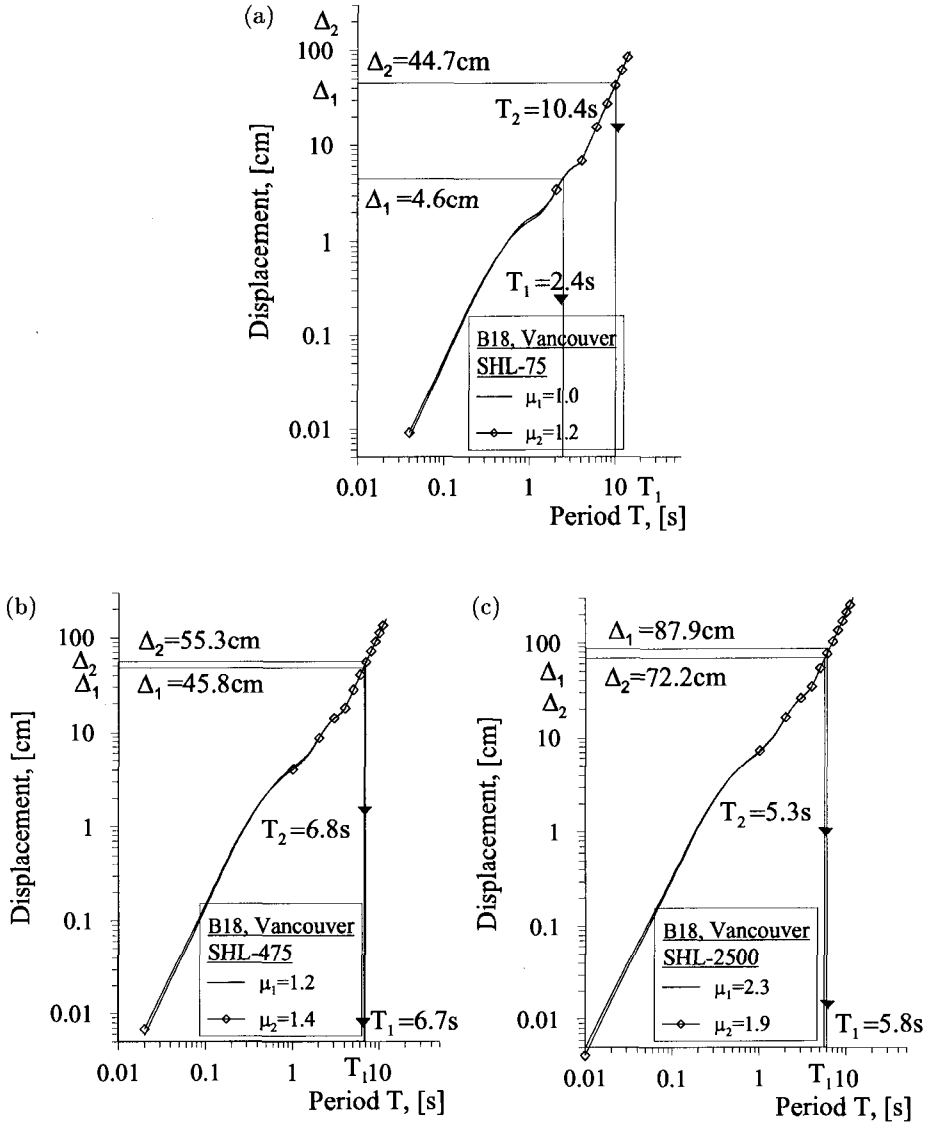

FIG. 5.23 Displacement Spectra for different ductility values μ for the B18 building in Vancouver : (a) Seismic Hazard Level SHL-75; (b) Seismic Hazard Level SHL-475 and (c) Seismic Hazard Level SHL-2500.

SHL in both cities. The final design results for the shear wall base shear and moment f_{req} and M_{req} are listed in the following table as V_u and M_u.

TAB. 5.11 Maximum displacement, design base shear and moment results from IDS method for a shear wall in B6, B12 and B18 under SHL-75, -475 and -2500.

	Montréal			Vancouver		
Buildings	Δ_{eff} (m)	V_u (kN)	M_u (kNm)	Δ_{eff} (m)	V_u (kN)	M_u (kNm)
Seismic Hazard Level SHL-2500						
B6	0.167	111	1783	0.166	720	11512
B12	0.405	356	10610	0.404	1212	36059
B18	0.724	805	35209	0.722	4345	189880
Seismic Hazard Level SHL-475						
B6	0.111	54	865	0.110	520	8366
B12	0.294	212	6326	0.291	932	27734
B18	0.554	247	10810	0.553	1524	66526
Seismic Hazard Level SHL-75						
B6	0.055	21	337	0.078	188	2954
B12	0.234	53	1583	0.233	397	11758
B18	0.367	111	4731	0.447	517	21968

CHAPTER 6

NONLINEAR TIME HISTORY DYNAMIC ANALYSES

6.1 Introduction

As described in Chapter 2, the NBCC 2005 (CCBFC 2005) avocates the use of linear and nonlinear dynamic analyses to establish design loads for building structures. For common structural design purposes, buildings and construction materials are generally considered to behave in a linear elastic manner. When subjected to important dynamic loads, nonlinear response has to be assessed, and this is particularly valid for buildings designed to dissipate inelastic energy. As principal seismic force resisting systems, shear walls should be designed to efficiently dissipate earthquake energy and their response to this type of loading is expected to extend to the nonlinear inelastic range. Nonlinear time history analyses are used in this chapter to assess the seismic performance of the three cantilever shear walls designed previously in Chapter 4. The buildings are subjected to historical and synthetic ground motions to evaluate their nonlinear response in light of the target performance objectives described in Chapters 2 and 5. Internal forces and maximum displacements at each floor are obtained and compared to results of the displacement-based approaches presented in Chapter 5. The computer program Ruaumoko 2D (Carr 2002) is used to perform nonlinear dynamic analyses of two-dimensional models of the three cantilever shear wall buildings B6, B12 and B18. It is to be mentioned that soil-structure interaction effects are not included in the present research.

6.2 Seismic Input

6.2.1 Selected Ground Motions

Ground motions used for seismic performance evaluation at a given location should reflect specific site characteristics such as tectonic environment, magnitude and epicentral

distance of expected earthquake events. The NBCC 2005 requires that ground motions selected as seismic input be compatible with the Geological Survey of Canada fourth-generation seismic hazard maps (Adams *et al.* 1999). This compatibility is ensured through spectrum matching with respect to the Uniform Hazard Spectra at 2% probability of exeedance in 50 years (CCBFC 2005). Two historical and five simulated accelerograms are used in this work as explained next.

Acceleration time histories recorded during the Saguenay and the Nahanni earthquakes are selected as seismic input. Earthquake data was taken from the Geological Survey of Canada (GSC 2006). Table 6.1 contains the main characteristics of the 4 horizontal components considered. The corresponding accelerograms are illustrated in Fig. 6.1.

TAB. 6.1 Main characteristics of selected historical ground motions.

No	Label	Event	Date	Component	Duration (s)	PGA (g)
1	Sag0	Saguenay	25-11-1988	0°	25.00	0.063
2	Sag90	Saguenay	25-11-1988	90°	25.00	0.091
3	Nah10	Nahanni	23-12-1985	10°	20.33	0.975
4	Nah280	Nahanni	23-12-1985	280°	20.42	1.345

In addition to the historical accelerograms described above, synthetic ground motions compatible with the 1/2475 per annum UHS prescribed by he NBCC 2005 for Montréal and Vancouver are considered. These synthetic accelerograms are assumed to realistically represent ground motions corresponding to combinations of earthquake magnitudes M and distances R that contribute most to hazard at the two cities. Table 6.2 shows the magnitude-distance combinations considered and the Fine-Tune Scale Factor (FTSF) used to calibrate the simulated earthquake signals (Atkinson and Beresnev 1998). The characteristics of the 10 resulting simulated earthquake signals used in this work are presented in Table 6.3.

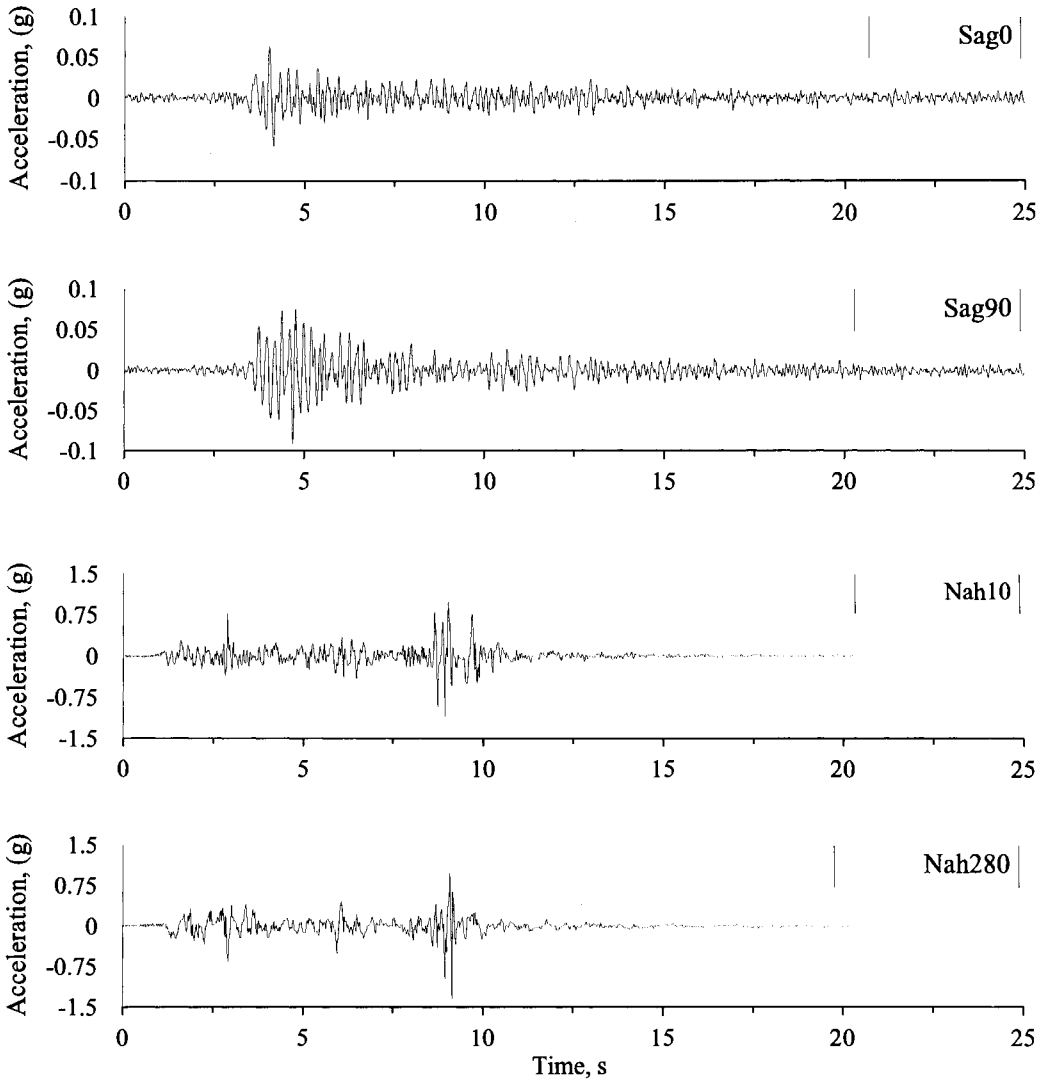

FIG. 6.1 Saguenay and Nahanni accelerograms used for nonlinear dynamic analyses.

TAB. 6.2 Magnitude-distance combinations and corresponding Fine-Tune Scale Factors (FTSF) used.

Location	Short-period event	FTSF	Long-period event	FTSF
Montréal	M6.0 at R=30 km	0.85	M7.0 at R=70 km	0.90
Vancouver	M6.5 at R=30 km	1.00	M7.2 at R=70 km	1.00
			M8.5 Cascadia	2.20

TAB. 6.3 Main characteristics of selected simulated ground motions.

No.	Event	Location	M	R (km)	Duration (s)	PGA (g)
1	AtkM6R30, Trial 1	Montréal (short-period)	6.0	30	8.87	0.430
2	AtkM6R30, Trial 2	Montréal (short-period)	6.0	30	8.87	0.522
3	AtkM7R70, Trial 1	Montréal (long-period)	7.0	70	24.06	0.301
4	AtkM7R70, Trial 2	Montréal (long-period)	7.0	70	24.06	0.286
5	AtkM65R30, Trial 1	Vancouver (short-period)	6.5	30	8.52	0.534
6	AtkM65R30, Trial 2	Vancouver (short-period)	6.5	30	8.52	0.537
7	AtkM72R70, Trial 1	Vancouver (long-period)	7.2	70	18.17	0.246
8	AtkM72R70, Trial 2	Vancouver (long-period)	7.2	70	18.17	0.259
9	AtkM85, Trial 1	Cascadia zone	8.5	–	121.62	0.045
10	AtkM85, Trial 2	Cascadia zone	8.5	–	121.62	0.049

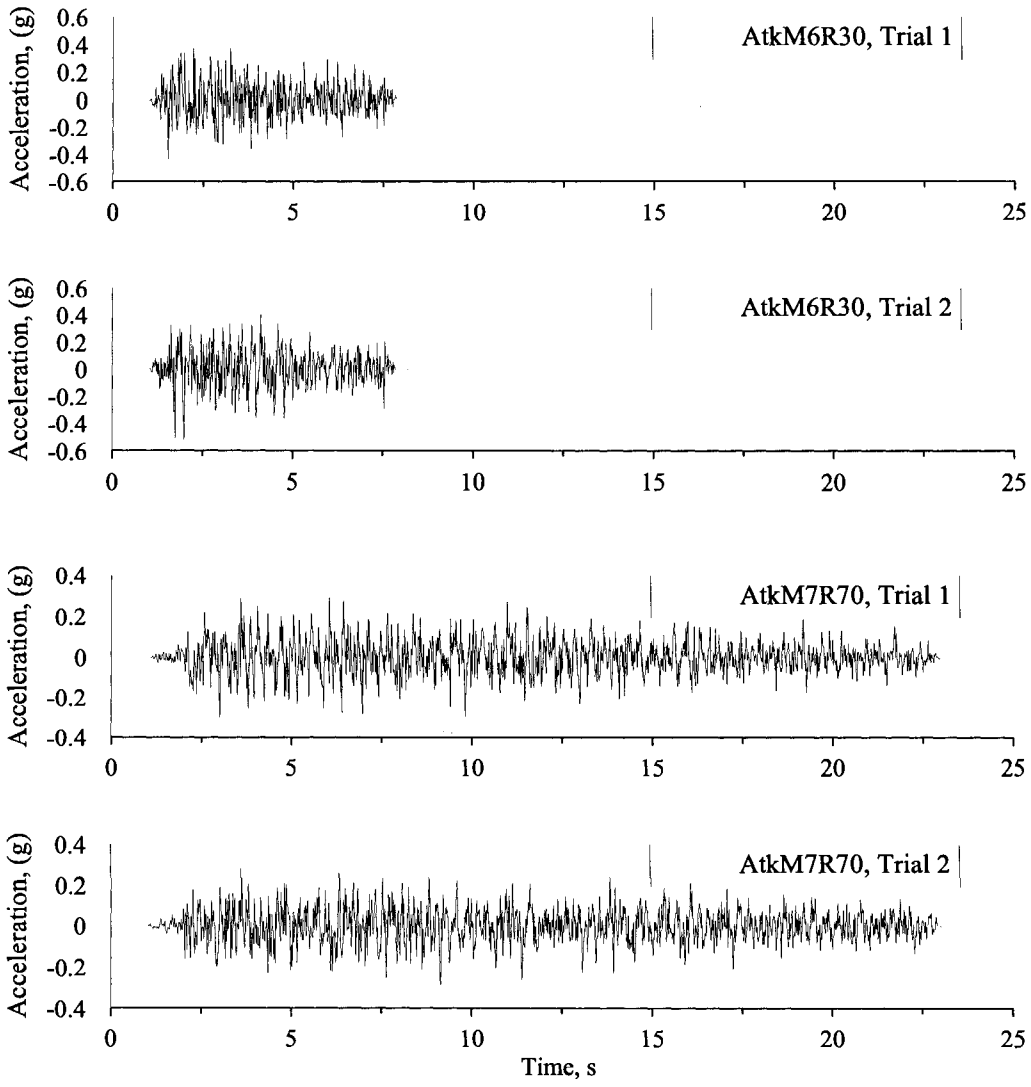

FIG. 6.2 Simulated accelerograms generated to represent short-period and long-period ground-motion hazards at Montréal.

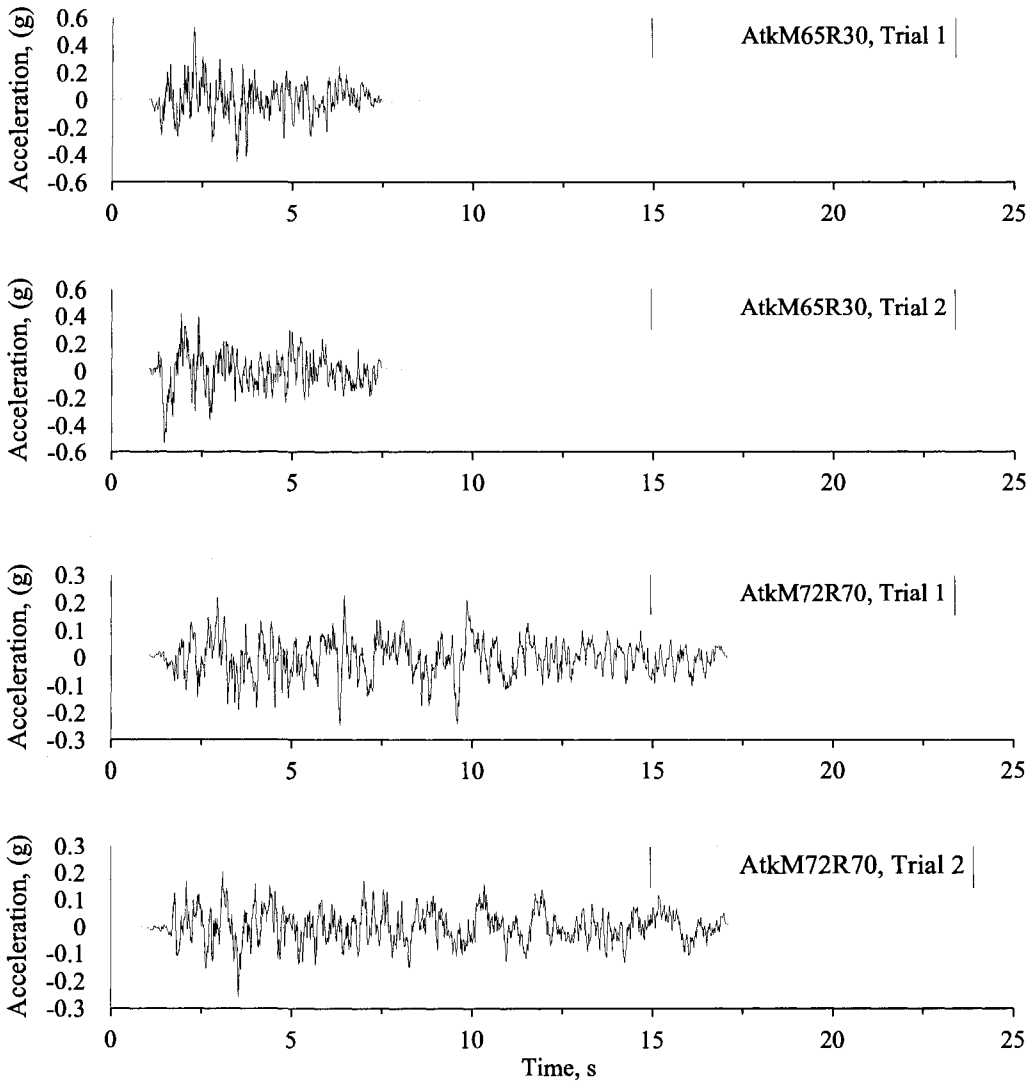

FIG. 6.3 Simulated accelerograms generated to represent short-period and long-period ground-motion hazards at Vancouver.

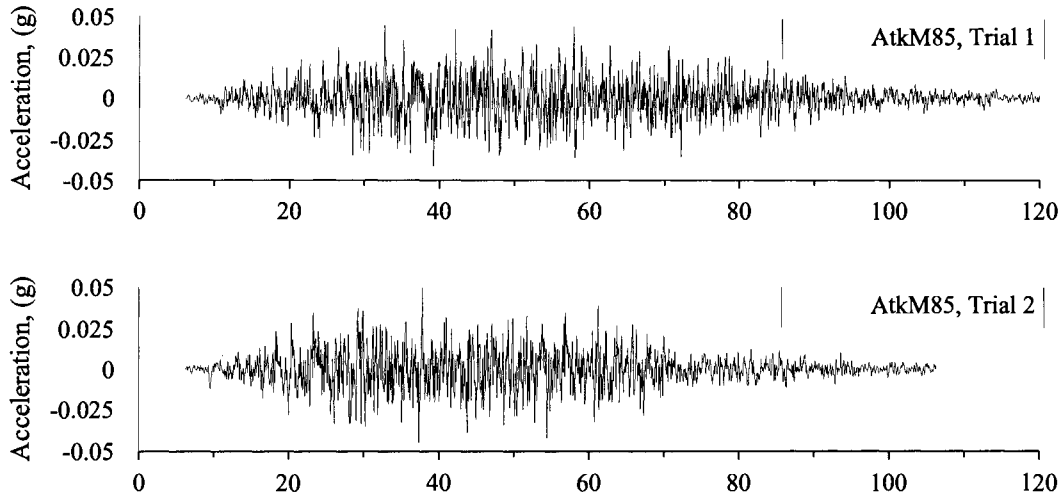

FIG. 6.4 Simulated accelerograms generated to represent ground-motion hazard for Cascadia Subduction Zone.

6.2.2 Time Domain Spectrum-Matching

As mentioned previously, the ground motions used for seismic analyses have to be scaled to match the target UHS at Montréal and Vancouver as prescribed by the NBCC 2005 [Art. 4.1.8.4 (1) and (6)]. To preserve the non-stationary character of the modified records, close spectrum-matching was performed in the time domain using the computer code RSPMATCH (Abrahamson 1998). This program implements the scaling algorithm proposed by Lilhanand and Tseng (1988), which produces a transformed signal by adding wavelets to the original record and adjusting the resulting spectral amplitude to *closely* fit the target spectrum. Using the FTSF factors shown in Table 6.3, the simulated ground motions are readily *loosely* matched to the target NBCC 2005 UHS. For comparison purposes, a close spectrum-matching is also performed on the simulated accelerograms.

Table 6.4 contains the signals used as seismic input for the non linear analyses conducted in this work. Figures 6.5 to 6.11 illustrate the original and scaled acceleration response spectra of the used earthquake signals as well as the NBCC 2005 2% in 50 year UHS at Montréal or Vancouver, correspondingly.

TAB. 6.4 Main characteristics of selected simulated and historical ground motions.

No.	Label of scaled signal	Label of original signal	Location	Type of scaling
1	1M6R30	AtkM6R30, Trial 1	Montréal	Loose : FTSF=0.85
2	2M6R30	AtkM6R30, Trial 2	Montréal	Loose : FTSF=0.85
3	1M6R30match	AtkM6R30, Trial 1	Montréal	Close : RSPMATCH
4	1M7R70	AtkM7R70, Trial 1	Montréal	Loose : FTSF=0.90
5	2M7R70	AtkM7R70, Trial 2	Montréal	Loose : FTSF=0.90
6	1M7R70match	AtkM7R70, Trial 1	Montréal	Close : RSPMATCH
7	Sag0Mtl	Sag0	Montréal	Close : RSPMATCH
8	Sag90Mtl	Sag90	Montréal	Close : RSPMATCH
9	Nah0Mtl	Nah0	Montréal	Close : RSPMATCH
10	Nah280Mtl	Nah280	Montréal	Close : RSPMATCH
11	1M65R30	AtkM65R30, Trial 1	Vancouver	Loose : FTSF=1.00
12	2M65R30	AtkM65R30, Trial 2	Vancouver	Loose : FTSF=1.00
13	1M65R30match	AtkM65R30, Trial 1	Vancouver	Close : RSPMATCH
14	1M72R70	AtkM72R70, Trial 1	Vancouver	Loose : FTSF=1.00
15	2M72R70	AtkM72R70, Trial 2	Vancouver	Loose : FTSF=1.00
16	1M72R70match	AtkM72R70, Trial 1	Vancouver	Close : RSPMATCH
17	1M85	AtkM85, Trial 1	Vancouver	Loose : FTSF=2.2
18	2M85	AtkM85, Trial 2	Vancouver	Loose : FTSF=2.2

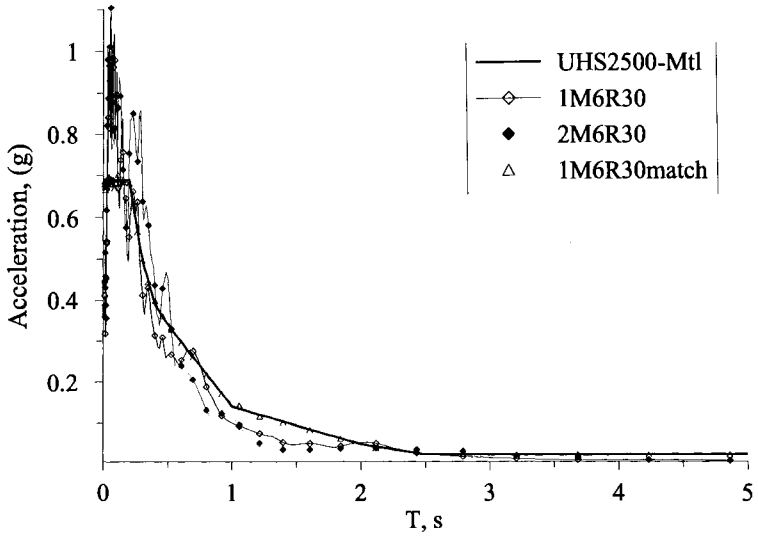

FIG. 6.5 Acceleration response spectra of short-period simulated ground-motions for Montréal, loosely and closely scaled to NBCC 2005 2% in 50 year UHS at Montréal.

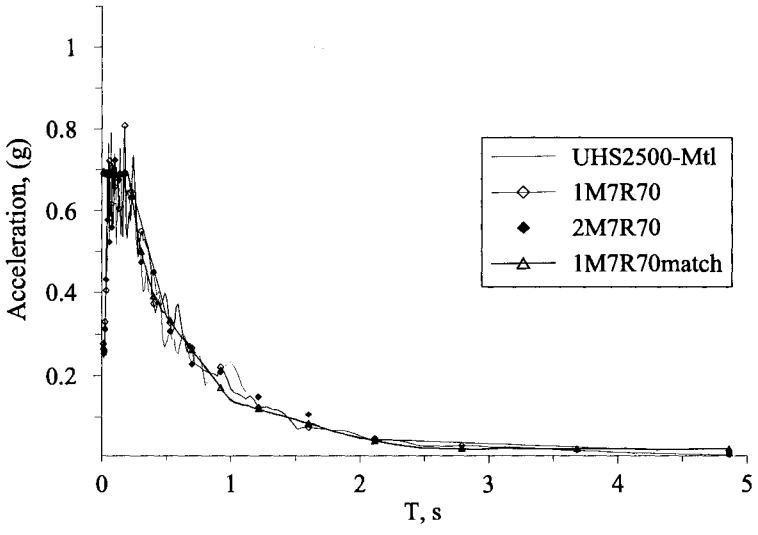

FIG. 6.6 Acceleration response spectra of long-period simulated ground-motions for Montréal, loosely and closely scaled to NBCC 2005 2% in 50 year UHS at Montréal.

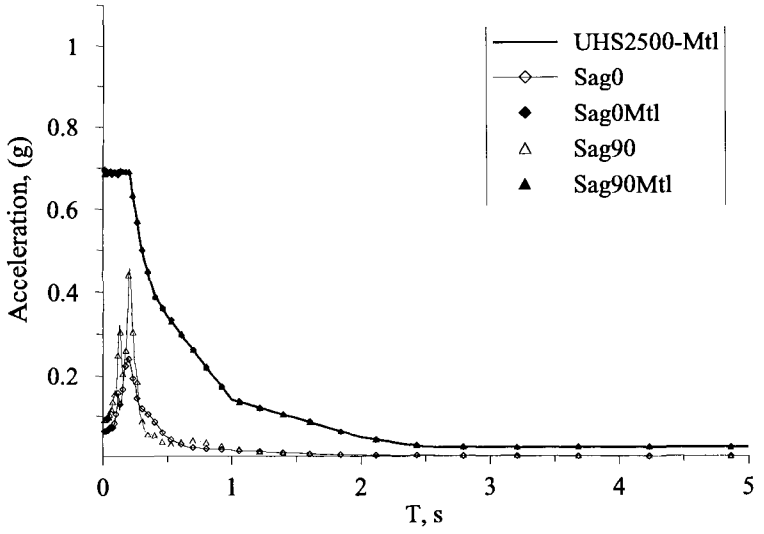

FIG. 6.7 Acceleration response spectra of original Saguenay ground motion and its close scaling to NBCC 2005 2% in 50 year UHS at Montréal.

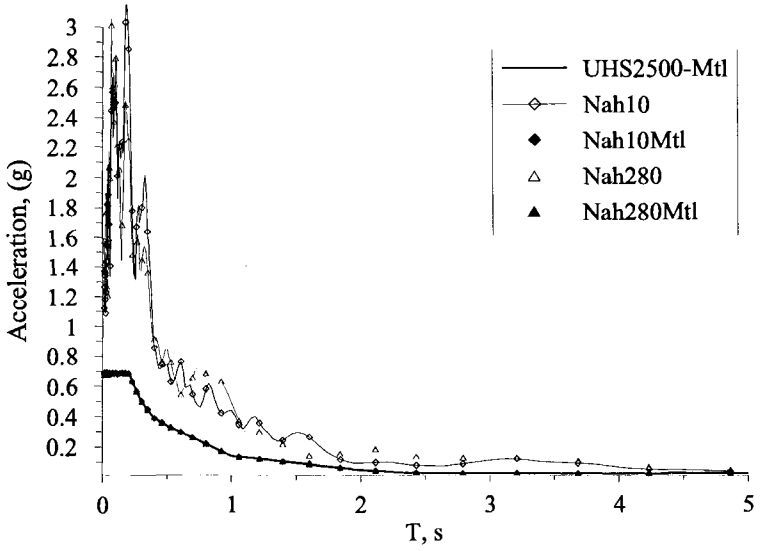

FIG. 6.8 Acceleration response spectra of original Nahanni ground motion and its close scaling to NBCC 2005 2% in 50 year UHS at Montréal.

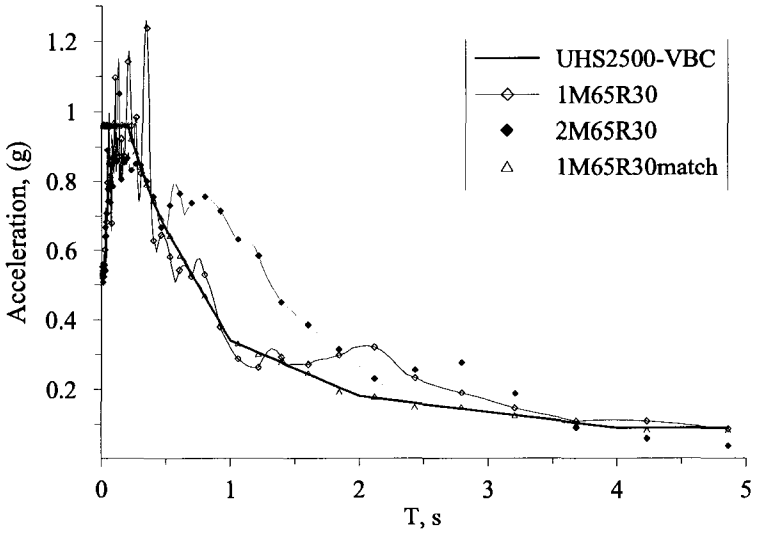

FIG. 6.9 Acceleration response spectra of short-period simulated ground-motions for Vancouver, loosely and closely scaled to NBCC 2005 2% in 50 year UHS at Vancouver.

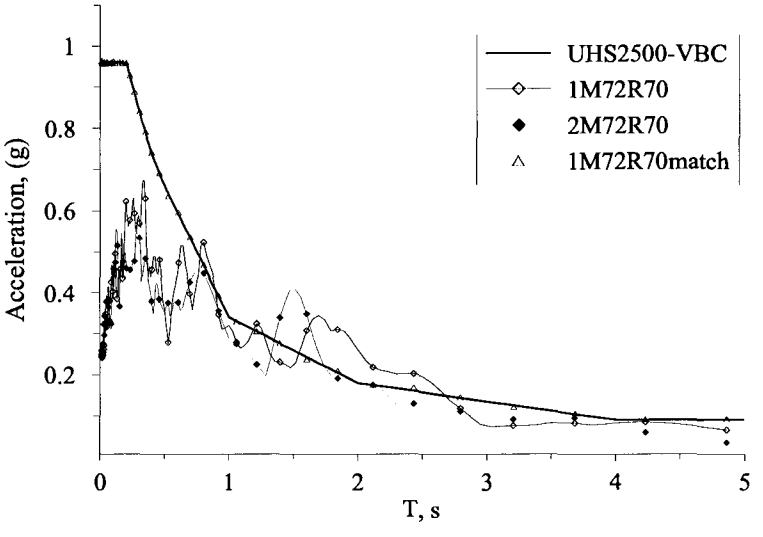

FIG. 6.10 Acceleration response spectra of long-period simulated ground-motions for Vancouver, loosely and closely scaled to NBCC 2005 2% in 50 year UHS at Vancouver.

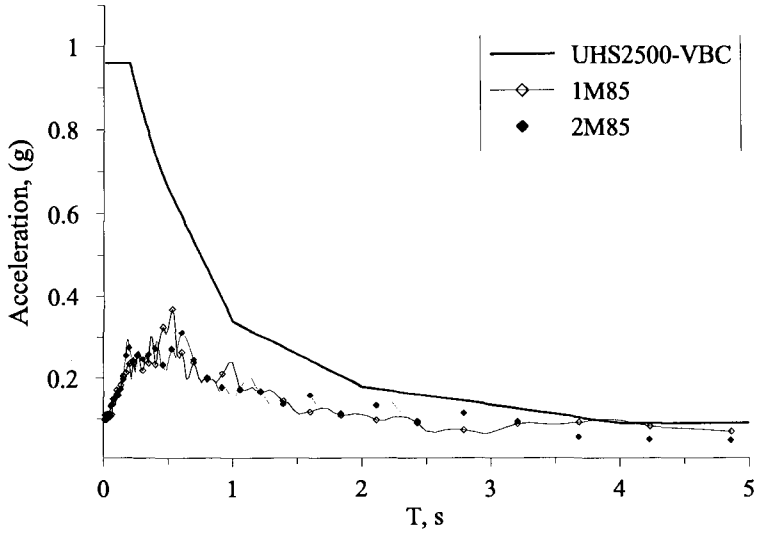

FIG. 6.11 Acceleration response spectra of simulated ground-motions for Cascadia Subduction zone, loosely and closely scaled to NBCC 2005 2% in 50 year UHS at Vancouver.

6.3 Numerical Modelling Aspects

6.3.1 Computer Program

As mentioned before, nonlinear dynamic analyses of the three cantilever shear walls are conducted using the computer program Ruaumoko 2D (Carr 2002). This program was initially developed to assess nonlinear time history response of building structures to earthquake loads (Carr 1982). The recent versions of the program can also be used to apply monotonic or cyclic loadings and to perform pushover analyses. It is chosen for the present work because of its widespread use by the earthquake engineering community, and most importantly due to the diversity of element types, hysteretic rules and other modelling options it offers.

6.3.2 Materials Definition

The *Kent and Park* relation between stress and strain in the concrete is chosen for analysis (see Fig.6.12), taking into account the following hypoteses [Carr 2002] :

- The concrete is assumed to carry no tensile stress once the material has cracked and the compressive strain has exceeded the concrete ultimate strain $EPSB$ is 0.0035, as per Cl.10.1.3 [Canadian Standard Association 2004].
- The concrete stress-strain law follows a quadratic rule until the stress $SIGA$ is reached.
- The peak stress $SIGA = -30000\,\text{kPa}$ and the elastic modulus of the concrete $EMODC = 24647\,\text{kPa}$ have been already defined in Chapter 4.
- The concrete peak strain is implemented in the program as $EPSA = 2{\times}SIGA/EMODC$.
- The concrete ultimate stress $SIGB$ is assumed as $-3000\,\text{kPa}$ and the concret cracking stress as $SIGCR = 1750\,\text{kPa}$.
- The steel hysteresis follows an elasto-plastic first yield rule, but subsequent cycles follow the *Al-Bermani* Bounding Surface one, where the deffault value of $ALFA$, accounting for the *Bauschinger* effect was overwritten to 1 in the present study, so to imply a bi-linear hysteresis, as shown in Fig. 6.13.

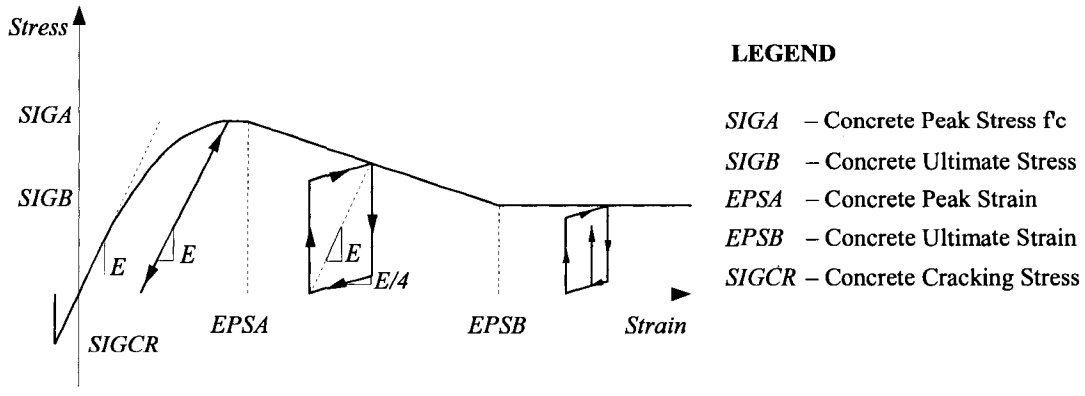

FIG. 6.12 'Kent and Park' Concrete Stress-Strain Relationship

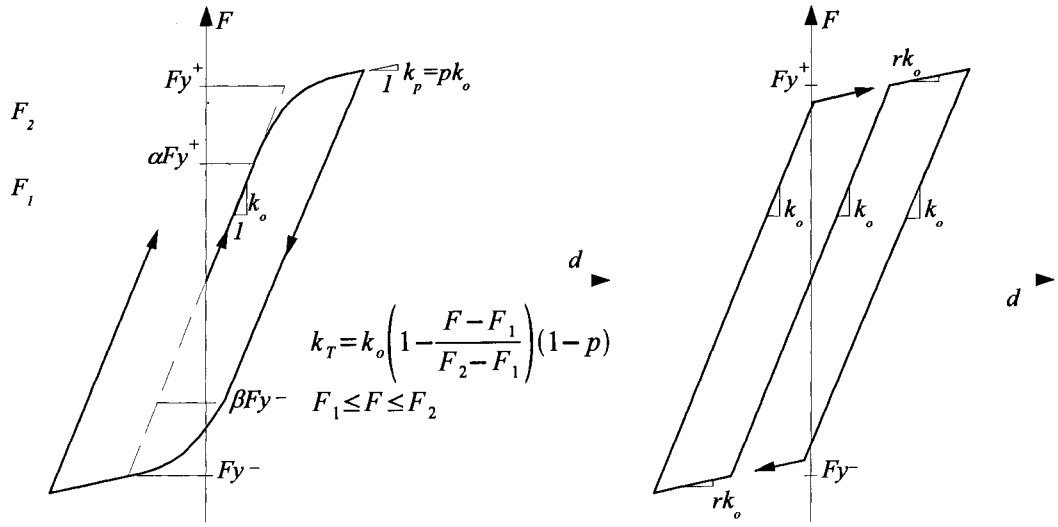

a) Al-Bermani Steel Hysteresis b) Bilinear Steel Hysteresis

FIG. 6.13 Steel Hysteresis

6.3.3 Element Type and Numerical Aspects

A *Structural-Wall* multi-fiber element proposed by Taylor (1977) is used to model the reinforced concrete shear walls. This element allows to represent the wall section as a concrete section with many fibers, taking into account the layout of steel rebars. In this case, the mechanical behaviour of both materials, concrete and reinforcing steel, is represented by their stress-strain diagrams, allowing for a suitable reproduction of the flexural behaviour of the section. The Ruaumoko Structural-Wall model was recently validated against experimental results on shear walls (Adebar and Ibrahim 2000 ; Velev 2006).

The mass distribution along the wall height was represented by a corresponding node number. In the present case - one node was assigned to each floor, so then the total floor mass was lumped at the corresponding node and the gravity loading tributary to the wall is lumped at the same node, as well. The wall is considered fixed at the base and the wall segments are assumed rigidly connected at all wall joints. The basic wall section properties are first represented by the number of Lobatto integration sections

along the member, which is supposed to be a number between three(3) and seven(7). Five(5) integration sections for all wall members were assumed, giving analysis results of satisfactory precision. Then, the number of the segments in a section is assigned, which shall be between 3 and 20, where a number of 18 is the maximum segment number for a standard wall section. For the present modeling purposes, a *Numerical Wall* section input was chosen and a number of thirteen (13) segments *NIP* per section was assigned for all structural wall types. A general case of the numerical definition of one wall cross-section, as assigned by Ruaumoko input requirements [Carr 2002], is shown in Figure 6.14.

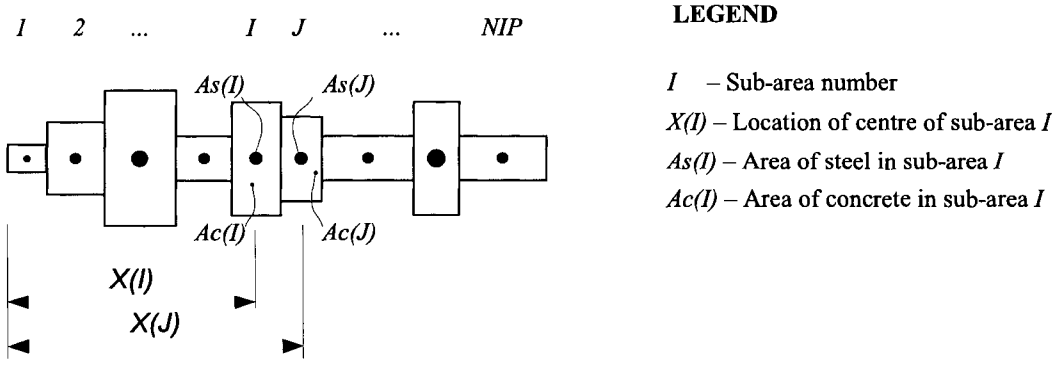

FIG. 6.14 Numerical Definition of Wall Cross-Section

According to afore-mentioned requirements, all segments are then modeled throughout three specific values : **A**, **B** and **C**, as shown in Figure III. Detailed calculations are presented herein for the six storey building in Montréal, as a typical exemple for modeling all shear wall sections by floors for both cities. The reinforcement has been previously defined in Chapter 4. As shown in the legend in Figure III, **A** is the horizontal coordinate of the corresponding modeled reinforcement on an assumed horizontal axis starting at the concrete section left corner. The second value **B** is the area of the modeled reinforcement, which for the present case is : $8/2 \times 500 = 2000\,\mathrm{mm}^2$ for the inner and outer layers of the concentrated reinforcement in both ends of the shear wall ($8M25$). The value of **B** for the uniformly distributed vertical reinforcing bars along the shear wall web would be then : $5400/260 \times 1/9 \times 2 \times 100 = 462\,\mathrm{mm}^2$, taking into account that $M10$@260mm have to be

modeled throughout 9 segments. Therefore a value of $\mathbf{B} = 465\,\mathrm{mm}^2$ is assigned on the model sketch for the assumed 2 layers of 21 vertical bars $M10$, uniformly distributed in 9 segments. The third value **C** is the concrete segment area, which is unified for all shear walls models and is specified by four (4) segments for the concentrated reinforcement in both shear wall ends and nine (9) segments for the uniformly distributed vertical reinforcing bars. So then the value of **C** is : $600/2 \times 600 = 180000\,\mathrm{mm}^2$ for the inner and outer layers of the concentrated reinforcement and $5400/9 \times 300 = 180000\,\mathrm{mm}^2$ for the shear wall web segments.

Nonlinear analyses were performed according the requirements of NBCC 2005. For the purpose of determining forces and deflections of the structure, effective properties for the shear walls per floor levels were calculated for the three models according the Canadian standard A23.3-04 [Canadian Standard Association 2004]. The effective properties, as fraction of the gross section properties, are obtained by multiplying the corresponding gross section property with a reduction coefficient. For a section area and moment of inertia, the reduction coefficient is $a_{\mathrm{w}} = 0.6 + \frac{P_{\mathrm{s}}}{f'_{\mathrm{c}} A_{\mathrm{g}}}$ according to Cl.21.2.5.2.1 [Canadian Standard Association 2004].

The damping model used is of the Rayleigh type with the damping matrix proportional to the mass and the initial stiffness matrices. Rayleigh type viscous damping equal to 5% of critical damping is assumed for all modes of vibration. Dynamic Time-history using Newmark numerical method, with a constant average acceleration $\beta = 0.25$, and a 5% Rayleigh damping model was used for all time-history analysis. The analysis time-step was chosen as 0.00002. $P - \Delta$ effects were not activated into the analysis. The maximum number of cycles of Newton-Raphson iteration per Time-step was chosen as 10. The norm of the out-of-balance force vector relative to the incremental force vector for the Newton-Raphson iteration was chosen as 0.00001, which value is the square of the iteration tolerance required (in the case, the value of 0.00001 implies a tolerance of 0.3% in the residual vector).

The following cross section properties were used for all models analysis for describing the

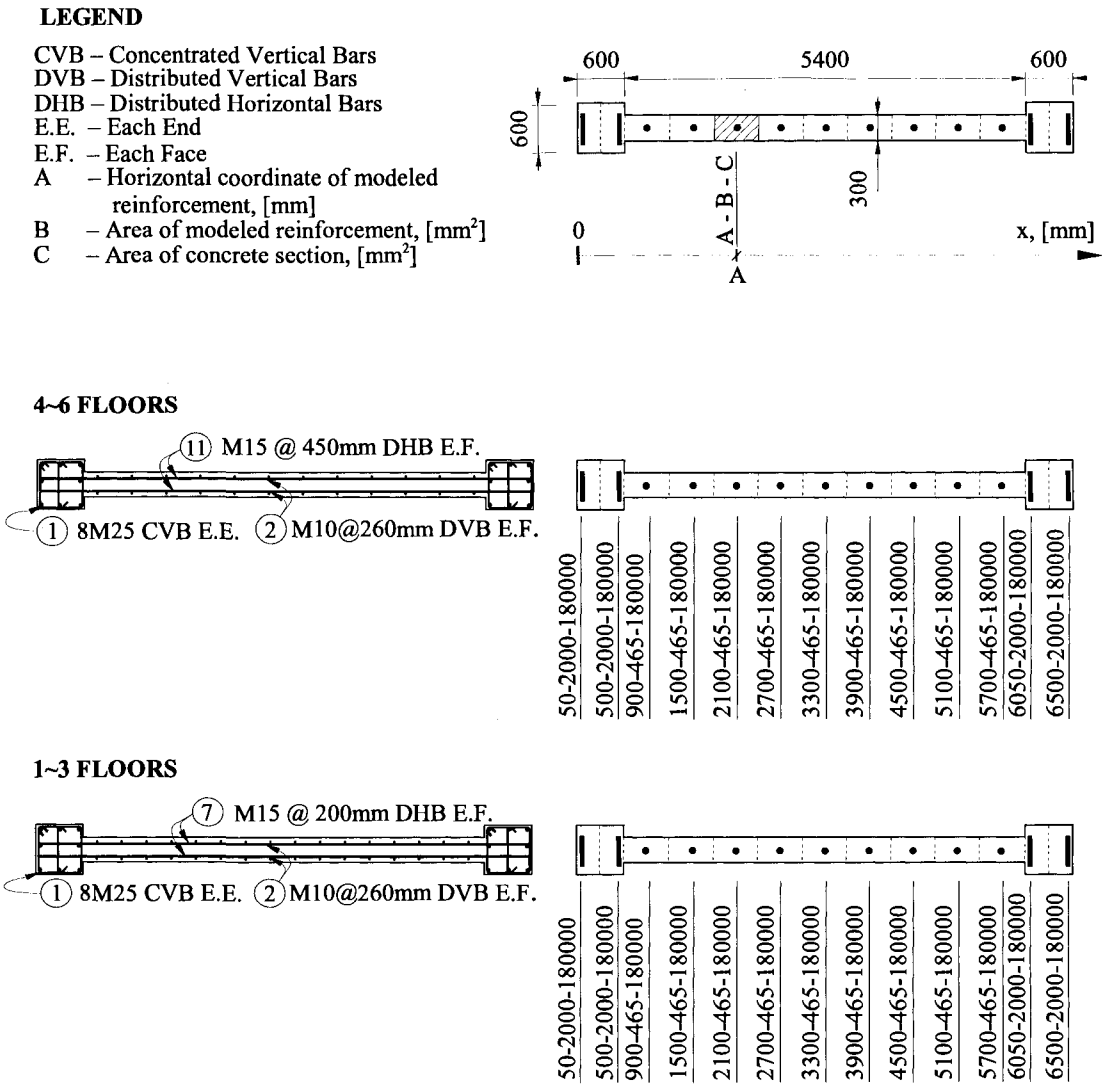

FIG. 6.15 Modeling of shear wall sections for 6 storey building located in Montréal

wall element :

- I_g - Moment of inertia of the gross concrete section about centroidal axis, neglecting reinforcement. A_g, I_g - the area and moment of inertia of the gross cross section.
  f'_c - the specified compressive strength of concrete ($f'_c = 30MPa$).
  f_y - the specified yield strength of reinforcement ($f_y = 400MPa$).
- I_{eff} - Effective moment of inertia, recommended in Cl.21.2.5.2.1, CSA 23.3-04 [Canadian Standard Association 2004]. $I_{eff} = (0.6 + \frac{P_s}{f'_c A_g})I_g$.

6.4 Dynamic Analysis Results

Inelastic dynamic analyses for the three models were performed through Ruaumoko program (Carr 2002). Time-history dynamic analysis results are presented with the maximum peak values of the structural response. Resulting maximum values, for the story shears, moments and maximum diaphragm point displacements, from the above discussed ground motions, are listed in Tables 6.5 to 6.25. Graphical representation of the those peak values is shown in Figures 6.16 to 6.45. It could be seen from that figures that even if the used time-history records have been matched up to 1% convergence with the NBCC uniform hazard spectra, resulting peak values vary for all models and for both cities. The reason for that results variability is the different profiles of the recorded or syntetically generated ground motions records. As assumed in the NBCC 2005 and the CSA A23.3-04, maximum peak response values from inelastic dynamic analysis have to be lower or equal to the design values, for which the SFRS members are designed. In fact, maximum peak values obtained by the inelastic time-history dynamic analysis may exceed the design code values, as it could be seen in that project. In general, few differences may be expected because of uncertainty in either ground motion inputs or structural modeling properties or even in both inherent to inelastic analysis.

TAB. 6.5 Story shear forces, moments and maximum displacements for a 6-storey shear wall subject to non-linear dynamic analysis for earthquakes 1M6R30, 2M6R30 and 1M6R30match.

	1M6R30			2M6R30			1M6R30match		
	V	M	Δ	V	M	Δ	V	M	Δ
Lev.	(kN)	(kNm)	(m)	(kN)	(kNm)	(m)	(kN)	(kNm)	(m)
6	1240	4096	0.032	956	3305	0.028	1106	3709	0.056
5	1128	6816	0.025	898	5865	0.021	1231	7050	0.044
4	882	7530	0.018	871	7265	0.014	1104	8472	0.032
3	1307	7870	0.012	1075	7834	0.010	1233	9328	0.020
2	1994	9852	0.007	1780	8424	0.006	1789	11320	0.010
1	2727	13880	0.002	2778	14050	0.002	2439	16030	0.003

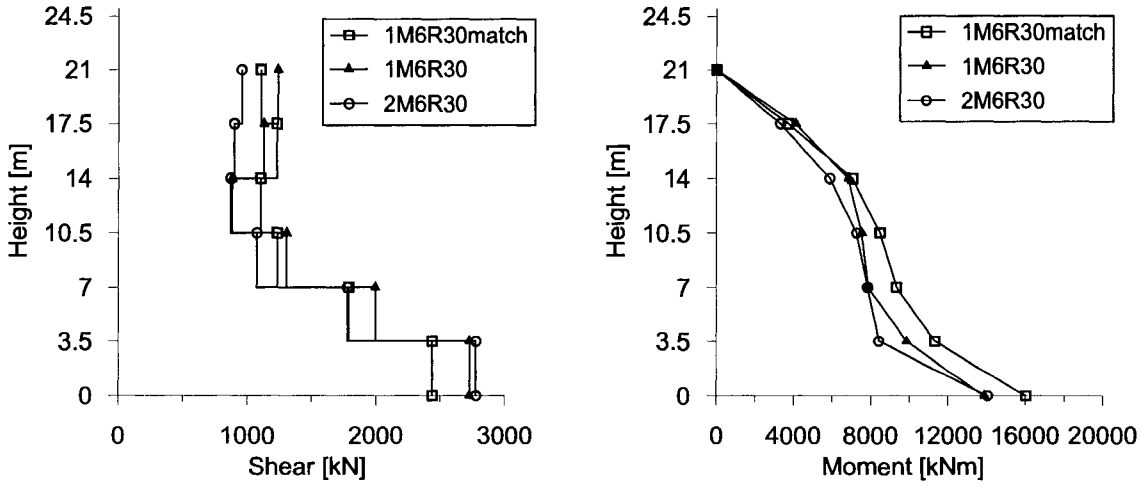

FIG. 6.16 Shear and moment results from non-linear dynamic analysis for events M6R30 - 6 storey shear wall in Montréal

TAB. 6.6 Story shear forces, moments and maximum displacements for a 6-storey shear wall subject to non-linear dynamic analysis for earthquakes 1M7R70, 2M7R70 and 1M7R70match.

	1M7R70			2M7R70			1M7R70match		
	V	M	Δ	V	M	Δ	V	M	Δ
Lev	(kN)	(kNm)	(m)	(kN)	(kNm)	(m)	(kN)	(kNm)	(m)
6	774	2700	0.059	815	2821	0.066	1279	4349	0.051
5	908	5849	0.046	847	5230	0.051	1227	7147	0.039
4	869	7498	0.033	943	7423	0.037	943	8328	0.029
3	1159	9421	0.020	1172	9583	0.024	1315	8374	0.018
2	1775	11710	0.010	1740	12280	0.012	2080	10660	0.009
1	2361	16440	0.003	2264	17060	0.003	3201	16030	0.003

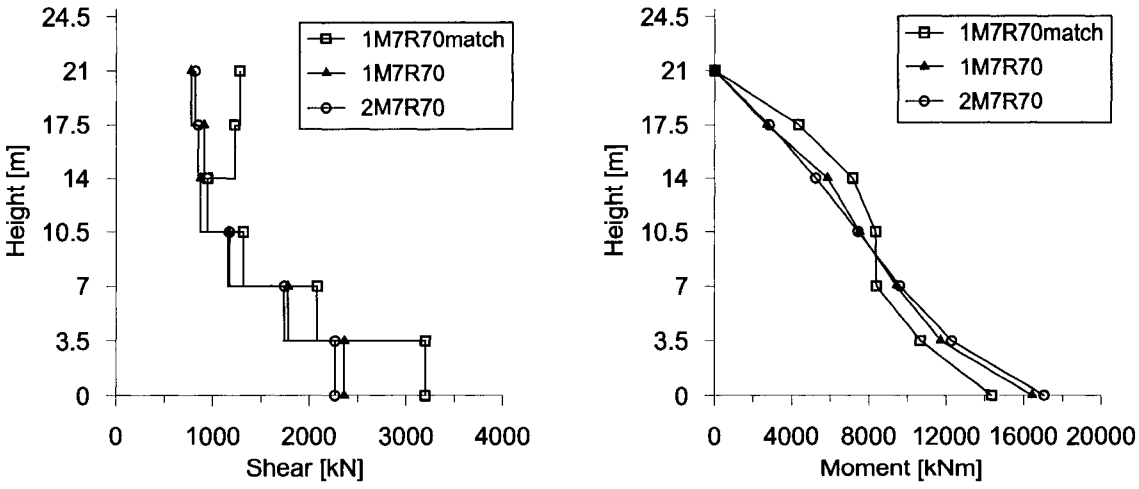

FIG. 6.17 Shear and moment results from non-linear dynamic analysis for earthquakes 1M7R70, 2M7R70 and 1M7R70match - 6 Storey

TAB. 6.7 Story shear forces, moments and maximum displacements for a 6-storey shear wall subject to non-linear dynamic analysis for earthquakes Nah10Mtl and Nah280Mtl

	Nah10Mtl			Nah280Mtl		
Lev.	V (kN)	M (kNm)	Δ (m)	V (kN)	M (kNm)	Δ (m)
6	1008	3483	0.053	1158	3956	0.053
5	955	5994	0.041	1049	6574	0.041
4	922	7754	0.030	881	7394	0.029
3	1385	9348	0.019	1217	9175	0.018
2	2373	11510	0.010	1858	11480	0.009
1	3897	15800	0.003	2857	15640	0.003

TAB. 6.8 Story shear forces, moments and maximum displacements for a 6-storey shear wall subject to non-linear dynamic analysis for earthquakes Sag0Mtl and Sag90Mtl .

	Sag0Mtl			Sag90Mtl		
Lev.	V (kN)	M (kNm)	Δ (m)	V (kN)	M (kNm)	Δ (m)
6	1242	4279	0.055	1175	3908	0.052
5	1215	7142	0.042	1265	6960	0.041
4	948	8482	0.031	1021	8577	0.029
3	1536	9546	0.019	1155	9184	0.018
2	2329	11570	0.010	1900	10850	0.009
1	3628	15240	0.003	2665	14170	0.002

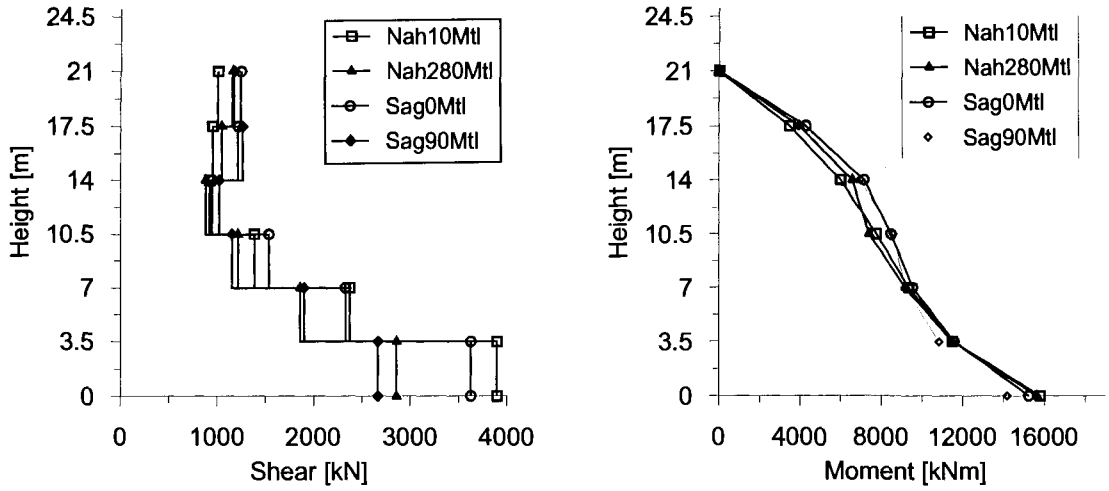

FIG. 6.18 Shear and moment results from non-linear dynamic analysis for earthquakes Nah10Mtl, Nah280Mtl, Sag0Mtl and Sag90Mtl - 6 Storey

TAB. 6.9 Story shear forces, moments and maximum displacements for a 12-storey shear wall subject to non-linear dynamic analysis for earthquakes 1M6R30, 2M6R30 and 1M6R30match.

	1M6R30			2M6R30			1M6R30match		
	V	M	Δ	V	M	Δ	V	M	Δ
Lev.	(kN)	(kNm)	(m)	(kN)	(kNm)	(m)	(kN)	(kNm)	(m)
12	620	2692	0.055	706	3047	0.082	770	3318	0.092
11	711	4906	0.042	790	5345	0.068	966	6249	0.078
10	759	6300	0.032	747	6546	0.058	1051	7579	0.068
9	894	7987	0.030	800	7972	0.051	916	9086	0.062
8	728	9267	0.027	869	9136	0.042	816	9815	0.052
7	729	10130	0.024	1018	10330	0.035	768	10410	0.042
6	841	10110	0.021	1224	11000	0.028	960	11080	0.034
5	1036	9086	0.017	1393	11680	0.022	1363	11200	0.026
4	1346	9567	0.013	1359	12220	0.016	1845	10270	0.018
3	1565	9365	0.009	1540	12120	0.010	2188	11350	0.012
2	2115	9330	0.005	1728	13420	0.005	2866	13640	0.006
1	2784	18250	0.001	2337	16750	0.001	4134	20330	0.002

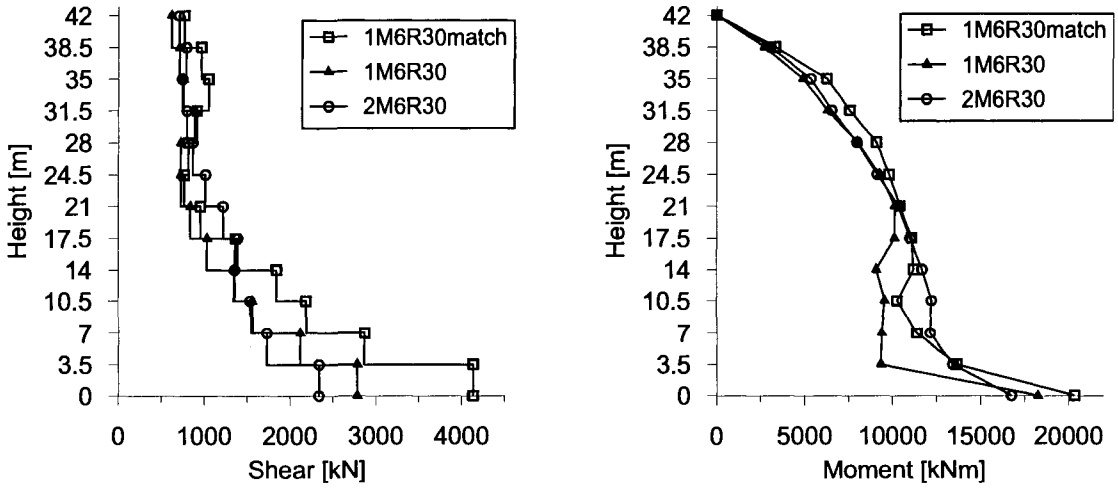

FIG. 6.19 Shear and moment results from non-linear dynamic analysis for earthquakes 1M6R30, 2M6R30 and 1M6R30match - 12 Storey

TAB. 6.10 Story shear forces, moments and maximum displacements for a 12-storey shear wall subject to non-linear dynamic analysis for earthquakes 1M7R70, 2M7R70 and 1M7R70match.

	1M7R70			2M7R70			1M7R70match		
	V	M	Δ	V	M	Δ	V	M	Δ
Lev.	(kN)	(kNm)	(m)	(kN)	(kNm)	(m)	(kN)	(kNm)	(m)
12	707	3145	0.086	657	2930	0.066	706	3127	0.078
11	910	6043	0.071	867	5766	0.056	899	6014	0.066
10	984	7309	0.062	1049	7229	0.050	1001	7206	0.057
9	832	8824	0.057	888	8891	0.046	849	8707	0.051
8	862	9184	0.049	833	9862	0.040	972	10460	0.042
7	918	10200	0.041	752	10540	0.035	1076	11080	0.037
6	1029	10610	0.034	873	11140	0.029	1030	10840	0.031
5	1160	11190	0.026	1044	11600	0.023	1208	11930	0.024
4	1296	11180	0.021	1224	11670	0.017	1395	12830	0.018
3	1651	12000	0.014	1645	11760	0.012	1802	13730	0.012
2	2069	14400	0.008	2062	13160	0.006	2868	14270	0.006
1	2667	20240	0.002	2450	19860	0.002	4243	18580	0.002

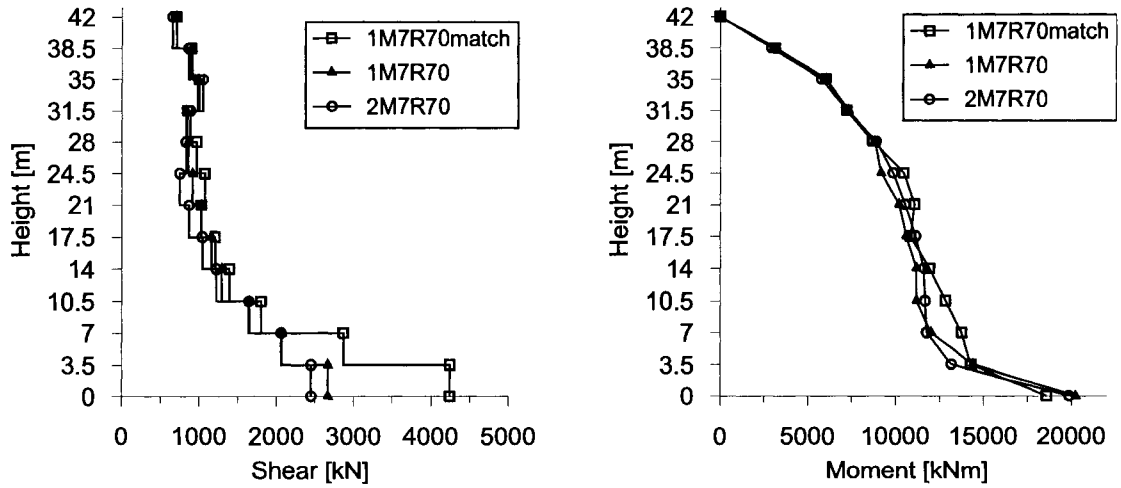

FIG. 6.20 Shear and moment results from non-linear dynamic analysis for earthquakes 1M7R70, 2M7R70 and 1M7R70match - 12 Storey

TAB. 6.11 Story shear forces, moments and maximum displacements for a 12-storey shear wall subject to non-linear dynamic analysis for earthquakes Nah10Mtl and Nah280Mtl .

	Nah10Mtl			Nah280Mtl		
	V	M	Δ	V	M	Δ
Lev.	(kN)	(kNm)	(m)	(kN)	(kNm)	(m)
12	760	3290	0.116	674	2971	0.104
11	972	6232	0.099	821	5603	0.088
10	1041	7613	0.084	1014	7036	0.076
9	977	9349	0.075	938	8655	0.068
8	1021	9917	0.064	879	9690	0.058
7	1044	10750	0.054	1033	10700	0.046
6	1104	11100	0.044	1137	11190	0.038
5	1326	11270	0.035	1229	11740	0.029
4	1571	11540	0.025	1433	11180	0.023
3	2175	11660	0.016	1676	12070	0.015
2	3161	15680	0.009	2095	14820	0.008
1	4458	20490	0.002	2816	20600	0.002

TAB. 6.12 Story shear forces, moments and maximum displacements for a 12-storey shear wall subject to non-linear dynamic analysis for earthquakes Sag0Mtl and Sag90Mtl .

	Sag0Mtl			Sag90Mtl		
	V	M	Δ	V	M	Δ
Lev.	(kN)	(kNm)	(m)	(kN)	(kNm)	(m)
12	786	3487	0.106	773	3441	0.098
11	972	6395	0.087	983	6411	0.084
10	1031	7507	0.073	1054	7566	0.073
9	832	8966	0.065	876	8929	0.065
8	790	10340	0.057	914	9302	0.055
7	901	10270	0.049	1095	9928	0.045
6	1050	10490	0.041	1173	9585	0.036
5	1353	10640	0.033	1251	9941	0.027
4	1645	10670	0.024	1391	11010	0.019
3	2042	11320	0.016	1644	12240	0.012
2	2935	15580	0.009	2194	13310	0.006
1	4272	21420	0.003	3675	17970	0.002

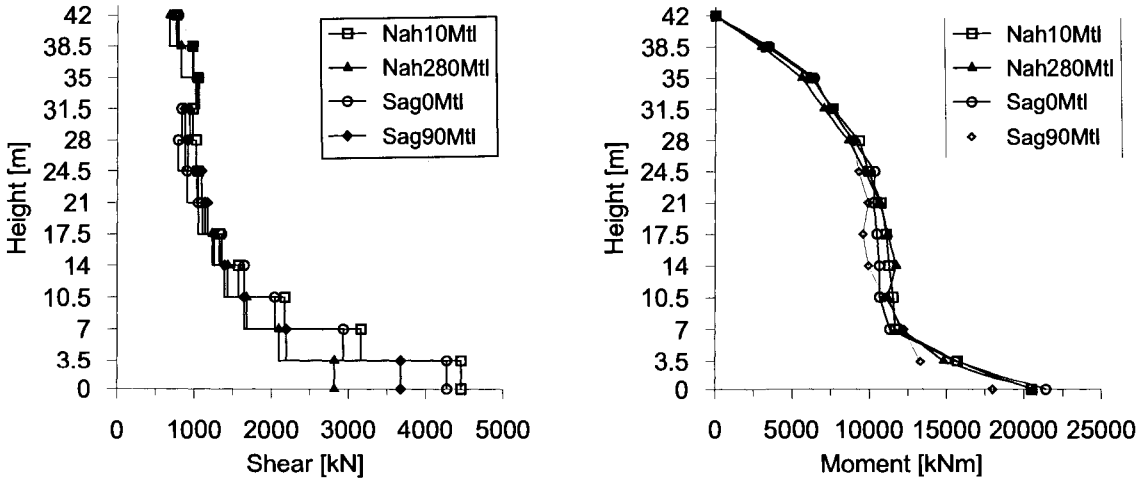

FIG. 6.21 Shear and moment results from non-linear dynamic analysis for earthquakes Nah10Mtl, Nah280Mtl, Sag0Mtl and Sag90Mtl - 12 Storey

TAB. 6.13 Story shear forces, moments and maximum displacements for a 18-storey shear wall subject to non-linear dynamic analysis for earthquakes 1M6R30, 2M6R30 and 1M6R30match.

	1M6R30			2M6R30			1M6R30match		
	V	M	Δ	V	M	Δ	V	M	Δ
Lev	(kN)	(kNm)	(m)	(kN)	(kNm)	(m)	(kN)	(kNm)	(m)
18	429	1361	0.067	535	1752	0.056	597	1959	0.306
17	568	3182	0.060	718	3949	0.051	844	4539	0.279
16	571	5006	0.052	773	6350	0.047	827	6989	0.254
15	509	6346	0.046	756	8133	0.044	750	8461	0.229
14	547	6963	0.039	682	9088	0.041	624	9098	0.205
13	541	7451	0.036	635	9750	0.038	778	9158	0.181
12	606	8567	0.034	842	10360	0.035	1027	10500	0.158
11	847	9356	0.031	949	10750	0.029	1159	11450	0.129
10	965	9528	0.028	928	10420	0.026	1261	11920	0.108
9	1008	9741	0.026	1054	9871	0.025	1431	13130	0.096
8	921	9491	0.023	1180	9442	0.022	1472	13930	0.077
7	797	8701	0.019	1120	9474	0.019	1424	14660	0.064
6	943	8256	0.015	1222	9909	0.017	1354	15370	0.051
5	1154	9152	0.012	1391	9926	0.013	1267	15740	0.037
4	1287	9662	0.008	1466	9537	0.009	1453	15950	0.026
3	1331	9364	0.005	1569	9849	0.006	1840	17040	0.016
2	1529	11600	0.002	1821	13050	0.003	2577	19760	0.008
1	2124	14260	0.001	2614	18020	0.001	4079	24910	0.002

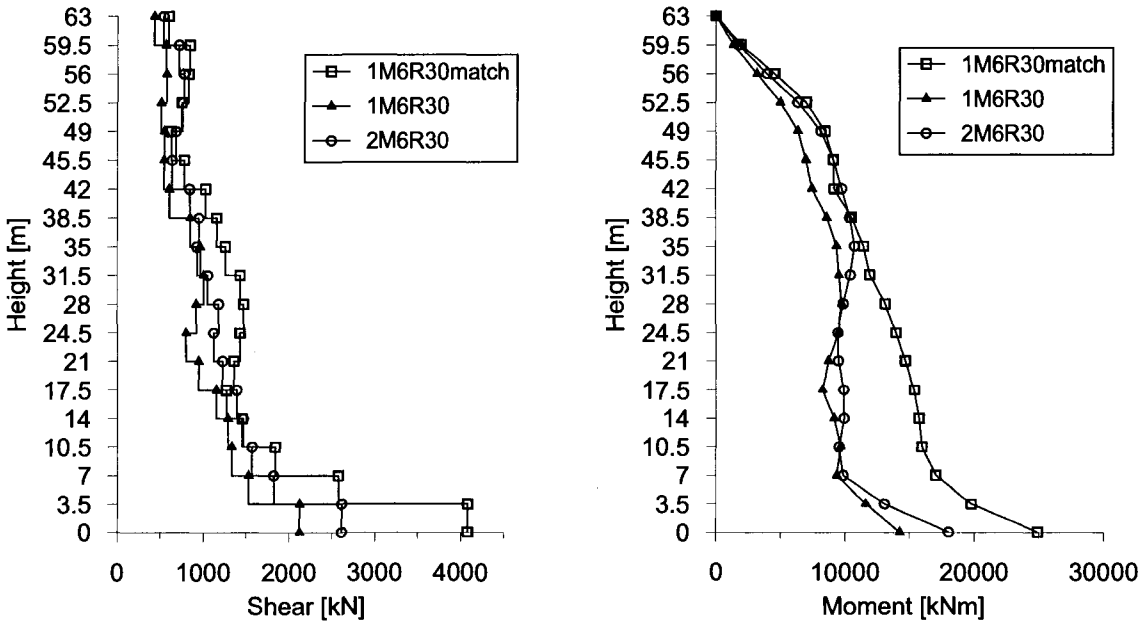

FIG. 6.22 Shear and moment results from non-linear dynamic analysis for earthquakes 1M6R30, 2M6R30 and 1M6R30match - 18 Storey

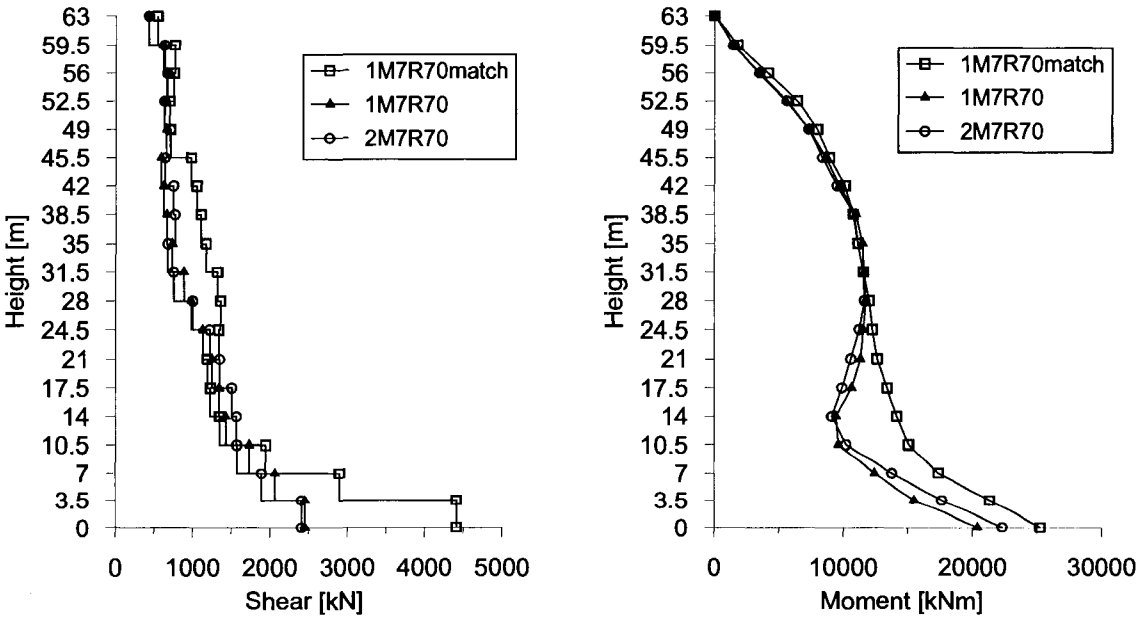

FIG. 6.23 Shear and moment results from non-linear dynamic analysis for earthquakes 1M7R70, 2M7R70 and 1M7R70match - 18 Storey

TAB. 6.14 Story shear forces, moments and maximum displacements for a 18-storey shear wall subject to non-linear dynamic analysis for earthquakes 1M7R70, 2M7R70 and 1M7R70match.

	1M7R70			2M7R70			1M7R70match		
L.	V (kN)	M (kNm)	Δ (m)	V (kN)	M (kNm)	Δ (m)	V (kN)	M (kNm)	Δ (m)
18	424	1439	0.086	429	1450	0.090	539	1793	0.248
17	613	3426	0.077	628	3499	0.079	766	4138	0.227
16	656	5494	0.068	666	5593	0.068	754	6411	0.206
15	625	7340	0.058	628	7301	0.060	697	7970	0.186
14	657	8605	0.050	707	8351	0.055	709	8891	0.166
13	587	9694	0.047	637	9490	0.053	975	10100	0.155
12	623	10950	0.044	746	10810	0.055	1050	10740	0.138
11	662	11450	0.042	766	11080	0.055	1104	11090	0.121
10	733	11590	0.041	674	11520	0.053	1168	11520	0.108
9	882	11690	0.039	749	11610	0.050	1317	11970	0.098
8	979	11530	0.035	997	11210	0.045	1356	12230	0.085
7	1127	11300	0.030	1218	10560	0.039	1337	12600	0.071
6	1246	10610	0.025	1345	9867	0.032	1187	13370	0.057
5	1338	9440	0.019	1502	9103	0.025	1224	14130	0.044
4	1426	9603	0.014	1565	10180	0.018	1346	15040	0.032
3	1730	12410	0.009	1570	13770	0.011	1944	17350	0.019
2	2066	15480	0.004	1891	17620	0.006	2900	21320	0.010
1	2452	20380	0.001	2407	22290	0.002	4410	25230	0.003

TAB. 6.15 Story shear forces, moments and maximum displacements for a 18-storey shear wall subject to non-linear dynamic analysis for earthquakes Nah10Mtl and Nah280Mtl.

	Nah10Mtl			Nah280Mtl		
	V	M	Δ	V	M	Δ
Lev.	(kN)	(kNm)	(m)	(kN)	(kNm)	(m)
18	584	1904	0.393	484	1308	0.352
17	829	4455	0.365	728	3284	0.325
16	849	6971	0.338	796	5514	0.300
15	803	8612	0.312	854	7505	0.280
14	702	9461	0.286	713	8845	0.258
13	847	9643	0.261	648	9922	0.231
12	959	10560	0.235	773	10520	0.208
11	917	11560	0.202	833	11350	0.178
10	999	12310	0.176	859	12020	0.154
9	1183	12990	0.158	967	12680	0.138
8	1310	13760	0.134	1073	13420	0.115
7	1421	15040	0.110	1070	13970	0.093
6	1452	16090	0.087	1106	14980	0.072
5	1333	17060	0.066	1287	16410	0.053
4	1354	19100	0.046	1506	17460	0.037
3	1568	20320	0.028	1740	20260	0.023
2	1906	24410	0.014	2504	23330	0.011
1	3506	28670	0.004	3985	27180	0.003

TAB. 6.16 Story shear forces, moments and maximum displacements for a 18-storey shear wall subject to non-linear dynamic analysis for earthquakes Sag0Mtl et Sag90Mtl.

	Sag0Mtl			Sag90Mtl		
	V	M	Δ	V	M	Δ
Lev.	(kN)	(kNm)	(m)	(kN)	(kNm)	(m)
18	469	1542	0.389	376	1286	0.322
17	649	3559	0.357	561	3144	0.301
16	607	5405	0.327	625	5128	0.279
15	610	6920	0.302	603	6925	0.257
14	687	8423	0.276	574	8180	0.236
13	600	9456	0.250	644	9240	0.214
12	766	10520	0.225	887	10630	0.192
11	889	11590	0.195	989	11390	0.164
10	1022	12300	0.171	986	11990	0.142
9	1198	13110	0.154	1004	12440	0.127
8	1307	13630	0.131	1064	13040	0.105
7	1380	14160	0.108	1096	14010	0.085
6	1405	14970	0.086	1103	14810	0.066
5	1304	16710	0.065	1169	15850	0.049
4	1159	18480	0.045	1243	17590	0.034
3	1484	20190	0.028	1461	18980	0.021
2	1879	23670	0.014	2534	22090	0.011
1	3454	27990	0.004	4424	26480	0.003

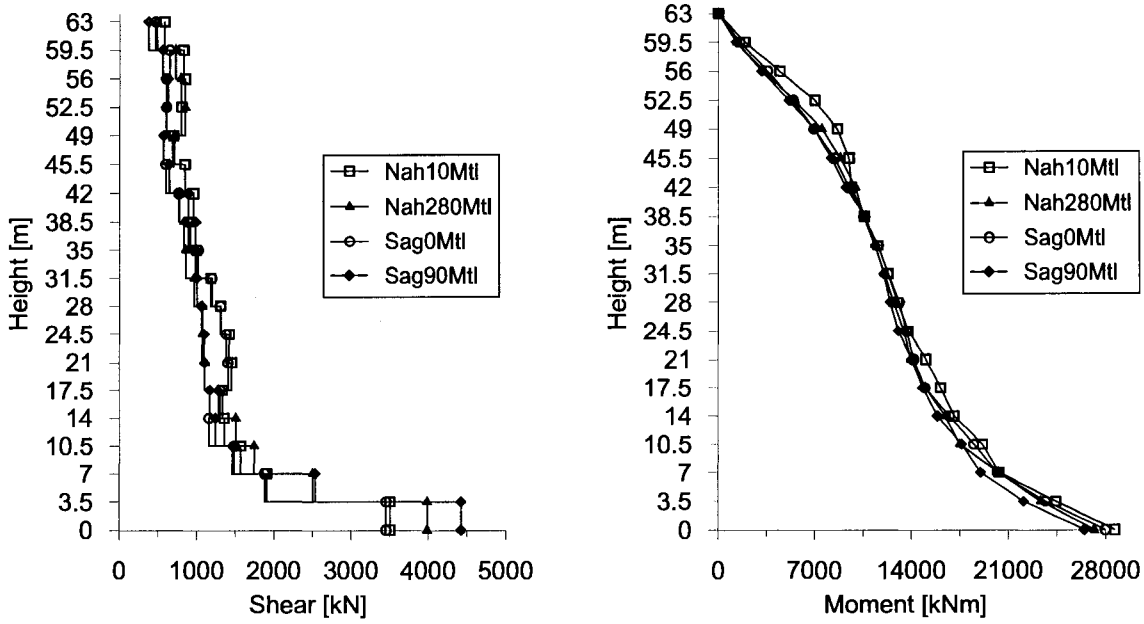

FIG. 6.24 Shear and moment results from non-linear dynamic analysis for earthquakes Nah10Mtl, Nah280Mtl, Sag0Mtl and Sag90Mtl - 18 Storey

TAB. 6.17 Story shear forces, moments and maximum displacements for a 6-storey shear wall subject to non-linear dynamic analysis for earthquakes 1M65R30, 2M65R30 and 1M65R30match.

	1M65R30			2M65R30			1M65R30match		
Lev.	V (kN)	M (kNm)	Δ (m)	V (kN)	M (kNm)	Δ (m)	V (kN)	M (kNm)	Δ (m)
6	1007	3485	0.253	997	3478	0.257	1291	4433	0.140
5	1345	7015	0.200	1406	7283	0.202	1284	7360	0.111
4	1343	10980	0.147	1410	11440	0.148	1230	10160	0.081
3	2133	13910	0.097	1637	14820	0.097	1925	13140	0.053
2	3115	17780	0.052	2626	18650	0.051	3418	16210	0.027
1	4693	25680	0.016	3958	25420	0.015	5719	21920	0.008

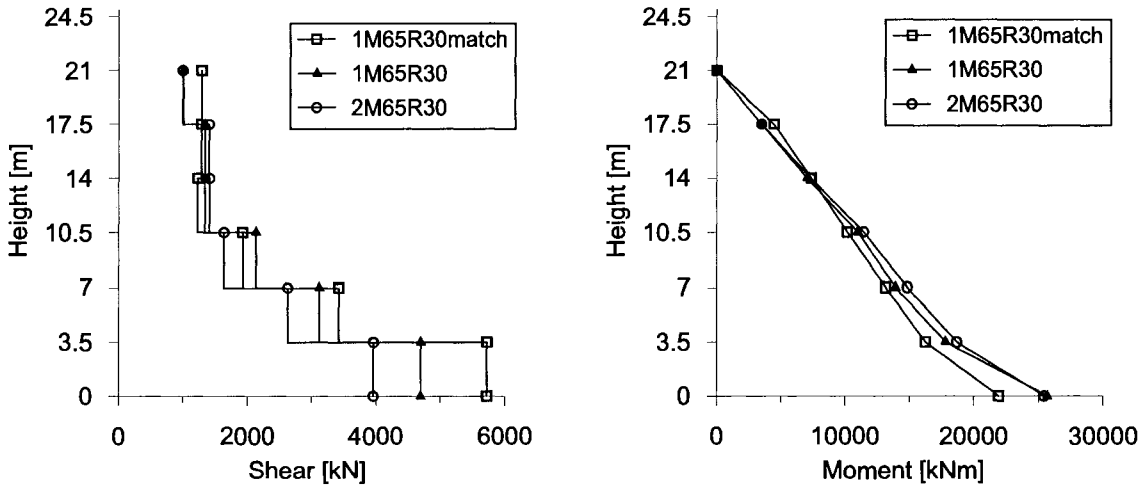

FIG. 6.25 Shear and moment results from non-linear dynamic analysis for earthquakes 1M65R30, 2M65R30 and 1M65R30match - 6 Storey

TAB. 6.18 Story shear forces, moments and maximum displacements for a 6-storey shear wall subject to non-linear dynamic analysis for earthquakes 1M72R70, 2M72R70 and 1M72R70match.

	1M72R70			2M72R70			1M72R70match		
Lev.	V (kN)	M (kNm)	Δ (m)	V (kN)	M (kNm)	Δ (m)	V (kN)	M (kNm)	Δ (m)
6	833	2910	0.142	668	2299	0.137	1698	5798	0.125
5	1085	6522	0.126	918	5394	0.107	1698	10280	0.096
4	1038	9183	0.093	1042	8607	0.078	1825	14750	0.068
3	1403	11670	0.063	1175	11850	0.050	2201	21330	0.043
2	1969	15150	0.035	1389	15120	0.026	3347	28590	0.022
1	2763	20780	0.011	1839	18850	0.008	5986	36970	0.006

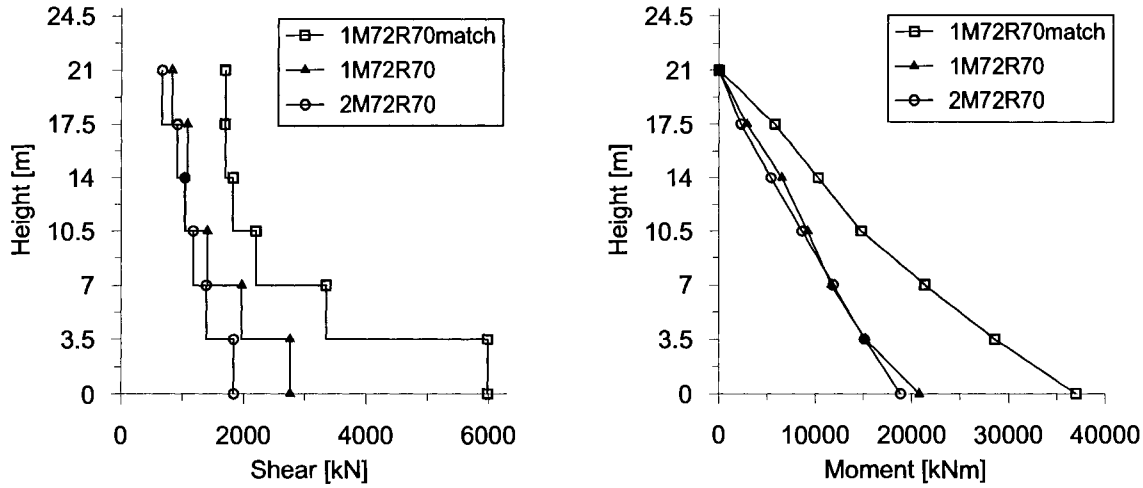

FIG. 6.26 Shear and moment results from non-linear dynamic analysis for earthquakes 1M72R30, 2M72R30 and 1M72R30match - 6 Storey

TAB. 6.19 Story shear forces, moments and maximum displacements for a 6-storey shear wall subject to non-linear dynamic analysis for earthquakes 1M85VBC and 2M85VBC .

	1M85VBC			2M85VBC		
Lev.	V (kN)	M (kNm)	Δ (m)	V (kN)	M (kNm)	Δ (m)
6	557	1926	0.079	505	1765	0.084
5	783	4371	0.062	744	4344	0.066
4	1039	7334	0.044	836	7145	0.049
3	990	10380	0.028	1005	9767	0.031
2	1199	13310	0.014	1173	13340	0.016
1	1379	16960	0.004	1345	17350	0.005

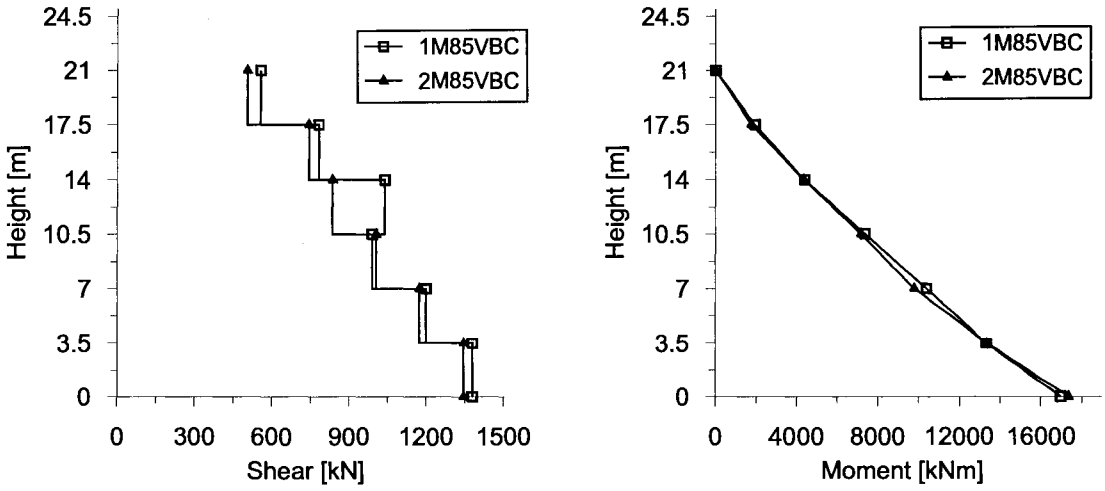

FIG. 6.27 Shear and moment results from non-linear dynamic analysis for earthquakes 1M85 and 2M85 - 6 Storey

TAB. 6.20 Story shear forces, moments and maximum displacements for a 12-storey shear wall subject to non-linear dynamic analysis for earthquakes 1M65R30, 2M65R30 and 1M65R30match.

	1M65R30			2M65R30			1M65R30match		
	V	M	Δ	V	M	Δ	V	M	Δ
Lev.	(kN)	(kNm)	(m)	(kN)	(kNm)	(m)	(kN)	(kNm)	(m)
12	1087	4839	0.630	994	4462	0.457	1102	4919	0.598
11	1603	8870	0.533	1532	9252	0.368	1649	9146	0.507
10	1488	12000	0.458	1629	13160	0.315	1582	12400	0.437
9	1541	15840	0.405	1663	18320	0.277	1559	16300	0.387
8	1529	18440	0.332	1568	21900	0.224	1729	18300	0.321
7	1588	20530	0.262	1329	24410	0.174	1822	19380	0.259
6	1763	21460	0.195	1573	25440	0.129	1806	20680	0.199
5	1800	23800	0.134	2039	24960	0.090	1768	23720	0.144
4	2315	26540	0.083	2678	23770	0.059	2235	26660	0.095
3	3156	30970	0.047	3489	25080	0.038	2695	32990	0.056
2	4162	36440	0.023	4078	31910	0.019	3337	37960	0.027
1	5375	44230	0.006	4950	45520	0.006	5565	43460	0.007

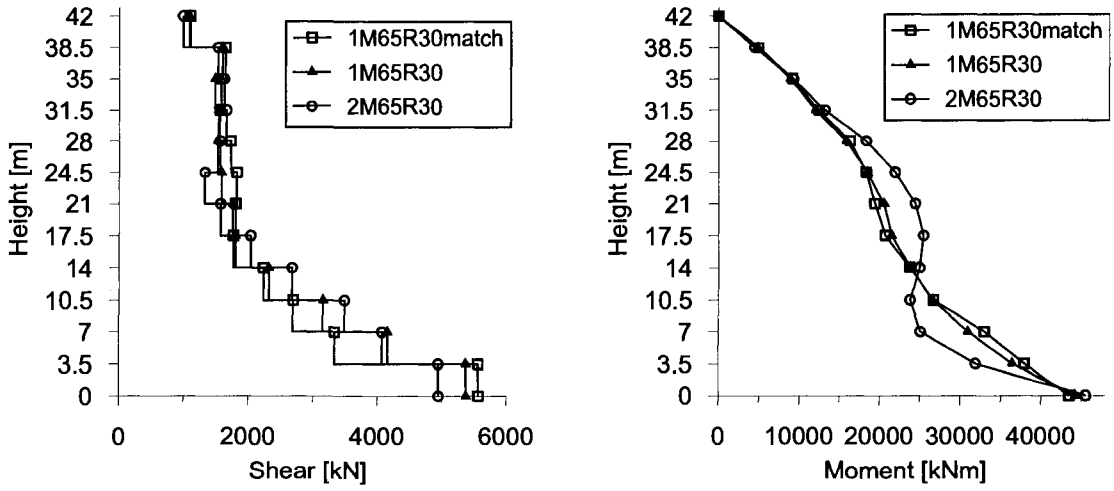

FIG. 6.28 Shear and moment results from non-linear dynamic analysis for earthquakes 1M65R30, 2M65R30 and 1M65R30match - 12 Storey

TAB. 6.21 Story shear forces, moments and maximum displacements for a 12-storey shear wall subject to non-linear dynamic analysis for earthquakes 1M72R70, 2M72R70 and 1M72R70match.

	1M72R70			2M72R70			1M72R70match		
	V	M	Δ	V	M	Δ	V	M	Δ
Lev.	(kN)	(kNm)	(m)	(kN)	(kNm)	(m)	(kN)	(kNm)	(m)
12	741	3330	0.506	741	3208	0.405	1175	5004	0.584
11	1113	7186	0.419	951	6048	0.339	1509	8411	0.499
10	1378	9760	0.353	1225	7898	0.287	1409	11580	0.434
9	1299	14130	0.309	995	10790	0.251	1325	14980	0.387
8	1241	17800	0.253	1011	13010	0.204	1280	17090	0.323
7	1337	20250	0.203	1035	16290	0.160	1429	18110	0.261
6	1437	21970	0.159	1114	19220	0.119	2069	20120	0.200
5	1882	23220	0.119	1194	21580	0.083	2505	22420	0.144
4	2319	25150	0.083	1562	23710	0.051	2664	26060	0.094
3	2652	29720	0.052	1819	27050	0.029	3394	31650	0.055
2	2995	36690	0.026	2299	29430	0.013	4727	38220	0.027
1	3519	44860	0.007	2755	33410	0.004	6838	51410	0.009

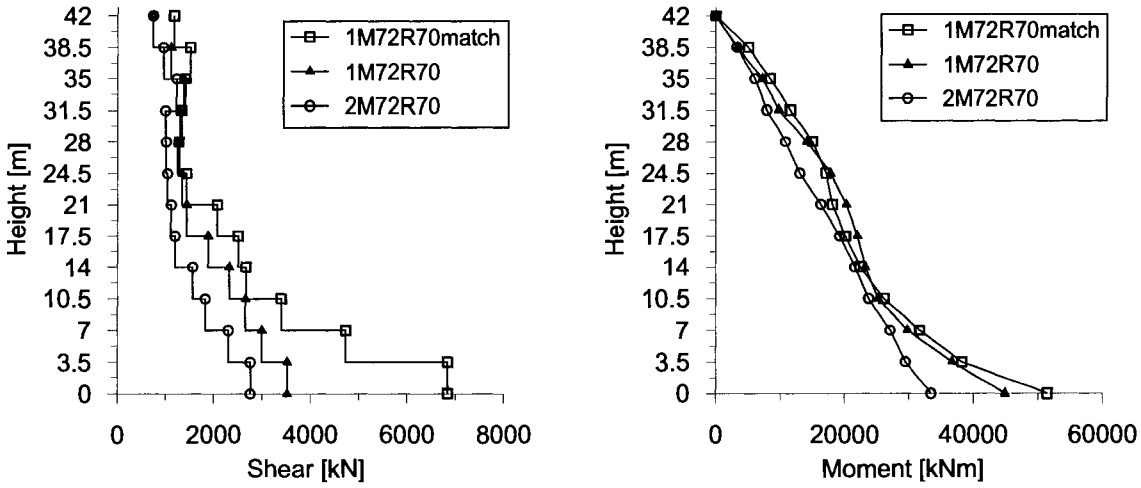

FIG. 6.29 Shear and moment results from non-linear dynamic analysis for earthquakes 1M72R70, 2M72R70 and 1M72R70match - 12 Storey

TAB. 6.22 Story shear forces, moments and maximum displacements for a 12-storey shear wall subject to non-linear dynamic analysis for earthquakes 1M85VBC and 2M85VBC .

	1M85VBC			2M85VBC		
Lev.	V (kN)	M (kNm)	Δ (m)	V (kN)	M (kNm)	Δ (m)
12	451	2023	0.421	561	2485	0.317
11	695	4440	0.364	700	4826	0.270
10	833	6474	0.316	745	6394	0.234
9	1076	9257	0.281	807	8246	0.208
8	1026	12310	0.233	931	10220	0.172
7	1042	15130	0.187	938	12510	0.137
6	1186	18370	0.142	1010	15240	0.104
5	1388	21310	0.101	1179	18320	0.074
4	1505	24260	0.065	1408	21710	0.048
3	1668	28940	0.037	1677	25280	0.028
2	1889	33160	0.018	1873	28720	0.013
1	2062	37640	0.005	2022	32060	0.003

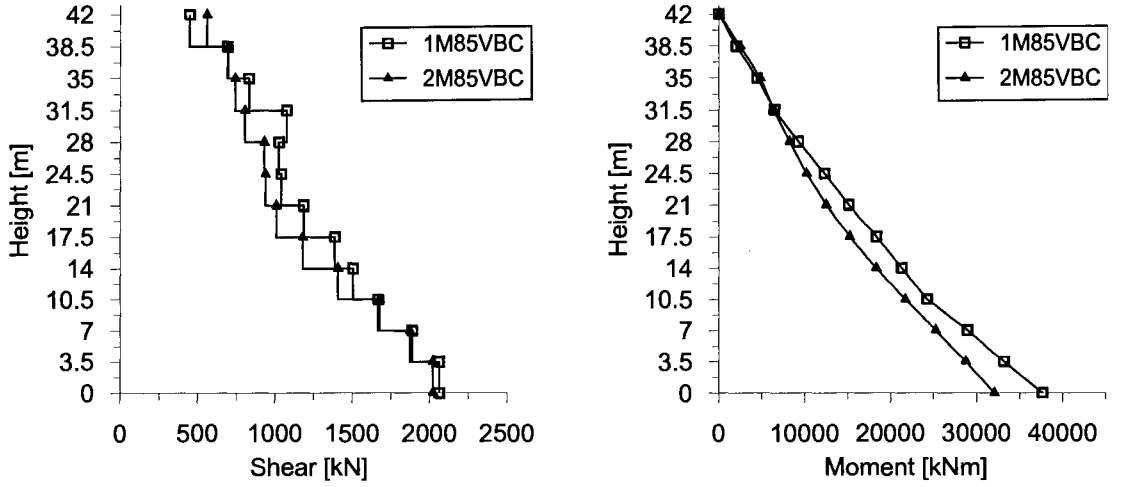

FIG. 6.30 Shear and moment results from non-linear dynamic analysis for earthquakes 1M85 and 2M85 - 12 Storey

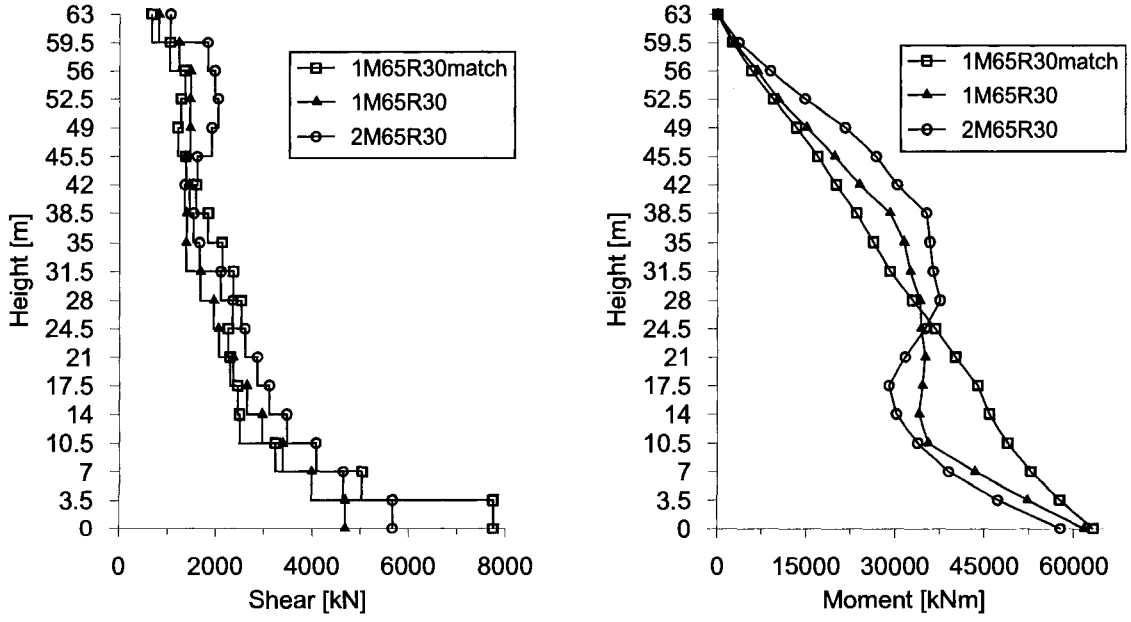

FIG. 6.31 Shear and moment results from non-linear dynamic analysis for earthquakes 1M65R30, 2M65R30 and 1M65R30match - 18 Storey

TAB. 6.23 Story shear forces, moments and maximum displacements for a 18-storey shear wall subject to non-linear dynamic analysis for earthquakes 1M65R30, 2M65R30 and 1M65R30match.

	1M65R30			2M65R30			1M65R30match		
	V	M	Δ	V	M	Δ	V	M	Δ
Lev.	(kN)	(kNm)	(m)	(kN)	(kNm)	(m)	(kN)	(kNm)	(m)
18	814	2764	0.616	1055	3606	0.462	661	2568	0.971
17	1234	6738	0.554	1824	8951	0.409	1044	5768	0.891
16	1473	10270	0.495	1973	14770	0.378	1354	9388	0.812
15	1457	15080	0.440	2038	21540	0.348	1270	13310	0.734
14	1466	19790	0.389	1910	26780	0.318	1208	16940	0.656
13	1375	23960	0.345	1609	30280	0.288	1369	20001	0.581
12	1446	29080	0.304	1353	35240	0.258	1586	23430	0.508
11	1391	31470	0.256	1535	35820	0.218	1832	26330	0.419
10	1380	32500	0.222	1657	36350	0.188	2122	29080	0.350
9	1673	34150	0.199	2097	37530	0.166	2355	32900	0.310
8	1952	34360	0.167	2340	35040	0.136	2521	36730	0.254
7	2054	35040	0.136	2597	31650	0.112	2248	40120	0.202
6	2354	34580	0.108	2854	28930	0.089	2287	43830	0.155
5	2637	34050	0.084	3099	30190	0.068	2445	45820	0.113
4	2955	35530	0.055	3461	33750	0.047	2486	48900	0.076
3	3381	43410	0.034	4071	38960	0.029	3225	52780	0.046
2	3977	52290	0.016	4632	47290	0.014	5024	57710	0.022
1	4683	61780	0.004	5665	57810	0.004	7750	63300	0.006

TAB. 6.24 Story shear forces, moments and maximum displacements for a 18-storey shear wall subject to non-linear dynamic analysis for earthquakes 1M72R70, 2M72R70 and 1M72R70match.

	1M72R70			2M72R70			1M72R70match		
	V	M	Δ	V	M	Δ	V	M	Δ
Lev.	(kN)	(kNm)	(m)	(kN)	(kNm)	(m)	(kN)	(kNm)	(m)
18	553	1899	0.509	538	1868	0.542	738	2556	1.107
17	890	4909	0.462	848	4758	0.493	1157	6462	1.011
16	1202	8302	0.416	983	7968	0.444	1355	9973	0.922
15	1173	11710	0.370	1072	10910	0.396	1266	14100	0.832
14	1118	15210	0.324	1007	14080	0.350	1162	17250	0.743
13	1135	18190	0.280	989	16820	0.304	1454	19360	0.660
12	1074	22390	0.253	959	19920	0.261	1836	23550	0.583
11	1215	25410	0.217	961	21520	0.209	2072	26690	0.488
10	1256	27050	0.189	939	22400	0.172	2176	29590	0.418
9	1320	28630	0.169	1105	23830	0.147	2256	33760	0.370
8	1611	29300	0.141	1396	25390	0.116	2181	37570	0.306
7	1867	29080	0.114	1665	27150	0.088	1958	41000	0.245
6	2000	29540	0.088	1970	29090	0.064	2213	44920	0.190
5	2074	29080	0.064	2216	30350	0.048	2545	48110	0.140
4	2372	34680	0.042	2462	30830	0.033	2936	51020	0.096
3	2600	39290	0.025	2741	31040	0.021	3446	55030	0.059
2	2771	42960	0.011	3105	37570	0.010	5149	60300	0.028
1	2947	47810	0.003	3430	48140	0.003	7561	67070	0.008

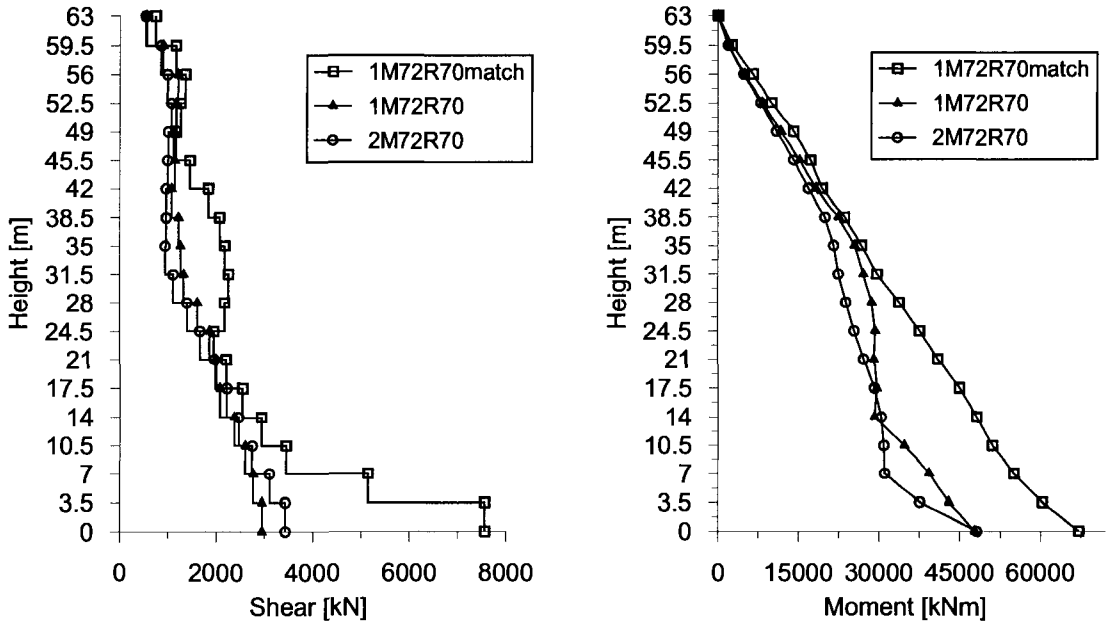

FIG. 6.32 Shear and moment results from non-linear dynamic analysis for earthquakes 1M72R70, 2M72R70 and 1M72R70match - 18 Storey

Following figures are graphical presentation of displacements results, as listed previously in Tables6.5 to 6.25, by floors for all models on both sites.

TAB. 6.25 Story shear forces, moments and maximum displacements for a 18-storey shear wall subject to non-linear dynamic analysis for earthquakes 1M85VBC et 2M85VBC.

	1M85VBC			2M85VBC		
	V	M	Δ	V	M	Δ
Lev.	(kN)	(kNm)	(m)	(kN)	(kNm)	(m)
18	406	1397	0.524	404	1390	0.611
17	646	3578	0.477	662	3623	0.558
16	761	6160	0.430	809	6393	0.507
15	809	8755	0.385	1006	9266	0.456
14	900	11010	0.340	1012	11560	0.406
13	905	13350	0.298	943	14410	0.357
12	913	16930	0.260	1062	18340	0.309
11	884	19380	0.214	1092	21160	0.252
10	1013	20950	0.181	1082	23030	0.214
9	1140	22880	0.158	1121	25560	0.188
8	1182	24440	0.129	1347	28090	0.152
7	1237	25730	0.103	1503	30390	0.119
6	1409	27150	0.079	1598	32400	0.092
5	1619	28960	0.057	1813	33850	0.068
4	1800	31510	0.038	1989	35900	0.047
3	1935	35340	0.023	2124	39080	0.028
2	2055	39940	0.011	2220	46580	0.013
1	2226	44770	0.003	2312	54240	0.004

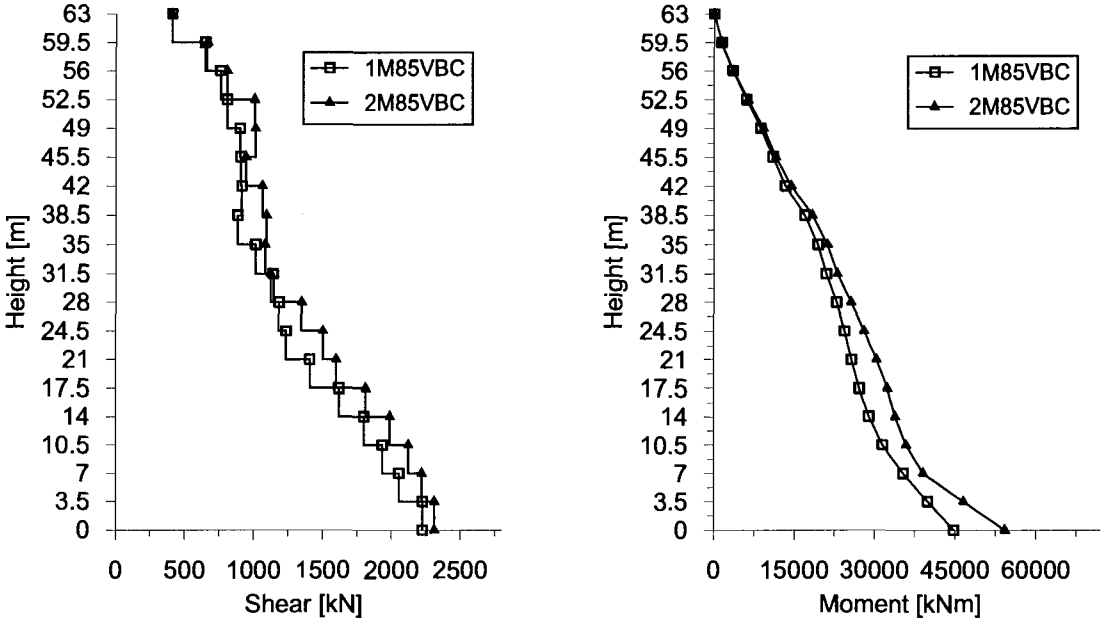

FIG. 6.33 Shear and moment results from non-linear dynamic analysis for earthquakes 1M85 and 2M85 - 18 Storey

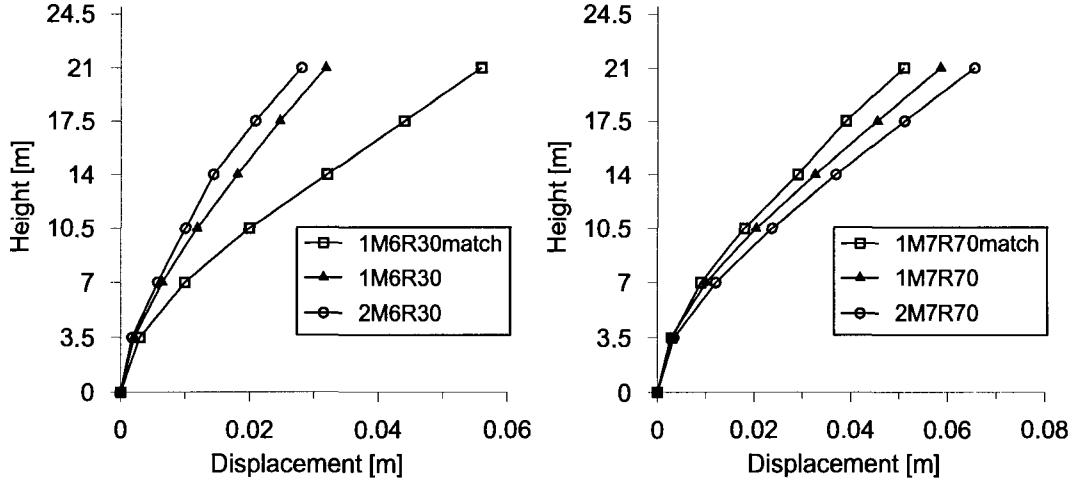

(a) M6R30 (b) M7R70

FIG. 6.34 Displacement results from non-linear dynamic analysis for 6 storey shear wall in Montréal

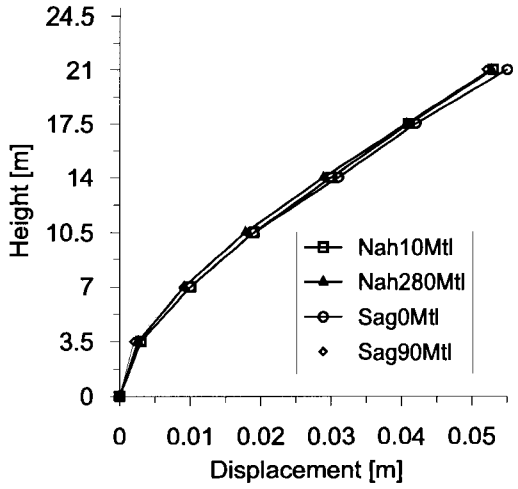

FIG. 6.35 Displacement results from non-linear dynamic analysis for earthquakes in Saguenay and Nahanni - 6 storey shear wall in Montréal

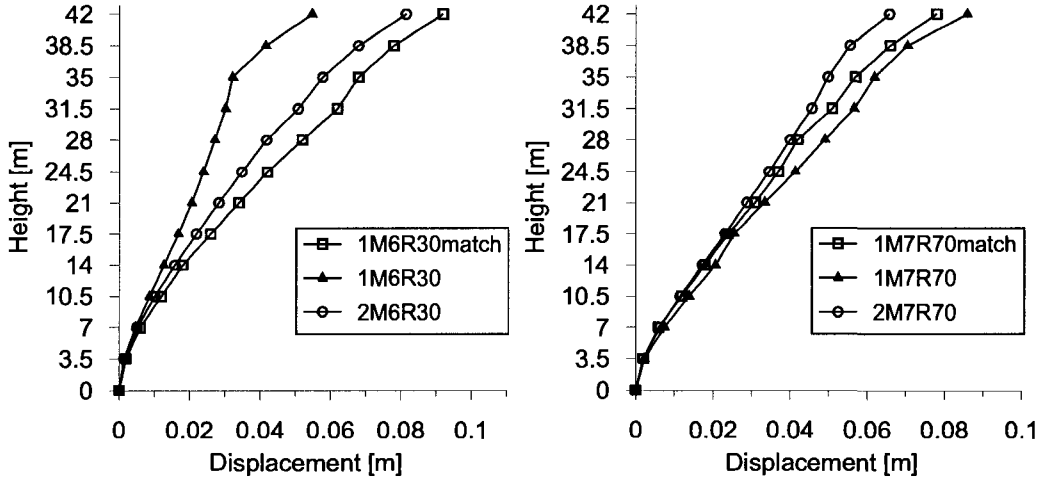

(a) M6R30 (b) M7R70

FIG. 6.36 Displacement results from non-linear dynamic analysis for 12 storey shear wall in Montréal

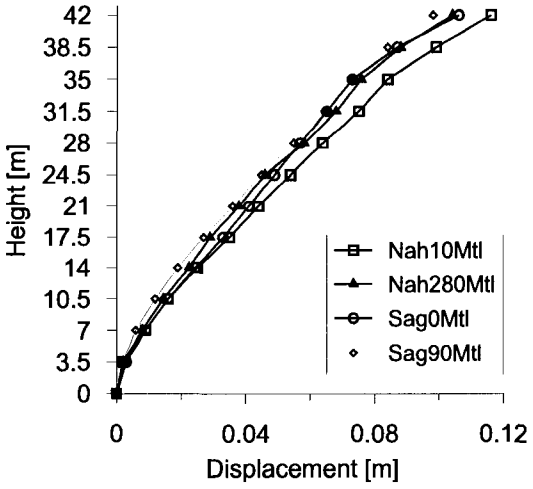

FIG. 6.37 Displacement results from non-linear dynamic analysis for earthquakes in Saguenay and Nahanni - 12 storey shear wall in Montréal

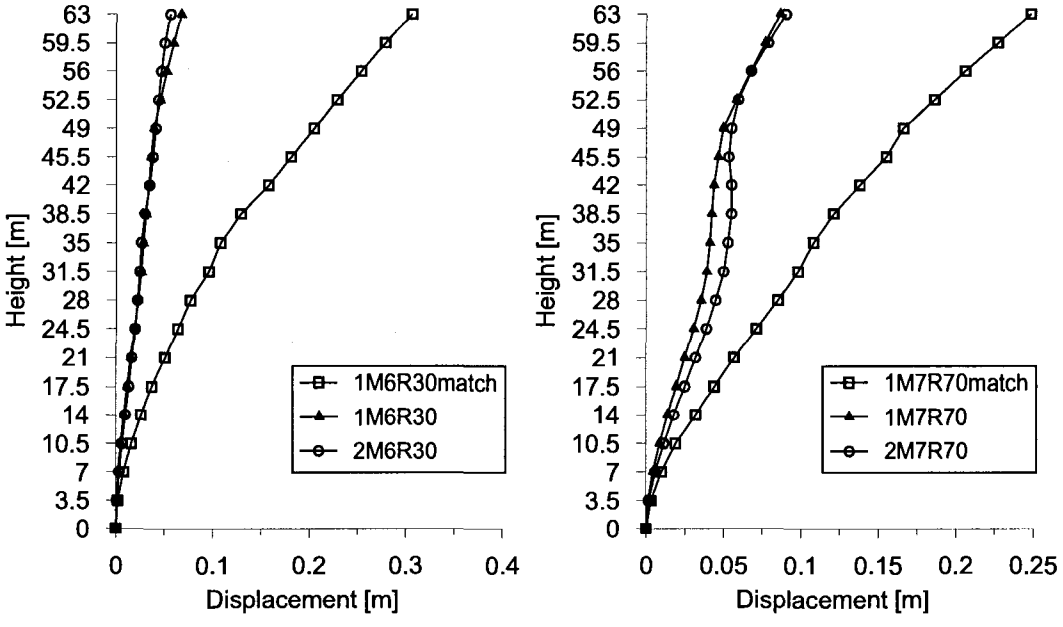

(a) M6R30 (b) M7R70

FIG. 6.38 Displacement results from non-linear dynamic analysis for 18 storey shear wall in Montréal

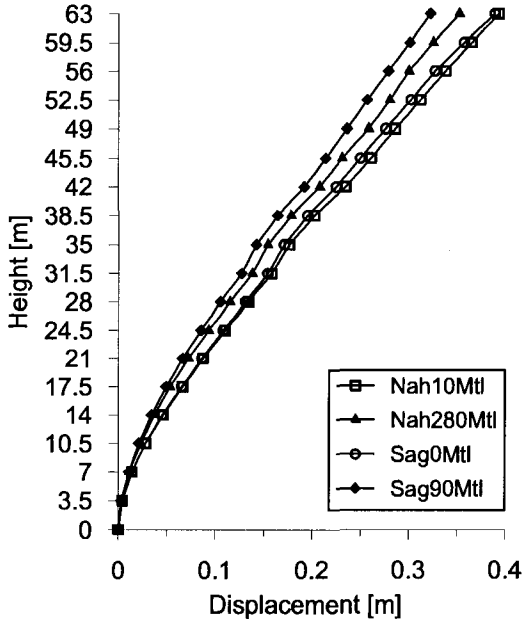

FIG. 6.39 Displacement results from non-linear dynamic analysis for earthquakes in Saguenay and Nahanni - 18 storey shear wall in Montréal

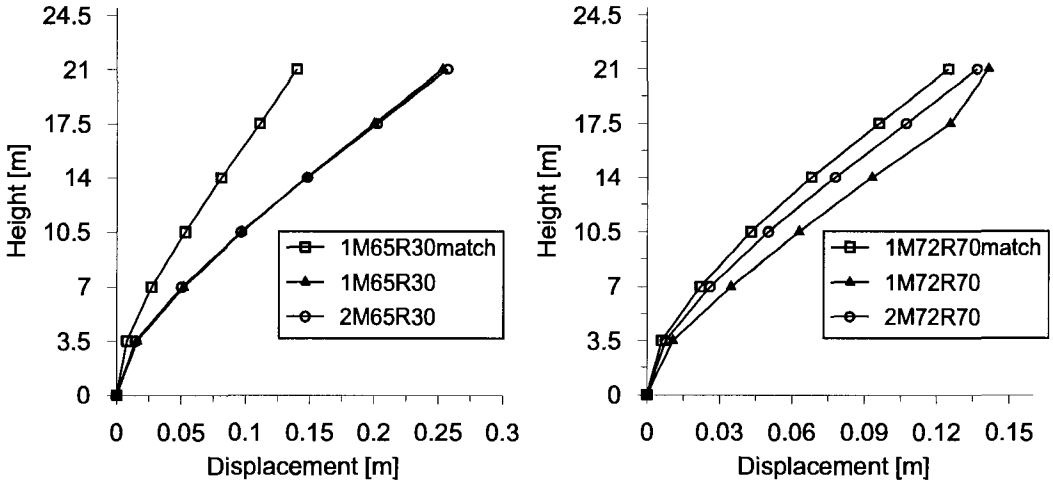

(a) M65R30

(b) M72R70

FIG. 6.40 Displacement results from non-linear dynamic analysis for 6 storey shear wall in Vancouver

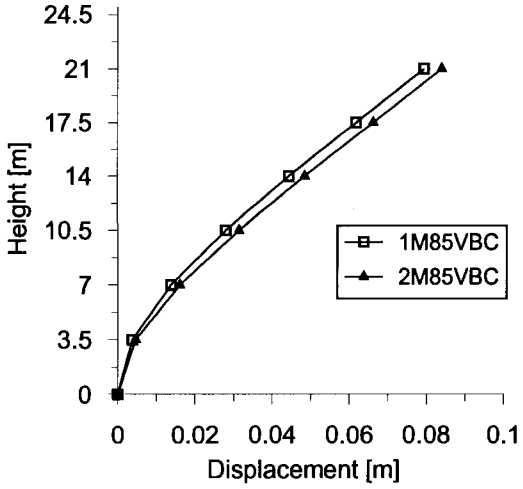

FIG. 6.41 Displacement results from non-linear dynamic analysis for earthquakes in Cascadia zone - shear wall in B6 in Vancouver

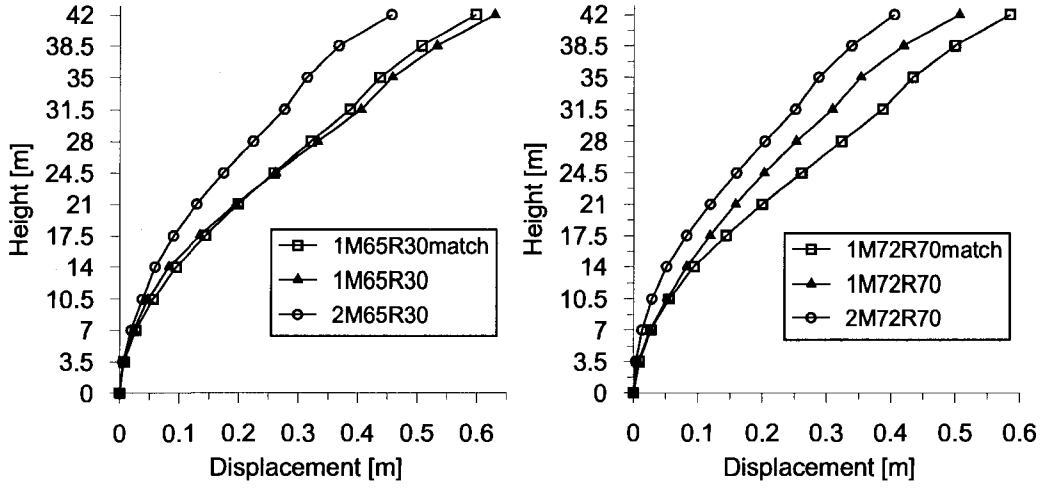

(a) M65R30

(b) M72R70

FIG. 6.42 Displacement results from non-linear dynamic analysis for shear wall in B12 in Vancouver

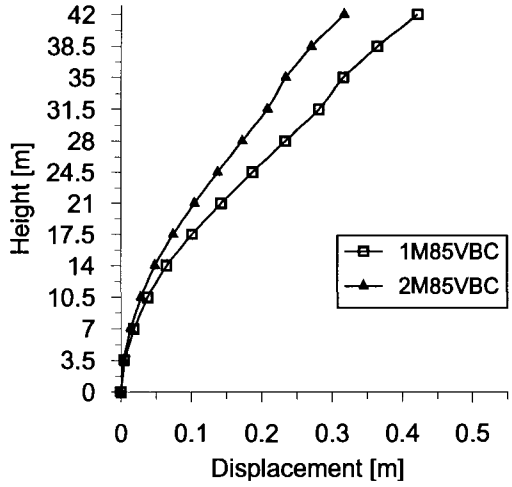

FIG. 6.43 Displacement results from non-linear dynamic analysis for earthquakes in Cascadia zone - shear wall in B12 in Vancouver

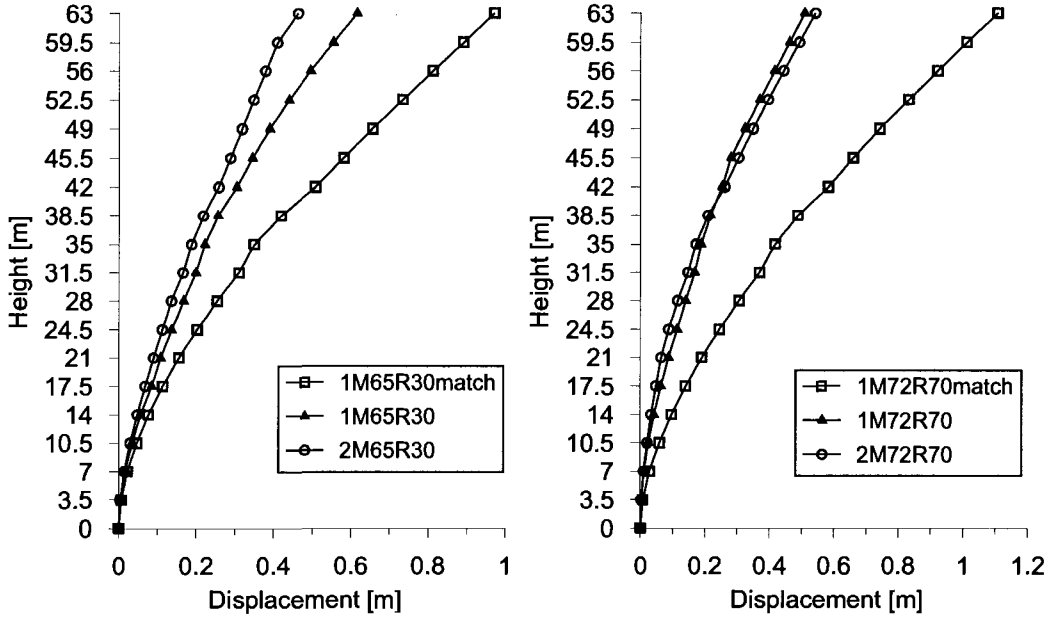

(a) M65R30 (b) M72R70

FIG. 6.44 Displacement results from non-linear dynamic analysis for shear wall in B18 in Vancouver

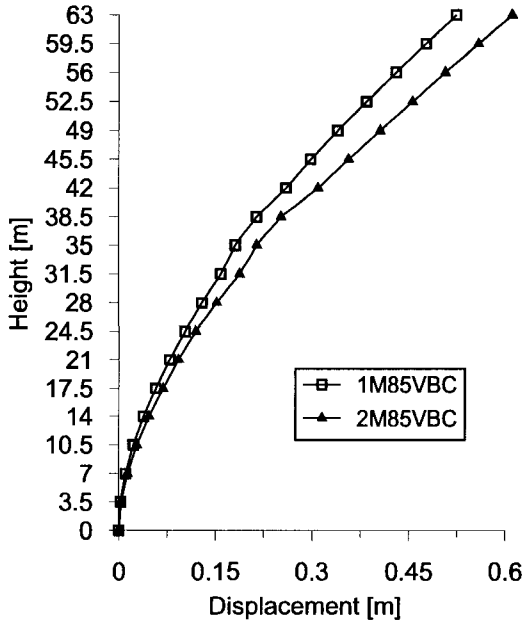

FIG. 6.45 Displacement results from non-linear dynamic analysis for earthquakes in Cascadia zone - shear wall in B18 in Vancouver

6.4.1 Concluding Remarks

Based on the obtained results from both applied historical and synthetical ground motions as input to the nonlinear time history analyses, a few conclusions could be commented.

6.4.1.1 Displacements

Nonlinear analyses results for the shear walls in Montréal and Vancouver showed that inter-storey drifts indexes meet the 2.5% limit, required in the NBCC 2005 for all shear walls in both cities, as shown in Figures 6.46 and 6.47. That conclusion is valid for all seismic demands, including the 'loose spectrum matched' and the 'close spectrum matched' earthquakes. For Montréal that ratio bearly reaches 1%, even for the low to mid-height buildings (i.e. B6 and B12), the inter-storey drift index is lower than 0.5%. That could be explained by the fact, that both geometric properties and ductility demand for

these shear walls have been conservatively assumed for design. For comparison purposes, an identical shear wall cross section was assumed for all buildings, and 'ductile' type has been assigned for all shear walls as well. However an economical design would rather require a different cross section (for example rectangular) for the shear walls in Montréal, as well as a 'moderately ductile' type for these shear walls with $R_d = 2.0$, especially for B6 and B12 in Montréal. The conservative design for the same shear walls has been validated with the minimum limit assumed for the inelastic rotational demand, as shown previously from the spectral analyses results in Table 4.28. For the shear walls in Vancouver, the inter-storey drift indexes are mainly between 1% and 2.5%, except for B6, where the maximum inter-storey drift index is 1.5% only for the short-period earthquake event (both 'loose' and 'close' spectrum matched). It must be noted, that similarly to the shear walls B6 and B12 in Montréal, for the B6 in Vancouver the minimum limit has been assigned for the inelastic rotational demand, as shown in the same Table 4.28, which means that the B6 shear wall design in Vancouver might be found conservative as well.

In the aspect of the shear wall height-to-width ratio, as shown in Figure 6.48, it must be noted that the peak roof displacements for the shear walls in Montréal give very simillar results for low to mid-height wall ratio, and the difference increases when increasing that ratio. A reason for that could be again the fact, that the B6 and B12 have been conservatively designed, as mentioned previously and their increased rigidity allow the top displacement to remain stable for periods up to two seconds in both cities.

It is noted as well, that the values of Δ_u for B12 are very similar to the results for B18 when using the 'loose' spectrum matched events for both cities, which is valid for both trials of the short and the long period events. A reason for that could be the fact, that fine-tune scaled events, both short and long period, provide 'loose' matched spectrums more than two times lower than the target spectra. In the same time the same 'loose' spectrums demonstrate almost constant values for structure periods bigger than two seconds, which is the present case for these buildings.

For shear walls in Vancouver, the peak roof displacements demonstrate a stable trend

in function of height-to-width wall ratios, as shown in the same Figure 6.48. Peak roof displacements increase when increasing the height-to-width ratio for all events, except the 'loose' spectrum matched ones. Reason for that could be the fact, that shear walls in Vancouver have been designed to satisfy the required moment factored resistance, contreversly to Montréal, where the minimum required reinforcement by the NBCC 2005 governed.

6.4.1.2 Shear strengths

Comparison of the base shear strengths peak values showed that results obtained through 'spectrum matched' earthquakes differ from those, obtained through 'factor scaled' ones. Analyses for 'Close' spectrum matched events give higher values than the 'loose' spectrum matched ones and that difference is valid for both short- and long-period events, as well as for both cities. Almost two times is the difference between the corresponding events for B18 in both cities. The reason for that, as mentioned previously for Δ_u could be the fact, that fine-tune scaled events, both short and long period, provide 'loose' matched spectrums more than two times lower than the target spectra for structure periods bigger than two seconds, which is the present case for these buildings.

6.4.1.3 Moment strength

Comparison for the base moment strengths values showed that the probable moment resistance of the shear walls is higher than the peak design values obtained from all non-linear analyses for the shear walls in Montréal. Therefore, the design for that shear walls which was found to be very conservative, validated by the fact that the minimum flexural reinforcement governed the factored moment resistance demand, satisfy the moment demands for both synthetically generated and historic records, as well as both 'loose' and 'close' spectrum matched events. However, for the shear walls in Vancouver, the probable moment resistance of the shear walls was overpassed for most of the analyses, even for

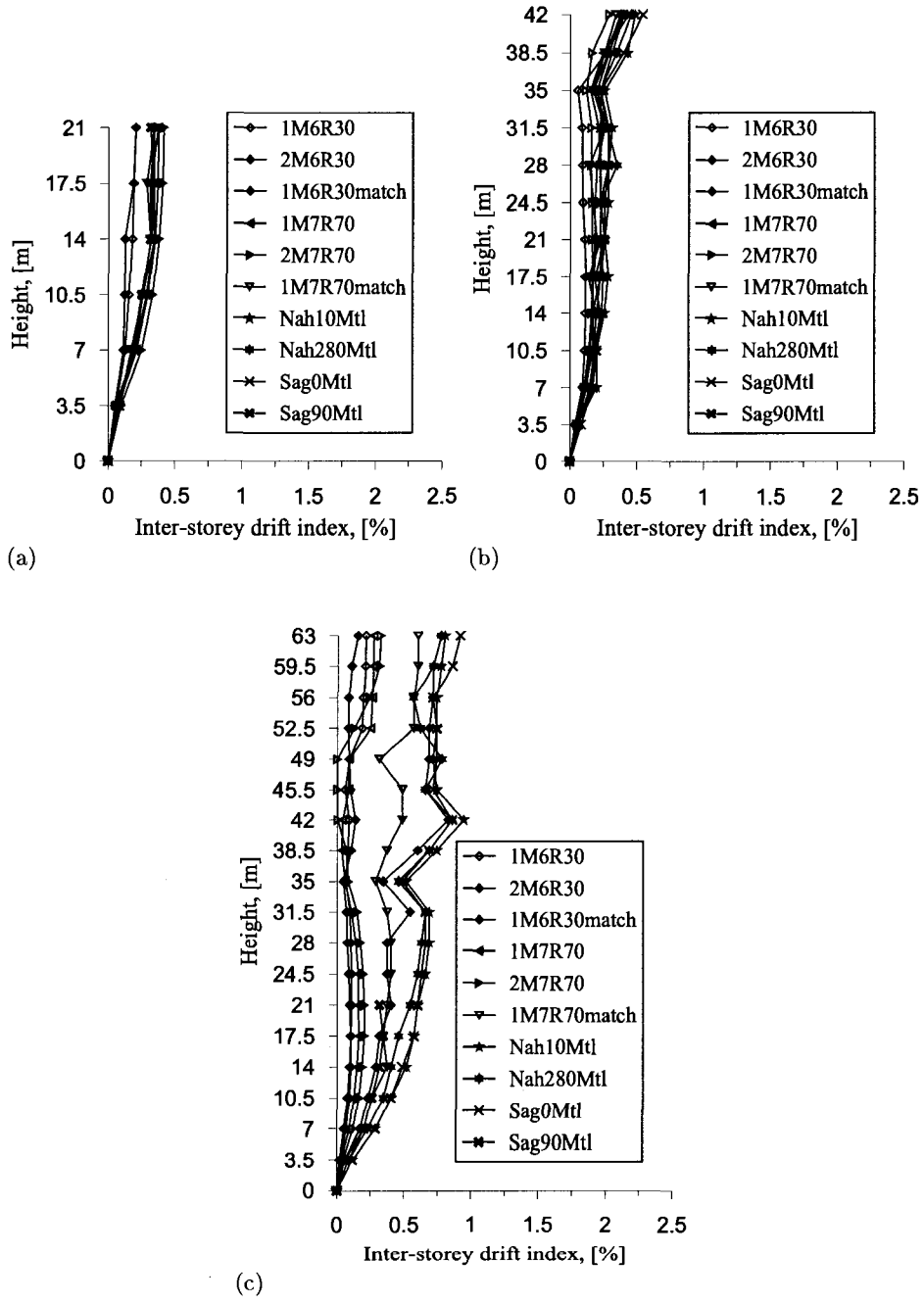

FIG. 6.46 Inter-storey drift indexes for shear walls in Montréal : (a) B6 ; (b) B12 ; and (c) B18.

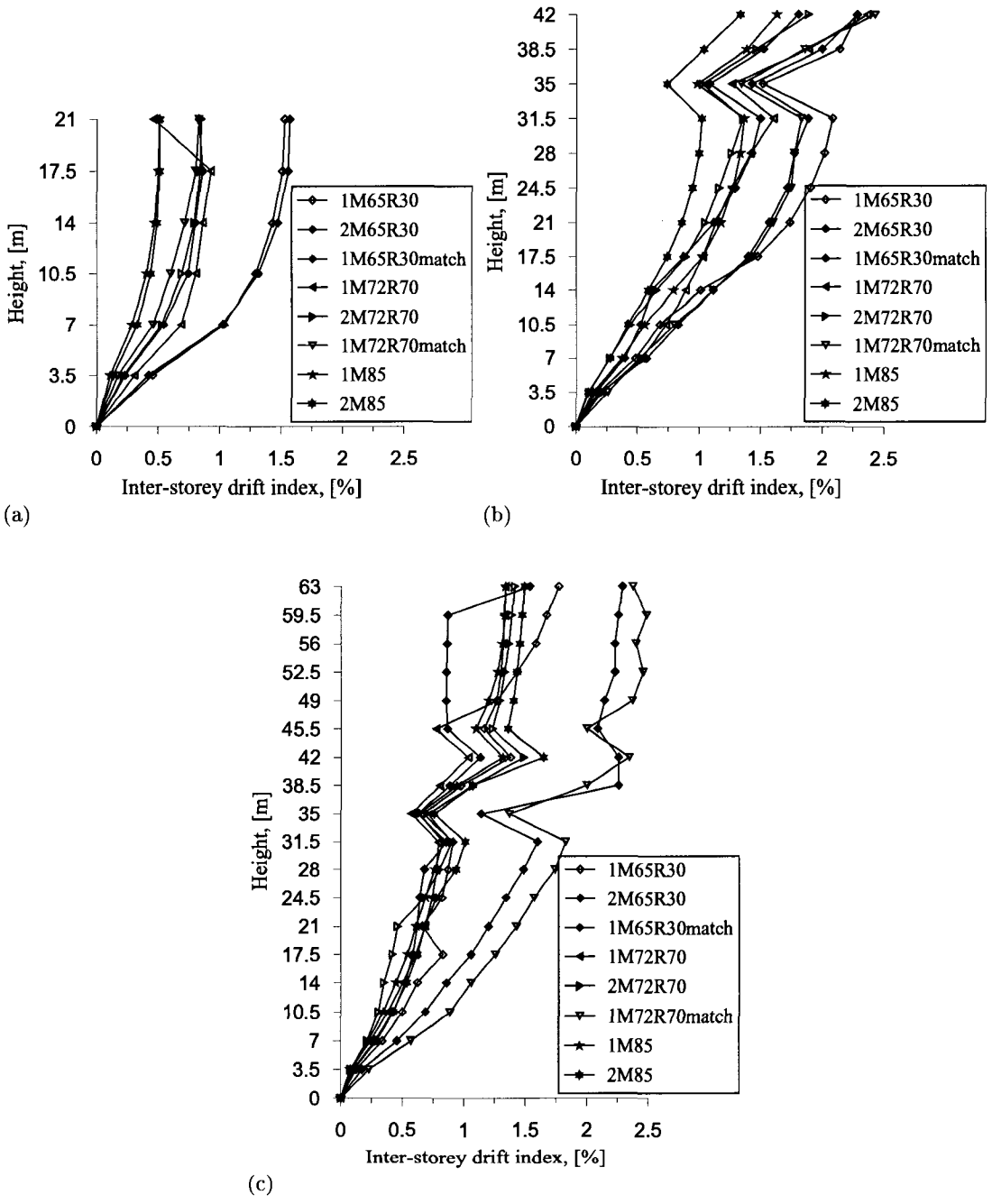

FIG. 6.47 Inter-storey drift indexes for shear walls in Vancouver : (a) B6; (b) B12; and (c) B18.

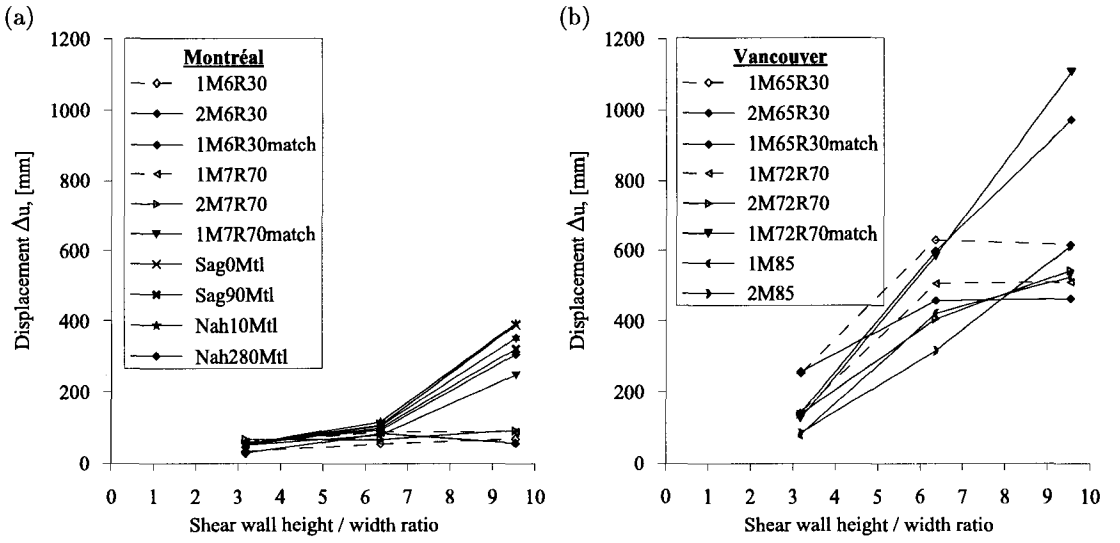

FIG. 6.48 Peak displacement results Δ_u at roof for different height-to-width wall ratio : (a) Montréal ; and (b) Vancouver ;

the low-rise buildings B6. Therefore, although the shear walls design satisfied the factored moment resistance demand for all shear walls, nonlinear analyses including both synthetically generated and historic records, as well as both 'loose' and 'close' spectrum matched events, seem to impose higher moment demands for the buildings in Vancouver, than provided by the spectral analysis.

CHAPTER 7

COMPARISON OF PERFORMED ANALYSES

7.1 Introduction

This chapter makes a comparative study of the shear force at the base of a shear wall and the displacement results obtained throughout the analyses in the present work. The graphical representation of the comparative study is given for the wall height to length ratio for the three models in both cities. The non-linear time-history analyses, described in details in Chapter 6 are represented in the graphical visualization only by the results from the highly converged excitations, both history records and synthetically generated. The analyses are denoted herein as following :

1. Linear spectral analysis - LSA,
2. Non-linear time-history analysis - NLTHA. According to the earthquake record used for analysis, non-linear time-history analyses are designated in the present chapter with the labels previously listed in Table 6.4.
3. Performance-based design methods analysis - PBDMA. According to the applied performance technique, performance methods are designated in the present chapter as following sub-types :
   - Yield Point Spectra method analysis (Ashheim) - YPS,
   - Direct Displacement-Based Design method (Priestley-Kowalsky) - DDBD,
   - Inelastic Design Spectra method (Chopra) - IDS.

7.2 Displacements

7.2.1 Yield Displacements

Table 7.1 compares the yield displacement Δ_y values at the top of the shear wall for the B6, B12 and B18 buildings located in Montréal and Vancouver. In order to calculate the

yield displacement at the top of the shear wall using the LSA, the equation $\Delta_y = \gamma_w \Delta_f$ is applied, where γ_w is listed in Table 4.27. Values in all tables for the displacement results are in (mm).

TAB. 7.1 Yield displacement (Δ_y) results for a shear wall using LSA and PBDMA analyses (mm).

	Montréal			Vancouver		
Shear wall in building	B6	B12	B18	B6	B12	B18
Shear wall height-to-length ratio	3.18	6.36	9.55	3.18	6.36	9.55
LSA	34	129	179	44	195	434
YPS	74	294	662	74	294	662
DDBD	50	179	389	50	178	388
IDS	52	180	387	52	179	385

7.2.2 Design Displacements

Table 7.2 compares the maximum design displacement Δ_u values (at the top of the shear walls) for the B6, B12 and B18 buildings located in Montréal and Vancouver. Both dynamic analysis procedures, recommended in the NBCC 2005, are represented in that table by their resulting design displacements (Δ_{des}) at the top of the shear walls. The maximum design displacements (Δ_u) for the linear spectral analysis (LSA) are represented by the values of $\Delta_{des} = \Delta_f R_d R_o$, summarized in Table 4.28. Similarly to the LSA, (Δ_u) for the non-linear time-history analysis (NLTHA) are represented by the values of Δ, listed in Tables 6.5 to 6.25. Regarding the performance-based design methods procedures, the target maximum displacement, the structure is designed for, corresponds to the design displacement Δ_u, represented in that section. For the YPS procedure (Ashheim, 2000), Δ_u is the target maximum displacement Δ_n at the top of the building. For the DDBD procedure (Priestley and Kowalsky, 2001), Δ_u is the target maximum displacement Δ_{eff}, listed in Tables 5.7 to 5.9. For the IDS procedure (Chopra and Goel, 2001), Δ_u is the

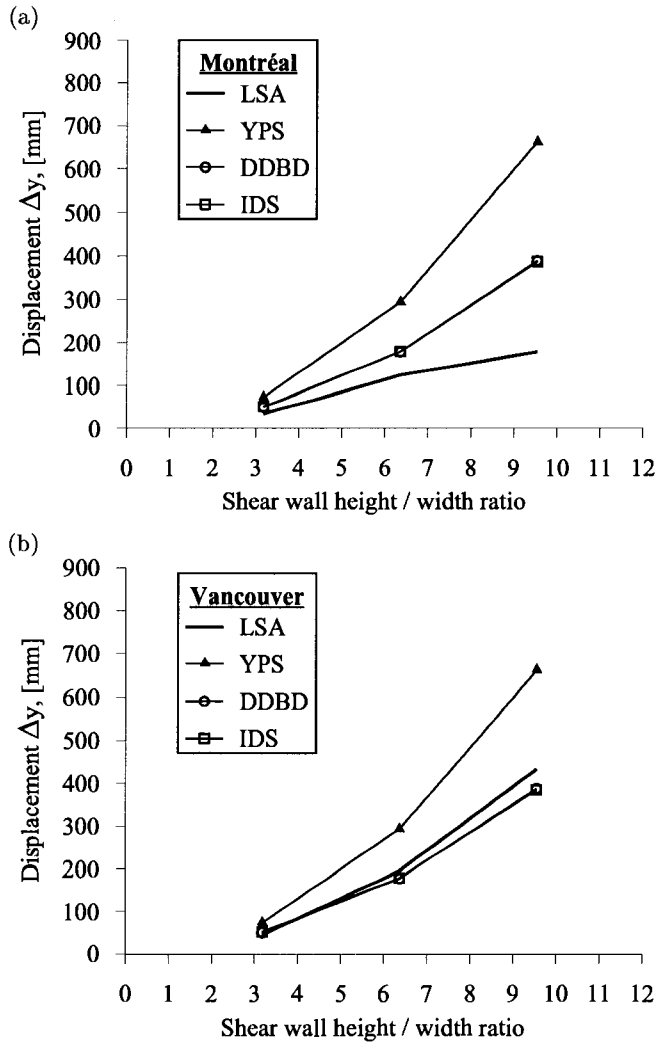

FIG. 7.1 Yield displacement (Δ_y) for different shear wall height-length ratios using LSA and PBDMA analyses for : (a) Montréal and (b) Vancouver.

target maximum displacement with the same designation Δ_{eff}, summarized in Table 5.11.

TAB. 7.2 Maximum design displacement (Δ_u) results for a shear wall using LSA, NLTHA and PBDMA analyses (mm) .

	Montréal			Vancouver		
Shear wall in building	B6	B12	B18	B6	B12	B18
Shear wall height-to-length ratio	3.18	6.36	9.55	3.18	6.36	9.55
LSA	50	187	346	116	625	1252
YPS	228	617	1152	228	617	1152
DDBD	166	631	881	165	630	879
IDS	167	405	724	166	404	722
1M6R30 / 1M62R30	32	55	67	253	630	616
2M6R30 / 2M62R30	28	82	56	257	457	462
1M6R30match / 1M62R30match	56	92	306	140	598	971
1M7R70 / 1M72R70	59	86	86	142	506	509
2M7R70 / 2M72R70	66	66	90	137	405	542
1M7R70match / 1M72R70match	51	78	248	125	584	1107
Sag0Mtl	56	106	389	–	–	–
Sag90Mtl	52	98	322	–	–	–
Nah10Mtl	53	116	393	–	–	–
Nah280Mtl	53	104	352	–	–	–
1M85	–	–	–	79	421	524
2M85	–	–	–	84	317	611

7.3 Shear Strength

7.3.1 Yield Shear Force

Table 7.3 compares the yield shear force V_y values at the base of a shear wall for the B6, B12 and B18 buildings located in Montréal and Vancouver. In order to calculate the

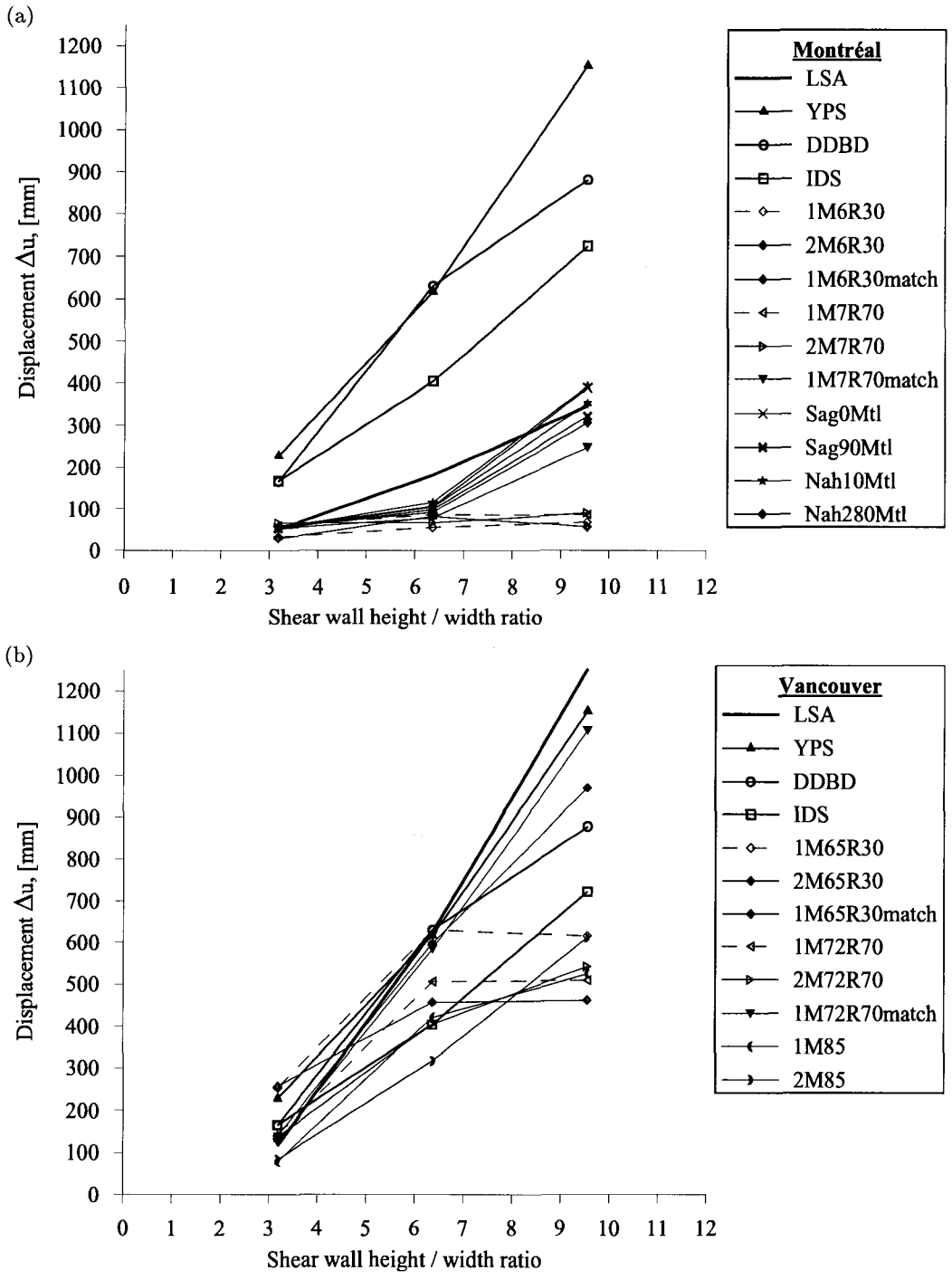

FIG. 7.2 Design displacement (Δ_u) for different shear wall height-length ratios using LSA, PBDMA and NLTHA analyses for : (a) Montréal and (b) Vancouver.

yield shear force at the shear wall base using the LSA, the following relation is applied $V_y = V_f R_o$, demonstrated in figure 3.1. Regarding the performance-based design methods procedures, the yield shear force V_y at the shear wall base is directly calculated following the YPS procedure (Ashheim, 2000). Values for V_y at the base of the buildings in both cities are summarized in Table 5.2. Values in all tables for the shear forces results are in (kN).

TAB. 7.3 Yield shear force (V_y) results at a shear wall base using LSA and PBDMA analyses .

	Montréal			Vancouver		
Shear wall in building	B6	B12	B18	B6	B12	B18
Shear wall height-to-length ratio	3.18	6.36	9.55	3.18	6.36	9.55
LSA	1266	1710	2283	2530	3738	4349
YPS	252	713	1292	1666	2523	4581

7.3.2 Design Shear Force

The design shear forces (V_u) for the non-linear time-history analyses (NLTHA) are represented in Table 7.4 by their resulting maximum shear force values (V_u) at the base of the shear walls. The values V_u are listed in Tables 6.5 to 6.25. Regarding the performance-based design methods procedures, the target shear force V_u, corresponds to the maximum target displacement Δ_u, afore-represented in that chapter. For the DDBD procedure (Priestley and Kowalsky, 2001), V_u is the design base shear force V_{eff}, listed in Tables 5.7 to 5.9. For the IDS procedure (Chopra and Goel, 2001), V_u is the required design base shear force with the same designation V_u, summarized in Table 5.11.

7.4 Comparative Study

Observation of the summarized in that chapter maximum displacements at the top of the shear walls Δ_y and Δ_u and the shear forces at the base of those walls V_y and V_u, conducts

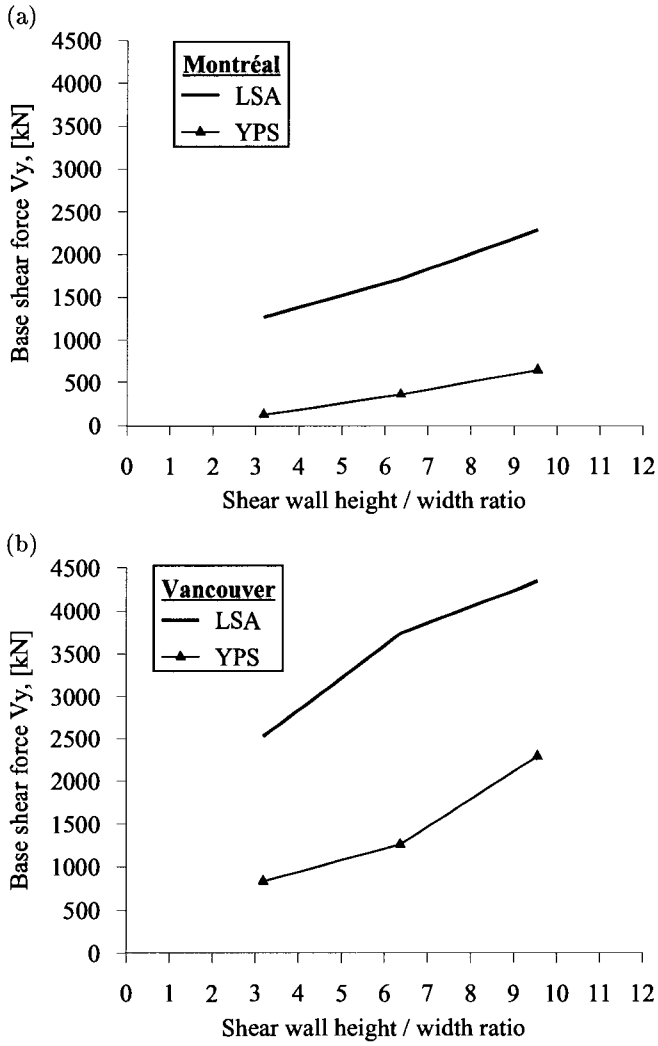

FIG. 7.3 Design shear force (V_y) for different shear wall height-length ratios using LSA and YPS analyses for : (a) Montréal and (b) Vancouver.

TAB. 7.4 Design shear force (V_u) results at a shear wall base using NLTHA and PBDMA analyses .

	Montréal			Vancouver		
Building	B6	B12	B18	B6	B12	B18
Height-to-length ratio	3.18	6.36	9.55	3.18	6.36	9.55
DDBD	212	429	704	924	1508	2488
IDS	245	576	919	863	2031	3251
1M6R30 / 1M62R30	2727	2784	2124	4693	5375	4683
2M6R30 / 2M62R30	2778	2337	2614	3958	4950	5665
1M6R30match / 1M62R30match	2439	4134	4079	5719	5565	7750
1M7R70 / 1M72R70	2361	2667	2452	2763	3519	2947
2M7R70 / 2M72R70	2264	2450	2407	1839	2755	3430
1M7R70match / 1M72R70match	3201	4243	4410	5986	6838	7561
Sag0Mtl	3628	4272	3454	–	–	–
Sag90Mtl	2665	3675	4424	–	–	–
Nah10Mtl	3897	4458	3506	–	–	–
Nah280Mtl	2857	2816	3985	–	–	–
1M85	–	–	–	1379	2062	2226
2M85	–	–	–	1345	2022	2312

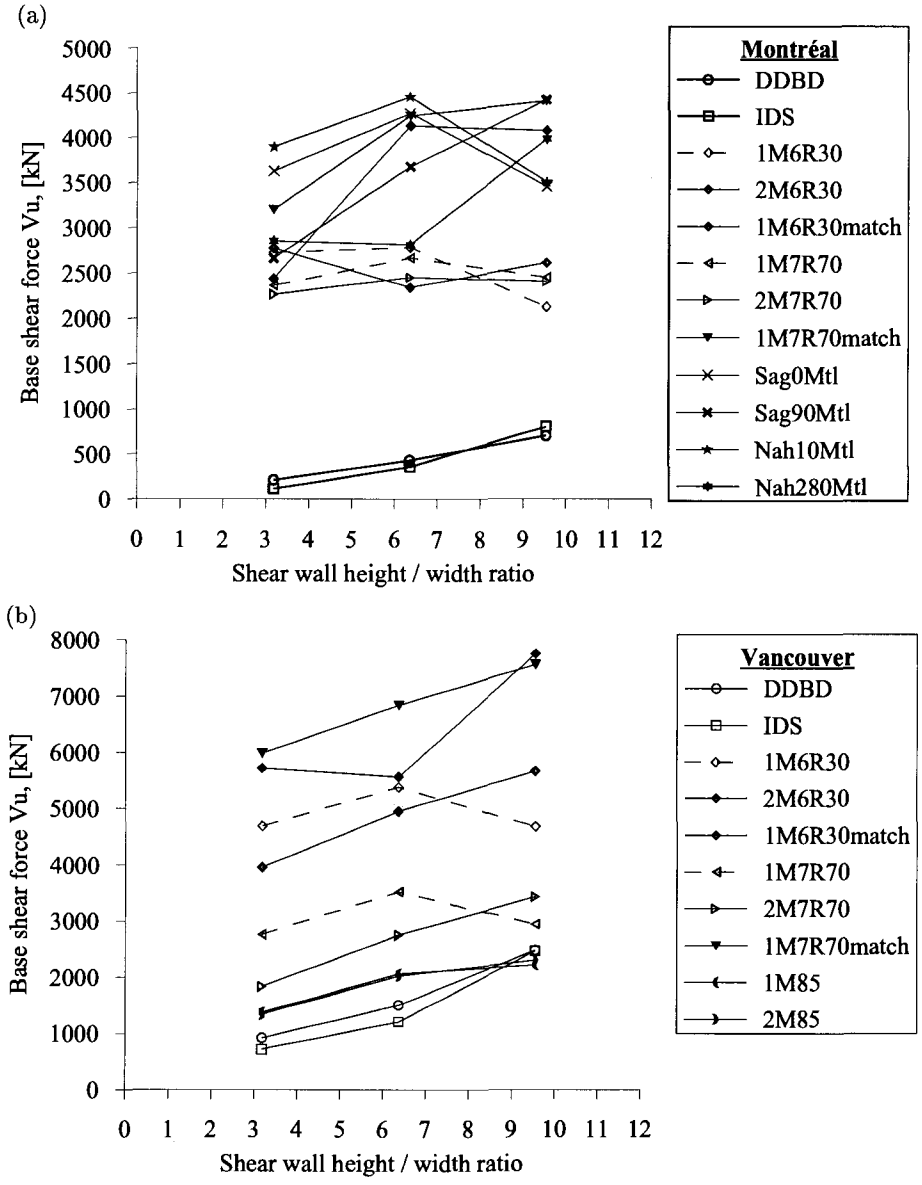

FIG. 7.4 Design shear force (V_u) for different shear wall height-length ratios using PBDM and NLTHA analyses for : (a) Montréal and (b) Vancouver.

to the following points :

1. Yield displacement Δ_y
   - There is a definite increasing trend for the yield displacement Δ_y as a function of the shear wall height-length ratio for both Montréal and Vancouver.
   - When applying the performance-based design methods, the encrease of Δ_y is amplified when the wall ratio increases. That trend is particularly reflected by the YPS method for both cities.
   - The yield displacement values, obtained from the LSA, representing the current code practice, and from the three DBD technics, used in the present work, are very close for the smaller wall ratio for both cities. For the DDBD and IDS methods, those values almost coincide with that obtained throughout the NBCC 2005 method (LSA).
   - The methods of Priestley and Kowalsky (DDBD) and Chopra and Goel (IDS), applied for the city of Vancouver, demonstrate very close values of the yield displacement to that obtained from the LSA for all wall ratios.
2. Design maximum displacement Δ_u
   - Similarly to Δ_y, an increasing trend exists for the maximum design displacement Δ_u, as well, as a function of the shear wall height-length ratio (wall ratio) for both Montréal and Vancouver. That trend is more clearly defined for the city of Vancouver for all methods, studied in that project, application. For the city of Montréal, the increasing trend is particularly demonstrated by the performance-based design methods nad the LSA, while the non-linear time-history analyses show such a trend for the higher wall height-to-length ratio.
   - Amplification of the design displacement (at the top of the building) as a function of the wall height-to-length is shown only for the NLTH analyses for the city of Montréal. For the three performance-based design methods and the LSA, the increase of Δ_u seems to follow a very alike linear distribution. For the city of Vancouver a linear increase of Δ_u can be observed in all analyses.
   - For Montréal the target design displacement values Δ_u, obtained from the performance-

based design methods, is significantly larger (two to three times), compared to the values of Δ_u, obtained from all the current code dynamic analyses, while for the city of Vancouver both PBDM and NBCC 2005 analyses show very close design results for all wall height-to-length ratio.

- Similarly to Δ_y, the methods of Priestley and Kowalsky (DDBD) and Chopra and Goel (IDS), applied for the city of Vancouver, demonstrate very close values of the design maximum displacement Δ_u to those obtained from all dynamic analyses (LSA and NLTHA) for all wall ratios. That is particularly visible for the target values from the DDBD and IDS methods, and the maximum design displacements from all dynamic analyses, which are very close for the lower to mid-height buildings.

3. Yield shear force V_y
   - A trend to increase is also valid for the yield shear force at the base of the building V_y as a function of the wall ratio for the NBCC 2005 dynamic (LSA) and performance-based (YPS) analyses. That trend is characteristic for both cities of Montréal and Vancouver.
   - A trend of yield force amplification as a function of the wall ratio may be noticed only when the YPS method is applied for the city of Vancouver. For the city of Montreal the raise of V_y as a function of the wall ratio is more alike linear.
   - The base yield shear force values obtained from the LSA, representing the current code practice, and from the YPS procedure differ considerably for both cities. For the city of Vancouver the values for V_y, obtained from LSA exceed two to three times those from YPS and the difference is inversly proportional to the wall ratio. For the city of Montréal the difference of V_y is even much bigger (three to ten times), but it is again inversly proportional to the wall ratio - the V_y difference decreases when increasing the wall ratio.
4. Shear design force V_u
   - There is a trend of increasing the shear design force at the base of the building V_u as a function of the wall ratio more specifically for the city of Vancouver. For Montréal such a trend is valid mostly for the PBDM analyses results.

- The design base shear force values obtained from the current code dynamic analyses, and those from the performance-based design methods differ considerably for both cities. For the city of Vancouver the values for V_u, obtained from NLTHA exceed five to six times those from PBDM (represented by DDBD and IDS) for lower buildings and two to three times for higher buildings results. Similarly to the yield force values V_y, for the city of Montreal, the difference of V_u is again much bigger between the Code prescribed dynamic analyses and the PBDM procedures. Forces V_u, obtained from NLTHA exceed ten to fifteen times those from PBDM (represented by DDBD and IDS) for lower buildings and six to three times for higher buildings results. Therefore, it may be seen, that the design shear force V_u difference is again inversly proportional to the wall ratio for both cities. More the wall ratio increases, more the design shear force difference decreases between the NBCC 2005 prescribed dynamic analyses and the PBDM procedures, studied in that project.

CHAPTER 8

CONCLUSIONS AND RECOMMENDATIONS

Three different displacement-based design procedures have been applied to three structural models of different height in two Canadian cities. It is important to note that these methods were not employed as design tools (i.e. the structure was designed using standard capacity-design approaches), but rather as the procedure to evaluate seismic performance of the building. The three models have an identical lateral force resisting system. Montréal and Vancouver have been chosen as representative for the Eastern and Western Canada seismic hazard spectra. The application of the three DBD methods and the code prescribed dynamic analysis procedures to all building models highlighted that all methods successfully sustained the target design parameters although the design strength varies significantly.

An interesting comparison of the design strenghts between DDBD and IDS methods is observed. Although both methods use a same target displacement profile as a start point, the resulting design maximum displacements differ by 50% when increasing the wall height-width ratio. In the same time the resulting design base shear strengths of both methods match within a small difference for all height-width ratio in both cities, except for the small buildings in Montréal, where the design shear from DDBD is twice that resulting from IDS. From the DBD methods, studied in that work, only the IDS method (Chopra and Goel, 2001) reflects the member design strength. In order to be consistent with the other DBD methods and for the purpose of their comparison, it was assumed in that project that the design moment, when applying the IDS method, is based on the required flexural resistance, which is times inferior than the required by the NBCC 2005 for all models in both cities. It would be interesting to compare then the design strengths obtained by the DBD methods when is used a minimum limitation for the required flexural resistance. It is expected that such limitation would govern the design shear strengths for all models and would approach the shear forces results from

the IDS to the code prescribed values, compared with the other DBD technics used in that project. It must be noted, that the correspondance of the flexural resistance for the used seismic hazard levels has to be validated as well.

Limitations are identified for all the DBD method. The YPS method (Aschheim, 2000) assumes that the structure will respond principally in the first mode. Therefore, values for the first mode participation factor relating the roof displacement to the displacement of an equivalent single degree of freedom system (SDOF) had to be assumed. The system effective mass also had to be assumed. The DDBD method (Priestley and Kowalsky, 2000) assumes the use of a preliminary defined target displacement profile. The IDS (Chopra, 2001) assumes a plastic rotation to be limited in the iterative procedures of the inelastic displacement. All these assumptions exclude the higer mode effect, which could be significant and must be furterly studied. No recommendations are made for the base shear distribution over the structure height.

An increasing trend has been noticed for all DBD methods, both for the design maximum and yield displacement, as well as for the design base shears in function of the wall ratio for both cities. Therefore a scaling effect may be studied further as for preliminary good approach to expected performance for the three DBD methods, studied in that work. Because those methods have been applied only to shear walls as a SRFS element and to regular structures, further study would be needed to verify that trend to other SRFS elements and to irregular structures.

Unless experimental validations are carried out, it would be difficult to state which method would perform best for design. Although the resulting maximum displacements have been found for some analyses much higher than the obtained by the NBCC 2005 dynamic analyses, they are based and satisfy the target objectives for interstorey drift limits. It is particularly shown for high wall ratio models in Montréal. In the same time the design base shear strengths are times lower than those obtained by the code prescribed procedures. In an economical meaning, all methods studied in that project give cost efficient design, while maintaining the target design parameters. Therefore an experimental validation of

the performance objectives for damage level index and their relation with the flexural and shear strengths limitations may conduct to much economical design.

BIBLIOGRAPHY

Abrahamson, N.A. 1998. Non-stationary spectral matching program RSPMATCH. PG&E Internal Report.

Adams, J., Weichert, D.H., and Halchuk, S. 1999. Trial seismic hazard maps of Canada : 2%/50 year values for selected Canadian cities. Geological Survey of Canada, Open File 3274.

Adams, J., Atkinson, G. 2003. Development of seismic hazard maps for the proposed 2005 edition of the National Building Code of Canada. Canadian Journal of Civil Engineering, Vol. 30, 255–271.

Adams, J., Halchuk, S. 2003. Fourth generation seismic hazard maps of Canada : Values for over 650 Canadian localities intended for the 2005 National Building Code of Canada. Geological Survey of Canada, Open File 4459

Report ARD 00-7. 2000. ADINA R&D, Inc.

Aschheim, M., and Black, E. 2000. Yield Point Spectra for seismic design and rehabilitation. Earthquake Spectra, **16**(2) : 317–335.

ATC-40. 1996. Seismic evaluation and retrofit of concrete buildings, Vol. 1, Applied Technology Council, Redwood City, California.

Atkinson, G., Beresnev, A. 1998. Compatible ground-motion time-histories for new national seismic hazard maps. Canadian Journal of Civil Engineering ; 25 : 305-318.

Aydinogly N.M. 2003. An Incremental Response Spectrum Analysis Procedure Based on Inelastic Spectral Displacements for Multi-Mode Seismic Performance Evaluation. Bulletin of Earthquake Engineering 2003 ; 1 : 3-36

Bertero, R.D., Bertero, V.V. 2002. Performance-based seismic engineering : the need for a reliable conceptual comprehensive approach. Earthquake Engineering Struct. Dyn. 2002 ; 31 : 627-652

Bommer, J.J., Elnashai, A.S. 1999. Displacement spectra for seismic design. J Earthquake Engineering 1999 ; 3(1) : 1-32

Bouaanani, N. and Alexieva, K. 2006. Use of Yield Point Spectra for seismic design of shear walls submitted to new Eastern Canadian seismic hazard. First International Structural Specialty Conference. May 23-26. Calgary, Alberta.

Browning, J.P., Proportioning of Earthquake-Resistant RC Building Structures. ASCE Journal of Structural Engineering, 2001 ; V.127 (2) : 145-151

Carr, A.J. 1982. Ruaumoko - Dynamic non-linear analysis. University of Canterbury, New Zealand

Carr, A.J. 2002. Ruaumoko - Inelastic Dynamic Analysis. University of Canterbury, New Zealand

CPCA. 1995. Concrete design handbook. Canadian Portland Cement Association, Ottawa, ON.

CSA. 2004. Design of Concrete Structres, CSA 23.3-04. Canadian Standards Association, Ottawa, Ontario.

Chopra, A.K.. 2001. Dynamics of Structures, Second edition, Prentice Hall, Upper Saddle River, NJ, U.S.A.

Chopra, A.K., Goel, R.K. 1999. Capacity-Demand-Diagram Methods Based on Inelastic Design Spectrum. Earthquake Spectra, Vol. 15, no. 4 : 637-656

Chopra, A.K. and Goel, R.K. 2001. Direct displacement-based design : Use of inelastic *vs* elastic design spectra. Earthquake Spectra, **17**(1) : 47–64.

Chopra, A.K., Goel, R.K. and Chintanapakdee, C. 2003. Statistics of Single-Degree-Of-Freedom Estimate of Displacement for Pushover Analysis of Buildings. Journal of Structural Engineering. 2003 ; April : 459-469

Bentz, E. and Collins, M. 2000. Response 2000 - Reinforced Concrete Sectional Analysis using the Modified Compression Field Theory. University of Toronto, ON.

Court, A.B., Kowalsky, M.J. 1998. Performance-based engineering of buildings displacement design approach. Structural Engineering World Wide, SEAOC, Paper No.T109-1.

Computers and Structures Inc. 2002. ETABS - Integrated Building Design Software. CSI Inc., Berkeley, CA, USA

Software and Solutions for Structural Engineers. 2006. W-Sect - General Purpose Structural Analysis and Design. CSC, Vancouver, BC.

DeVall, R. 2003. Background information for some of the proposed earthquake design provisions for the 2005 edition of the National Building Code of Canada. Canadian Journal of Civil Engineering, **30**(2) :279–286.

Dincer, E. 2003. Seismic drift demands of reinforced concrete buildings. Faculty of Engineering, University of Ottawa, ON.

EUROCODE EC8. 1998. Design provisions for earthquake resistance of structures. European Union, European Prestandarts, Brussel.

Fajfar, P., Capacity spectrum method based on inelastic demand spectra. 1999. Earthquake Engineering Structural Dynamics ; 28 : 979-993

Fajfar, P. 2000. A Nonlinear Analysis Method for Performance-Based Seismic Design. Earthquake Spectra ; V.16, 3 : 573-592

Gulkan, P. and Sozen, M. 1974. Inelastic response of reinforced concrete structures to earthquake motions. ACI Journal, **71**(12) :604-–610.

Kowalsky M.J., Priestley, M., McRae, G. 1994. Displacement-based design, a methodology for seismic design applied to single degree of freedom reinforced concrete structures. Report No.SSRP-94/16. Structural Systems Research, University of California, San Diego, La Jolla, California.

Kowalsky, M. J., Priestley, M., and McRae, G. 1995. Displacement-based design of RC bridge columns in seismic regions. Earthquake Engineering and Structural Dynamics, **24**(12) :1623—1642.

Kowalsky, M. 2001. RC Structural Walls Designed according to UBC and Displacement-Based Methods. Journal of Structural Engineering. May : 506-516

Lilhanad, K. and Tseng, W. 1988. Development and application of realistic earthquake time histories compatible with multiple damping response spectra, Ninth World Conf. Earth. Engin., Tokyo, Japan, Vol. II, 819–824.

Medhekar, M. and Kennedy, D. 2000. Displacement-based seismic design of buildings - theory. Engineering Structures ; 22 : 201-209

Medhekar, M.S., Kennedy, D. 2000. Displacement-based seismic design of buildings - application. Engineering Structures ; 22 : 210-221

Miranda, E. 1993. Site-dependent strength reduction factors. ASCE Journal of Structural Engineering, **119**(12), 3503–3519.

Miranda, E. and Bertero, V. 1994. Evaluation of Strength Reduction Factors for Earthquake-Resistant Design. Earthquake Spectra, **10**(2) : 357–379.

Mitchell, D., and Paultree, P. Ductility and overstrength in seismic design of reinforced concrete structures. Canadian Journal of Civil Engineering, **21**(6) :1049–1060.

Nassar, A. and Krawinkler, H. 1991. Seismic Demands for SDOF Report No. 95, The John A. Blume Earthquake Engrg. Center, Stanford University.

Canadian Commission on Building and Fire Codes. National Building Code of Canada. Ottawa, Ontario : National Research Council of Canada, 1995

Canadian Commission on Building and Fire Codes. National Building Code of Canada. Ottawa, Ontario : National Research Council of Canada, 2004

Newmark, N. and Hall, W. 1982. Earthquake spectra and design. Berkeley : Earhtquake Engineering Research Institute.

Panagiotakos, T. and Fardis, M. 1999. Deformation-controlled earthquake-resistant design of RC buildings. J Earthquake Eng. ; 3(4) : 495-518

Panagiotakos, T. and Fardis, M. 2001. A displacement-based seismic design procedure for RC buildings and comparison with EC8. Earthquake Engng Struct. Dyn. ; 30 : 1439-1462

Paulay, T. 2001. Seismic response of structural walls : Recent developments. Canadian Journal of Civil Engineering, **28**(6) :922–937.

Paulay, T. 2002. Displacement-Focused Seismic Design of Mixed Building Systems. Earthquake Spectra, Vol. 18, No. 4, 689–718

GSC, Earthquakes Canada, Geological Survey of Canada, http ://earthquakescanada.nrcan.gc.ca, Date accessed : 27 septembre 2006.

Priestley, M., Kowalsky, M., Ranzo, G. and Benzoni, G. 1996. Preliminary developpement of direct displacement-based design for multi degree of freedom systems. Proceedings of 65th Annual Convention. SEAOC, Maui, Hawaii.

Priestley, M. and Kowalsky, M. 2000. Direct Displacement-Based Design of Concrete Buildings. Bulletin of the New Zealand National Society for Earthquake Engineering, **33**(4) :421–444.

SEAOC Vision 2000 Committee. 1995. Performance based seismic engineering of buildings. Structural Engineers Association of California, CA, USA.

SEAOC Blue Book. 1999. Recommended lateral force requirements and commentary. Seventh Edition, Seismology Committee, Structural Engineers Association of California, CA, USA.

Shibata, A. and Sozen, M. 1976. Substitute structure method for seismic design in reinforced concrete. ASCE Journal of the Structiral Division, **102**(1) :1–18.

Takeda, T., Sozen, M. and Nielsen, N. 1970. Reinforced concrete response to simulated earthquakes. ASCE Journal of the Structural Division, **96**(12) :2557-–2573.

Taylor, R. 1977. The nonlinear sesimic response of tall shear wall structures. Ph.D. thesis, Departement of civil engieering, University of Canterbury, New Zealand.

Tinawi, R. 2004. An Overview of fifty years of development for the Canadian seismic building code. Egyptian Society for Earthquake Engineering, EGYQUAKE3 Conference, Cairo University, Egypt.

Tremblay, R. 2005. Seismic aspects in the new 2005 edition of the NBCC and in the CSA A23.3-04 and CSA-S16 standards. CISMIQ conference, 30 may 2005, Orford, Sherbrooke.

UBC. 1997. Uniform Building Code. International Conference of Building Officials (ICBO), Whittier, CA, USA.

Vidic, T., Fajfar, P. and Fishinger, M. 1992. A procedure for determining consistent inelastic design spectra. Proceedings of the Workshop on Nonlinear Seismic Analysis of RC Structures, Bled, Slovenia.

Vision 2000 Committee. 1995. Performance Based Seismic Engineering of Buildings. Structural Engineers Association of California (SEAOC), CA, USA.

ANNEXE I

AXIAL LOADING FOR A SINGLE SHEAR WALL AND A BUILDING FOR ALL MODELS

* Live Load Reduction Factor :

(1) $F_{\text{rld}}^{office} = 0.3 + \sqrt{9.8/Area}$ - Reduction factor for Live Loading over trib. areas bigger than $20\,\text{m}^2$ and surcharges other than specified per Clause 4.1.6.9,1&2 [CCBFC 2005].

(2) $F_{\text{rld}}^{Corr.} = 0.5 + \sqrt{20/Area}$ - Reduction factor for Live Loading over trib. areas bigger than $80\,\text{m}^2$ and surcharges bigger than 4.8 kPa, as per Clause 4.1.6.9 [CCBFC 2005].

** Combination loading $P_{\text{D}} + 0.25P_{\text{S}}$ includes the attributed snow loading.

TAB. I.1 Shear wall trib. loading in B6 in Montréal

Lev.	Live Occupancy		Cumulated Trib. Area		Reduction* Factor		Live Load Cumul.	Live Load per Floor	Dead Load	Cumulated load Combination		Factored Loading
	Off	Corr	Off	Corr	F_{rld}^{off}	F_{rld}^{corr}				$P_{\text{D}} + 0.25P_{\text{S}}$**	$P_{\text{D}} + 0.5P_{\text{L}}$	per floor
-	kPa	kPa	m^2	m^2	-	-	kN	kN	kN	kN	kN	kN
6	2.48	-	49.50	-	-	-	123	123	423	453	453	453
5	2.40	4.8	29.16	18	0.88	1.00	148	148	405	859	933	479
4	2.40	4.8	58.32	36	0.71	1.00	272	124	405	1264	1400	467
3	2.40	4.8	87.48	54	0.63	1.00	392	120	405	1669	1866	465
2	2.40	4.8	116.64	72	0.59	1.00	511	118	405	2075	2330	464
1	2.40	4.8	145.80	90	0.56	0.97	615	105	405	2480	2788	458

TAB. I.2 Shear wall trib. loading in B12 in Montréal

Lev.	Live Occupancy		Cumulated Trib. Area		Reduction* Factor		Live Load		Dead Load	Cumulated load Combination		Factored Loading
	Off	Corr	Off	Corr	F_{rld}^{off}	F_{rld}^{corr}	Cumul.	per Floor		$P_{\text{D}} + 0.25P_{\text{S}}$**	$P_{\text{D}} + 0.5P_{\text{L}}$	per floor
-	kPa	kPa	m^2	m^2	-	-	kN	kN	kN	kN	kN	kN
12	2.48	-	49.50	-	-	-	123	123	423	453	453	453
11	2.40	4.8	29.16	18	0.88	1.00	148	148	405	859	933	479
10	2.40	4.8	58.32	36	0.71	1.00	272	124	405	1264	1400	467
9	2.40	4.8	87.48	54	0.63	1.00	392	120	405	1669	1866	465
8	2.40	4.8	116.64	72	0.59	1.00	511	118	405	2075	2330	464
7	2.40	4.8	145.80	90	0.56	0.97	615	105	405	2480	2788	458
6	2.40	4.8	174.96	108	0.54	0.93	708	92	408	2888	3242	454
5	2.40	4.8	204.12	126	0.52	0.90	798	90	408	3296	3695	453
4	2.40	4.8	233.28	144	0.50	0.87	886	88	408	3704	4147	452
3	2.40	4.8	262.44	162	0.49	0.85	973	87	408	4111	4598	451
2	2.40	4.8	291.60	180	0.48	0.83	1058	86	408	4519	5048	451
1	2.40	4.8	320.76	198	0.47	0.82	1143	85	408	4927	5499	450

TAB. I.3 Shear wall trib. loading in B18 in Montréal

Lev.	Live Occupancy		Cumulated Trib. Area		Reduction* Factor		Live Load	per	Dead Load	Cumulated load Combination		Factored Loading
	Off	Corr	Off	Corr	F_{rld}^{off}	F_{rld}^{corr}	Cumul.	Floor		$P_{\text{D}} + 0.25P_{\text{S}}$**	$P_{\text{D}} + 0.5P_{\text{L}}$	per floor
-	kPa	kPa	m^2	m^2	-	-	kN	kN	kN	kN	kN	kN
18	2.48	-	49.50	-	-	-	123	123	423	453	453	453
17	2.40	4.8	29.16	18	0.88	1.00	148	148	405	859	933	479
16	2.40	4.8	58.32	36	0.71	1.00	272	124	405	1264	1400	467
15	2.40	4.8	87.48	54	0.63	1.00	392	120	405	1669	1866	465
14	2.40	4.8	116.64	72	0.59	1.00	511	118	405	2075	2330	464
13	2.40	4.8	145.80	90	0.56	0.97	615	105	405	2480	2788	458
12	2.40	4.8	174.96	108	0.54	0.93	708	92	405	2885	3239	451
11	2.40	4.8	204.12	126	0.52	0.90	798	90	405	3291	3690	450
10	2.40	4.8	233.28	144	0.50	0.87	886	88	408	3699	4141	452
9	2.40	4.8	262.44	162	0.49	0.85	973	87	408	4106	4593	451
8	2.40	4.8	291.60	180	0.48	0.83	1058	86	408	4514	5043	451
7	2.40	4.8	320.76	198	0.47	0.82	1143	85	408	4922	5494	450
6	2.40	4.8	349.92	216	0.47	0.80	1226	84	408	5330	5943	450
5	2.40	4.8	379.08	234	0.46	0.79	1309	83	408	5738	6392	449
4	2.40	4.8	408.24	252	0.45	0.78	1391	82	408	6146	6841	449
3	2.40	4.8	437.40	270	0.45	0.77	1473	81	408	6554	7290	449
2	2.40	4.8	466.56	288	0.44	0.76	1554	81	408	6961	7738	448
1	2.40	4.8	495.72	306	0.44	0.76	1634	80	408	7369	8186	448

TAB. I.4 Loading applied at mass center for B6 in Montréal

Lev.	Elev.	Live Occupancy		Cumulated Trib. Area		Reduction* Factor		Live Load		Dead Load	Cumulated load Combination		Factored Loading
		Off	Corr	Off	Corr	F_{rld}^{off}	F_{rld}^{corr}	Cumul.	per Floor		$P_{\text{D}} + 0.25P_{\text{S}}$**	$P_{\text{D}} + 0.5P_{\text{L}}$	per floor
-	m	kPa	kPa	m^2	m^2	-	-	kN	kN	kN	kN	kN	kN
6	21.0	2.48	-	1041.25	-	-	-	2582	2582	6647	7293	7293	7293
5	17.5	2.40	4.8	789.25	252	0.41	0.78	1725	1725	6509	13802	14664	7371
4	14.0	2.40	4.8	1578.50	504	0.38	0.70	3127	1402	6509	20311	21874	7210
3	10.5	2.40	4.8	2367.75	756	0.36	0.66	4475	1348	6509	26819	29057	7183
2	7.0	2.40	4.8	3157.00	1008	0.36	0.64	5796	1321	6509	33328	36226	7169
1	3.5	2.40	4.8	3946.25	1260	0.35	0.63	7099	1303	6509	39837	43387	7161

TAB. I.5 Loading applied at mass center for B12 in Montréal

Lev.	Elev.	Live Occupancy		Cumulated Trib. Area		Reduction* Factor		Live Load	per	Dead Load	Cumulated load Combination		Factored Loading
		Off	Corr	Off	Corr	F_{rld}^{off}	F_{rld}^{corr}	Cumul.	Floor		$P_{\text{D}} + 0.25P_{\text{S}}$**	$P_{\text{D}} + 0.5P_{\text{L}}$	per floor
-	m	kPa	kPa	m^2	m^2	-	-	kN	kN	kN	kN	kN	kN
12	42.0	2.48	-	1041.25	-	-	-	2582	2582	6647	7293	7293	7293
11	38.5	2.40	4.8	789.25	252	0.41	0.78	1725	1725	6509	13802	14664	7371
10	35.0	2.40	4.8	1578.50	504	0.38	0.70	3127	1402	6509	20311	21874	7210
9	31.5	2.40	4.8	2367.75	756	0.36	0.66	4475	1348	6509	26819	29057	7183
8	28.0	2.40	4.8	3157.00	1008	0.36	0.64	5796	1321	6509	33328	36226	7169
7	24.5	2.40	4.8	3946.25	1260	0.35	0.63	7099	1303	6509	39837	43387	7161
6	21.0	2.40	4.8	4735.50	1512	0.35	0.62	8390	1291	6632	46469	50664	7277
5	17.5	2.40	4.8	5524.75	1764	0.34	0.61	9671	1281	6632	53100	57936	7272
4	14.0	2.40	4.8	6314.00	2016	0.34	0.60	10945	1274	6632	59732	65204	7268
3	10.5	2.40	4.8	7103.25	2268	0.34	0.59	12213	1268	6632	66363	72470	7265
2	7.0	2.40	4.8	7892.50	2520	0.34	0.59	13476	1263	6632	72995	79733	7263
1	3.5	2.40	4.8	8681.75	2772	0.33	0.58	14734	1258	6632	79626	86993	7261

TAB. I.6 Loading applied at mass center for B18 in Montréal

Lev.	Elev.	Live Occupancy		Cumulated Trib. Area		Reduction* Factor		Live Load		Dead Load	Cumulated load Combination		Factored Loading
		Off	Corr	Off	Corr	F_{rld}^{off}	F_{rld}^{corr}	Cumul.	per Floor		$P_{\text{D}} + 0.25P_{\text{S}}$**	$P_{\text{D}} + 0.5P_{\text{L}}$	per floor
-	m	kPa	kPa	m^2	m^2	-	-	kN	kN	kN	kN	kN	kN
18	63.0	2.48	-	1041.25	-	-	-	2582	2582	6647	7293	7293	7293
17	59.5	2.40	4.8	789.25	252	0.41	0.78	1725	1725	6509	13802	14664	7371
16	56.0	2.40	4.8	1578.50	504	0.38	0.70	3127	1402	6509	20311	21874	7210
15	52.5	2.40	4.8	2367.75	756	0.36	0.66	4475	1348	6509	26819	29057	7183
14	49.0	2.40	4.8	3157.00	1008	0.36	0.64	5796	1321	6509	33328	36226	7169
13	45.5	2.40	4.8	3946.25	1260	0.35	0.63	7099	1303	6509	39837	43387	7161
12	42.0	2.40	4.8	4735.50	1512	0.35	0.62	8390	1291	6560	46397	50592	7205
11	38.5	2.40	4.8	5524.75	1764	0.34	0.61	9671	1281	6560	52957	57793	7201
10	35.0	2.40	4.8	6314.00	2016	0.34	0.60	10945	1274	6632	59589	65061	7268
9	31.5	2.40	4.8	7103.25	2268	0.34	0.59	12213	1268	6632	66220	72327	7265
8	28.0	2.40	4.8	7892.50	2520	0.34	0.59	13476	1263	6632	72852	79589	7263
7	24.5	2.40	4.8	8681.75	2772	0.33	0.58	14734	1258	6632	79483	86850	7261
6	21.0	2.40	4.8	9471.00	3024	0.33	0.58	15988	1254	6632	86115	94109	7259
5	17.5	2.40	4.8	10260.25	3276	0.33	0.58	17239	1251	6632	92746	101366	7257
4	14.0	2.40	4.8	11049.50	3528	0.33	0.58	18488	1248	6632	99378	108621	7256
3	10.5	2.40	4.8	11838.75	3780	0.33	0.57	19733	1246	6632	106009	115876	7254
2	7.0	2.40	4.8	12628.00	4032	0.33	0.57	20976	1243	6632	112641	123129	7253
1	3.5	2.40	4.8	13417.25	4284	0.33	0.57	22217	1241	6632	119272	130381	7252

TAB. I.7 Shear wall tribuary loading for B6 in Vancouver

Lev.	Live Occupancy		Cumulated Trib. Area		Reduction* Factor		Live Load		Dead Load	Cumulated load Combination		Factored Loading
	Off	Corr	Off	Corr	F_{rld}^{off}	F_{rld}^{corr}	Cumul.	per Floor		$P_{\text{D}} + 0.25P_{\text{S}}$**	$P_{\text{D}} + 0.5P_{\text{L}}$	per floor
-	kPa	kPa	m^2	m^2	-	-	kN	kN	kN	kN	kN	kN
6	1.64	-	49.50	-	-	-	81	81	423	443	443	443
5	2.40	4.8	29.16	18	0.88	1.00	148	148	405	848	922	479
4	2.40	4.8	58.32	36	0.71	1.00	272	124	405	1254	1390	467
3	2.40	4.8	87.48	54	0.63	1.00	392	120	405	1659	1855	465
2	2.40	4.8	116.64	72	0.59	1.00	511	118	405	2064	2320	464
1	2.40	4.8	145.80	90	0.56	0.97	615	105	405	2470	2777	458

TAB. I.8 Shear wall trib. loading in B12 in Vancouver

Lev.	Live Occupancy		Cumulated Trib. Area		Reduction* Factor		Live Load	per	Dead Load	Cumulated load Combination		Factored Loading
	Off	Corr	Off	Corr	F_{rld}^{off}	F_{rld}^{corr}	Cumul.	Floor		$P_{\text{D}} + 0.25P_{\text{S}}$**	$P_{\text{D}} + 0.5P_{\text{L}}$	per floor
-	kPa	kPa	m^2	m^2	-	-	kN	kN	kN	kN	kN	kN
12	1.64	-	49.50	-	-	-	81	81	423	443	443	443
11	2.40	4.8	29.16	18	0.88	1.00	148	148	405	848	922	479
10	2.40	4.8	58.32	36	0.71	1.00	272	124	405	1254	1390	467
9	2.40	4.8	87.48	54	0.63	1.00	392	120	405	1659	1855	465
8	2.40	4.8	116.64	72	0.59	1.00	511	118	405	2064	2320	464
7	2.40	4.8	145.80	90	0.56	0.97	615	105	405	2470	2777	458
6	2.40	4.8	174.96	108	0.54	0.93	708	92	408	2877	3231	454
5	2.40	4.8	204.12	126	0.52	0.90	798	90	408	3285	3684	453
4	2.40	4.8	233.28	144	0.50	0.87	886	88	408	3693	4136	452
3	2.40	4.8	262.44	162	0.49	0.85	973	87	408	4101	4587	451
2	2.40	4.8	291.60	180	0.48	0.83	1058	86	408	4509	5038	451
1	2.40	4.8	320.76	198	0.47	0.82	1143	85	408	4917	5488	450

TAB. I.9 Shear wall trib. loading in B18 in Vancouver

Lev.	Live Occupancy		Cumulated Trib. Area		Reduction* Factor		Live Load		Dead Load	Cumulated load Combination		Factored Loading
	Off	Corr	Off	Corr	F_{rld}^{off}	F_{rld}^{corr}	Cumul.	per Floor		$P_{\text{D}} + 0.25P_{\text{S}}$**	$P_{\text{D}} + 0.5P_{\text{L}}$	per floor
-	kPa	kPa	m^2	m^2	-	-	kN	kN	kN	kN	kN	kN
18	1.64	-	49.50	-	-	-	81	81	423	443	443	443
17	2.40	4.8	29.16	18	0.88	1.00	148	148	405	848	922	479
16	2.40	4.8	58.32	36	0.71	1.00	272	124	405	1254	1390	467
15	2.40	4.8	87.48	54	0.63	1.00	392	120	405	1659	1855	465
14	2.40	4.8	116.64	72	0.59	1.00	511	118	405	2064	2320	464
13	2.40	4.8	145.80	90	0.56	0.97	615	105	405	2470	2777	458
12	2.40	4.8	174.96	108	0.54	0.93	708	92	405	2875	3229	451
11	2.40	4.8	204.12	126	0.52	0.90	798	90	405	3280	3679	450
10	2.40	4.8	233.28	144	0.50	0.87	886	88	408	3688	4131	452
9	2.40	4.8	262.44	162	0.49	0.85	973	87	408	4096	4582	451
8	2.40	4.8	291.60	180	0.48	0.83	1058	86	408	4504	5033	451
7	2.40	4.8	320.76	198	0.47	0.82	1143	85	408	4912	5483	450
6	2.40	4.8	349.92	216	0.47	0.80	1226	84	408	5320	5933	450
5	2.40	4.8	379.08	234	0.46	0.79	1309	83	408	5727	6382	449
4	2.40	4.8	408.24	252	0.45	0.78	1391	82	408	6135	6831	449
3	2.40	4.8	437.40	270	0.45	0.77	1473	81	408	6543	7280	449
2	2.40	4.8	466.56	288	0.44	0.76	1554	81	408	6951	7728	448
1	2.40	4.8	495.72	306	0.44	0.76	1634	80	408	7359	8176	448

TAB. I.10 Loading applied at mass center for B6 in Vancouver

Lev.	Elev.	Live Occupancy		Cumulated Trib. Area		Reduction* Factor		Live Load		Dead Load	Cumulated load Combination		Factored Loading
		Off	Corr	Off	Corr	F_{rld}^{off}	F_{rld}^{corr}	Cumul.	per Floor		$P_{\text{D}} + 0.25P_{\text{S}}$**	$P_{\text{D}} + 0.5P_{\text{L}}$	per floor
-	m	kPa	kPa	m^2	m^2	-	-	kN	kN	kN	kN	kN	kN
6	21.0	1.64	-	1041.25	-	-	-	1708	1708	6647	7074	7074	7074
5	17.5	2.40	4.8	789.25	252	0.41	0.78	1725	1725	6509	13583	14445	7371
4	14.0	2.40	4.8	1578.50	504	0.38	0.70	3127	1402	6509	20092	21655	7210
3	10.5	2.40	4.8	2367.75	756	0.36	0.66	4475	1348	6509	26601	28838	7183
2	7.0	2.40	4.8	3157.00	1008	0.36	0.64	5796	1321	6509	33110	36008	7169
1	3.5	2.40	4.8	3946.25	1260	0.35	0.63	7099	1303	6509	39619	43168	7161

TAB. I.11 Loading applied at mass center for B12 in Vancouver

Lev.	Elev.	Live Occupancy		Cumulated Trib. Area		Reduction* Factor		Live Load	per	Dead Load	Cumulated load Combination		Factored Loading
		Off	Corr	Off	Corr	F_{rld}^{off}	F_{rld}^{corr}	Cumul.	Floor		$P_{\text{D}} + 0.25P_{\text{S}}$**	$P_{\text{D}} + 0.5P_{\text{L}}$	per floor
-	m	kPa	kPa	m^2	m^2	-	-	kN	kN	kN	kN	kN	kN
12	42.0	1.64	-	1041.25	-	-	-	1708	1708	6647	7074	7074	7074
11	38.5	2.40	4.8	789.25	252	0.41	0.78	1725	1725	6509	13583	14445	7371
10	35.0	2.40	4.8	1578.50	504	0.38	0.70	3127	1402	6509	20092	21655	7210
9	31.5	2.40	4.8	2367.75	756	0.36	0.66	4475	1348	6509	26601	28838	7183
8	28.0	2.40	4.8	3157.00	1008	0.36	0.64	5796	1321	6509	33110	36008	7169
7	24.5	2.40	4.8	3946.25	1260	0.35	0.63	7099	1303	6509	39619	43168	7161
6	21.0	2.40	4.8	4735.50	1512	0.35	0.62	8390	1291	6632	46179	50374	7277
5	17.5	2.40	4.8	5524.75	1764	0.34	0.61	9671	1281	6632	52738	57574	7272
4	14.0	2.40	4.8	6314.00	2016	0.34	0.60	10945	1274	6632	59370	64843	7268
3	10.5	2.40	4.8	7103.25	2268	0.34	0.59	12213	1268	6632	66001	72108	7265
2	7.0	2.40	4.8	7892.50	2520	0.34	0.59	13476	1263	6632	72633	79371	7263
1	3.5	2.40	4.8	8681.75	2772	0.33	0.58	14734	1258	6632	79264	86631	7261

TAB. I.12 Loading applied at mass center for B18 in Vancouver

Lev.	Elev.	Live Occupancy		Cumulated Trib. Area		Reduction* Factor		Live Load		Dead Load	Cumulated load Combination		Factored Loading
		Off	Corr	Off	Corr	F_{rld}^{off}	F_{rld}^{corr}	Cumul.	per Floor		$P_{\text{D}} + 0.25P_{\text{S}}$**	$P_{\text{D}} + 0.5P_{\text{L}}$	per floor
-	m	kPa	kPa	m^2	m^2	-	-	kN	kN	kN	kN	kN	kN
18	63.0	1.64	-	1041.25	-	-	-	1708	1708	6647	7074	7074	7074
17	59.5	2.40	4.8	789.25	252	0.41	0.78	1725	1725	6509	13583	14445	7371
16	56.0	2.40	4.8	1578.50	504	0.38	0.70	3127	1402	6509	20092	21655	7210
15	52.5	2.40	4.8	2367.75	756	0.36	0.66	4475	1348	6509	26601	28838	7183
14	49.0	2.40	4.8	3157.00	1008	0.36	0.64	5796	1321	6509	33110	36008	7169
13	45.5	2.40	4.8	3946.25	1260	0.35	0.63	7099	1303	6509	39619	43168	7161
12	42.0	2.40	4.8	4735.50	1512	0.35	0.62	8390	1291	6560	46179	50374	7205
11	38.5	2.40	4.8	5524.75	1764	0.34	0.61	9671	1281	6560	52738	57574	7201
10	35.0	2.40	4.8	6314.00	2016	0.34	0.60	10945	1274	6632	59370	64843	7268
9	31.5	2.40	4.8	7103.25	2268	0.34	0.59	12213	1268	6632	66001	72108	7265
8	28.0	2.40	4.8	7892.50	2520	0.34	0.59	13476	1263	6632	72633	79371	7263
7	24.5	2.40	4.8	8681.75	2772	0.33	0.58	14734	1258	6632	79264	86631	7261
6	21.0	2.40	4.8	9471.00	3024	0.33	0.58	15988	1254	6632	85896	93890	7259
5	17.5	2.40	4.8	10260.25	3276	0.33	0.58	17239	1251	6632	92527	101147	7257
4	14.0	2.40	4.8	11049.50	3528	0.33	0.58	18488	1248	6632	99159	108403	7256
3	10.5	2.40	4.8	11838.75	3780	0.33	0.57	19733	1246	6632	105790	115657	7254
2	7.0	2.40	4.8	12628.00	4032	0.33	0.57	20976	1243	6632	112422	122910	7253
1	3.5	2.40	4.8	13417.25	4284	0.33	0.57	22217	1241	6632	119053	130162	7252

ANNEXE II

TORSIONAL SENSITIVITY FOR 6B, 12B AND 18B BUILDINGS IN MONTREAL AND VANCOUVER

The torsional sensitivity for the three models 6B, 12B and 18B is determined according Article 4.1.8.11, Sentence (9), NBCC 2005 and explained in Section 2.2 of that project. It is schematically represented in Figure 2.1 (Tremblay 2005). The torsional effects in the present work are accounted by applying the equivalent static forces, determined in Chapter 4 with concurently acting torsional moments due to accidental eccentricities at each level, which are : $T_x = F_x(e_x \pm 0.10D_{nx})$. The lateral deflections δ_{max}, δ_{ave} resulting from those analyses and listed in the following Tables II.1, II.2 and II.3 have to be multiplied by $(R_d R_o / I_E)$ in order to give realistic values of the anticipated deflections, according to Article 4.1.8.13, Sentence (2), NBCC 2005.

TAB. II.1 Maximum to average displacement ratio at the extreme points of 6B model in Montreal and Vancouver.

		Montreal			Vancouver		
	Level	Displacement		B	Displacement		B
		δ_{max}	δ_{ave}		δ_{max}	δ_{ave}	
Floor	(m)	(m)	(m)		(m)	(m)	
6	21.0	0.0147	0.0124	1.185	0.018	0.015	1.195
5	17.5	0.0114	0.0096	1.188	0.014	0.012	1.193
4	14.0	0.0081	0.0069	1.183	0.010	0.009	1.195
3	10.5	0.0051	0.0043	1.186	0.007	0.006	1.189
2	7.0	0.0026	0.0022	1.182	0.004	0.003	1.207
1	3.5	0.0008	0.0007	1.231	0.001	0.001	1.158

TAB. II.2 Maximum to average displacement ratio at the extreme points of 12B model in Montreal and Vancouver.

		Montreal			Vancouver		
	Level	Displacement		B	Displacement		B
		δ_{max}	δ_{ave}		δ_{max}	δ_{ave}	
Floor	(m)	(m)	(m)		(m)	(m)	
12	42.0	0.087	0.074	1.171	0.175	0.150	1.171
11	38.5	0.077	0.065	1.171	0.155	0.133	1.172
10	35.0	0.067	0.057	1.171	0.135	0.116	1.172
9	31.5	0.057	0.049	1.173	0.116	0.099	1.172
8	28.0	0.048	0.041	1.173	0.096	0.082	1.173
7	24.5	0.038	0.033	1.173	0.079	0.067	1.181
6	21.0	0.030	0.025	1.174	0.060	0.051	1.175
5	17.5	0.022	0.019	1.175	0.044	0.038	1.176
4	14.0	0.015	0.013	1.179	0.030	0.026	1.177
3	10.5	0.009	0.008	1.179	0.018	0.015	1.177
2	7.0	0.003	0.004	1.178	0.009	0.007	1.176
1	3.5	0.001	0.001	1.182	0.003	0.002	1.182

TAB. II.3 Maximum to average displacement ratio at the extreme points of 6B model in Montreal and Vancouver.

		Montreal			Vancouver		
	Level	Displacement		B	Displacement		B
		δ_{max}	δ_{ave}		δ_{max}	δ_{ave}	
Floor	(m)	(m)	(m)		(m)	(m)	
18	63.0	0.343	0.299	1.146	0.650	0.568	1.146
17	59.5	0.317	0.276	1.146	0.600	0.524	1.146
16	56.0	0.290	0.253	1.147	0.550	0.480	1.147
15	52.5	0.264	0.230	1.148	0.501	0.437	1.147
14	49.0	0.238	0.207	1.148	0.451	0.393	1.148
13	45.5	0.212	0.185	1.149	0.403	0.351	1.149
12	42.0	0.187	0.163	1.149	0.355	0.309	1.150
11	38.5	0.163	0.141	1.150	0.309	0.268	1.150
10	35.0	0.139	0.121	1.151	0.264	0.229	1.151
9	31.5	0.116	0.101	1.152	0.221	0.192	1.152
8	28.0	0.095	0.083	1.152	0.180	0.157	1.152
7	24.5	0.075	0.065	1.153	0.143	0.124	1.153
6	21.0	0.057	0.050	1.154	0.109	0.094	1.154
5	17.5	0.041	0.036	1.155	0.078	0.068	1.155
4	14.0	0.027	0.024	1.156	0.052	0.045	1.156
3	10.5	0.016	0.014	1.158	0.031	0.027	1.135
2	7.0	0.008	0.007	1.160	0.015	0.012	1.177
1	3.5	0.002	0.002	1.158	0.004	0.004	1.167

ANNEXE III

MODELING OF CONCRETE SHEAR WALLS

LEGEND

CVB – Concentrated Vertical Bars
DVB – Distributed Vertical Bars
DHB – Distributed Horizontal Bars
E.E. – Each End
E.F. – Each Face
A – Horizontal coordinate of modeled reinforcement, [mm]
B – Area of modeled reinforcement, [mm^2]
C – Area of concrete section, [mm^2]

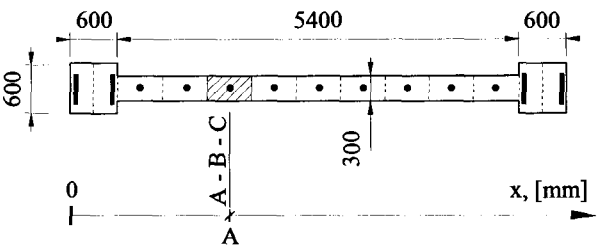

4~6 FLOORS

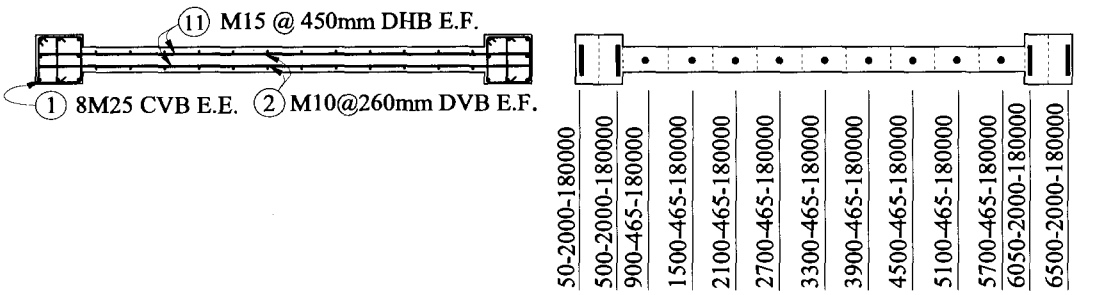

1~3 FLOORS

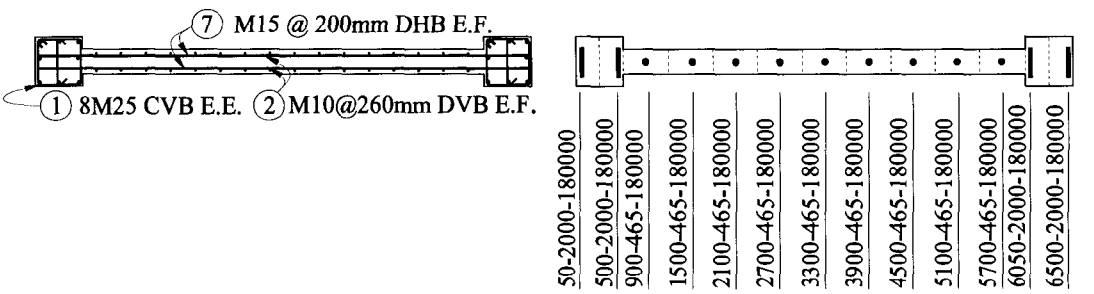

FIG. III.1 Modeling of shear wall sections for B6 located in Montréal

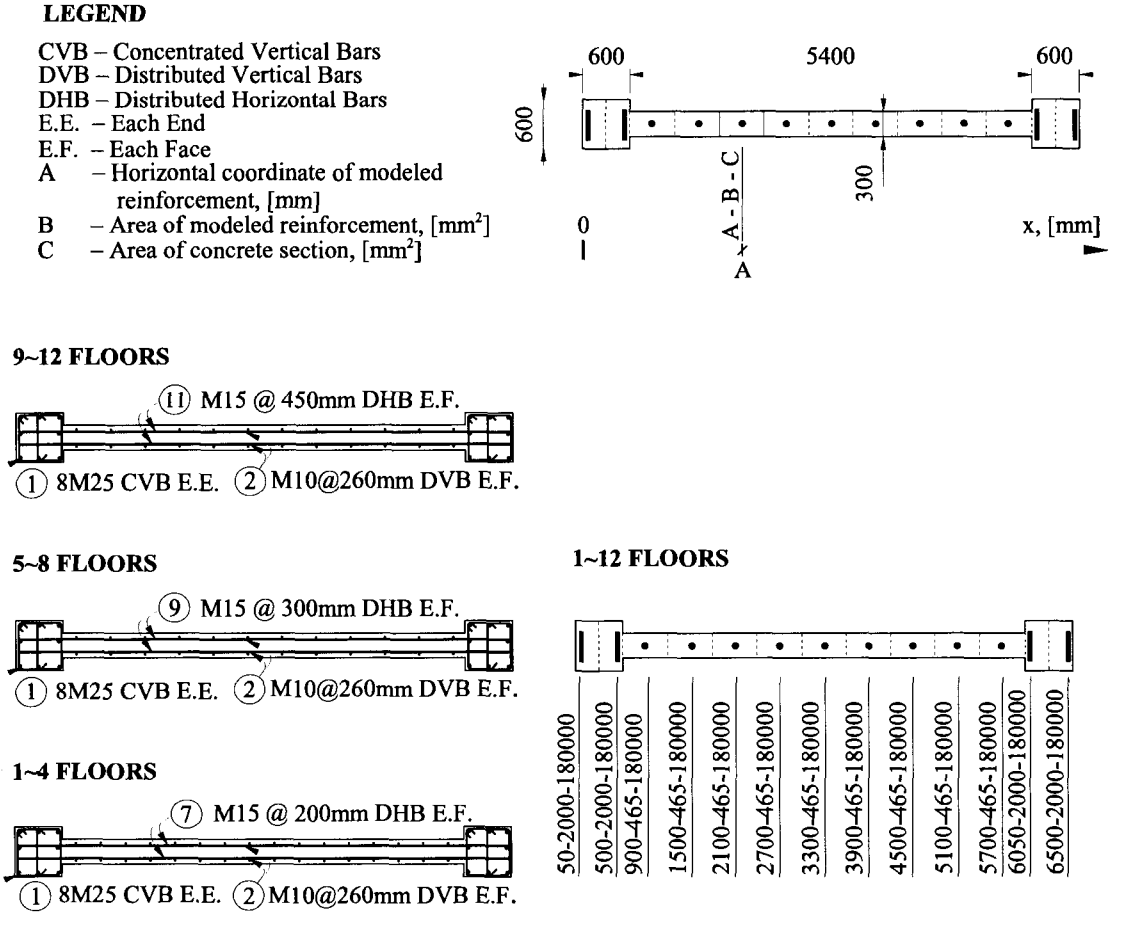

FIG. III.2 Modeling of shear wall sections for B12 located in Montréal

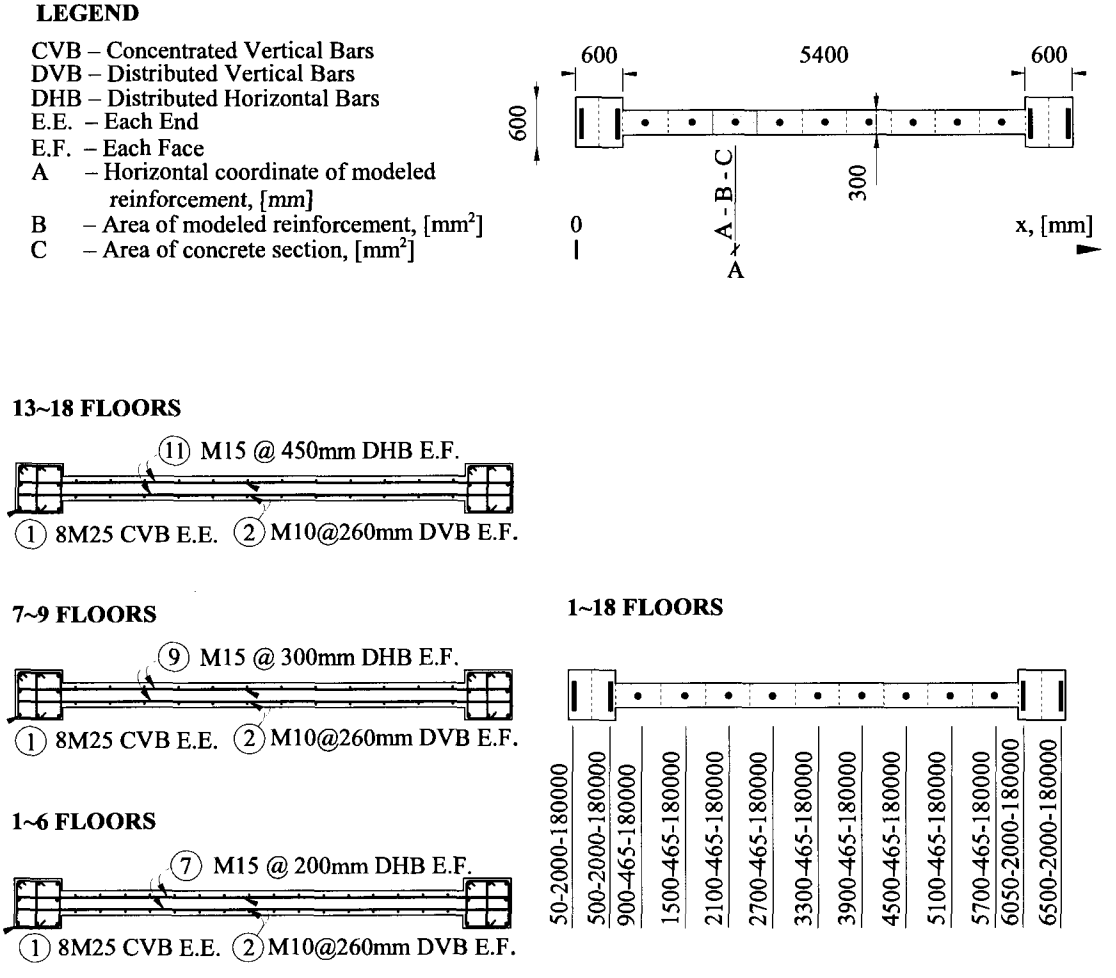

FIG. III.3 Modeling of shear wall sections for B18 located in Montréal

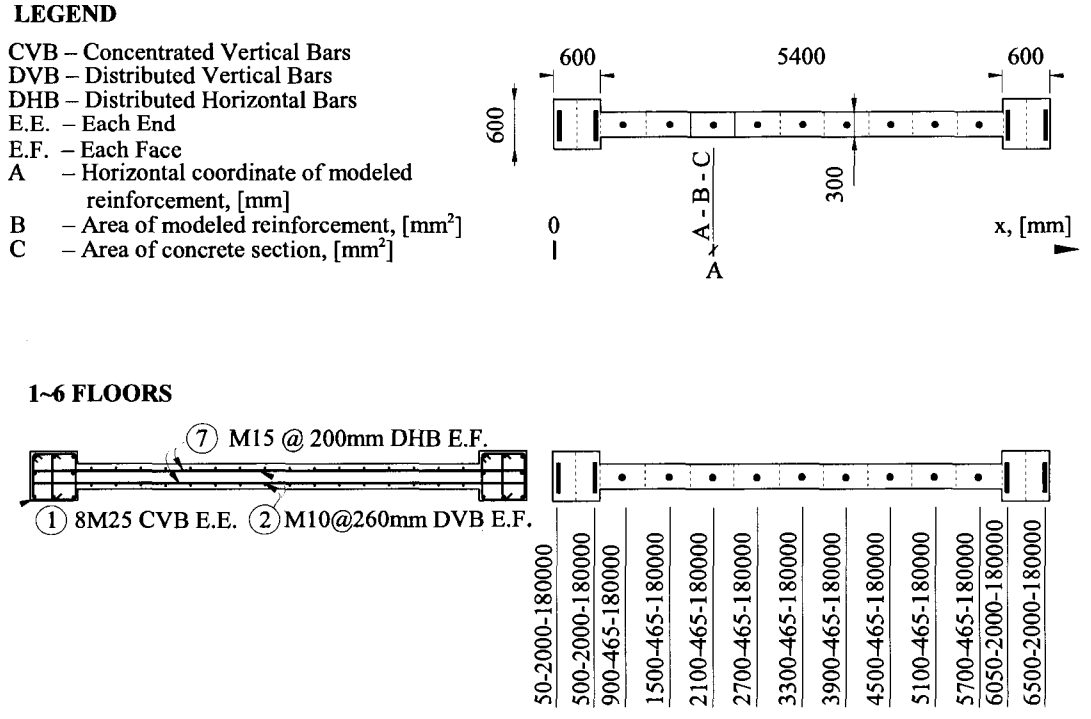

FIG. III.4 Modeling of shear wall sections for B6 located in Vancouver

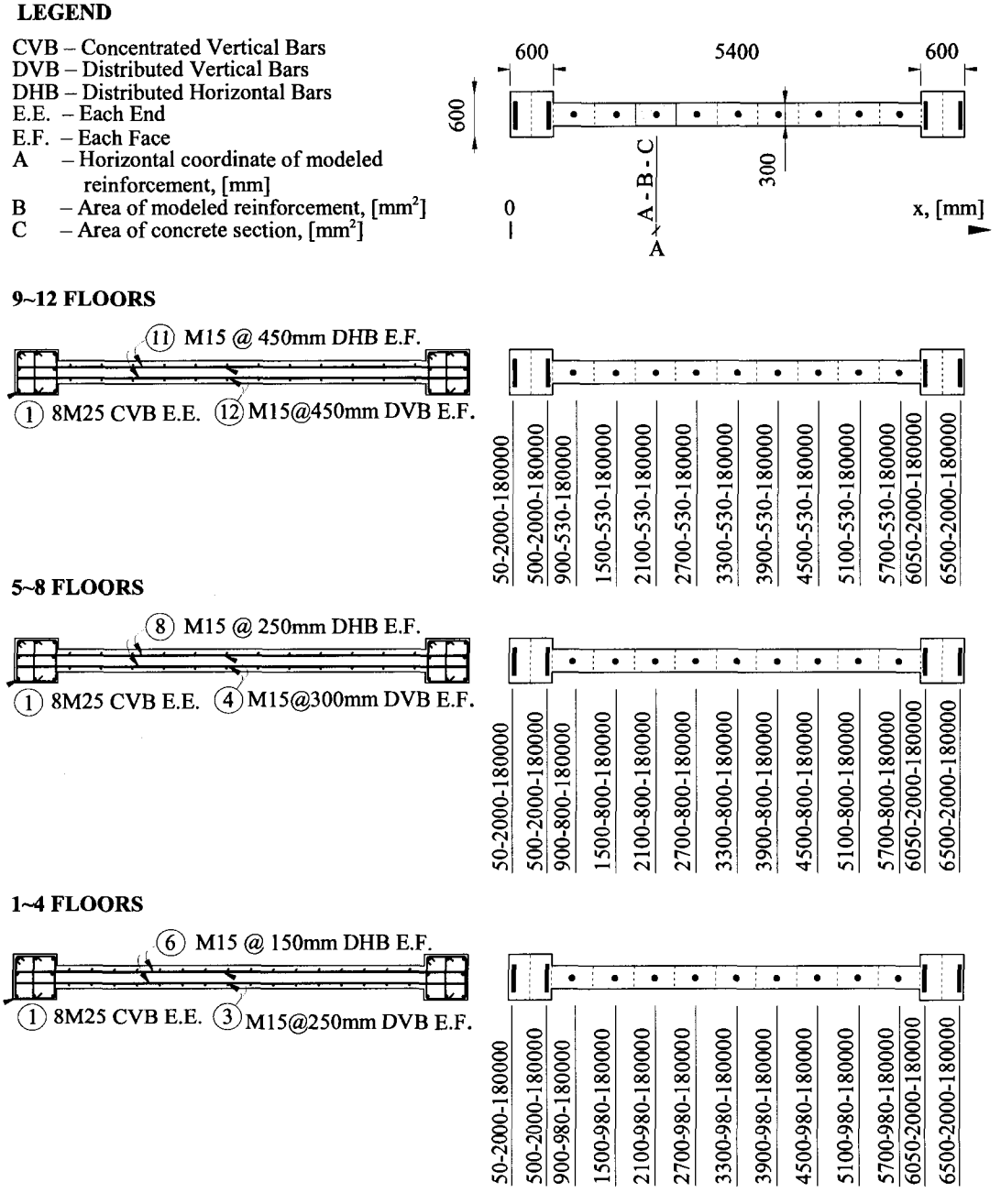

FIG. III.5 Modeling of shear wall sections for B12 located in Vancouver

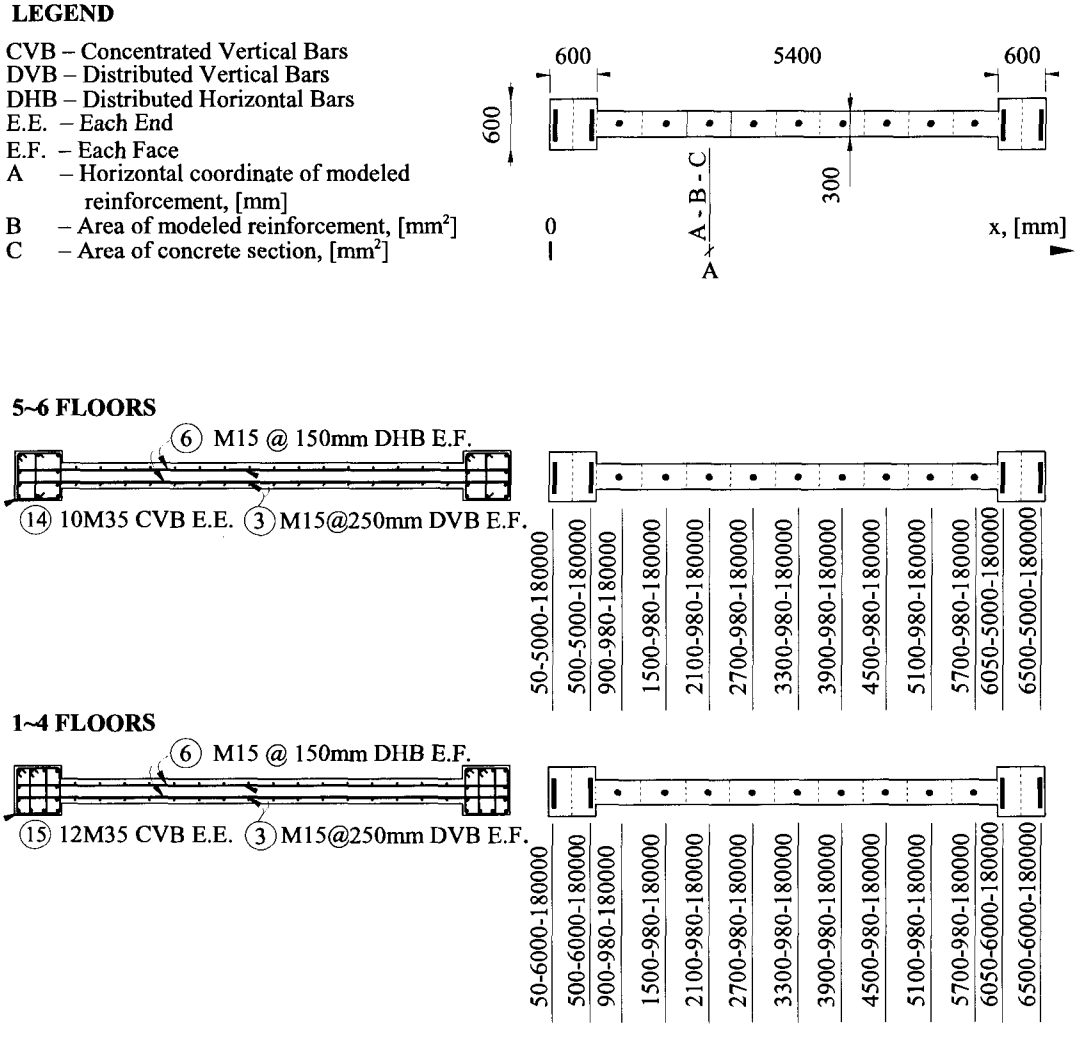

FIG. III.6 Modeling of shear wall sections for B18 located in Vancouver

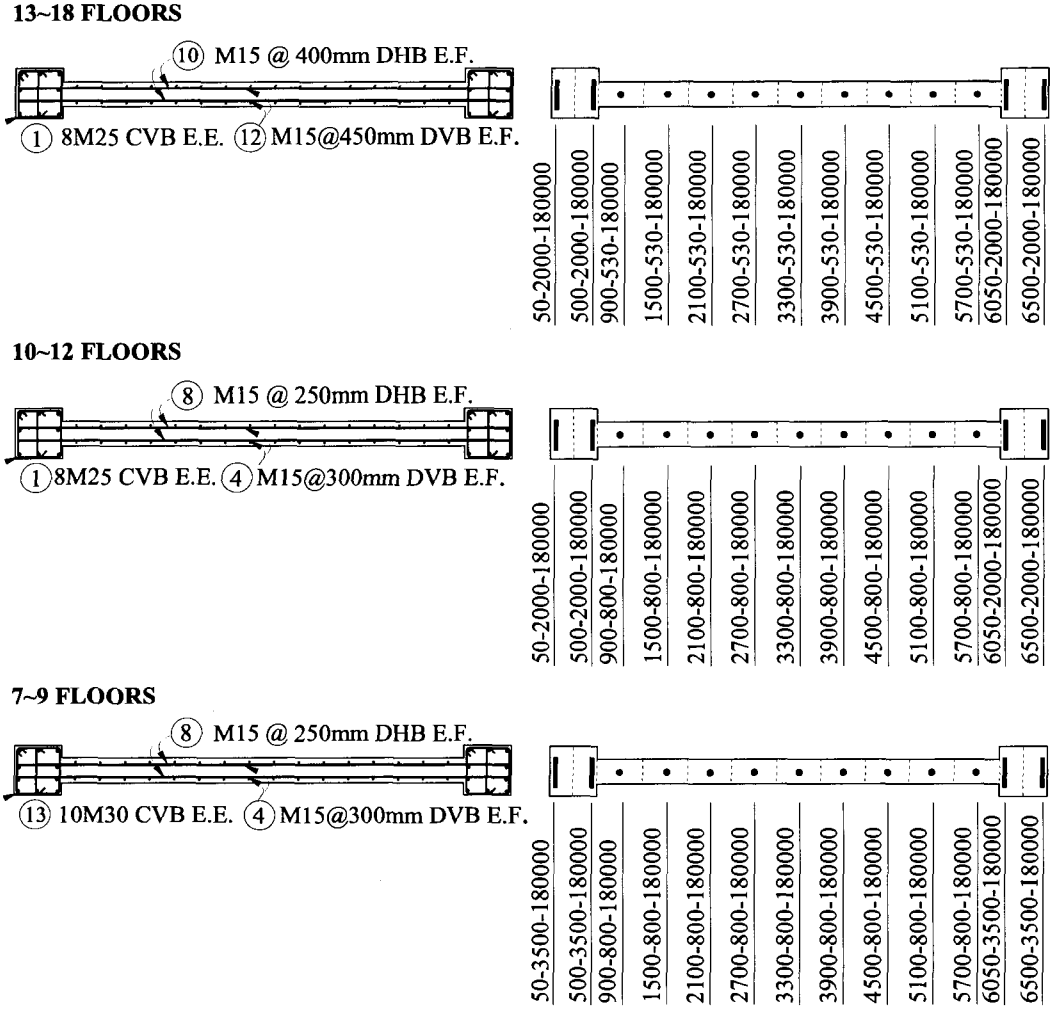

FIG. III.7 Modeling of shear wall sections for B18 located in Vancouver(cont.)

ANNEXE IV

CHOPRA METHOD - DISPLACEMENT-BASED DESIGN USING INELASTIC DESIGN SPECTRUM FOR 6-, 12- AND 18-STOREYS SHEARWALLS IN MONTRÉAL AND VANCOUVER

TAB. IV.1 Results of iterative DBD procedure for 6-storey shearwall in Montréal using inelastic design spectrum for SHL-2500.

No	Δ_y (cm)	Δ_{eff} (cm)	μ	T (s)	k (kN/cm)	f_{req} (kN)	M_{req} (kNm)	EI_{eff} (kNm^2)	k_{des} (kN/cm)	$\Delta_{y,des}$ (cm)
1	5.00	16.6	3.3	5.2	21.68	108	1731	28+E5	20.9	5.19
2	5.19	16.7	3.2	5.3	21.43	111	1783	29+E5	21.4	5.19

TAB. IV.2 Results of iterative DBD procedure for 6-storey shearwall in Montréal using inelastic design spectrum for SHL-475.

No	Δ_y (cm)	Δ_{eff} (cm)	μ	T (s)	k (kN/cm)	f_{req} (kN)	M_{req} (kNm)	EI_{eff} (kNm^2)	k_{des} (kN/cm)	$\Delta_{y,des}$ (cm)
1	5.00	10.9	2.2	7.4	10.7	54	865	14+E5	10.2	5.27
2	5.27	11.1	2.1	7.5	10.3	54	878	14+E5	10.3	5.27

TAB. IV.3 Results of iterative DBD procedure for 6-storey shearwall in Montréal using inelastic design spectrum for SHL-75.

No	Δ_y (cm)	Δ_{eff} (cm)	μ	T (s)	k (kN/cm)	f_{req} (kN)	M_{req} (kNm)	EI_{eff} (kNm^2)	k_{des} (kN/cm)	$\Delta_{y,des}$ (cm)
1	4.90	5.5	1.1	11.8	4.4	21	337	5+E5	4.3	5.02
2	5.02	7.8	1.6	12.0	4.2	21	337	5+E5	4.3	5.02

TAB. IV.4 Results of iterative DBD procedure for 12-storey shearwall in Montréal using inelastic design spectrum for SHL-2500.

No	Δ_y (cm)	Δ_{eff} (cm)	μ	T (s)	k (kN/cm)	f_{req} (kN)	M_{req} (kNm)	EI_{eff} (kNm^2)	k_{des} (kN/cm)	$\Delta_{y,des}$ (cm)
1	17.90	63.1	3.5	8.2	17.94	321	9578	158+E5	17.9	17.95
2	17.95	40.5	2.3	7.8	19.83	356	10610	175+E5	19.8	17.95

TAB. IV.5 Results of iterative DBD procedure for 12-storey shearwall in Montréal using inelastic design spectrum for SHL-475.

No	Δ_y (cm)	Δ_{eff} (cm)	μ	T (s)	k (kN/cm)	f_{req} (kN)	M_{req} (kNm)	EI_{eff} (kNm^2)	k_{des} (kN/cm)	$\Delta_{y,des}$ (cm)
1	17.80	34.9	1.9	12.1	8.27	147	4388	72+E5	8.2	17.94
2	17.94	29.2	1.6	10.1	11.83	212	6326	104+E5	11.8	17.94

TAB. IV.6 Results of iterative DBD procedure for 12-storey shearwall in Montréal using inelastic design spectrum for SHL-75.

No	Δ_y (cm)	Δ_{eff} (cm)	μ	T (s)	k (kN/cm)	f_{req} (kN)	M_{req} (kNm)	EI_{eff} (kNm^2)	k_{des} (kN/cm)	$\Delta_{y,des}$ (cm)
1	17.70	6.8	1.0	11.6	8.93	158	4689	77+E5	8.9	17.76
2	17.76	23.4	1.3	20.3	3.0	53	1583	26+E5	3.0	17.76

TAB. IV.7 Results of iterative DBD procedure for 18-storey shearwall in Montréal using inelastic design spectrum for SHL-2500.

No	Δ_y (cm)	Δ_{eff} (cm)	μ	T (s)	k (kN/cm)	f_{req} (kN)	M_{req} (kNm)	EI_{eff} (kNm^2)	k_{des} (kN/cm)	$\Delta_{y,des}$ (cm)
1	38.90	88.1	2.3	11.0	14.9	580	25370	418+E5	14.9	38.70
2	38.70	72.4	1.9	9.3	20.8	805	35209	580+E5	20.8	38.70

TAB. IV.8 Results of iterative DBD procedure for 18-storey shearwall in Montréal using inelastic design spectrum for SHL-475.

No	Δ_y (cm)	Δ_{eff} (cm)	μ	T (s)	k (kN/cm)	f_{req} (kN)	M_{req} (kNm)	EI_{eff} (kNm^2)	k_{des} (kN/cm)	$\Delta_{y,des}$ (cm)
1	38.80	45.9	1.2	16.7	6.46	251	10966	180+E5	6.5	38.6
2	38.61	55.4	1.4	16.8	6.40	247	10810	178+E5	6.4	38.6

TAB. IV.9 Results of iterative DBD procedure for 18-storey shearwall in Montréal using inelastic design spectrum for SHL-75.

No	Δ_y (cm)	Δ_{eff} (cm)	μ	T (s)	k (kN/cm)	f_{req} (kN)	M_{req} (kNm)	EI_{eff} (kNm^2)	k_{des} (kN/cm)	$\Delta_{y,des}$ (cm)
1	37.30	4.6	1.0	10.0	15.2	566	24131	398+E5	15.4	36.7
2	36.70	44.9	1.2	22.4	3.03	111	4731	78+E5	3.0	36.7

TAB. IV.10 Results of iterative DBD procedure for 6-storey shearwall in Vancouver using inelastic design spectrum for SHL-2500.

No	Δ_y (cm)	Δ_{eff} (cm)	μ	T (s)	k (kN/cm)	f_{req} (kN)	M_{req} (kNm)	EI_{eff} (kNm^2)	k_{des} (kN/cm)	$\Delta_{y,des}$ (cm)
1	5.00	16.5	3.3	2.0	143.83	719	11492	190+E5	139.4	5.16
2	5.16	16.6	3.2	2.1	139.65	720	11512	190+E5	139.7	5.16

TAB. IV.11 Results of iterative DBD procedure for 6-storey shearwall in Vancouver using inelastic design spectrum for SHL-475.

No	Δ_y (cm)	Δ_{eff} (cm)	μ	T (s)	k (kN/cm)	f_{req} (kN)	M_{req} (kNm)	EI_{eff} (kNm^2)	k_{des} (kN/cm)	$\Delta_{y,des}$ (cm)
1	5.00	10.9	2.2	2.4	103.5	517	8330	140+E5	98.8	5.24
2	5.24	11.0	2.1	2.4	99.2	520	8366	140+E5	98.2	5.24

TAB. IV.12 Results of iterative DBD procedure for 6-storey shearwall in Vancouver using inelastic design spectrum for SHL-75.

No	Δ_y (cm)	Δ_{eff} (cm)	μ	T (s)	k (kN/cm)	f_{req} (kN)	M_{req} (kNm)	EI_{eff} (kNm^2)	k_{des} (kN/cm)	$\Delta_{y,des}$ (cm)
1	4.80	5.5	1.1	3.4	52.7	253	3976	65+E5	50.8	4.99
2	4.99	7.8	1.6	4.0	37.7	188	2954	48+E5	37.7	4.99

TAB. IV.13 Results of iterative DBD procedure for 12-storey shearwall in Vancouver using inelastic design spectrum for SHL-2500.

No	Δ_y (cm)	Δ_{eff} (cm)	μ	T (s)	k (kN/cm)	f_{req} (kN)	M_{req} (kNm)	EI_{eff} (kNm^2)	k_{des} (kN/cm)	$\Delta_{y,des}$ (cm)
1	17.80	63.0	3.5	5.6	38.00	676	20131	332+E5	37.8	17.89
2	17.89	40.4	2.3	4.2	67.72	1212	36059	594+E5	67.7	17.89

TAB. IV.14 Results of iterative DBD procedure for 12-storey shearwall in Vancouver using inelastic design spectrum for SHL-475.

No	Δ_y (cm)	Δ_{eff} (cm)	μ	T (s)	k (kN/cm)	f_{req} (kN)	M_{req} (kNm)	EI_{eff} (kNm^2)	k_{des} (kN/cm)	$\Delta_{y,des}$ (cm)
1	17.80	34.9	2.0	5.1	46.0	819	24390	402+E5	45.8	17.88
2	17.88	29.1	1.6	4.8	52.1	932	27734	457+E5	52.1	17.88

TAB. IV.15 Results of iterative DBD procedure for 12-storey shearwall in Vancouver using inelastic design spectrum for SHL-75.

No	Δ_y (cm)	Δ_{eff} (cm)	μ	T (s)	k (kN/cm)	f_{req} (kN)	M_{req} (kNm)	EI_{eff} (kNm^2)	k_{des} (kN/cm)	$\Delta_{y,des}$ (cm)
1	17.60	6.8	1.0	4.1	71.22	1253	37088	611+E5	70.9	17.7
2	17.69	23.3	1.3	7.1	22.46	397	11758	194+E5	22.5	17.7

TAB. IV.16 Results of iterative DBD procedure for 18-storey shearwall in Vancouver using inelastic design spectrum for SHL-2500.

No	Δ_y (cm)	Δ_{eff} (cm)	μ	T (s)	k (kN/cm)	f_{req} (kN)	M_{req} (kNm)	EI_{eff} (kNm^2)	k_{des} (kN/cm)	$\Delta_{y,des}$ (cm)
1	38.80	87.9	2.3	5.8	53.02	2057	89895	14+E7	53.3	38.58
2	38.58	72.2	1.9	5.0	72.08	2475	108155	17+E7	64.2	38.58

TAB. IV.17 Results of iterative DBD procedure for 18-storey shearwall in Vancouver using inelastic design spectrum for SHL-475.

No	Δ_y (cm)	Δ_{eff} (cm)	μ	T (s)	k (kN/cm)	f_{req} (kN)	M_{req} (kNm)	EI_{eff} (kNm^2)	k_{des} (kN/cm)	$\Delta_{y,des}$ (cm)
1	38.70	45.8	1.2	6.7	40.19	1555	67888	11+E7	40.4	38.49
2	38.49	55.3	1.4	6.8	39.6	1524	66526	10+E7	39.6	38.49

TAB. IV.18 Results of iterative DBD procedure for 18-storey shearwall in Vancouver using inelastic design spectrum for SHL-75.

No	Δ_y (cm)	Δ_{eff} (cm)	μ	T (s)	k (kN/cm)	f_{req} (kN)	M_{req} (kNm)	EI_{eff} (kNm^2)	k_{des} (kN/cm)	$\Delta_{y,des}$ (cm)
1	37.10	4.6	1.0	2.4	263.45	9774	415394	68+E7	267.8	36.49
2	36.49	44.7	1.2	10.4	14.17	517	21968	3+E7	14.2	36.49